STABILITY OF MIXED CONVECTION FLOW IN VERTICAL CHANNEL FILLED WITH POROUS MEDIUM

Ph.D. THESIS

by

ABHISHEK KUMAR SHARMA

DEPARTMENT OF MATHEMATICS
INDIAN INSTITUTE OF TECHNOLOGY ROORKEE
ROORKEE – 247 667 (INDIA)
DECEMBER, 2017

STABILITY OF MIXED CONVECTION FLOW IN VERTICAL CHANNEL FILLED WITH POROUS MEDIUM

A THESIS

Submitted in partial fulfilment of the requirements for the award of the degree

of

DOCTOR OF PHILOSOPHY

in

MATHEMATICS

by

ABHISHEK KUMAR SHARMA

DEPARTMENT OF MATHEMATICS
INDIAN INSTITUTE OF TECHNOLOGY ROORKEE
ROORKEE – 247 667 (INDIA)
DECEMBER, 2017

INDIAN INSTITUTE OF TECHNOLOGY ROORKEE
ROORKEE

CANDIDATE'S DECLARATION

I hereby certify that the work which is being presented in the thesis entitled "**STABILITY OF MIXED CONVECTION FLOW IN VERTICAL CHANNEL FILLED WITH POROUS MEDIUM**" in partial fulfilment of the requirements for the award of the Degree of Doctor of Philosophy and submitted in the Department of Mathematics of the Indian Institute of Technology Roorkee, Roorkee is an authentic record of my own work carried out during a period from July, 2012 to December, 2017 under the supervision of Dr. P. Bera, Assosciate Professor, Department of Mathematics, Indian Institute of Technology Roorkee, Roorkee.

The matter presented in this thesis has not been submitted by me for the award of any other degree of this or any other Institution.

(ABHISHEK KUMAR SHARMA)

This is to certify that the above statement made by the candidate is correct to the best of my knowledge.

(Premananda Bera)
Supervisor

Date:

Abstract

The thesis reports a linear as well as weakly non-linear stability analysis of non-isothermal parallel flow in a vertical channel filled with porous medium. The flow is induced by external pressure gradient and buoyancy force due to maintenance of non-isothermal walls of the channel. Two different boundary conditions are considered: (i) when both walls of the channel are kept at constant but different temperatures (called as differentially heated), and (ii) when the temperature of both walls varies linearly with respect to the vertical coordinate. The non-Darcy model which gives rise to the volume averaged Navier-Stokes (VANS) equation is used except for some comparative study where Darcy model is also used. In porous medium, two different situations: local thermal equilibrium state (LTE) and local thermal non-equilibrium state (LTNE) are possible to explain the mechanism of heat transfer. Both these situations are considered in the thesis. The spectral method has been adopted to solve the governing equations of the problem. The weakly nonlinear analysis of parallel mixed convective flow in vertical channel filled with porous medium is developed on the basis of pioneering work of Stuart [99, 100], Stuart and Stewartson [101] and Yao & Rogers [130]. Motivation for the present study is based on the following three facts: (i) mixed convection through wall bounded domain filled with porous medium has numerous applications, (ii) stability analysis has not been extended to parallel mixed convective flow in a differentially heated channel, (iii) there are subtle differences between parallel mixed convective flow in a linearly heated channel and differentially heated channel.

The entire study is split into six chapters and a brief description of each chapter is given below.

The first chapter contains some basic concepts related to porous medium as well as hydrodynamic stability, a brief state of the art in this direction, and a note on considered models in this thesis is presented.

In Chapter 2, the linear stability of parallel mixed convective flow (PMCF) in a differentially heated vertical channel filled with incompressible fluid saturated porous medium is analyzed . Here, it is assumed that the two phases of porous medium: fluid and the solid matrix are in LTE state. The flow is controlled by six governing parameters: Darcy number (Da), ratio of Grashof number to Reynolds number ($Gr' = Gr/Re$), Reynolds number (Re), product of Forchheimer number and Reynolds number ($F' = FRe$), Prandtl number (Pr), and porosity (ε). The stability analysis of PMCF is carried out after a partial reinvestigation of Kwok and Chen's [62] numerical study which confirms that Gill's [41] result on stability of parallel natural convection flow (PNCF) is not valid when no-slip condition and inertia impact are taken into account. Similar to the parallel flow due to linearly varying wall temperature [5], in the present problem also the basic flow possesses three different types of instability, namely thermal-shear, interactive, and thermal-buoyant, which depends on controlling parameters, mainly Pr. The regimes of above three instabilities over the domain of Pr are functions of Da as well as Re. Stability analysis also reveals that when Re is fixed at 1000, the appearance of point of inflection in the basic velocity for fluid with Pr less than 30 acts as a necessary condition for instability for all considered values of Da. For a very small range of Pr, in the vicinity of $Pr = 0.01$, velocity disturbances are more responsible for the instability and kinetic energy production due to shear force is most dominant in balancing the dissipation of disturbance kinetic energy (KE). So, for these values of Pr the type of instability of the basic flow is thermal-shear. On the other hand, for relatively larger values of Pr (i.e., water or heavy oil), the instability is primarily due to the thermal disturbances and KE production due to buoyant term is most dominant in the energy balance and results in thermal-buoyant instability of the flow. In contrast to the flow in purely fluid medium, where the production of KE is solely suppressed by viscous dissipation (E_d), in porous medium the KE can be suppressed by surface drag (E_D),

form drag (E_F) and viscous dissipation (E_d). For relatively low permeable medium (i.e., for $Da = 10^{-4}$) dissipation through E_D dominates in the entire range of Pr for $Re = 1000$. From the influence of modified Forchheimer number it has been found that for Pr equal to 7 or 100 there exist a minimum value (F_o) of F' below which the effect of form drag on the critical Gr' as well as corresponding wave number is negligible and above this minimum value F' stabilizes the flow. It is also found that form drag may destabilize the flow for very less viscous (i.e., $Pr < 1$) fluid. For the range of parameters considered in this study, the scale analysis reveals that when the permeability of the medium is less than or equal to $2.5 \times 10^{-6}\text{m}^2$ and half width of the channel is 5cm, then the critical value of ΔT (i.e, temperature difference between the channel walls) for PMCF of water is higher than the same for PNCF (e.g., ΔT for PNCF and PMCF when $K = 2.5 \times 10^{-6}\text{m}^2$ are 8.58^oC and 13.3^oC, respectively), which may be the consequence of thermal-buoyant instability of the flow. In the case of PMCF there exists an optimum value of Re, depending on Da and F', at which the value of ΔT corresponding to critical Gr' is least. Thus, the flow will remain stable for all Re if the value of ΔT is less than this least value. Also it is expected that for a given media permeability there will be a least value of Pr above which the instability of the flow will take place for ΔT less than 20^oC, i.e., results from linear stability analysis using Boussinesq approximation will be more realistic.

Chapter 3 is an extension of the previous chapter by considering the two phases of porous medium in LTNE state. This study is carried out to get a better perspective of how two different modes, namely local thermal equilibrium and local thermal non-equilibrium, of transfer of energy between solid and fluid phases inside the porous medium affect the instability of the considered flow. The interphase heat transfer coefficient (H) and porosity scaled thermal conductivity ratio of fluid and solid phases (γ) are new parameters in LTNE state whose effects are analyzed. The linear instability boundary shows that for a given value of Da, the interphase heat transfer coefficient has a stabilizing effect on the instability of the flow. The relative change in critical Gr' as a function of H for different values of Da shows that the impact of local thermal non-equilibrium state is relatively higher in the case

of high permeable porous medium. In comparison to the LTE state, the disturbance kinetic energy balance at the critical level in LTNE state shows that shear instability is dominant in larger range of Pr for all considered values of Da. For $Pr = 7$, the disturbance kinetic energy balance shows that the contribution of E_b decreases whereas the contribution of E_s increases by almost 10% as compared to LTE state. The interphase heat transfer coefficient affects the instability of the flow when quadratic form drag is relatively low, i.e., up to $F' = 100$.

The finite amplitude instablity of stably stratified parallel mixed convective flow due to linearly varying wall temperature in vertical channel filled with porous medium has not been carried out yet. Thus, before studying the finite amplitude instability of the flow considered in Chapter 2, we consider the finite amplitude instability of stably stratified parallel mixed convective flow of air as well as water in a vertical channel filled with porous medium in Chapter 4. The objective of this study is to analyze the nature of bifurcation and the finite amplitude behavior of unstable disturbances that occur beyond the linear instability boundary, specially when the permeability of the medium and strength of the flow are reasonably high. This is accomplished by reviewing the linear stability results, and then a weakly nonlinear analysis is made to trace the evolution of finite amplitude perturbation. From the review it has been checked through dimensional analysis that the non-isothermal PMCF becomes unstable under mild heating conditions. For example, when the channel is filled with water saturated porous medium with permeability equal to $10^{-7}\mathrm{m}^2$, PMCF becomes unstable even when the temperature gradient, C, is equal to 3.7. In the case when channel is filled with air saturated porous medium with permeability equal to $9 \times 10^{-7}\mathrm{m}^2$, PMCF becomes unstable when $C = 13.9$. The results obtained using Boussinesq approximation remains valid for a wide range of input parameters. To study the evolution of finite amplitude perturbation, we have analyzed the variation of real part of Landau constant ($(a_1)_r$) and amplitude in the vicinity of the least linearly stable point as a function of Re for air as well as water. Depending on the flow strength as well as media permeability, the weakly nonlinear analysis predicts both supercritical and subcritical bifurcations for air

and only supercritical bifurcation for water. In the case of air, an increase in Forchheimer number or decrease in media permeability delays the shift of bifurcation from supercritical to subcritical or vice versa in Reynolds number space. In general, compared to subcritical bifurcation, the supercritical bifurcation occurs at relatively lower values of *Re*. The amplitude profile shows a peak, due to change in sign of $(a_1)_r$, at the Reynolds number where the shift in bifurcation from supercritical to subcritical takes place. The similar characteristic is also observed in physical quantities such as Nusselt number and friction coefficient, which is a consequence of the distortion in basic flow velocity and temperature. For air, when $Da = 10^{-3}$, the nonlinear spectrum of kinetic energy in supercritical regime of *Re* shows that due to change in the shape of fundamental wave, modification in the buoyant production of KE (T_{11}) becomes main destabilizing factor, however modification in the gradient production (P_{110}) as well as modification in the surface drag dissipation (K_{11}) become major stabilizing factors. On the other hand in the subcritical regime of *Re*, P_{110} is a destabilizing factor along with T_{11}. Furthermore, based on very small value of imaginary part of complex linear eigenvalue (c_i), we have analyzed the bifurcation away from the critical point for particular choice of *Re* in super as well as subcritical regimes. It has been found that for all the considered values of *Da* the supercritical bifurcation as a function of Rayleigh number (*Ra*) remains supercritical whereas for *Re* in subcritical regime it may change to supercritical one. Also, the heat transfer rate (skin friction) increases (decreases) significantly and experiences jump in the neighbourhood of *Ra* where the change of bifurcation takes place. The nonlinear balance of kinetic energy for the finite disturbances also supports the results obtained through Landau constant. It is important to mention here that while studying mixed convection flow in vertical annulus, Rogers *et. al.* [88] have found that the buoyant instability is supercritical at all wavenumbers whereas with the shear and interactive (or mixed) instabilities, both subcritical and supercritical branches appear on the neutral curves. In contrast to the above results it has been observed in the present study that with the buoyant and mixed instabilities both subcritical and supercritical branches appear

on the neutral curves. Finally, for values of *Re* in supercritical regime, the disturbance temperature contours maintain the same shape but due to nonlinear interaction of waves they move towards the center of the channel. In the case of *Re* in subcritical regime, the shape of disturbance velocity as well as temperature contours gets changed drastically which in turn enhances the destabilizing characteristic of T_{11}.

In Chapter 5, we have analyzed the finite amplitude instability of fully developed mixed convection flow in differentialy heated vertical channel filled with porous medium. The results are presented with respect to two different fluids with Prandtl number equal to 0.7 and 7 using non-Darcy model. In contrast to the non-isothermal flow in linearly heated channel where subcritical bifurcations were observed, in this case the finite amplitude analysis predicts only supercritical bifurcation of the flow at and beyond the critical points for both fluids as the sign of real part of Landau constant $(a_1)_r$ is found to be negative for all the considered values of *Da*. The magnitude of equilibrium amplitude experiences sharp fall when the Reynolds number is increased form 0 to 1000 and remains almost constant beyond $Re = 1000$ due to non-linear saturation. Also, only supercritical bifurcation is predicted in the neighborhood of critical wavenumbers. Due to the interaction of different harmonics, increased heat transfer rate is obtained for distorted flow as compared to the same for basic flow. Considering the importance of results in practical situations, higher order weakly nonlinear stability analysis and direct numerical simulation could be used to further explore the stability behavior of the present flow.

In the end, Chapter 6 presents the summary and concluding remarks of the thesis and some possible directions for future work.

Acknowledgements

First and foremost, I would like to thank my supervisor Dr. P. Bera, for his guidance, support and encouragement throughout my research work at IIT Roorkee and making the completion of this thesis possible. I am very grateful to my thesis committee members, Prof. V. K. Katiyar, Department of Mathematics and Dr. P. K. Sahoo, Department of Mechanical Engineering, IIT Roorkee for their help and suggestions throughout my Ph.D. program.

I am grateful to the Department of Mathematics, IIT Roorkee and its Computational Fluid Dynamics (CFD) lab for providing the necessary facilities to carry out my research work. I would like to thank all my lab members and friends, Dr. Manish K. Khandelwal, Dr. Saurabh Kapoor, Dr. Sarita Pippal, Dr. Moumita Bhowmik, Mr. Ajay Kumar and Mr. Arshan Khan for their valuable suggestions and kind support. I can't forget to say thanks to Mrs. Rajashree Bera for her warm nature through out these years.

I would like to express my gratitude to my parents Mr. Mritunjai Sharma & Mrs. Asha Sharma and my sister Mrs. Archana Sharma. I would like to acknowledge the sacrifices that my family made to ensure that I had an excellent upbringing as well as education. It is to them that I dedicate this work.

Finally, I would like to acknowledge the financial support by the Ministry of Human Resource and Development (MHRD), New Delhi, India to carry out this research work.

Roorkee **Abhishek Kumar Sharma**

December , 2017

Table of Contents

List of Tables

List of Figures

Chapter 1

Introduction

The hydrodynamic stability of mixed convection in vertical ducts filled with porous medium is of fundamental importance in practical applications. It is known that a steady and parallel flow may exist in a vertical channel bounded by impermeable and isothermal parallel planes kept at different temperatures. The flow may be due to the action of buoyancy force which in turn causes natural convection, or may be due to the action of both buoyancy force as well as constant pressure gradient along the vertical direction resulting in mixed convection. The former flow is defined by parallel natural convective flow (PNCF) which takes place with zero vertical mass flow rate, whereas the latter one is defined by parallel mixed convective flow (PMCF) which is endowed with nonzero vertical mass flow rate. The stability analysis of this flow has directed intense research efforts toward its understanding. These types of flow may be configured, with different features, either for a fluid filling the channel or for a fluid-saturated porous slab/channel.

Due to the presence of inter-connected voids porous medium has large surface area to volume fraction and are good candidates for heat transfer enhancement applications. One of the major heat transfer applications is in the electronic industry. Use of porous medium such as metal foam has attracted the attention of many researchers due to their desirable flow and thermal characteristics. A metal foam consists of a solid matrix containing a large volume fraction of voids or pores. Open cell metal foams have interconnected voids

and are used for heat exchangers, compact electronics cooling, energy absorption, etc. For example, in order to exchange the heat of an electronic device from the system to the surrounding, a vertical rectangular duct filled with open cell metal foam can be considered inside the system. The heat generated from the system can be treated as constant heat flux or constant temperature on one of the surfaces of the duct. A steady fluid flow due to an external pressure gradient can be considered through it to exchange the heat from the system to the surrounding. For fast cooling one may enhance the velocity of steady flow, or, increase the gap between the two channel (for rectangular cylinder) walls. In this situation steady flow may not remain stable and the exchange of heat from the system to surrounding may be affected due to mixing of different fluid layers. Therefore, before installing such type of heat exchanger in the system it is essential to understand the fluid flow and heat transfer mechanism through a channel filled with open cell metal foam or high permeable porous medium, specially in the transition state. Understanding the dynamic behavior of non-isothermal flow in porous media, especially flow-transition, is also a highly active and challenging area of research due to its wide applications in geothermal systems, building thermal insulation, nuclear waste disposal, thermal energy storage, cooling of nuclear reactors during emergency shutdown, etc.

The understanding of nonlinear stability mechanism in porous media may be a special interest because linear stability analysis cannot be accomplished when the larger amplitudes are obtained. Linear stability analysis is used to determine the point at which an infinitesimal disturbance becomes unstable as well as to predict the form of developing disturbances. There are shear flows in literature where the linear stability analysis cannot predict remarkable results. For example, the well known result given by Orszag [79] that the plane Poiseuille flow is linearly unstable at a Reynolds number of 5772, but in practice the transition for this flow often occurs at very low Reynolds number. Apart from this, the linear stability analysis addresses only the initial growth of the disturbance, however, when the disturbance reaches such a size that Reynolds stresses (i.e., the mean force per unit area imposed on the mean flow by turbulent fluctuation) affect the mean flow then it becomes

difficult to explain the stability of the flow by means of linear theory.

1.1 Basic definitions and governing equations in porous medium

In this section some important basic definitions related to porous media which are used for this study are given. For theoretical treatment the physical quantities in porous medium are measured over areas that cross many pores because these space-averaged (macroscopic) quantities vary in a regular manner with respect to space and time. The laws governing these macroscopic variables are derived by considering the standard equations obeyed by the fluid and average them over volumes or areas containing many pores (i.e., representative elementary volume (r.e.v.)). The r.e.v. is sufficiently large as compared to pore volume for reliable volume averages. Once a continuum model is obtained, the differential equations expressing conservation laws can be derived.

1.1.1 Porous medium

"By a porous medium we mean a material consisting of a solid matrix with an interconnected void" [76]. In this work we have assumed that the solid matrix is rigid non-deformable medium. The flow of one or more fluids in the porous medium takes place through the interconnnected voids or pores. We have assumed the simplest situation (i.e., single-phase flow) where the porous medium is saturated by a single fluid. Many natural substances such as sand, wood, rocks, limestone, biological tissues (e.g. skin, bones) and man made materials such as cements, metallic foams and ceramics can be considered as a porous media. The porosity of a porous medium, denoted by ε, is defined as the fraction of the total volume of the porous medium occupied by void spaces assuming that all the void space is connected. The value of porosity can vary from 0 to 1. Generally, the porosity does not exceed 0.6 in natural porous media. But, the porosity of man made porous medium such

as metallic foams can be very close to 1. The permeability of a porous medium is simply its ability to allow fluids to pass through it under some external pressure gradient. The value of permeability (K) depends on the geometry of porous medium. For example, in the case of beds of spherical particles with diameters in a narrow range, Carman-Kozeny gave the relationship between permeability and porosity as

$$K = \frac{D_p^2 \varepsilon^3}{180(1-\varepsilon)^2}, \tag{1.1}$$

where, D_p is the effective average particle diameter.

1.1.2 Mass conservation equation

When the rate of increase of mass of the fluid within a representative elementary volume (under the assumption of continuum model) of porous medium is equated with the net mass flux into the volume, it results in the equation of continuity given as

$$\varepsilon \frac{\partial \rho_f}{\partial t} + \nabla.(\rho_f \mathbf{v}) = 0. \tag{1.2}$$

Here, ρ_f is the fluid density and $\mathbf{v}$ is the Darcy velocity (or, seepage velocity) which is related to the intrinsic average velocity $\mathbf{V}$ by the Dupuit-Forchheimer relationship $\mathbf{v} = \varepsilon \mathbf{V}$. It should be noted that $\mathbf{v}$ is average of the fluid velocity over volume element of the porous medium incorporating both fluid and solid phases, whereas $\mathbf{V}$ is average of the fluid velocity over volume element consisting of fluid only.

1.1.3 Momentum conservation equation

The momentum conservation equation for fluid is well established and known as the Navier-Stokes equation. But the governing equations of flow through porous media are not straight forward and it is still a challenging problem to understand the dynamic behavior of fluid flow through porous medium using a proper model. In fact, different approaches to the formulation of the momentum balance equation for fluid flow in saturated porous medium

have been proposed in the literature. A brief description of different models used in porous medium is given below [76].

The Darcy's law given by Henry Darcy (1856), is a proportionality between applied pressure gradient and the flow rate for a steady unidirectional flow in a uniform porous medium. The law was formulated by Henry Darcy based on results of experiments on the flow of water through beds of sand. The Darcy's law can be written as

$$\nabla P = -\frac{\mu}{K}\mathbf{v}, \tag{1.3}$$

where, P is the pressure, μ is the dynamic viscosity of the fluid, K is the permeability of the medium and $\mathbf{v}$ is the Darcy velocity. It should be noted that unlike other conservation equations, equation (1.3) does not represent balance of forces averaged over any representative elementary volume. Furthermore, Darcy model fails to satisfy the no-slip boundary condition in physical problems where the porous medium is adjacent to a solid wall.

Brinkman, while deriving relationship between permeability and porosity, proposed an equation of the form

$$\nabla P = -\frac{\mu}{K}\mathbf{v} + \tilde{\mu}\nabla^2\mathbf{v}. \tag{1.4}$$

containing the Laplacian term which is important if a no-slip boundary condition is to be satisfied. It has a significant effect in the boundary layer near a solid wall. The thickness of boundary layer is of order $(\tilde{\mu}K/\mu)^{1/2}$ which is much smaller than the macroscopic length scale (L) of the problem. This is due to continuum hypothesis requiring $K^{1/2} \ll L$. Lundgren [70] and Rubinstein [91] showed that such an equation is valid for porous medium with $\varepsilon > 0.6$. It is a common practice to assume effective vicosity ($\tilde{\mu}$) to be equal to μ for high porosity cases.

The acceleration and other inertial effects were also incorporated into the Darcy equation to account for non-linear development of the flow inside the porous medium. Many authors, for example Wooding [124], added the convective term in the Darcy equation in analogy with the Navier-Stokes equation to get

$$\rho_f \left(\frac{1}{\varepsilon}\frac{\partial \mathbf{v}}{\partial t} + \frac{1}{\varepsilon^2}(\mathbf{v}.\nabla)\mathbf{v} \right) = -\nabla P - \frac{\mu}{K}\mathbf{v} \tag{1.5}$$

But, this equation had severe flaws. First, it was inconsistent with slip boundary condition as the order of differential equation with respect to spatial derivatives was raised. Second, it could not explain the inertial effects arising in steady incompressible unidirectional flow no matter how large the fluid velocity as in such cases $(\mathbf{v}.\nabla)\mathbf{v}$ is identically zero. The time derivative term is generally small as the transients decay rapidly in the case of a flow in porous medium. However, the time derivative term is retained to study the temporal stability of a flow in porous medium.

The Forchheimer term in the form of a quadratic drag generally dominates the $(\mathbf{v}.\nabla)\mathbf{v}$ term. This quadratic drag or form drag is due to solid obstacles inside the porous medium. When it becomes comparable to surface drag due to friction on increasing the Reynolds number (based on $K^{1/2}$) up to 10^2, the smooth transition from Darcy flow to non-linear drag takes place according to the equation

$$\nabla P = -\frac{\mu}{K}\mathbf{v} - \frac{c_F \rho_f}{K^{1/2}}|\mathbf{v}|\mathbf{v}, \tag{1.6}$$

where, c_F is the form drag constant whose value vary with the nature of the porous medium. For example, c_F is close to 0.1 for metal foams.

Following the work of Vafai and Tien [120] and Whitaker [123], a generalized non-Darcy model through volume-averaging method is given as

$$\rho_f \left[\frac{1}{\varepsilon}\frac{\partial v}{\partial t} + \frac{1}{\varepsilon^2}(\mathbf{v}.\nabla)\mathbf{v} + \frac{c_F}{K^{1/2}}|\mathbf{v}|\mathbf{v}\right] = -\nabla P + \rho g + \tilde{\mu}\nabla^2\mathbf{v} - \frac{\mu}{K}\mathbf{v}. \tag{1.7}$$

where, g is the gravitational acceleration. The density (ρ) is obtained through Boussinesq approximation as

$$\rho = \rho_f\{1 - \beta_T(T - T_0)\}, \tag{1.8}$$

where, β_T, T and T_0 are volumetric thermal expansion coefficient, dimensional temperature and reference temperature, respectively.

1.1.4 Energy equations in porous medium

The energy equation in a porous medium is derived by volume averaging method over a representative elementary volume. This results in two different energy equations for an

isotropic porous medium, one for the fluid phase and one for the solid phase given as

$$\varepsilon(\rho c_P)_f \frac{\partial T_f}{\partial t} + (\rho c_P)_f \mathbf{v}.\nabla T_f = \varepsilon k_f \nabla^2 T_f + h(T_s - T_f), \tag{1.9}$$

$$(1-\varepsilon)(\rho c)_s \frac{\partial T_s}{\partial t} = (1-\varepsilon) k_s \nabla^2 T_s + h(T_f - T_s). \tag{1.10}$$

Here, c_p is the specific heat at constant pressure of the solid, c is the specific heat of the solid, k is the thermal conductivity, h is the interphase heat transfer coefficient, the subscripts s and f denote solid and fluid phases of the porous medium, respectively. The use of two different energy equations, where $T_f \neq T_s$, is referred as local thermal non-equilibrium (LTNE) state. A simple and widely used concept of heat transfer in porous medium is local thermal non-equilibrium (LTE) state in which the local temperatures of the fluid and solid phases of porous medium are assumed to be identical such that $T_s = T_f = T$, where T_f and T_s are the temperatures of the fluid and solid phases respectively. The one energy equation model under local thermal equilibrium state is obtained by assuming $T_s = T_f$ and adding equations (1.9) and (1.10). It is given as

$$(\rho c)_m \frac{\partial T}{\partial t} + (\rho c)_f \mathbf{v}.\nabla T = k_m \nabla^2 T, \tag{1.11}$$

where, $(\rho c)_m$ is the overall heat capacity per unit volume, k_m is the overall thermal conductivity given by,

$$(\rho c)_m = (1-\varepsilon)(\rho c)_s + \varepsilon(\rho c_P)_f, \tag{1.12}$$

$$k_m = (1-\varepsilon)k_s + \varepsilon k_f. \tag{1.13}$$

1.2 Hydrodynamics Stability

In general, the ability of a dynamical system to remain unaffected to small disturbances is called as stability. The stability of a dynamical system can be examined only after establishing the possibility of equilibrium. The problem of stability in fluid mechanics also has these important features. First, using well defined initial/boundary conditions, a specific flow is fully determined through a proper choice of co-ordinate system. Then, a flow

which is in equilibrium is identified. Such a flow should not be accelerated due to the balance of forces involved, but it may be time dependent. This laminar and equilibrium flow is called as base mean flow which is broadly categorized into parallel (e.g., channel and pipe flows) or almost parallel (e.g., free shear and boundary layer flows) , with curved streamlines (e.g., flow in concentric circular cylinder) and mean flow with zero value (e.g., Rayleigh-Benard flows). Notably, the important initial contributions to hydrodynamic stability theory and related experiments are due to Hagen (1855), Helmholtz (1868), Rayleigh (1879), Kelvin (1880) and Reynolds (1883). It should be mentioned that whereas Kelvin and Rayleigh used inviscid hypothesis in their theoretical work, Orr (on plane Couette flow) and Sommerfeld (on plane Poiseuille flow) independently did their theoretical work on viscous stability problem, later the combination formed the basic equation of hydrodynamic stability theory using perturbation analysis known as Orr-Sommerfeld equation. The aim of hydrodynamic stability is to find out the conditions under which a given laminar flow may become unstable and how an unstable flow breaks down into some other laminar/non-laminar flow. The rapid development of this theory in recent decades has resulted in huge number of studies in various fields such as petroleum industries, chemical technology and geophysical sciences, etc. Many important developments of stability theory are given in literature ([25, 32]).

It is important to sketch the important physical mechanisms of instability. Instability occurs when the equilibrium of external forces, inertia and viscous stresses on the fluid gets disturbed. For example, the instability of plane Poiseuille flow is affected by the dual nature of viscosity, inertia and the presence of solid boundaries. On applying some slight disturbance to a basic flow, the disturbance may either die away, persist as a disturbance of similar magnitude or grow so much that the basic flow becomes a different laminar or turbulent flow. Broadly speaking, such disturbances are called (asymptotically) stable, neutrally stable or unstable respectively. The connection between laminar flow and turbulent flow may not be a direct one, but more often than not laminar flow is a prelude to transition to turbulence. In the case of laminar flow, particles of fluid can be considered to

travel along smooth continuous paths, i.e., no mixing between fluid layers occurs unlike a turbulent flow (see few examples in figure 1.1).

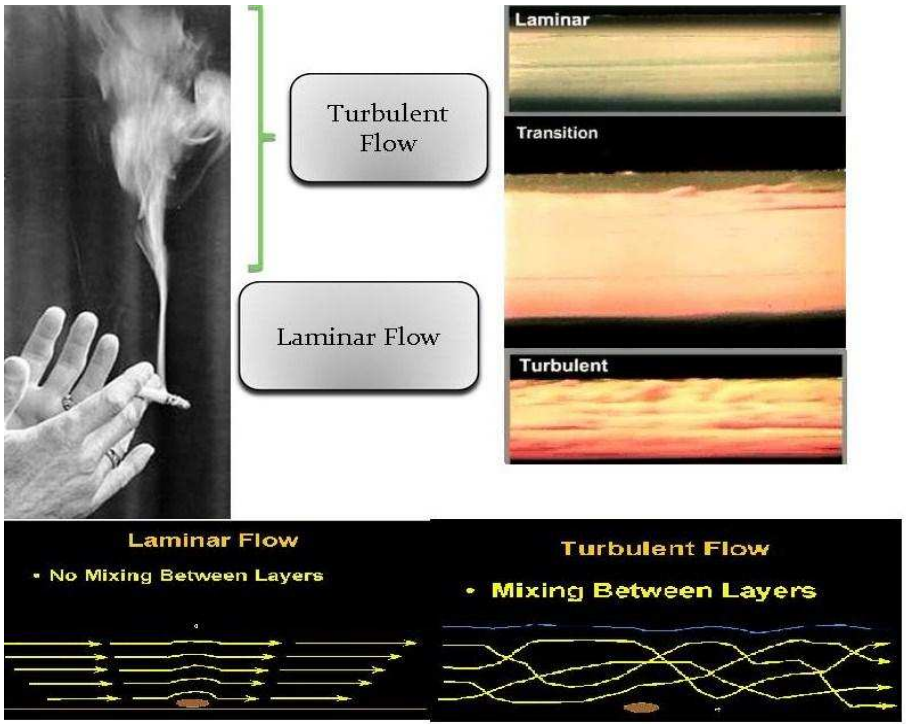

Figure 1.1: Laminar and turbulent flow examples (pictures are taken from internet).

Mathematically, using the concept of stability of system of ordinary differential equations, a basic flow is stable (in the sense of Liapounov) if, for any $\varepsilon > 0$, there exists some positive number δ (depending upon ε) such that if $|| V(x,0) - V_0(x,0) ||$, $|| P(x,0) - P_0(x,0) ||$, etc. $< \delta$, then $|| V(x,t) - V_0(x,t) ||$, $|| P(x,t) - P_0(x,t) ||$, etc $< \varepsilon$ for all $t \geq 0$, where V is the velocity field and P is the pressure field. This definition means that the flow is stable if the perturbation remains small for all time provided it is small initially. Some perturbations that might lead to instability arise from small changes in the boundary conditions due to irregularities in nature or imperfections in laboratory equipment. The mathematical treatment of these perturbations is closely related to that of a small initial disturbance of the basic flow. Also, it must be recognized that an unstable basic flow free of any disturbance can not instantaneously be set up in the laboratory or arise in nature. Rather a stable basic flow evolves in space or time until it becomes unstable [32].

Consider a steady basic flow and assume that the equations of motion and the boundary conditions may be linearized for sufficiently small disturbances. The principle of linearization is straightforward where the products of the increments $v'(x,t) = (V - V_0)$, $p'(x,t) = (P - P_0)$ etc., that is, of the total velocity $v(x,t)$ and pressure $p(x,t)$ etc., of the disturbed flow less their respective values for the basic flow, are neglected. This results in a linear homogeneous system of partial differential equations and boundary conditions. The coefficients in this system of equations may vary in space but not time because the basic flow is steady. Our vast experience with the method of separation of variables and Laplace transform for the solution of such systems suggests that in general the solutions can be expressed as the real parts of the integrals of components, each component varying with time like e^{st} for some complex number $s = \sigma + iw$, also known as normal modes. The values of s and the spatial variation of corresponding components are called as eigenvalues and eigenfunctions, determined from the linear system. If $\sigma > 0$ for a mode, then the corresponding disturbance will be amplified, growing exponentially with time until it is so large that non linearity becomes significant. If $\sigma = 0$ the mode is said to be neutrally stable, and if $\sigma < 0$ then asymptotically stable or stable. Thus a mode is unstable if $\sigma > 0$, and stable if $\sigma \leq 0$ because then it remains small for all time. A small disturbance of the basic flow will in general excite all modes, so that if $\sigma > 0$ for at least one mode then the flow is unstable. Conversely, if $\sigma \leq 0$ for all of a complete set of modes then the flow is stable. A mode is marginally stable if $\sigma = 0$ for critical values of the parameters on which the eigenvalue s depends but $\sigma > 0$ for some neighboring values of the parameters. Plane Poiseuille flow, with basic velocity $V = V_o(1 - r^2/a^2\hat{i})$ between rigid walls at $z = \pm a$, provides an example of this.

1.3 Review of Literature

Despite theoretical and technological advancements in recent years, the flow mechanics and heat transfer characteristics in porous media are still difficult to comprehend as they lack

a unified governing theory. This is due to the presence of a wide range of length scales in porous media and extremely complex boundary conditions at pore level. To treat a porous medium as continuum, the appropriate set of governing equations in terms of volume averaged dependent variables are derived using the method of volume averaging [55] where primarily the large scale (macroscopic) behavior of the flow in porous regions is considered. The continuity, momentum and energy equations are integrated in a representative elementary volume whose length scale is much larger than the average pore and particle length but much smaller than the characteristic macroscopic length of the porous medium. The energy equation can be volume averaged in two ways: (i) assuming local thermal equilibrium (LTE) between the fluid and the solid phases, in which the volume averaged fluid temperature is assumed to be equal to the solid phase, (ii) assuming local thermal non-equilibrium (LTNE) between the fluid and the solid phases, in which the volume averaged fluid temperature is assumed to be different from the solid phase. Chanpreet *et. al.* [28] have given some experimental validation of above mentioned heat transfer models.

Let us first discuss about important applications of flow and heat transfer in porous medium. Due to the presence of inter-connected voids porous medium has large surface area to volume fraction and are good candidates for heat transfer enhancement applications. One of the major heat transfer applications is in the electronic industry. Starting with micro-scale (due to the miniaturization of integrated circuits and the assemblage in small volumes) electronics equipment [57] to macro-scale electrical Transformer [116] or giant UPS, design of good heat transfer equipment has become a challenge to the industry. Mixed convection in ducts (commonly channel, pipe and annulus) filled with porous medium is relevant in many engineering systems such as geothermal systems, building thermal insulation, nuclear waste disposal, thermal energy storage, transportation biofuels, etc. The growing volume of work in this area is amply documented in the books by Nield and Bejan [76] and Vafai [122]. Use of porous medium such as metal foam has attracted the attention of many researchers due to their desirable flow and thermal characteristics [11, 17]. A metal foam consists of a solid matrix containing a large volume fraction of voids or pores. Open

cell metal foams have interconnected voids and are used for heat exchangers [33, 61, 131], compact electronics cooling [10, 86], energy absorption [66], *etc*. For example, in order to exchange the heat of an electronic device from the system to the surrounding, a vertical rectangular duct filled with open cell metal foam can be considered inside the system. The heat generated from the system can be treated as constant heat flux or constant temperature on one of the surfaces of the duct. A steady fluid flow due to an external pressure gradient can be considered through it to exchange the heat from the system to the surrounding. For fast cooling one may enhance the velocity of steady flow, or, increase the gap between the two channel (for rectangular cylinder) walls. In this situation steady flow may not remain stable and the exchange of heat from the system to surrounding may be affected due to mixing of different fluid layers. Therefore, before installing such type of heat exchanger in the system it is essential to understand the fluid flow and heat transfer mechanism through a channel filled with open cell metal foam or high permeable porous medium, specially in the transition state.

Based on important applications (in microwave heating [34], in fuel cells [35], in heat exchangers [52, 131] and references therein) convection in porous media under local thermal non-equilibrium state becomes an area of intense research. Different important works which utilize the local thermal non-equilibrium theory are well documented in the literature (e.g., [1, 36, 76, 92, 109]). The regenerator used in Stirling cycle is an important application of heat exchanger using porous medium in which thermal energy is stored and reused at a later time. The transfer of heat from solid to fluid phase of the porous medium inside the regenerator takes place under local thermal non-equilibrium state [109].

A comprehensive literature review is presented, first pertaining to local thermal equilibrium theory and then local thermal non-equilibrium theory covering a wide range of natural, forced and mixed convection flows mainly in vertical systems filled with porous medium. It is known that a steady and parallel flow may exist in a vertical channel bounded by impermeable and isothermal parallel planes kept at different temperatures. The flow may be due to the action of buoyancy force which in turn causes natural convection, or may be

due to the action of both buoyancy force as well as constant pressure gradient along the vertical direction resulting in mixed convection. The former flow is defined by parallel natural convective flow (PNCF) which takes place with zero vertical mass flow rate, whereas the latter one is defined by parallel mixed convective flow (PMCF) which is endowed with non-zero vertical mass flow rate. These types of flow may be configured, with different features, either for a fluid filling the channel or for a fluid-saturated porous slab/channel [76].

A fundamental result from the analysis of natural convection in a vertical porous slab governed by Darcy's law was obtained by Gill [41]. Using linear stability analysis the author has proved that the PNCF in a vertical porous slab is always stable. In spite of this conclusion further investigations were carried out by other authors. For example, Gill's [41] problem was reinvestigated: using nonlinear analysis by Wolanski [125] and Straughan [106], considering the no-slip condition by Kwok and Chen [62], including the time derivative term in momentum balance equation by Rees [89], in a regime of very large Darcy-Rayleigh numbers by Lewis *et. al.* [67]. Payne *et. al.* [83a] derived *a priori* bounds for the Darcy equation when the Newton cooling type boundary condition is imposed on the porous medium. Note that the main motivation for these studies was the suggestion stated by Gill [41] at the end of his paper that possible instability could be obtained by including inertial effects in the local momentum balance equation, i.e., by altering the classical formulation. However, except the work of Kwok and Chen [62] where the basic flow is different from the basic flow of Gill [41], all these investigations finally lead to the basic conclusion reached by Gill [41]. Recently, Barletta, while studying natural convection in a vertical channel [3] and the same as a limiting case of mixed convection [4], has found that Gill's finding does not remain valid even under Darcy model. Kwok and Chen [62] investigated the effect of no-slip boundary conditions for velocity, implemented by Brinkman's model of momentum balance instead of Darcy's law, and the effect of temperature-dependent viscosity within Darcy's law. In both the cases they considered a quadratic dependence of the density on temperature. Through linear stability analysis the authors found that both

no-slip conditions and variable viscosity are able to yield instability and, hence, modify the conclusion implied by Gill's proof. While studying the double-diffusive natural convection in rectangular enclosure filled with anisotropic porous medium, Bera *et. al.* [15] found that the permeability orientation angle has important effect on heat and mass transfer. Unsing linear stability theory, the thermosolutal convection in a ferromagnetic fluid saturating a porous medium has been studied by considering constant viscosity [40] and magnetic field dependent viscosity [114].

The hydrodynamic stability of mixed convection in vertical ducts filled with porous medium is of fundamental importance in practical applications. Although, several studies in vertical channel/layer have already been made directly or indirectly in this direction but most of these are restricted to laminar fluid flow and heat transfer only (e.g., with uniform heating of walls [21, 48, 58, 63, 108], with differential heating: [47, 81, 118]), which are well documented in the book by Nield and Bejan [76]. Studies related to transition state are restricted to either linearly heating or imposing constant heat flux condition on the walls. To gain a better perspective of results to be presented, we summarize their primary conclusions.

A good number of articles [5–8, 19, 22, 23, 60] focus on linear stability of PMCF due to linear variation of wall temperature and external pressure gradient to understand the stability of the flow in various aspects. In these studies the non-Darcy volume-averaged Navier-Stokes (VANS) equation was used and assumed that the solid porous matrix and saturated fluid are in local thermal equilibrium (LTE) state. It has been reported that higher media permeability results in lower stability of the flow, whereas induced form drag stabilizes the flow. Fully developed flow can become unstable under mild heating condition [23]. Furthermore, it has also been pointed out that when buoyancy force acts in the direction of forced flow, three different types of instability, namely shear (or thermal-shear), mixed (or interactive), and buoyant (or thermal buoyant) are possible [5–7, 19, 60]. The type of instability depends on the type of fluid, media permeability, strength of bulk velocity, as

well as on induced form drag. In the case when buoyancy force acts in the opposite direction of forced flow (i.e., buoyancy opposed flow) the fully developed flow has two types of instabilities: Rayleigh-Taylor and buoyant (or, thermal buoyant) [6, 7]. Note that their study for buoyancy opposed flow was limited to very low permeable porous media. Recently, Bera and Khandelwal [9] have extended the linear stability analysis of above flow with the assumption that the solid porous matrix and saturated fluid are in local thermal non-equilibrium state with buoyancy force in the direction of forced flow. They have found that higher value of interphase heat transfer coefficient results in more stable flow, i.e., interphase heat transfer coefficient stabilizes the flow. Its stabilizing impact for fluid with low Prandtl number becomes high when disturbance kinetic energy due to non-isothermal effect is lost to the basic flow. For relatively low permeable medium thermal-buoyant instability is the most dominant instability in the entire range of Prandtl number. Stability of the mixed convection in the same geometry, where buoyant force is induced by symmetric uniform heat flux on the vertical planes, is investigated by Barletta [2]. The details of these studies can be found in Bera and Khandelwal [9].

Investigation of mixed convection in a differentially heated channel filled with porous medium is carried out numerically by Hadim and Chen [47] as well as Umavathi *et. al.* [118], and experimentally by Pu *et. al.* [81]. Hadim *et. al.* [47] have studied the mixed convective flow in the developing region and have shown that on increasing the Darcy number the distortions in the velocity profile result in an increased velocity near the walls leading to increased heat transfer. Using perturbation method Umavathi *et. al.* [118] have shown that the viscous dissipation enhances the flow reversal in the case of downward flow while it counters the flow in the case of upward flow and the Darcy as well as inertial drag terms suppress the flow. Pu *et. al.* [81] experimentally found the existence of a secondary convective cell in the mixed-convection regime. Apart from these, Kamath *et. al.* [57] conducted an experimental study of hydraulic performance and heat transfer in flow assisted mixed convection (induced by external pressure gradient and constant heat flux on one vertical side and maintenance of adiabatic condition on the other vertical side) on aluminium

metal foams of high porosity. Through the results of the hydraulic experiments the authors have shown, for the air velocity range used, that the metal foam characteristics deviate from the Darcy flow. Apart from this the mixed convection flow and heat transfer phenomena with various types of fluids are also available in the literature. For example, laminar mixed convective flow and heat transfer in Newtonian and power law fluids have been investigated by Dhiman *et al.* [37]. Also, Dhiman *et al.* [38] investigated the dependence of drag and lift coefficients on Richardson number while studying the mixed convection across an isothermal square cylinder confined in a channel. Some computational studies of heat transfer in a liquid-saturated porous annulus with a heated inner wall and a cold outer wall have been reported by Muralidhar [73–75]. Using similarity analysis Partha *et. al.* [83] studied simultaneous thermal radiation and mixed convection in a porous medium. Bhargavi *et. al.* [16] examined changes in physical quantities such as skin friction coefficient and Nusselt number inside a channel with walls attached with porous layer. Further, Dey *et. al.* [39] have presented an analytical study of unsteady flow through a channel lined with asymmetric porous lining. Analysis of isothermal flow in flexible tube is also interesting and complicated in the area of hydrodynamic stability. A rigorous study of such problems can be found in the work of Shankar *et. al.* [112, 113] and Kumaran [113a]. The hydrodynamic stability of channel flow with compliant boundaries has been studied by Sibanda *et. al.* [45, 72, 111].

From the above literature review it is clear that the stability characteristic of PMCF has not been extended to differentially heated channel. Furthermore, in a linearly heated vertical channel the direction of pressure driven forced flow and the direction of buoyancy force can be either same or opposite, i.e., fully developed parallel flow will be either buoyancy assisted or buoyancy opposed flow. In the case of a differentially heated vertical channel with the pressure driven forced flow from bottom to top, parallel flow can be either buoyancy assisted or assisted near the hot wall but opposed near the cold wall. Therefore, plausible different instability mechanism in a differentially heated channel is expected.

Being motivated from the applications, in the present thesis an attempt is made to

understand the stability to small-amplitude perturbations of the parallel mixed convective flow in a differentially heated vertical channel filled with fluid-saturated high permeable porous medium. The flow is caused by a pressure gradient from the bottom of the channel aided by buoyancy effects induced by heating of side walls. It is important to mention that the flow instability characteristics depend on the boundary conditions at the walls of the channel.

The temperature of fluid and solid phases of a porous medium are accounted separately when there is a significant between conductivities of the solid and fluid phases. The flow dynamics as well as heat transfer mechanism in such a situation is governed by a model of two medium treatment in the single phase flow, formulated by Carbonell and Whitaker [24] which is well accepted in the literature [55]. These equations are coupled with an additional term that models the mode of interfacial heat transfer between the two phases. This situation is known as local thermal non-equilibrium (LTNE) state. Kaviany [55] and many other authors (e.g., [17, 121]) have shown that when the porous medium is under local thermal non-equilibrium state then mechanism of heat transfer and fluid flow are different form the same under local thermal equilibrium state. When metal foams are used with low-conductivity fluids like air or water then it is preferable to use LTNE hypothesis.

Natural convection in high porosity metal foams was studied numerically and experimentally by, among others, Phanikumar and Mahajan [82]. The authors have found that the LTNE model provides a more realistic description of heat transfer phenomena in metal foams. Recently, Rees [90] has extended the work of Gill [41] by considering the effect of local thermal nonequilibrium on the stability properties of natural convection in a vertical porous channel heated and cooled from the sides. The flow is governed by Darcy's law and Boussinesq approximation. On using an energy stability analysis of the linearised stability equations, the author has shown that the system remains unconditionally stable to small-amplitude disturbances. Later, Scott and Straughan [104] studied the problem considered by Rees [90] by using nonlinear energy stability theory to derive a Rayleigh

number threshold below which convection will not occur no matter how large the initial data. The authors have given a generalized nonlinear analysis to show that convection cannot occur for any Rayleigh number provided the initial data is suitably restricted. Using energy method, Sunil *et. al.* [115] have studied the nonlinear stability analysis of a rotating thermoconvective magnetized ferrofluid layer using LTNE model.

In comparison to the natural convection in fluid-saturated vertical porous slab, the theoretical investigation of parallel mixed convective flow in a differentially heated vertical channel filled with porous medium under local thermal non-equilibrium state is largely overlooked. Analysis of mixed convection in a vertical porous layer using non-equilibrium model is investigated by Saeid [108]. He has found the total average Nusselt number depends strongly on the thermal conductivity ratio parameter and depends slightly on the heat transfer coefficient parameter i.e. increasing the thermal conductivity ratio leads to increase in the total average Nusselt number Recently, Bera and Khandelwal [9] have studied the linear stability analysis of PMCF with linearly varying wall temperatures of the channel with the assumption that the solid porous matrix and saturated fluid are in local thermal non-equilibrium state with buoyancy force in the direction of forced flow. They have found that higher value of interphase heat transfer coefficient results in more stable flow, i.e., interphase heat transfer coefficient stabilizes the flow. Its stabilizing impact for fluid with low Prandtl number becomes high when disturbance kinetic energy due to non-isothermal effect is lost to the basic flow. Al-Sumaily *et. al.* [1] investigated the effect of particle diameter of a packed bed of spherical particles on forced convection about an embedded cylinder numerically. They found that the agreement between experimental results and numerical results under LTNE model is much better than the same between experimental results and analytical results under LTE model. In this thesis, we have made an attempt to understand the stability to infinitesimal perturbations of the parallel mixed convective flow in a differentially heated vertical channel filled with fluid-saturated high permeable porous medium under LTNE state.

The flow transition (laminar to turbulent) phenomena of non-isothermal Poiseuille

flow in a vertical channel using direct numerical simulation is investigated by [26, 27]. The flow transition phenomena in buoyancy assisted case [26] is supercritical and transition is gradual. However, in buoyancy-opposed case [27] the transition is sudden and abrupt. Linear stability analysis is used to determine the point at which an infinitesimal disturbance becomes unstable as well as to predict the form of developing disturbances. There are shear flows in literature where the linear stability analysis cannot predict remarkable results. For example, the well known result given by [79] that the plane Poiseuille flow is linearly unstable at a Reynolds number of 5772, but in practice the transition for this flow often occurs at very low Reynolds number. The linear stability analysis gives only the initial growth of the disturbance, but eventually the disturbance reaches such a size that Reynolds stresses (i.e., the mean force per unit area imposed on the mean flow by turbulent fluctuation) affect the mean flow and then it becomes difficult to explain the stability of the flow by linear theory. Nonlinear stability analysis gives some important information about size of disturbance and flow field that results from the linear instability. Weakly nonlinear theories developed in [93, 100, 101, 127] have been shown to be very powerful tools for the analysis of stability of various flows. These nonlinear analyses are centered around the derivation of the Landau equation for the amplitude of disturbance wave.

From the best of our knowledge, though some attempts [84, 104] are made to understand the nonlinear stability problem in natural convection but it has not been extended to mixed convection in vertical channel. Among them, [104] derived a threshold Raleigh number below which convection will not occur regardless of how large the initial data may be. Using a generalized nonlinear analysis they have also shown that convection cannot occur for any Rayleigh number provided the initial data is suitably restricted.

The understanding of nonlinear stability mechanism in porous media may be a special interest because linear stability analysis cannot be accomplished when the larger amplitudes are obtained. Especially, when the permeability of the medium and strength of the flow are reasonably high then nonlinear interaction of different harmonic modes may have significant role in the flow mechanism [30, 87, 98].

As pointed out in the literature [50], in general, the transition from smooth laminar to disorder turbulent flow can involve a sequence of instabilities in which the system realizes progressively more complicated states [77] or it can occur suddenly [44, 49]. In the former case, the complexity arises in well defined steps in the name of sequence of bifurcations [12]. The prediction of wide band nature of sequence of instabilities of the detailed flow pattern and temperature distribution at a point away from the critical is beyond the scope of linear stability analysis. In this situation, a nonlinear analysis is required to trace the evolution of finite amplitude perturbations. To analyze the nonlinear phenomena of a flow, mainly two different approaches:(i) weakly nonlinear stability analysis, and (ii) direct numerical simulation (DNS) can be used. The advantages of weakly nonlinear stability theory using finite amplitude expansion method are relatively small computational cost and easy to adopt. It tells us something significant when a full DNS calculation is infeasible. The role of normal modes in nonlinear analysis is different from that in the linear analysis because of the interaction of different harmonic modes. The nonlinear stability analysis modifies the unbounded exponential growth predicted by the linear stability analysis. This analysis is valid near the linear stability boundary, and it addresses the question of what happens to an unstable flow.

The above literature review reveals that so far the investigation on stability of non-isothermal parallel flow in a vertical channel filled with fluid saturated porous medium is restricted to the linear theory only for both situations: (i) differentially heated channel walls, and (ii) linearly varying temperature of channel walls. Apart from this, the instability mechanism of above flow in a purely fluid medium [20] under linear theory predicts significant different results from the same in a fluid-saturated porous medium [5, 19]. Consequently, the nonlinear stability analysis made for purely fluid medium [59] may not predict similar results when the channel is filled with porous medium. Being motivated from the above applications and limitation of linear stability theory, in the present study we consider a weakly nonlinear instability analysis of stably stratified (i.e., when buoyant force is in the

direction of forced flow) non-isothermal parallel mixed convection flow (PMCF) in a vertical channel filled with porous medium. The linear stability analysis of this flow is already examined by some authors (for example, [5, 19, 60]). Here we determine the the nature of bifurcation (supercritical/subcritical) and the finite amplitude behavior of disturbance that occurs beyond the linear instability boundary. The present analysis is carried out using the theory given in the references [59, 100, 101, 130] and therein. This nonlinear analysis is centered around the derivation of the Landau equation to study the nonlinear interaction of different harmonic waves. The mechanism behind subcritical transition has been explained by Brandt [14]. Samanta *et. al.* [107] have studied the effect of permeable wall on secondary flow through porous duct. A comprehensive note on stability, receptivity and sensitivity analysis of fluid systems is given by Schmid *et. al.* [110].

1.4 Motivation and Objective of the Study

As mentioned in the literature review, in comparison to the natural convection in fluid-saturated vertical porous slab, the theoretical investigation of parallel mixed convective flow in a vertical channel filled with porous medium especially when channel walls are kept at different temperatures is largely overlooked. Motivation for the present study is based on the following three facts:

1. Mixed convection through wall bounded domain filled with porous medium has numerous applications in science and engineering.

2. Stability analysis has not been extended to parallel mixed convective flow in a differentially heated channel.

3. There are subtle differences between the flow and heat transfer characteristics of a parallel mixed convective flow in a linearly heated channel and differentially heated channel.

To gain a comprehensive knowledge of the stability characteristics of the flow being considered, the objectives of the present study are as follows:

1. To analyze the stability characteristics of parallel mixed convective flow in a differentially heated vertical channel filled with high permeable porous medium under local thermal equilibrium state for a range of fluids including mercury, air, water and heavy oils.

2. To find the appropriate non-isothermal parameter space as a function of Prandtl number, Reynolds number as well as Forchheimer number in which the parallel flow will remain stable, and identify the type of instability through energy analysis.

3. Using dimensional analysis, find the critical temperature difference between the walls of the channel below which the fully developed parallel flow will remain parallel and stable.

4. To examine the mean flow characteristics in a vertical channel filled with porous medium under LTNE state for fluids such as air and water.

5. To develop a cubic Landau equation to analyze the nature of bifurcation and amplitude of most unstable wave at and beyond the critical value using a weakly nonlinear stability theory for parallel mixed convective flow in a vertical channel filled with porous medium under local thermal equilibrium state for both situations: (i) differentially heated channel walls, and (ii) linearly varying temperature of channel walls.

Chapter 2

Linear stability of mixed convection flow in differentially heated vertical channel filled with porous-medium

Linear stability analysis is used to analyze the stability of parallel flow induced by external pressure gradient and buoyancy force in a differentially heated vertical channel filled with a fluid-saturated high permeable porous medium. In the case of a differentially heated vertical channel with the pressure driven forced flow from bottom to top, parallel flow can be either buoyancy assisted or assisted near the hot wall but opposed near the cold wall. Therefore, plausible different instability mechanism in a differentially heated channel is expected.

The objective of the present study is two folds. The first is to analyze the stability characteristics of PMCF in a differentially heated channel filled with high permeable porous medium for a range of fluids including mercury, air, water and heavy oils. Also, we want to find the appropriate non-isothermal parameter space as a function of Prandtl number, Reynolds number as well as Forchheimer number in which the parallel flow will remain stable, and identify the type of instability through energy analysis. Second, using scale analysis, to find the critical temperature difference between the walls of the channel

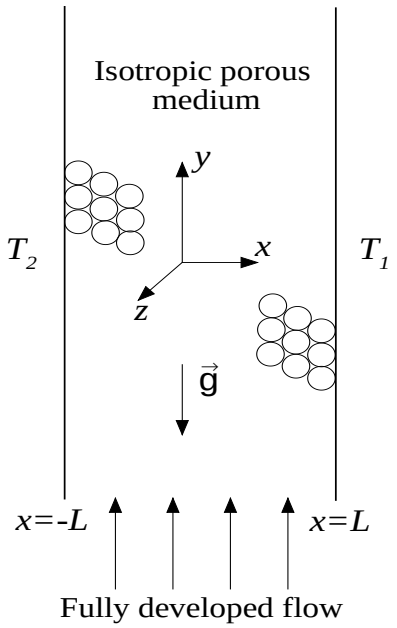

Figure 2.1: Schematic of the physical problem.

below which the fully developed parallel flow will remain parallel and stable.

2.1 Mathematical Model

2.1.1 Problem definition and governing equations

The flow investigated in this paper is mixed convection in a long vertical channel of width $2L$ and filled with fluid saturated porous medium. It is driven by an external pressure gradient and buoyancy force due to a constant temperature difference between the two channel walls. The right wall at $x = L$ and the left wall at $x = -L$ are maintained at constant temperatures T_1 and T_2 ($T_1 > T_2$) respectively, as shown in Figure 2.1. It is assumed that the fluid and porous medium are everywhere in local thermal equilibrium state, the porous medium is homogeneous and hydro-dynamically as well as thermally isotropic, and the fluid is

incompressible. The thermo-physical properties of the fluid are assumed to be constant except for the density dependence of the buoyancy term in the momentum equation which is satisfied by the Boussinesq approximation, i.e., density varies linearly with temperature as $\rho = \rho_f[1-\beta_T(T-T_0)]$, where $T_0 = (T_1+T_2)/2$. The gravitational force is aligned in the negative y-direction. Following [9, 107, 117] the volume averaged Navier-Stokes (VANS) equation derived by Whitaker [123] is used as the momentum balance equation for the above flow.

The non-dimensional space coordinates (x^*, y^*, z^*), dependent variables $(\mathbf{v}^*, \theta, P^*)$ and time t^* are calculated after scaling the dimensional variables as follows:

$$\left.\begin{aligned}(x^*,y^*,z^*) = \frac{(x,y,z)}{L},\ \ \mathbf{v}^* = \frac{\mathbf{v}}{\overline{V}_0},\ \ \theta = (T-T_0)/(T_1-T_2),\\ P^* = \frac{P}{\rho_f \overline{V}_0^2},\ \ t^* = \frac{t\overline{V}_0}{L}\end{aligned}\right\}, \tag{2.1}$$

where, $\mathbf{v}^* = (u^*, v^*, w^*)$, θ, P^* and t^* are the dimensionless Darcy velocity vector, temperature, pressure and time, respectively. Furthermore, $\overline{V}_0$ and ρ_f are dimensional average basic velocity (bulk velocity) and fluid density, respectively.

After dropping asterisk, the non-dimensional governing equations can be written as

$$\nabla.\mathbf{v} = 0, \tag{2.2}$$

$$\frac{1}{\varepsilon}\frac{\partial \mathbf{v}}{\partial t} + \frac{1}{\varepsilon^2}(\mathbf{v}.\nabla)\mathbf{v} + F\mathbf{v}|\mathbf{v}| = -\nabla P + \frac{\lambda}{Re}(\nabla^2\mathbf{v}) - \frac{1}{DaRe}\mathbf{v} + \frac{Gr}{Re^2}\theta\hat{e}_y, \tag{2.3}$$

$$\sigma\frac{\partial \theta}{\partial t} + (\mathbf{v}.\nabla)\,\theta = \frac{1}{PrRe}(\nabla^2\theta). \tag{2.4}$$

In the above equations Gr, Pr, Da, Re and F are Grashof number, Prandtl number, Darcy number, Reynolds number and Forchheimer number, respectively. They are defined as

$$Gr = \frac{g\beta_T(T_1-T_2)L^3}{\nu^2},\ \ Pr = \frac{\nu}{k},\ \ Da = \frac{K}{L^2},\ \ Re = \frac{\overline{V}_0 L}{\nu},\ \text{ and }\ F = \frac{C_F L}{|K|^{1/2}}. \tag{2.5}$$

Furthermore, g, $\hat{e}_y$, K, k, β_T, ν, ε and C_F denote the acceleration due to gravity, unit vector along y-direction, permeability of the porous medium, thermal diffusivity, volumetric

thermal expansion coefficient, kinematic viscosity, porosity and dimensionless form-drag constant, respectively. Also, λ is the ratio of effective viscosity to fluid viscosity ($\tilde{\mu}/\mu_f$), whereas, σ is ratio of overall heat capacity per unit volume of the fluid saturated porous medium to heat capacity at constant pressure per unit volume of the fluid ($(\rho c_m)_m/(\rho c_p)_f$). Here, $(\rho c_m)_m = (1-\varepsilon)(\rho c_s)_s + \varepsilon(\rho c_p)_f$ [76], where c_s denotes specific heat of the solid and c_p denotes specific heat at constant pressure of the fluid. Due to lack of any specific measured value of $(\rho c_m)_m$ in this study where porosity is high, $\sigma = 1$ is considered. Again, different values have been reported for $\tilde{\mu}$ in the literature [43, 55] leading to a λ other than unity. However, in the absence of any specific measured value, $\lambda = 1$ has been taken in this study.

2.1.2 Parallel mixed convective flow: Basic state

The basic flow whose stability analysis is going to be carried out is steady, fully developed, and one dimensional, i.e., PMCF. Under these conditions the governing Equations (2.2)-(2.4) are simplified into following coupled ordinary differential equations.

$$\frac{d^2V_0}{dx^2} - \frac{1}{Da}V_0 + Gr'\Theta_0 - F'|V_0|V_0 = Re\frac{dP_0}{dy}, \tag{2.6}$$

$$\frac{d^2\Theta_0}{dx^2} = 0. \tag{2.7}$$

where, V_0, Θ_0 and P_0 are the basic velocity, basic temperature and basic pressure, respectively. Here, $F' = FRe$ and $Gr' = Gr/Re$. The boundary conditions for the above basic state equations are given as:

$$V_0 = 0 \ \text{ at } \ x = \pm 1, \ \ \Theta_0 = \pm 1/2 \ \text{ at } \ x = \pm 1. \tag{2.8}$$

To solve the Equations (2.6)-(2.8), the axial pressure gradient is determined using the global mass conservation,

$$\int_{-1}^{1} V_0 dx = 2. \tag{2.9}$$

Note that the above basic flow can be solved in three different cases: (i) for Darcy flow, i.e., dropping the second order derivative and quadratic terms in the momentum equation, (ii) for Darcy-Brinkman flow without form drag, i.e., $F = 0$, and, (iii) for Darcy-Brinkman flow with form drag. The basic temperature for all the three cases is given by

$$\Theta_0 = x/2. \tag{2.10}$$

The basic flow velocity functions for the first two cases are given as,

$$V_0 = \begin{cases} Gr'Da\left(\frac{x}{2}\right) + 1; & \text{(Darcy flow)} \\ s\left(1 - \frac{cosh(mx)}{cosh(m)}\right) + \frac{Gr'Da}{2}\left(x - \frac{sinh(mx)}{sinh(m)}\right); & \text{(when } F\text{= 0)} \end{cases} \tag{2.11}$$

where, $m = \frac{1}{\sqrt{Da}}$ and $s = m\left(\frac{sinh(2m)}{m(sinh(2m)) - cosh(2m) + 1}\right)$. However, in the third case, the basic flow velocity is obtained numerically using spectral method by solving Equation (2.6) along with Equations (2.8)-(2.10). The basic flow in the first two cases is governed by $Gr'Da$ while in the third case by $\{Gr', Da, F'\}$. To understand the stability of PMCF under Darcy-Brinkman-Forchheimer model, a comparative study of the basic flow velocity under the above three cases is made by considering three different values $\{10^{-2}, 10^{-3}, 10^{-4}\}$ of Da. The velocity profiles for three different values 0.01, 2.4 and 3 of the product of Gr' and Da are shown in Figures 2.2(a) to 2.2(c). From the observation of the above figures following four interesting facts can be disclosed. First, irrespective of the value of Da as well as the model, for $Gr'Da = 10^{-2}$ the profile is free from back flow (or, negative flow) and point of inflection, i.e., the temperature difference between the walls is so small that the flow in the channel is mainly due to the external pressure gradient. Second, velocity profile under the Darcy model is always free from point of inflection, which is a consequence of it's linear nature. However, it may have back flow depending on the product of Gr' and Da. Third, for $Da = 10^{-2}$ and $Gr'Da = 2.4$ the non-Darcy velocity profile possesses point of inflection without back flow for $F' = 0$. But, when $F' = 0$ is replaced by $F' = 1000$, the profile becomes free from inflection point. Finally, for $Gr'Da = 2.4$ or 3, in contrast to the case of $Da = 10^{-4}$ where the non-Darcy velocity profile possesses point of inflection as

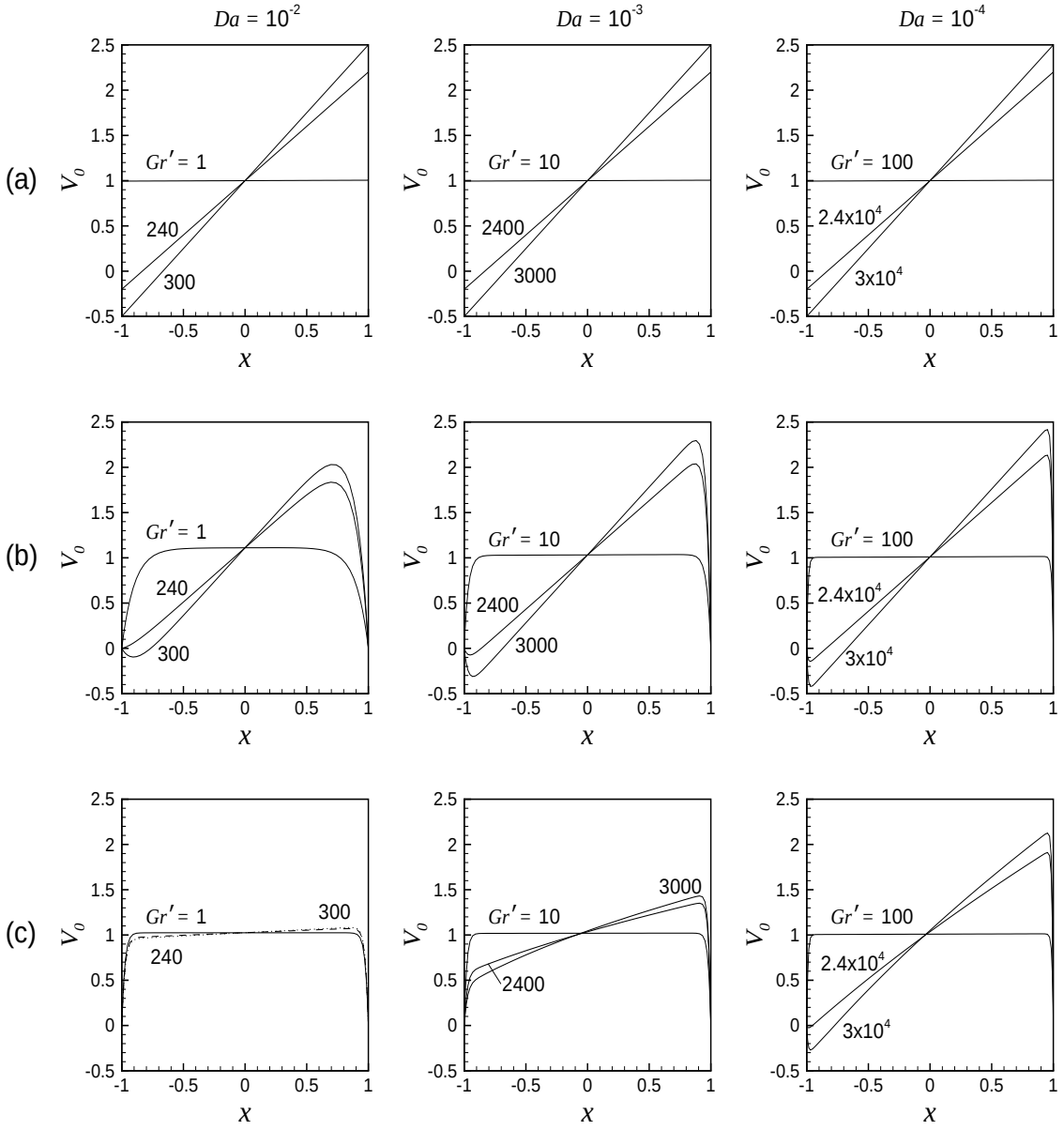

Figure 2.2: Basic velocity profile: (a) Darcy flow, (b) $F' = 0$, (c) $F' = 1000$.

	F'=0		F'=1000	
Da	Gr'_i	Gr'_b	Gr'_i	Gr'_b
10^{-2}	223	248	2559	2765
10^{-3}	2065	2134	4493	4669
10^{-4}	20204	20428	22815	23066

Table 2.1: Values of minimum Gr'.

well as back flow for both $F' = 0$ as well as 1000, in the case of $Da = 10^{-3}$ the point of inflection as well as back flow characteristic of the non-Darcy velocity profile for $F' = 0$ gets completely removed on replacing $F' = 0$ by 1000. This indicates that the Forchheimer term in the momentum equation has significant impact on the flow regime.

As it has been pointed out in the literature (ref. Yao and Rogers [129]), the point of inflection in the velocity profile is a potential for instability, so we are curious to know the minimum value of Gr' for which non-Darcy flow will have point of inflection for a given value of Da and how does it depend on the form drag of the medium. For this, the least values of Gr' for which the point of inflection and back flow appear in the velocity profile have been calculated for different values of Da (considered in this paper) as well as F' and shown in Table 2.1. Here, Gr'_i and Gr'_b denote the respective least values of Gr' for which point of inflection and back flow appear in the velocity profile. It can be seen from this table that $Gr'_i < Gr'_b$. Above observations bring us to a crossroad: whether the appearance of the point of inflection in the basic flow influence the stability boundary? Similar to the purely fluid domain [129] does the back flow in the basic flow profile give an indication of the instability of the flow?

2.1.3 Temporal linear stability

The linear stability of the above basic flow is investigated by imposing an infinitesimal disturbance on it. So, the field variables are split into the basic state and an infinitesimal

disturbance, as

$$(\mathbf{v},\theta,P) = (V_0(x)\hat{e}_y,\Theta_0(x),P_0(y)) + (\mathbf{v}',\theta',p'). \tag{2.12}$$

These infinitesimal disturbances of corresponding field variables are separated into the normal mode form [32] as,

$$(\mathbf{v}',\theta',p') = (\hat{\mathbf{v}}(x),\hat{\theta}(x),\hat{p}(x))e^{i(\alpha y+\beta z-\alpha ct)}, \tag{2.13}$$

where, α and β are the wavenumbers in streamwise and spanwise directions respectively, and $c = c_r + ic_i$ is a complex wave speed. The sign of c_i determines the growth or decay of the disturbances, i.e., the disturbances are classified as stable, neutrally stable, or unstable depending on whether $c_i < 0$, $c_i = 0$, or $c_i > 0$, respectively. On substituting the Equations (2.12) and (2.13) into the governing Equations (2.2)-(2.4), and subtracting the Equations (2.6)-(2.7), the linear equations for the infinitesimal disturbances are obtained which are given in Appendix A. These equations form a generalized eigenvalue problem with complex disturbance wavespeed as the eigenvalue.

2.1.4 Numerical method

The system of differential equations along with their boundary conditions in this paper are discretized in the interval $[-1,1]$ along x-direction at Gauss-Lobatto points by implementing the Chebyshev spectral collocation method [18] that uses Chebyshev polynomials as the basis functions.

The linear disturbance Equations (A.6)-(A.8) along with homogeneous boundary conditions (A.9) are formulated as a generalized eigenvalue problem in the form

$$\mathbf{A}X = c\mathbf{B}X, \tag{2.14}$$

where, c is the complex eigenvalue, X is the representation of the eigenfunction, and $\mathbf{A}$ and $\mathbf{B}$ are the square complex matrices of order $3N+3$, where N represents order of the

base polynomial in the collocation method. The eigenvalues of the above system are determined using the complex QZ algorithm [71] inbuilt in MATLAB. In the complete paper, the integrals are calculated by Gauss-Chebyshev quadrature formula.

The validation of our numerical code is carried out in three different ways. First, by performing a grid independence test of the least stable eigenvalue for the mixed convection flow in a porous medium. Second, by making a comparison with published results in vertical channel without porous medium for (i) natural convection, (ii) forced convection (isothermal flow) and, (iii) mixed convection flow. Third, by ensuring that the balance of disturbance kinetic energy and disturbance thermal energy at the critical level must be zero.

The convergence of the numerical scheme is checked by varying the number of terms in the Chebyshev collocation method. Table 2.5 (see Appendix C) shows that the least stable eigenvalue achieve 6-digit point accuracy with 51 terms at randomly selected values for various parameters. The results remain consistent with increase in number of terms. The same trend is observed with other values of parameters. It is observed that 51 terms of Chebyshev polynomials, i.e. $N = 51$, are usually sufficient to perform the numerical calculations with high accuracy.

In the case of natural convection flow of air, Lee and Korpela [68] have found the critical value of $Gr = 8038$ and $\alpha = 2.8$ by taking characteristic length as the width of the channel. This result can be obtained exactly from our code when $Re = 1$, $Da = 10^{10}$, $\varepsilon = 1$, $Pr = 0.7$ and $F = 0$. Also, our definition of Gr needs to be modified by including $2L$ as characteristic length instead of L. In the case of isothermal channel flow without porous medium the critical value of Reynolds number ($Re_c = 3848.13$ based on average velocity) and wavenumber (α=1.02) obtained by Orszag [79] for plane Poiseuille flow of water matches exactly with the results of our code when $Gr/Re = 0$, $Da = 10^{10}$, $\varepsilon = 1$, $Pr = 7$ and $F = 0$. Some particular results of published work of Chen and Chung [23] in mixed convection are also used to validate our numerical code. Again, we had to modify our definition of Gr to include $2L$ instead of L to get the same critical value of Gr/Re . Table 2.2 shows that the agreement is good. The final check is made by calculating energy

	Current results	Chen and Chung [23]
Gr'_c	115.20	115.25
α_c	1.03	1.032

Table 2.2: Comparison of critical Gr' and wavenumber with those obtained in Chen and Chung[23] at $Re = 1500$, $Pr = 7$, $Da = 10^{10}$, $\varepsilon = 1$, and $F = 0$.

growth rate around the critical point, which is discussed in Appendix B.

2.1.5 Energy spectra

As pointed out by Hart [46], the driving mechanisms of flow instability may be determined by the production and dissipation of disturbance kinetic energy (hereafter, KE). Therefore, to ascertain the role played by heat transfer during the flow instability, it is necessary to keep track of KE. The balance of KE is given as,

$$\begin{aligned} Re\frac{1}{\varepsilon}\frac{\partial}{\partial t}\left\langle \frac{1}{2}(u'^2+v'^2+w'^2)\right\rangle &= -Re\frac{1}{\varepsilon^2}\left\langle u'v'\frac{dV_0}{dx}\right\rangle + Gr'\left\langle v'\theta'\right\rangle - F'\left\langle |V_0|(u'^2+2v'^2+w'^2)\right\rangle \\ &\quad -\frac{1}{Da}\left\langle (u'^2+v'^2+w'^2)\right\rangle - \left\langle (\nabla u')^2+(\nabla v')^2+(\nabla w')^2\right\rangle \\ &= E_s+E_b+E_F+E_D+E_d \end{aligned} \tag{2.15}$$

where, the symbol $<>$ imply integration over the volume: $[-1,1]\times[0,2\pi/\alpha]\times[0,2\pi/\beta]$ of the disturbance cell. The integrals in above equation can be evaluated using the eigenvectors from the linear stability analysis. On the curve of neutral stability, the disturbances neither grow nor decay, and the left-hand side of equation (2.15) is zero. The first term on the right-hand side represents the gain (loss) of the KE from(to) the mean flow through Reynolds stress, referred to as shear production (destruction), represented as E_s. The second term represents the production of KE through work done by the fluctuating body force, and defined as (E_b). The third term (E_F) represents the dissipation of KE due to form drag. The fourth term (E_D) represents the dissipation of KE energy due to work done by surface drag. The last term (E_d) represents the dissipation of energy due to viscous effects. Therefore, the Equation (2.15) represents a balance of the production of KE by buoyant and shear

mechanism with the dissipation of KE by surface drag, form drag, and viscous action.

Similar to the KE balance, thermal energy balance is also defined by

$$\sigma\frac{d}{dt}\left\langle\frac{1}{2}\theta'^2\right\rangle=\frac{1}{RePr}\left\langle-\left[\left(\frac{d\theta'}{dx}\right)^2+\left(\frac{d\theta'}{dy}\right)^2+\left(\frac{d\theta'}{dz}\right)^2\right]\right\rangle+\left\langle-\left(\theta'v'\frac{d\theta_0}{dy}\right)\right\rangle=T_d+T_c \tag{2.16}$$

where, T_c and T_d are production of disturbance thermal energy due to thermal convection and dissipation of disturbance thermal energy due to diffusion, respectively. Since, at the critical level, the sum of all KE components as well as the sum of all disturbance thermal energy components must be equal to zero, therefore the relative errors of the kinetic and thermal energy balance are defined by $\delta_K=\frac{|E_s+E_b+E_D+E_F+E_d|}{|E_s+E_b|}$ and $\delta_T=\frac{|T_c+T_d|}{|T_c|}$, respectively. For all the calculations presented in the following study δ_K and δ_T are less than 3%.

2.2 Importance of Prandtl number

It is to be noted that the PMCF is independent of Pr. Therefore, before addressing its effect on the stability of the flow, the role played by Prandtl number in a non-isothermal flow is first examined. It has been done by finding the first ten least stable eigenvalues of the eigen-spectrum of system (2.14) when Gr' is equal to zero and when it is equal to 10^{-3}, for different values of Pr keeping α equal to 1. For $Gr'=0$ the system (2.14) is solved without energy equation. In this case each least stable mode is classified as kinetic (K) type. When $Gr'=10^{-3}$, the modes which have common eigenvalue with the spectrum corresponding to $Gr'=0$ are classified as K type, whereas other modes are classified as thermal (T) type. A comparative Table 2.3 is made when Re, F', and Da are fixed at 10^3, 10^3, and 10^{-3}, respectively. It can be seen from the above table that except the first three all other modes are of K-type for $Pr=0.02$. It is other way when Pr is replaced by 0.1, i.e., except the last two all other modes are of T-type. For Pr = 0.7 all the first ten least stable modes are of T-type which also holds for $Pr>0.7$. Similar impact of Pr for other considered values of Da as well as Re is also checked and it is observed that the impact of Pr on the first ten least

$Gr/Re = 0$	Type	$Pr = 0.02$	Type	$Pr = 0.1$	Type	$Pr = 0.7$	Type
0.01133-0.01820i	K	0.01019-0.00173i	T	0.01019-0.00034i	T	0.01019-0.00004i	T
0.01132-0.01827i	K	0.01019-0.00543i	T	0.01019-0.00108i	T	0.01019-0.00015i	T
0.01132-0.01838i	K	0.01019-0.01160i	T	0.01019-0.00232i	T	0.01019-0.00033i	T
0.01131-0.01853i	K	0.01133-0.01820i	K	0.01018-0.00404i	T	0.01018-0.00057i	T
0.01130-0.01873i	K	0.01132-0.01827i	K	0.01018-0.00626i	T	0.01018-0.00089i	T
0.01129-0.01897i	K	0.01132-0.01838i	K	0.01017-0.00898i	T	0.01017-0.00128i	T
0.01128-0.01925i	K	0.01131-0.01853i	K	0.01017-0.01219i	T	0.01017-0.00174i	T
0.01127-0.01958i	K	0.01130-0.01873i	K	0.01016-0.01589i	T	0.01016-0.00227i	T
0.01126-0.01995i	K	0.01129-0.01897i	K	0.01133-0.01820i	K	0.01015-0.00287i	T
0.01125-0.02036i	K	0.01128-0.01925i	K	0.01132-0.01827i	K	0.01014-0.00354i	T

Table 2.3: The first ten least stable eigenvalues of isothermal flow ($Gr/Re = 0$) and nearly isothermal flow ($Gr/Re \to 0$).

stable modes is significant. So, from this analysis it can be concluded that an important role of Prandtl number in the instability mechanism of the PMCF in the fluid saturated porous medium is expected.

2.3 Stability boundary of PNCF

To understand the stability boundary of PMCF comparatively with that of PNCF, the results of linear stability analysis of PNCF are also required. Therefore, a brief linear stability results of PNCF that includes a revisit to the problem of Kwok and Chen [62] is given in this section. Here, using non-Darcy model, first we have tried to reproduce the numerical result of Kwok and Chen [62] in a differentially heated vertical porous layer (a tall narrow box 30cm high $\times$ 2cm wide $\times$ 11.5cm deep, filled with porous medium consisting of 3mm diameter glass beads saturated by distilled water) where permeability and porosity of the medium are $0.85\times10^{-8}\text{m}^2$ and 0.4, respectively. Based on the depth of the box it is assumed that the flow is independent of the direction of depth, i.e., the flow is considered in a slender cavity. Following Kwok and Chen [62] we have also found the similar result, i.e., PNCF is linearly unstable.

A note is made about the above results. We have reviewed the work done by Kwok

and Chen [62] in three different ways. First, the problem of natural convection is solved as proposed by them using Galerkin method. Second, the same problem is solved using Chebyshev collocation method. Third, the natural convection flow (PNCF) is studied as a limiting case of mixed convection flow (PMCF) in the limit $Re \to 0$ using Chebyshev collocation method. In the third case the quadratic dependence of density on the temperature in the Boussinesq approximation is also used and the coefficient $1/\varepsilon^2$ of advective term in Equation (2.3) is replaced by $1/\varepsilon$ as given in their paper . The authors have mentioned that the values of coefficients C_2 and C_3 in their momentum equation are of the order 10^{-4} but as per their given data and the property values of water at 25^oC the coefficients are found to be equal to 9.2×10^{-6} which is one order less than what they have reported. Also, the authors have used a ten term Galerkin expansion to evaluate the critical Rayleigh number (Ra) but we have found that it is not sufficient. Table 2.6 (see Appendix C) shows the convergence of least stable eigenvalue at $Ra = 308$ and $\alpha = 2.6$ for both Galerkin and Collocation method. It can be seen that a reasonable convergence is achieved for $N = 35$ and for this value of N the critical Ra is 3610 in both the cases which corresponds to a temperature difference (ΔT) of 1100 ^{o}C across the walls. Also, when this problem is studied as a limiting case of the present PMCF in the limit $Re \to 0$ the same value of ΔT is obtained. For $N = 10$, which is considered by the above authors, ΔT is calculated and it is around 600^oC. However, when the values of coefficients C_2 and C_3 are taken as 10^{-4} and $N = 10$ then the value of ΔT comes out to be 390^oC which is very large as compared to the one reported by them which is 135.9^oC. Although, it is a non-realistic approximation since it is far away from the experimental value of 29.2^oC, but it reconfirms that inclusion of no-slip condition causes instability of PNCF under linear stability analysis.

Apart from this, the instability boundary of PNCF as a limiting case of PMCF for some other permeability and porosity are also calculated, where the quadratic relationship between density and temperature in the body force term is replaced by the Boussinesq approximation and the governing equations by VANS with F=0. For example, when the permeability of the medium is replaced by 2.5×10^{-6}m^2 and the porosity by 0.9 then the

critical values of ΔT for different half widths: 1.58cm, 5cm, and 15.8cm of the channel are given as 4.18^oC, 8.58^oC, and 4.75^oC, respectively, for water saturated porous medium channel. Furthermore, when the half width of the channel is fixed at 5cm then the critical values of ΔT are 0.13^oC, 8.58^oC, and 150.4^oC for media permeability $2.5\times10^{-5}m^2$, $2.5\times10^{-6}m^2$, and $2.5\times10^{-7}m^2$, respectively. This indicates that the decrease in media permeability increases the critical value of ΔT. Similar results are also observed when the porous medium is saturated by air.

2.4 Results and Discussion

The present work intends to offer a comprehensive account of linear stability analysis of parallel mixed convective flow (PMCF) in a differentially heated vertical channel filled with fluid saturated high permeable porous medium. Accordingly, the following analysis is made when the channel is filled with metallic foam or any other porous medium having permeability in the range of $10^{-5}m^2$ to $10^{-7}m^2$ in SI unit with porosity of 0.9. Rigorous numerical computations reveal that the least stable mode is two-dimensional and spanwise independent (i.e. $\beta = 0$). This is in agreement with the results obtained while studying the linear stability of mixed convection with linearly varying wall temperature of the vertical channel [5, 23]. Special attention is given on the influence of Prandtl number on instability mechanism of the flow. We present the results for a wide range of Pr to describe the effect of important parameters related to the porous medium such as Darcy number and modified Forchheimer number on the instability boundary along with scale analysis at the least linearly stable point. It has been done by considering a wide range [10^{-2}, 10^3] of Pr and different values of Da. Furthermore, the range for parameters such as Re and F' considered in this study are [100, 5000] and [0, 5×10^3], respectively. The results are described using stability boundaries formed by critical modified Grashof number and wave numbers with respect to Prandtl number, Reynolds number and modified Forchheimer number.

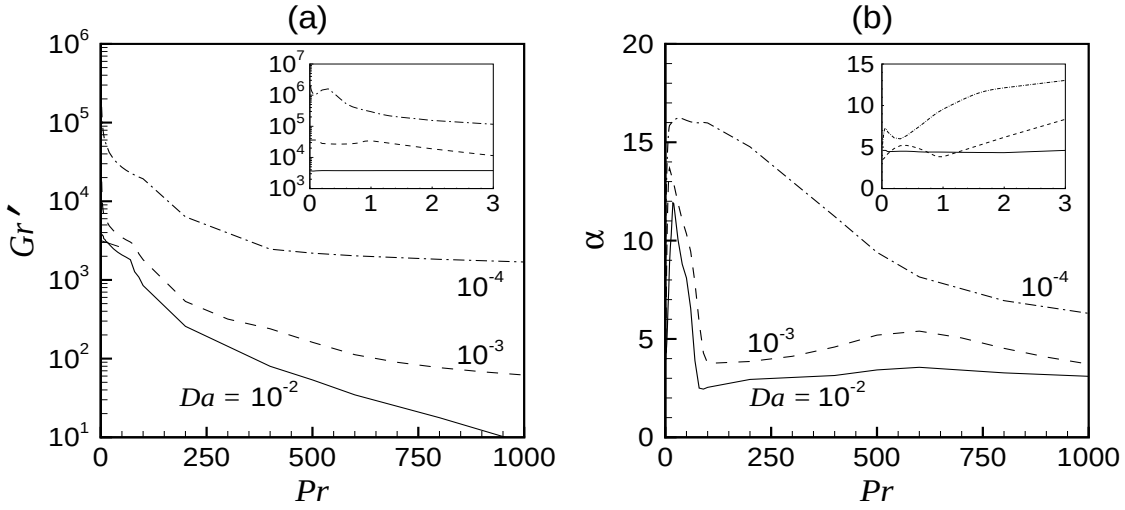

Figure 2.3: Instability boundaries in (a) (Pr, Gr')-plane and, (b) (Pr, α)-plane when $Re = 1000$ and, $F' = 1000$.

2.4.1 Influence of Prandtl number

To understand the relative influence of momentum diffusivity and thermal diffusivity on the instability boundary points, we have discussed about the instability boundary as a function of Pr for three different values (10^{-2}, 10^{-3}, 10^{-4}) of Da when Re and modified Forchheimer number are fixed at 10^3. The instability boundary curves in (Pr, Gr') and (Pr, α) planes are shown in Figure 2.3. It can be seen from this figure that a higher value of Da results in a lower value of critical Gr', i.e., Da has a destabilizing effect on the flow. For example, the basic flow becomes unstable even at $Da = 10^{-2}$ and Gr' around 849 when the fluid is oil ($Pr = 100$). This may be the consequence of the fact that in a higher permeable porous medium the velocity of the basic flow is high (see Figure 2.2), which can be made unstable for a relatively smaller value of Gr' (i.e., for a low temperature difference between the walls). Furthermore, from the above figure as well as Table 2.1 it can be pointed out that for $Da = 10^{-2}$ the critical $Gr' < Gr'_i (= 2560)$ for $Pr > 30$. This indicates that the appearance of point of inflection in PMCF is necessary for instability when $Pr \leq 30$, which is also true for $Da = 10^{-3}$. For $Da = 10^{-4}$, the critical value of Gr' is less than 22815 for $Pr > 80$, therefore the appearance of point of inflection acts as a necessary condition for

instability when $Pr \leq 80$.

A close inspection of the above graph (see inset Figure 2.3(a)) reveals an important feature of the instability curve in the vicinity of $Pr = 0.01$, where a wavy characteristic of the profile can be seen. Let this vicinity be defined as first regime. The length of this regime is highly sensitive to Da. From our numerical experiments it has been found that the first regime for Da equal to 10^{-2} sustains upto a threshold value of Pr ($Pr = 2$), whereas the same for Da equal to 10^{-3} and 10^{-4} sustains upto $Pr = 1.3$ and $Pr = 0.3$, respectively. Similar observation is also reported by Su and Chung [102] while studying the linear stability analysis of mixed-convection flow in a vertical pipe. Note that the variation of wavenumber also shows a wavy profile in the first regime (see inset Figure 2.3(b)). Let the complement of the first regime of Pr be defined as second regime, where a monotonic decrease in Gr' on increasing Pr takes place.

To understand the instability mechanism in the above two regimes we recall that the importance of momentum and thermal diffusions is measured by $(Re)^{-1}$ and $(RePr)^{-1}$, respectively. So, the Prandtl number signifies the relative efficiency of momentum and thermal diffusion. Hence, in general a low value of Pr causes an increase in the thermal diffusivity which itself suppresses the thermal fluctuations in the flow field. As a result, the flow remains stable even for larger values of Gr'. Although it gives a qualitative explanation of destabilizing characteristic of Pr, i.e., an increase in Pr decreases the critical value of Gr' which can be seen in the second regime; but it does not give any clue regarding the wavy nature of the instability curve in the first regime and its dependence on media permeability. To shed more light on the above results we have plotted the growth rate of disturbance in the neighborhood $(Gr' = Gr'(1 + 0.01))$ of the critical point in Figure 2.14. As can be seen the growth rate in the first regime is sinuous for all Da, whereas in the second regime, depending on the value of Da, initially the growth rate oscillates upto a small value of Pr and beyond that it decreases smoothly with Pr. The characteristic of the instability boundary curve in Figure 2.3 could be further explained through the plots of eigenfunctions at the critical level for $\hat{u}$, $\hat{v}$, and $\hat{\theta}$, specially for very low and high values of Pr. It is known

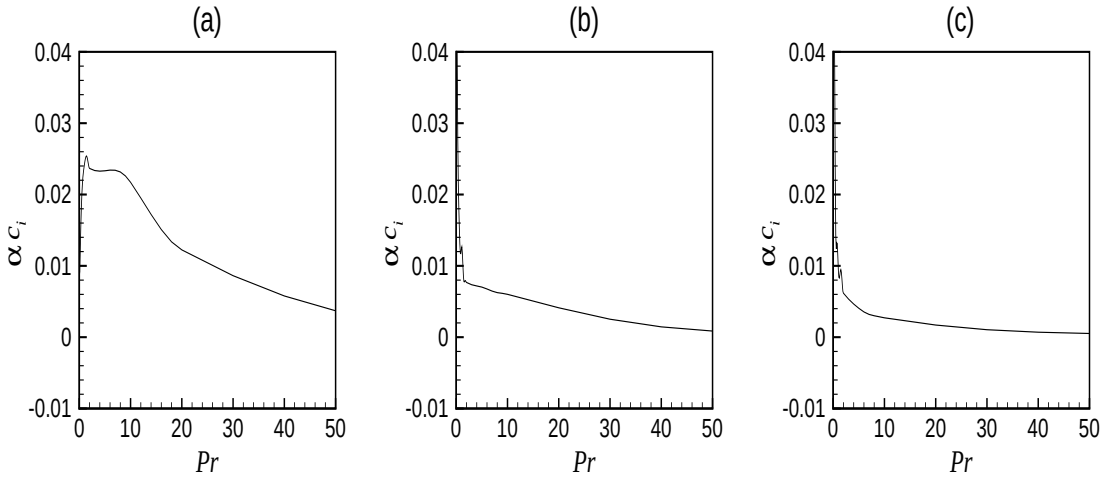

Figure 2.4: Growth rate (αc_i) as a function of Pr for (a) $Da = 10^{-2}$, (b) $Da = 10^{-3}$ and, (c) $Da = 10^{-4}$.

from the literature [20, 102] that in purely fluid domain the instability in the liquids ($Pr = 7$) or heavy oil ($Pr = 100$) is primarily due to thermal buoyant force or thermal disturbances while velocity disturbances are more responsible for the instability in mercury ($Pr = 0.02$) or gaseous fluids ($Pr = 0.7$).

Figure 2.5, which presents eigenfunction curves for four values 0.02, 0.7, 7, and 100 of Pr at $Da = 10^{-3}$, gives similar impression for all the above mentioned fluids except for fluid with $Pr = 7$, where the magnitude of the velocities is higher than the magnitude of the temperature disturbance eigenfunction. The magnitude of the temperature disturbance eigenfunction is much higher than those of the velocity for fluid with $Pr = 100$ and it is reverse for fluid with $Pr = 0.02$. Apart from these, compared to $Pr = 100$ the eigenfunctions for $Pr = 0.02$ or 0.7 or 7 are more wavy in nature, which may be the consequence of the fact that the corresponding PMCF velocity profile contains point of inflection and has back flow characteristic. Similar characteristics of eigenfunctions are also observed for other two values 10^{-2} and 10^{-4} of Da but not shown here. The difference for $Pr = 7$ in Figure 2.5 may be justified through the suggestion by Yao and Rogers [129] that "for larger-Prandtl number fluids, the flow becomes unstable mainly due to the disruption of the

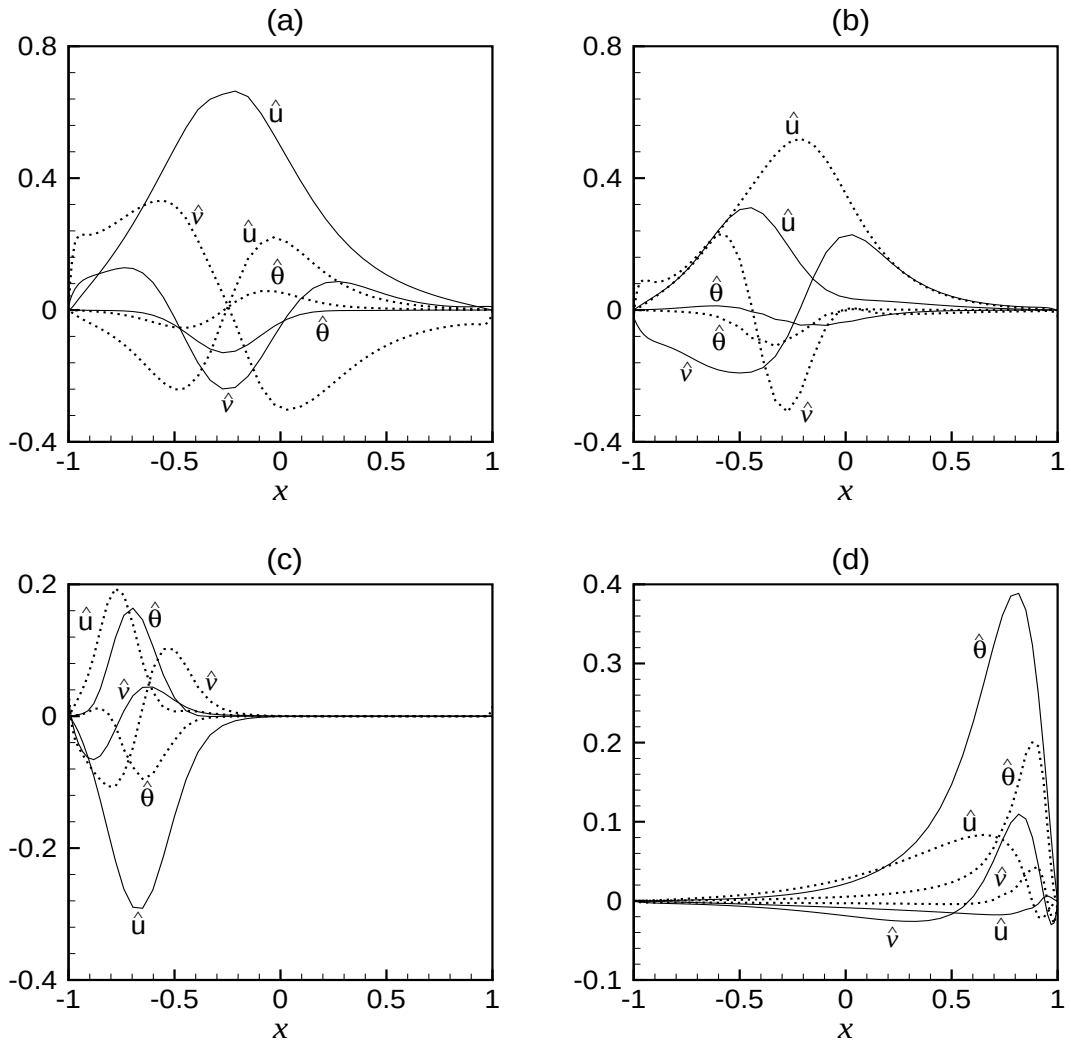

Figure 2.5: Eigenfunctions ('——' real part, '.....' imaginary part) of $\hat{u}$, $\hat{v}$ and $\hat{\theta}$ for (a) $Pr = 0.02$, (b) $Pr = 0.7$, (c) $Pr = 7$, (d) $Pr = 100$ when $Da = 10^{-3}$, $Re = 1000$ and, $F' = 1000$.

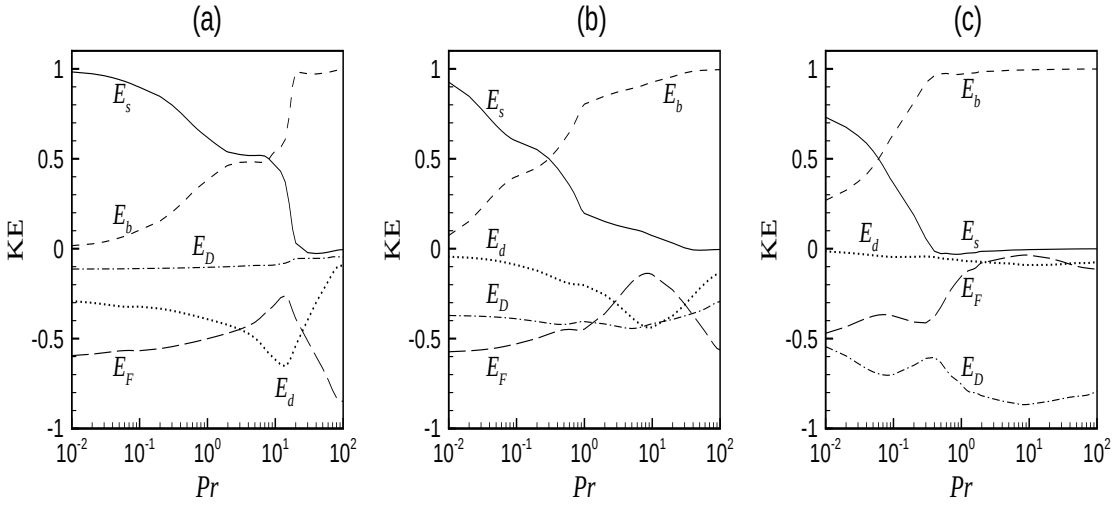

Figure 2.6: KE spectrum as a function of Pr for (a) $Da = 10^{-2}$, (b) $Da = 10^{-3}$, (c) $Da = 10^{-4}$, when $F' = 1000$ and $Re = 1000$.

velocity profile, induced by the temperature fluctuation", however it will be clarified via energy spectrum analysis at critical level.

Note that the stability of the mixed convection flow depends on the suppression of both thermal as well as kinetic fluctuations. Therefore, both kinetic as well as thermal energy spectrum at the critical level must be analyzed. However, our numerical experiments reveal that the terms T_d and T_c in thermal energy balance Equation (2.16) are negative and positive definite quantities respectively, and balance each other completely. So, we have taken the help of KE spectrum to identify the type of instability as well as to understand the instability mechanism. In contrast to the purely viscous medium, where the production of KE is solely suppressed by viscous dissipation, in porous medium it can be suppressed by surface drag, form drag as well as viscous dissipation.

The variation of KE as a function of Pr at the critical level for three different values 10^{-2}, 10^{-3}, 10^{-4} of Da is shown in Figures 2.6(a) to 2.6(c). Since the variation of instability boundary beyond $Pr = 100$ is similar in nature, so we have taken the domain of Pr as [0.01, 100] to plot the KE. Before identifying the type of instability we define the three possible types: thermal-shear, interactive, and thermal-buoyant instability. Here, the type

of instability is defined on the basis of contribution of energy production (or, destruction) by shear term (E_s) and buoyant term (E_b). If in the energy balance, contribution of E_s (E_b) is more than 70% then the type of instability is defined as thermal-shear (thermal-buoyant) else it is defined as interactive. As can be seen from Figure 2.6 that in a very small range of Pr in the vicinity of $Pr = 0.01$ KE production due to shear force is most dominant in balancing the dissipation of KE due to surface drag (E_D), viscous dissipation (E_d), as well as form drag (E_F). So similar to purely fluid domain in linearly heating case [102], here also for these value of Pr the type of instability of the basic flow is thermal-shear. Based on the value of Da the thermal-shear type of instability continues upto a least value of Pr. Beyond that least value the contribution of both terms E_s and E_b becomes equally important giving rise to interactive type of instability. It continues upto a threshold value of Pr. However, on increasing Pr beyond that threshold value the contribution of E_s becomes less than 30% and the type of instability becomes thermal-buoyant. Furthermore, the range of Pr in which above types of instability appear is sensitive to the value of Da. For example, the range of Pr in which thermal-shear type of instability appears for Da equal to 10^{-2}, 10^{-3} and 10^{-4} are [0.01,0.05], [0.01,0.04] and [0.01,0.02], respectively. However, the corresponding range of Pr in which the type of instability is interactive are [0.06, 16], [0.05, 0.8] and [0.03, 0.1], respectively. Apart from these, a close inspection of the dissipation of KE reveals three following important facts. First, on decreasing Da the dissipation of KE through form drag (E_F) decreases and through surface drag (E_D) increases, which may be the consequence of fixing the value of F' for all the three considered values of Da and also the fact that decreasing media permeability increases the surface drag. Second, the dissipation of KE via viscous dissipation (E_d) is negligible for $Da = 10^{-4}$. Third, for Da equal to 10^{-2} or 10^{-3}, dissipation of KE via form drag takes dominant role for $Pr < 1$ as well as for $Pr > 30$, and dissipation of KE for $1 \leq Pr \leq 30$ is not straight forward. Furthermore, the contribution of viscous dissipation deceases on decreasing media permeability. For relatively low permeable medium (i.e., for $Da = 10^{-4}$) dissipation through E_D dominates in the entire range of Pr.

		$Re = 1000$		$Re = 5000$	
Da	Pr	${Gr'}_c$	α_c	${Gr'}_c$	α_c
10^{-2}	10^4	0.083	1.7	0.022	1.2
	10^5	0.011	2.0	0.015	1.4
	10^6	0.015	0.7	0.005	0.3
10^{-3}	10^4	4.249	7.4	1.101	1.5
	10^5	0.214	4.0	0.102	1.4
	10^6	0.015	2.7	0.011	1.4
10^{-4}	10^4	136.8	2.5	9.817	4.1
	10^5	8.292	2.1	1.246	5.7
	10^6	0.243	16	0.027	8.7

Table 2.4: Critical Gr' and critical wavenumber for extremely high Pr.

Above discussion does not give any clear cut hint about the physics behind sinuous characteristic of the instability boundary curve in first regime. In general, fluid with $Pr < 1$ at a relatively high temperature is compressible in nature. Also, an increase in momentum diffusion stabilizes the flow [85]. May be the incompressible hypothesis for such type of fluid, when the temperature difference between the two walls is reasonably high, has resulted in such type of sinuous profile of the instability boundary curve in the first regime.

2.4.1.1 Instability in extremely high *Pr* fluid flow

To understand the instability boundary as well as instability mechanism when Pr is extremely high (i.e., when the fluid is cane molasses, lava or engine oil ($Pr = 10^4 \sim 10^6$) the critical value of Gr' for different values of Da at $F' = 1000$ is calculated and displayed in Table 2.4. It shows that the fully developed flow in this case is unstable in a differentially heated vertical porous medium channel even for $Gr' < 10$. From this table it can also be pointed out that the critical Gr' tends to zero for relatively lower value of Pr for flow in a high permeable porous medium. An increase in Reynolds number further reduces the value of critical Gr'. This may be the consequence of the fact that fluid flow through a higher permeable medium requires relatively lower momentum diffusion to be unstable.

2.4.1.2 Scale analysis at critical level

It is important to check the minimum value of wall temperature difference (ΔT) for which the mixed convective parallel flow will become unstable. From the scale analysis we have $\Delta T = \frac{Gr\nu^2}{g\beta_T L^3}$. Using our numerical data set of instability curve we have calculated the critical value of ΔT for water at $Re = 1000$ and found that it is 16.7^{o}C for Da equal to 10^{-3} and 168.6^{o}C for Da equal to 10^{-4}. Here, considered half width of the channel is 5cm. However, if the value L equal to 5cm is replaced by 10cm then the value of critical ΔT becomes 20^{o}C for Da equal to 10^{-4}. The critical value of ΔT for air is also calculated at same Re for Da equal to 10^{-3} and 10^{-4}. It has been found that the value of ΔT is 12^{o}C and 178^{o}C, respectively when the value of L is taken as 25cm. However, by changing the value of L to 50cm the same for Da equal to 10^{-4} will be 22.32^{o}C. Note that the temperature difference between the channel walls has been calculated from the definition of Gr which involves the characteristic length scale L. For a given value of Darcy number, the characteristic length is determined by the permeability (K) of the porous medium. So, for a given fluid, the choice of permeability decides the temperature difference which can be controlled by the experimentalist to obtain realistic and feasible results within the Boussinesq limit. Here, we have used the value of ν and β_T for water as 8.7×10^{-7}m^2/s and 2.5×10^{-4}/^{o}C, respectively, whereas for air as 1.5×10^{-5}m^2/s and 3.4×10^{-3}/^{o}C, respectively. As, this is a theoretical study, so the choice of permeability is at our disposal to suit our requirements.

May be the value of ΔT would differ on changing the bulk velocity, i.e., on changing the value of Re. Therefore, it is necessary to understand the variation of critical Gr' in the (Re, Gr')-plane for different values of Pr, which is undertaken in the next subsection.

2.4.2 Influence of Reynolds number

From our rigorous numerical analysis we have found that for $Da = 10^{-3}$ the saturation of Gr' as a function of Re could be achieved in the range [100, 5000] of Re. Consequently, the value of F' is fixed at 10^3. Figure 2.7 shows the variation of instability boundary in

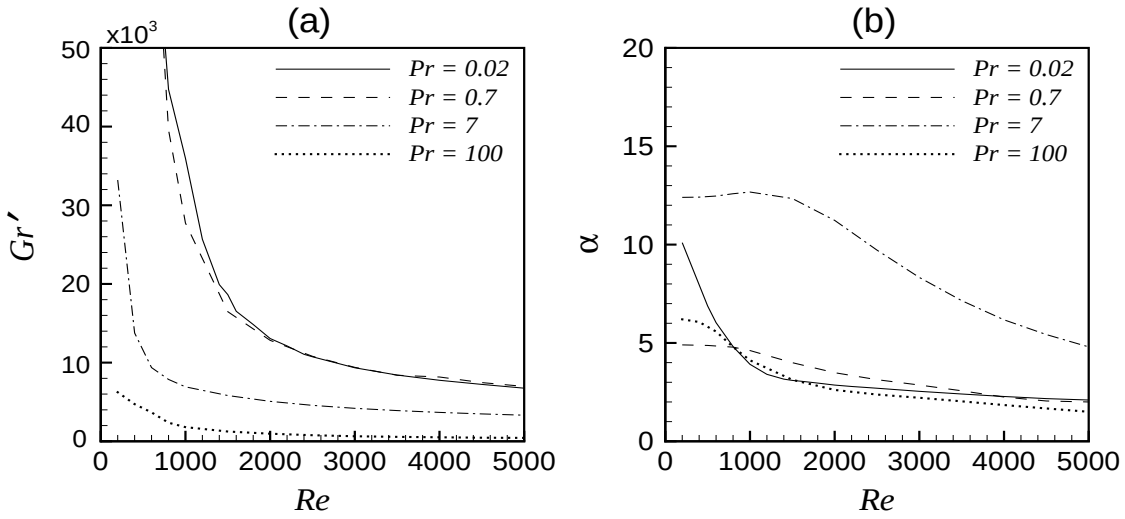

Figure 2.7: Instability boundaries in (a) (Re, Gr')-plane and, (b) (Re, α)-plane when $F' = 1000$ and $Da = 10^{-3}$.

(Re, Gr') and (Re, α)-planes. The first notable feature is that similar to the mixed convection in linearly heated channel flow (purely fluid medium [20], channel filled with porous medium [6]) here also each instability boundary curve in (Re, Gr')-plane shows a rapid decrease in Gr' as Re is increased from very small value to a threshold value. However, as Re is increased beyond this threshold value the change in Gr' is gradual and negligible, and finally leads to saturation. The corresponding wave profile also shows the same characteristic of gradual decreasing (see Figure 2.7(b)). Here, the threshold value of Re is defined by that value of Re beyond which the rate of change in the critical Gr' as a function of Re is less than 5%.

The second notable feature is that the saturation of instability curve with higher Pr is achieved much earlier than the same with lower Pr. The rapid change in the critical value of Gr' for smaller values of Re is the consequence of following fact. When the flow is slow then under the considered heating condition denser fluid from the left part of the channel has the tendency to move into the lighter region. The denser fluid will also carry its inertia when it moves into the region of lighter fluid which has a higher velocity. This invites a change in the concavity of the velocity profile (see Figure 2.2)

and introduces a local shear layer as well as surface drag. As a consequence, a point of inflection appears in the velocity profile. In this situation, a mild increase in Re accelerates the tendency of advection in the direction of the hot wall and more denser fluid can be transported upward to destabilize the flow. Hence, the critical value of Gr' falls drastically. This mechanism is similar to the 'lift-up' mechanism in the boundary layer in the presence of streamwise vortices [69]. Note that when the Reynolds number is higher than a certain value, which is a function of other governing parameters, further increase will result in a negligible change in the convection effect to destabilize the flow and the change in critical Gr' becomes negligible. This threshold value of Re is a function of Pr. Furthermore, it can be pointed out from Figure 2.7(a) that the instability boundary curves of mercury as well as air merged with each other beyond Re equal to 2500. The corresponding wave profiles also give similar impression. To elucidate the type of instability as well as underlying instability mechanism as a function of Re for mercury, air, water, and oil, Figure 2.8 is plotted. From this figure three interesting observations can be highlighted. First, the type of instability for mercury is thermal-shear, for water and heavy oil it is thermal-buoyant, and for air it is interactive in the entire range of Re. Second, as Re is increased from 0 to 5000, the contribution of E_D in the dissipation of disturbance KE for fluids with lower Pr such as 0.02(mercury) and 0.7(air) increases, but for fluids with higher Pr, such as water or oil, the contribution from E_D decreases whereas E_F increases and plays a dominant role in the dissipation of the disturbance KE. Finally, though the contribution of E_d increases in balancing the disturbance KE as a function Re but its maximum contribution remains less than 25%. The characteristic of E_d is opposite for fluid with $Pr = 100$, whereas it depends on Re for $Pr = 7$.

Before closing this subsection we have calculated the minimum value of ΔT as a function of Re for which the PMCF will be unstable. It has been found that when Da is equal to 10^{-3} the minimum ΔT for water is achieved at $Re = 400$ (see Figure 2.9) whereas the same for air is achieved at $Re = 1500$ (figure not shown). The minimum values for these two fluids are 13.3^oC (when $K = 2.5 \times 10^{-6}m^2$) and 22.3^oC (when $K = 4 \times 10^{-5}m^2$),

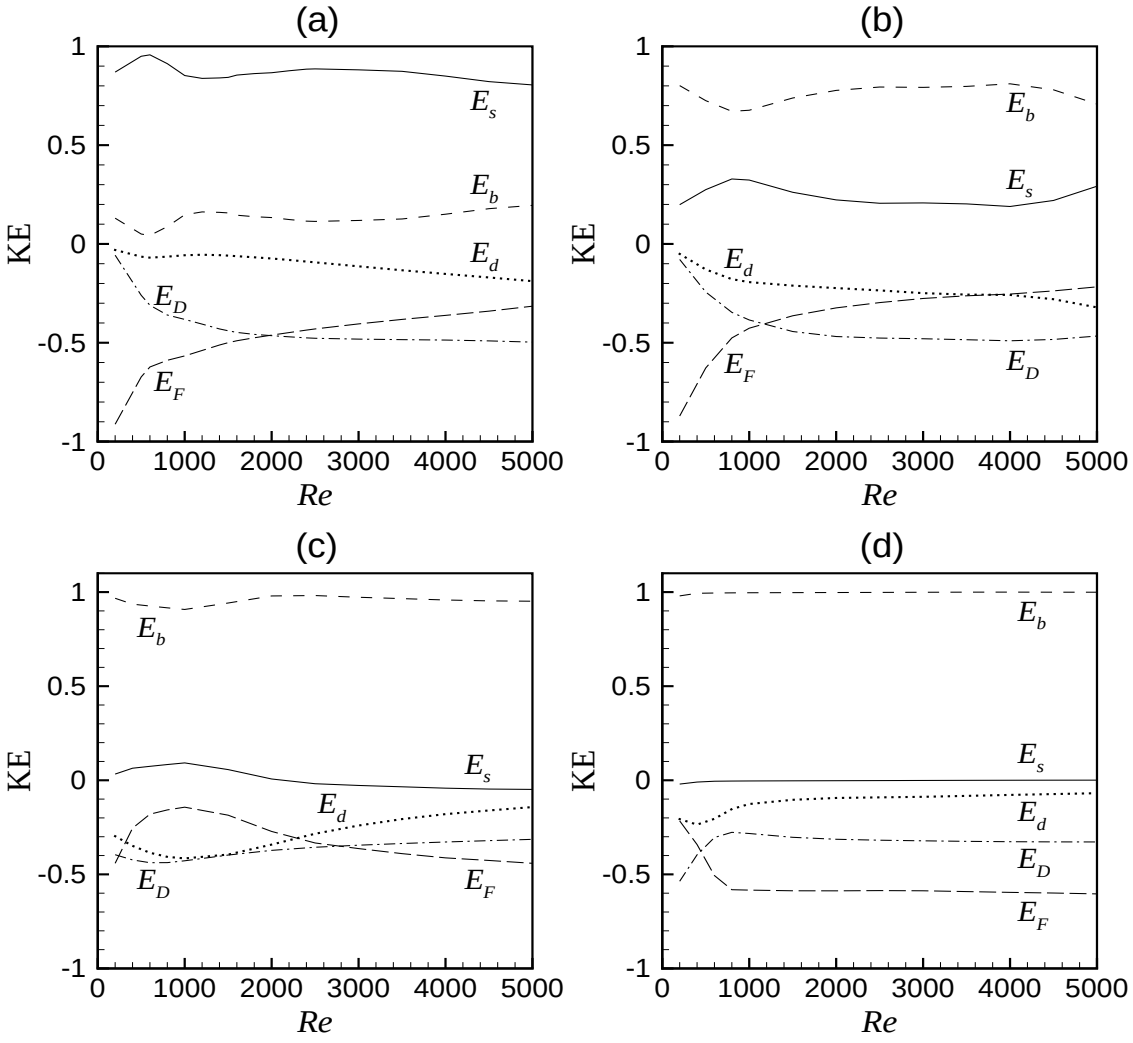

Figure 2.8: KE spectrum as a function of Re for (a) $Pr = 0.02$, (b) $Pr = 0.7$, (c) $Pr = 7$, (d) $Pr = 100$ when $F' = 1000$ and $Da = 10^{-3}$.

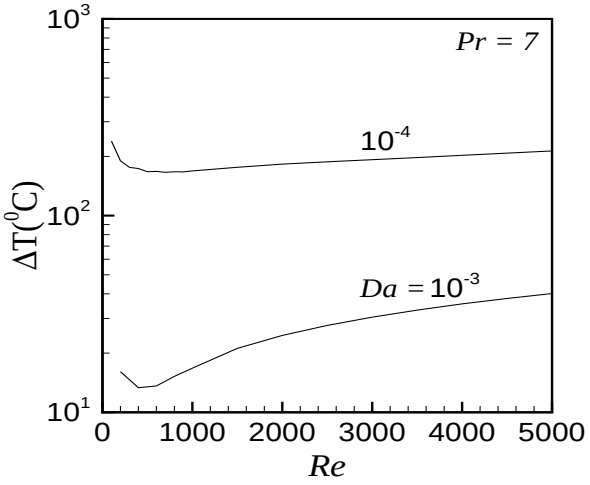

Figure 2.9: ΔT as a function of Re when $L = 5cm$, $Pr = 7$ and $F' = 1000$.

respectively. We have also seen that the minimum values of ΔT for which the PNCF of water and air become unstable are 8.58^oC (when $K = 2.5 \times 10^{-6}m^2$) and 24.5^oC (when $K = 4 \times 10^{-5}m^2$), respectively. This indicates that the forced convection stabilizes the flow in the case of water whereas it destabilizes the flow for fluid such as air. However, if media permeability is changed to $2.5 \times 10^{-7}m^2$ by considering $Da = 10^{-4}$ our numerical experiments reveal that the minimum value of ΔT for PMCF of water is 166^oC which is achieved at $Re = 700$, whereas the same for PNCF of water is achieved at 150.4^oC. This implies that the forced convection in this situation does not play significant role on the stability of the flow. We have also checked that when instability of PMCF is characterized by E_s then the critical ΔT for PNCF is greater than the same for PMCF. So, it can be generalized that when the type of instability is interactive or thermal-shear the minimum critical ΔT for PMCF will be less than the same for PNCF and it will be other way when the type of instability is thermal-buoyant.

2.4.3 Influence of modified Forchheimer number

So far in our discussion we have fixed the value of F'. But, the inertia due to form drag may play a significant role in the flow dynamics as well as instability mechanism [60]. Apart from this, it is also known that Forchheimer term alongside the Darcy term is appropriate under such conditions where Brinkman's (Laplacian) term looks incongruous. In the present problem Brinkman's term has been considered to satisfy the no-slip boundary condition. Therefore, the appropriateness of Forchheimer term should be checked by studying the flow regime with and without Forchheimer term in the momentum equation. Consequently, the impact of form drag on the flow was seen in the parallel flow and basic state subsection through Figure 2.2. It was found that the point of inflection in the flow profile as well as back flow characteristic of the flow die out on incorporating the form drag in the momentum balance equation. Of course, how fast the above characteristics of the flow will damp out depends on the permeability of the medium. For relatively high permeable medium the damping characteristic of F' will be relatively high. Now we are curious to see this impact on the instability boundary. Furthermore, it is also expected that the inertia force should depend on type of fluid. Therefore, in what follows, the effect of form drag on the instability boundary for different Pr is discussed. Figures 2.10(a) and 2.10(b) show the variation of critical Gr' in (F', Gr')-plane as well as critical α in (F', α)-plane, when Da and Re are fixed at 10^{-3} and 10^{3}, respectively. Figure 2.10(a) discloses three important findings. First, for Pr equal to 0.7, 7 or 100 there exist a minimum value (F_o) of F' below which the effect of form drag on the critical Gr' as well as corresponding wave number is negligible. From the numerical data set we have found that the value of F_o is around 50. Second, depending on the value of Pr, there exist a threshold value of F' above which F' stabilizes the flow. Third, it is not necessary that the inclusion of form drag into the momentum balance equation will always stabilize the flow. It depends on the type of fluid. As an example, for fluid as mercury, when F' is increased from 1 to 10 the critical value of Gr' decreases linearly with the relation: log Gr' = -0.3743 log F' + 5.317. The critical value of Gr' also decreases on further increasing the value of F' upto 300. However, as

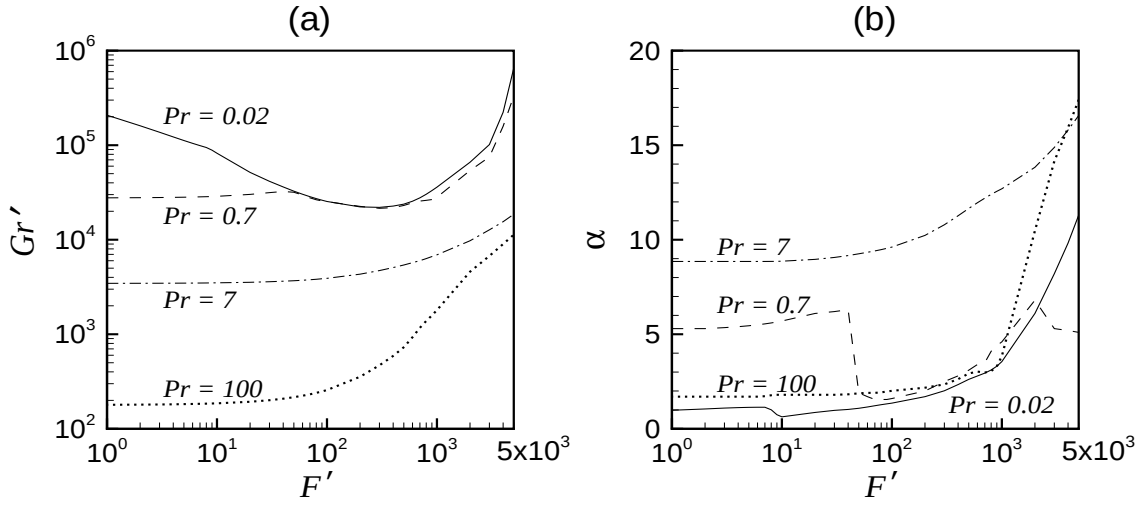

Figure 2.10: Instability boundaries in (a) (F', Gr')-plane and, (b) (F', α)-plane when $Da = 10^{-3}$ and $Re = 1000$.

F' is increased beyond 300 the scenario becomes reverse, i.e., increasing the value of F' increases Gr'. In the case of $Pr = 0.7$ it can be seen that the critical value of Gr' decreases as F' is increased from 50 to 300 and increases as F' is increased beyond 300.

To understand the variation of energy spectrum as a function of F' for above four values of Pr, Figures 2.11(a) to 2.11(d) are drawn. As can be seen from this graph, the type of instability for Pr equal to 7 or 100 is thermal-buoyant and remain unaffected by F', however, the same for Pr equal to 0.02 or 0.7 is affected by F'. The type of instability for mercury is mainly thermal-shear except in a small neighborhood around $F' = 100$ where it is interactive. In the case of air the flow instability is interactive for $F' \leq 50$ and in a small neighborhood around $F' = 1000$. The change of type of instability from interactive to thermal-buoyant at $F' = 51$ is sudden, however, the same around $F' = 1000$ is gradual. Note that the corresponding wavenumber profile changes smoothly as a function of F' except at $F' = 51$ where it experiences a sudden fall (see Figure 2.10(b)). Furthermore, the energy spectrum of $Pr = 0.02$ also shows that in the region of F' in which the critical logarithmic value of Gr' decreases linearly with the logarithmic value of F', there is a destruction of disturbance KE due to the action of buoyant force in the energy balance.

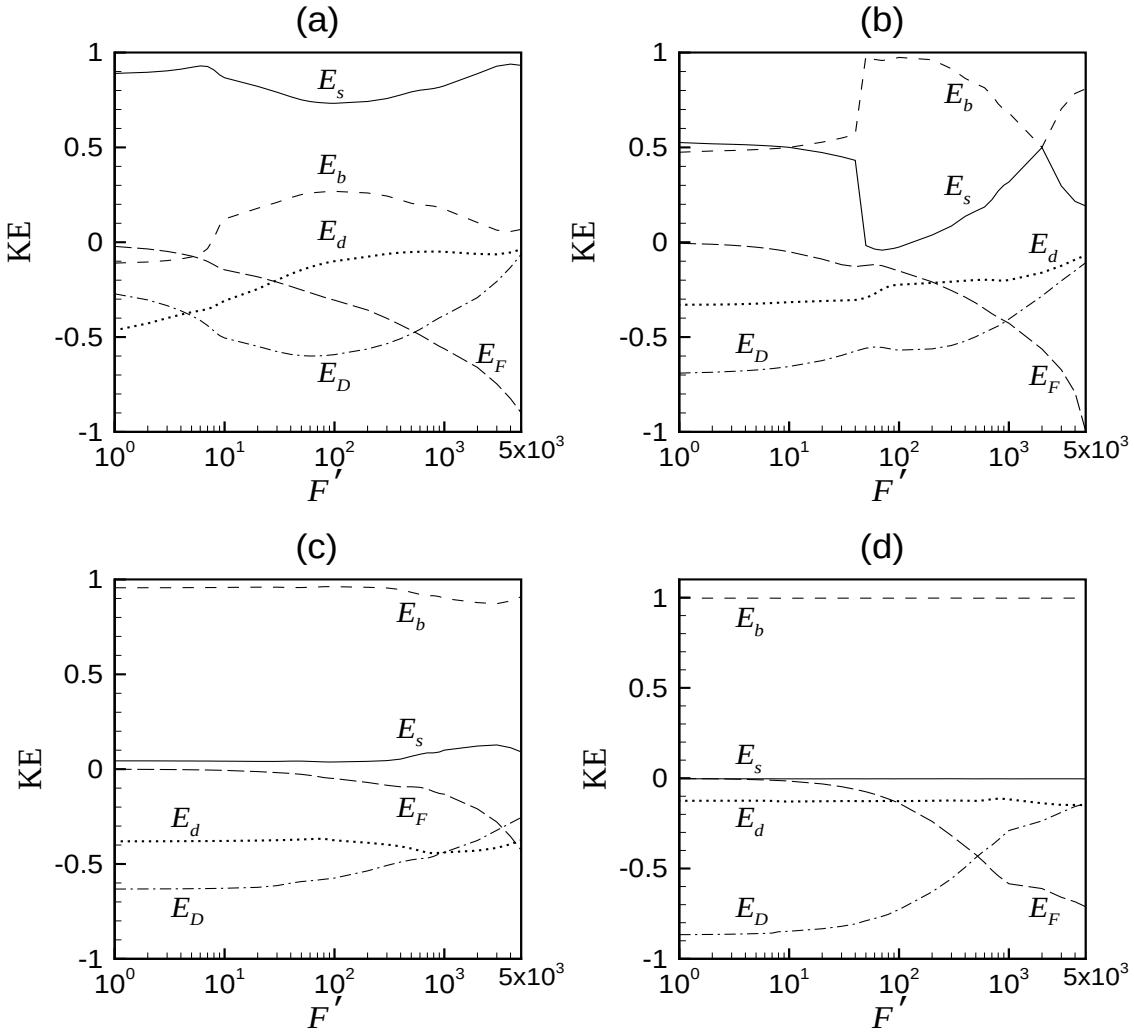

Figure 2.11: KE spectrum as a function of F' for (a) $Pr = 0.02$, (b) $Pr = 0.7$, (c) $Pr = 7$, (d) $Pr = 100$ when $Re = 1000$ and $Da = 10^{-3}$.

Note that in order to understand stability mechanism under non-Darcy model Volume average Navier-Stoke's (VANS) equation without convective term $\rho_f \mathbf{v}.\nabla\mathbf{v}/\varepsilon^2$ an attempt is also made in Appnendix D.

2.5 Summary and Conclusions

We have analyzed the stability of parallel mixed convective flow (PMCF) in a differentially heated vertical channel filled with incompressible fluid saturated porous medium. The non-Darcy VANS equation is used to understand the stability mechanism of PMCF. The flow is controlled by six governing parameters: Da, Gr', Re, F', Pr, and ε. The stability of the basic flow is examined primarily for the effect of Pr in the range of $[0.01, 1000]$. The instability boundary for extremely large values of Pr is also investigated. The entire study is made mainly for three different values (10^{-2}, 10^{-3}, 10^{-4}) of Da with porosity fixed at 0.9. Furthermore, the range of Re and F' considered in this study are [100, 5000] and [0, 5000], respectively. The stability analysis of PMCF is carried out after a partial reinvestigation of Kwok and Chen's [62] numerical study. Reinvestigation of the Kwok and Chen's [62] numerical study confirms that Gill's [41] result on stability of PNCF is not valid when no-slip condition and inertia impact are taken into account.

Similar to parallel flow due to linearly varying wall temperature [5], in the present problem also the basic flow possesses three different types of instability, namely thermal-shear, interactive, and thermal-buoyant, which depends on controlling parameters, mainly Pr. The regimes of above three instabilities over the domain of Pr are functions of Da as well as Re. Stability analysis also reveals that when Re is fixed at 1000, the appearance of point of inflection in the basic velocity for fluid with Pr less than 30 acts as a necessary condition for instability for all considered values of Darcy number. For a very small range of Pr, in the vicinity of $Pr = 0.01$, velocity disturbances are more responsible for the instability and kinetic energy production due to shear force is most dominant in balancing the dissipation of KE. So, for these values of Pr the type of instability of the basic flow

is thermal-shear. On the other hand, for large values of Pr (i.e., in the case of water or heavy oil), the instability is primarily due to the thermal disturbances and KE production due to buoyant term is most dominant in the energy balance and results in thermal-buoyant instability of the flow. The instability boundary for very larges value of Pr, say engine oil, indicates that PMCF in the channel becomes unstable even for $Gr' < 10$. In contrast to the flow in purely fluid medium, where the production of KE is solely suppressed by viscous dissipation, in porous medium the KE can be suppressed by surface drag, form drag and viscous dissipation. For relatively low permeable medium (i.e., for $Da = 10^{-4}$) dissipation through E_D dominates in the entire range of Pr for $Re = 1000$. From the influence of modified Forchheimer number it has been found that for Pr equal to 7 or 100 there exist a minimum value (F_o) of F' below which the effect of form drag on the critical Gr' as well as corresponding wave number is negligible and above this minimum value F' stabilizes the flow. It is also found that form drag may destabilize the flow for very less viscous (i.e., $Pr < 1$) fluid. The type of instability for Pr equal to 7 and 100 is thermal-buoyant and remains unaffected on varying F', however, the same for Pr equal to 0.02 and 0.7 gets affected by F'.

For the range of parameters considered in this study, the scale analysis reveals that when the permeability of the medium is less than or equal to $2.5 \times 10^{-6}\text{m}^2$ and half width of the channel is 5cm, then the critical value of ΔT for PMCF of water is higher than the same for PNCF (e.g., ΔT for PNCF and PMCF when $K = 2.5 \times 10^{-6}\text{m}^2$ are 8.58^oC and 13.3^oC, respectively), which is the consequence of thermal-buoyant instability of the flow. Note that in the case of PMCF there exists an optimum value of Re, depending on Da and F', at which the value of ΔT corresponding to critical Gr' is least (see Figure 2.9). Thus, the flow will remain stable for all Re if the value of ΔT is less than the above mentioned least value. Apart from these, when the type of instability is interactive or thermal-shear the minimum critical ΔT for PMCF will be less than the same for PNCF and will be other way when the type of instability is thermal-buoyant. Also it is expected that for a given media permeability there will be a least value of Pr above which the instability of the flow will

take place for wall temperature difference less than 20^oC, i.e., results from linear stability analysis using Boussinesq approximation will be more realistic. Overall, we hope that these findings will motivate and act as a guideline for those who are interested to study mixed convective flow through fluid saturated metallic foam or high permeable porous media used as a heat exchanger in some realistic problems.

We have investigated the instability of fully developed mixed convective flow using Boussinesq approximation along with the assumption that the solid porous matrix and saturated fluid are in local thermal equilibrium state. However, the present study reveals that when the porous medium is saturated by certain type of fluids the instability takes place for very large value of wall temperature difference. So, in that situation non-Boussinesq approximation along with local thermal non-equilibrium state between the two phases of saturated porous medium will be more appropriate. Apart from this, the prediction of wide band nature of sequence of instabilities of the detailed flow pattern and temperature distribution at a point away from the critical is beyond the scope of linear stability analysis. Consequently, a weakly non-linear stability analysis or direct numerical simulation of the present problem is required to understand the same, which could be worked out in the framework of future studies.

Appendix A: Linear disturbance equations

The governing linear equations for the infinitesimal disturbances are given as,

$$\frac{d\hat{u}}{dx} + i\alpha\hat{v} + i\beta\hat{w} = 0, \tag{A.1}$$

$$i\alpha Re\frac{1}{\varepsilon}\left(\frac{1}{\varepsilon}V_0 - c\right)\hat{u} + Re\frac{d\hat{p}}{dx} - \left(\frac{d^2\hat{u}}{dx^2} - (\alpha^2+\beta^2)\hat{u}\right) + \frac{1}{Da}\hat{u} + F'|V_0|\hat{u} = 0, \tag{A.2}$$

$$i\alpha Re\frac{1}{\varepsilon}\left(\frac{1}{\varepsilon}V_0 - c\right)\hat{v} + Re\frac{1}{\varepsilon^2}\frac{dV_0}{dx}\hat{u} + i\alpha Re\hat{p} - \left(\frac{d^2\hat{v}}{dx^2} - (\alpha^2+\beta^2)\hat{v}\right) + \frac{1}{Da}\hat{v} + 2F'|V_0|\hat{v} - Gr'\hat{\theta} = 0, \tag{A.3}$$

$$i\alpha Re\frac{1}{\varepsilon}\left(\frac{1}{\varepsilon}V_0 - c\right)\hat{w} + i\beta Re\hat{p} - \left(\frac{d^2\hat{w}}{dx^2} - (\alpha^2+\beta^2)\hat{w}\right) + \frac{1}{Da}\hat{w} + F'|V_0|\hat{w} = 0, \tag{A.4}$$

$$\frac{d\Theta_0}{dx}\hat{u} + i\alpha(V_0 - c)\hat{\theta} - \frac{1}{PrRe}\left(\frac{d^2\hat{\theta}}{dx^2} - (\alpha^2+\beta^2)\hat{\theta}\right) = 0, \tag{A.5}$$

and, after eliminating the pressure we get,

$$\frac{d^4\hat{u}}{dx^4} - 2(\alpha^2+\beta^2)\frac{d^2\hat{u}}{dx^2} + (\alpha^2+\beta^2)^2\hat{u} + i\alpha Re\frac{1}{\varepsilon^2}\frac{d^2V_0}{dx^2}\hat{u} + i\frac{\alpha\beta}{\alpha^2+\beta^2}F'\frac{d}{dx}(|V_0|\hat{\eta}) + \left(i\alpha cRe\frac{1}{\varepsilon} - \frac{1}{Da} - i\alpha Re\frac{1}{\varepsilon^2}V_0\right)\left[\frac{d^2\hat{u}}{dx^2} - (\alpha^2+\beta^2)\hat{u}\right] + (\alpha^2+\beta^2)F'|V_0|\hat{u} - F'\left(\frac{\alpha^2}{\alpha^2+\beta^2}+1\right)\frac{d}{dx}\left(|V_0|\frac{d\hat{u}}{dx}\right) - i\alpha Gr'\frac{d\hat{\theta}}{dx} = 0, \tag{A.6}$$

$$\beta Re\frac{1}{\varepsilon^2}\frac{dV_0}{dx}\hat{u} + i\frac{\alpha\beta}{\alpha^2+\beta^2}F'|V_0|\frac{d\hat{u}}{dx} - \beta Gr'\hat{\theta} - \left(\frac{d^2\hat{\eta}}{dx^2} - (\alpha^2+\beta^2)\hat{\eta}\right) + \frac{1}{Da}\hat{\eta} + i\alpha Re\frac{1}{\varepsilon}\left(\frac{1}{\varepsilon}V_0 - c\right)\hat{\eta} + \left(\frac{\beta^2}{\alpha^2+\beta^2}+1\right)F'|V_0|\hat{\eta} = 0, \tag{A.7}$$

$$\frac{d\Theta_0}{dx}\hat{u} + i\alpha(V_0 - c)\hat{\theta} - \frac{1}{PrRe}\left(\frac{d^2\hat{\theta}}{dx^2} - (\alpha^2+\beta^2)\hat{\theta}\right) = 0, \tag{A.8}$$

where, $\hat{\eta} = \beta\hat{v} - \alpha\hat{w}$. Boundary conditions on the velocity as well as temperature perturbations are applied at both walls. The velocity fluctuations satisfy the no-slip condition at the walls and the temperature perturbation satisfy the isothermal condition at the walls, i.e.,

$$\hat{u} = \frac{d\hat{u}}{dx} = \hat{\theta} = \hat{\eta} = 0 \text{ at } x = \pm 1. \tag{A.9}$$

Appendix B: Eenergy growth rate around the critical point

To see the variation of δ_K around the critical Gr', the energy graph in (Gr', δ_K) plane for four different values (mercury, air, water, and oils) of Pr has been plotted in Figure 2.12, where Da, Re, and F' are fixed at 10^{-3}, 10^3 and 10^3, respectively. Note that the above graph is plotted at corresponding critical α. It is clear from the figure that for all the above fluids, growth rate of KE is negative when $Gr' < Gr_c$ and equal to zero at Gr'_c. However, as Gr' is increased further the growth rate becomes positive.

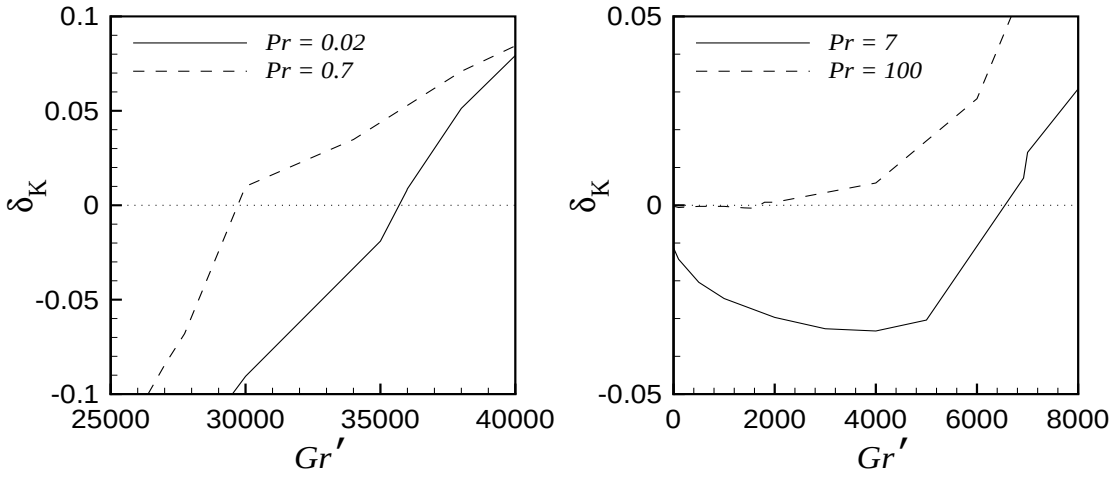

Figure 2.12: δ_K as a function of Gr' for Pr=0.02, 0.7, 7, 100 when $Re = 1000$, $Da = 10^{-3}$, and $F' = 1000$.

Appendix C: Convergence of numerical methods

N	Least stable eigenvalue
30	1.676468955047174 - 0.016075576125170i
40	1.676447163990309 - 0.016065443627865i
50	1.676447117345247 - 0.016065306170580i
51	1.676447163863406 - 0.016065361568882i
55	1.676447067018138 - 0.016065296350136i
60	1.676447157345265 - 0.016065362329521i

Table 2.5: Convergence of the least stable eigenvalue by Chebyshev collocation method for PMCF. Here, Pr=7, Re=1000, Gr'=5000, F'=1000, $Da = 10^{-3}$, ε=0.9, α=1, β=0.

	Least stable eigenvalue	
N	Galerkin method	Chebyshev Collocation method
5	-0.252070700630408 - 0.028228437240528i	-0.223186954854920 - 0.017936853498893i
10	-0.250547422539085 - 0.030461649384641i	-0.247597084941830 - 0.028924833000287i
15	-0.249444380595507 - 0.030999795632102i	-0.248961909113281 - 0.031218579850456i
20	-0.248515265197424 - 0.031295513726534i	-0.248358581351306 - 0.031429730361078i
25	-0.248216361382521 - 0.031399358180723i	-0.248234567013510 - 0.031429434415217i
30	-0.248183532738252 - 0.031407053725102i	-0.248177272797637 - 0.031423269854840i
35	-0.248170353673825 - 0.031418483695819i	-0.248171166586757 - 0.031423879120650i

Table 2.6: Convergence of the least stable eigenvalue by Galerkin and Chebyshev collocation method for the problem of Kwok and Chen [62]. Here, Ra=308, α=2.6.

Appendix D: Linear stability analysis

The prime intension in this section is to study the instability mechanism of fully developed mixed convection flow in a differentially heated vertical channel filled with porous medium by using a model that does not contain *convective term* in the volume averaged Navier-Stokes equations. Accordingly, we present the results to describe the effect of important parameters related to porous medium such as Darcy number and porosity on instability boundary curve. It has been done mainly for two distinct category of fluids with $Pr = 7$ (i.e., water) and 70 (i.e., oil), considering a wide range 10^{-7} to 10^{-2} of Da. The permeability of the medium is a function of porosity, consequently when $10^{-7} \leq Da \leq 10^{-5}$

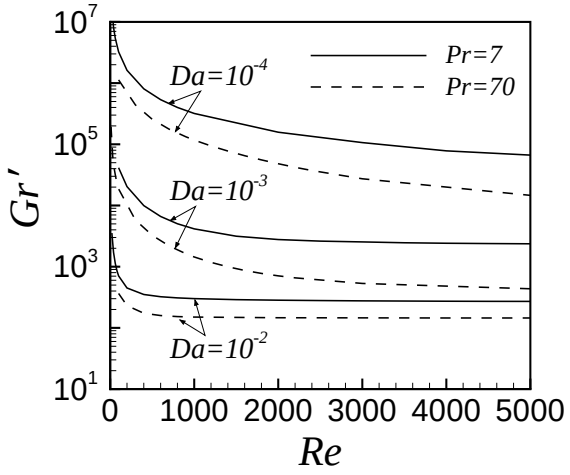

Figure 2.13: Variation of critical Gr' as a function of Re when $F' = 1$.

porosity is fixed at 0.4 and when $10^{-4} \leq Da \leq 10^{-2}$ the same is fixed at 0.9. Following the work by Bera *et. al.*[5, 6], the range of Reynold's number considered in this appendix for porosity 0.9 and 0.4 are $[10, 5 \times 10^3]$. and [10^3, 5×10^4], respectively. Heat capacity ratio is fixed at 1. Based on the media permeability, two situations: (i) HP and (ii) LP are introduced. HP is defined as flow in high permeable porous medium ($10^{-4} \leq Da \leq 10^{-2}$) with porosity equal to 0.9, whereas LP is defined as flow in relatively low permeable porous medium ($10^{-7} \leq Da \leq 10^{-5}$) with porosity equal to 0.4. Instability mechanism of the basic flow under both situations is discussed subsequently.

The results are described using stability boundaries formed by critical (Gr') as well as critical wavenumber with respect to Reynolds number (Re). In the case of HP the linear instability boundaries in the (Re, Gr') plane are plotted in figure 2.13 for different values Da and both values of Pr. As can be observed from the above figure, a higher value of Da results in a lower value of critical Gr'. That is, the effect of increasing media permeability destabilizes the flow. The basic flow becomes unstable even at very low values of Gr', i.e., around $270(145)$ when fluid is water (oil) for $Da = 10^{-2}$. The $Pr = 70$ case is very close to that of $Pr = 7$ except that it is comparatively less stable for $Pr = 70$. Although the general trend for $Pr = 7$ is similar to that of $Pr = 70$, but there is a fundamental difference between

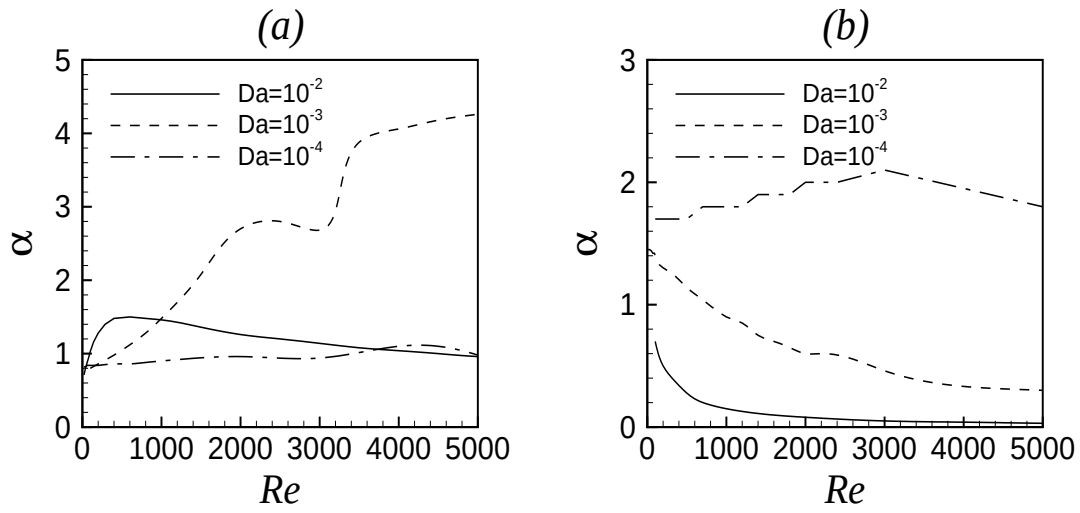

Figure 2.14: Variation of critical α as a function of Re: *(a)* $Pr = 7$ and *(b)* $Pr = 70$.

the instability of these two fluids. The basic laminar flow does contain point of inflection for $Pr = 7$ becasue the least value of critical Gr' as a function of Re is greater than Gr'_i for all the three values (10^{-2}, 10^{-3}, 10^{-4}) of Da (see table 2.1). However, for $Pr = 70$ there exist a minimum value of Re shown in table 2.1 beyond which the laminar basic flow does not contain point of inflection even though the flow is linearly unstable. This fundamental difference in the profile of the laminar base flow causes non-similar trends in the neutral stability curves in (Re, α) plane for $Pr = 7$ and $Pr = 70$ for all the above values Da. This is shown in figure 2.14.

Furthermore, each instability boundary curve in (Re, Gr') plane also shows a rapid decrease in critical Gr' as Re is increased from very small value to a threshold value. However, as Re is increased beyond this threshold value the change in critical Gr' is negligible. The threshold value of Re is a function of Da as well as Pr. Quantitatively, when Re is fixed at 100, a stepwise decrease in Da from 10^{-2} to 10^{-3} and 10^{-3} to 10^{-4} changes the critical Gr' from 707 to 41367 and 41367 to 3.2464×10^6, respectively. Hence, for the same order of reduction in permeability of the porous medium, the critical Gr' first increases by 58.5 times and then 78 times. However, when the critical Gr' becomes almost independent of Re (for $4000 \leq Re \leq 5000$) the increase in its value for the above stepwise decrease of Da

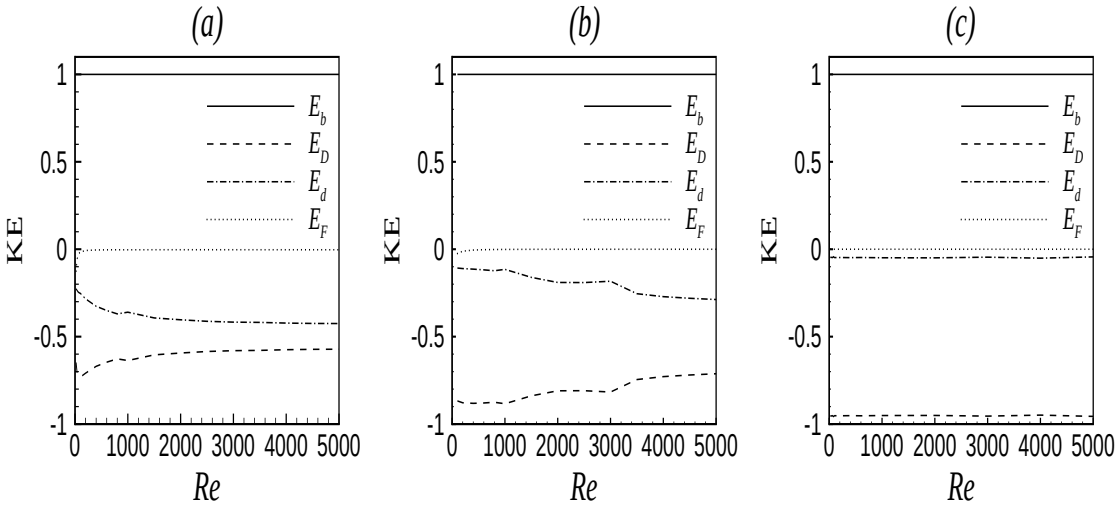

Figure 2.15: Kinetic energy spectrum at the critical level for *(a)* $Da = 10^{-2}$, *(b)* $Da = 10^{-3}$, and *(c)* $Da = 10^{-4}$ when $Pr = 7$ and $F' = 1$.

is around 8 and 32 times, respectively.

The rapid change in critical Gr' for smaller values of Re is best on the mechanism similar to the 'lift-up' mechanism in the boundary layer in the presence of streamwise vortices, which is already explained in the result section of this chapter. Note that when the Reynolds number is higher than a certain value, which is a function of other governing parameters, further increase will result in a negligible change in the convection to destabilize the flow so that the change in critical Gr' becomes negligible. As compared to the disturbance energy due to shear, bouyant and viscous forces in fluid flow without porous medium, a new source of disturbance energy caused by surface drag appears in the porous medium. For the present flow, the appearance of point of inflection in the velocity profile is a result of these three disturbance forces acting on the flow inside porous medium: viscous, bouyant and surface drag. To shed more light on the instability mechanism as well as to understand the role of Laplacian operator in it, kinetic energy spectrum at the critical level as a function of Re is plotted in figure 2.15 for $Pr = 7$. As can be seen from the above figure, first, the major part of dissipation in the whole domain of Re is due to surface drag. Second, the contribution of viscous dissipation decreases on decreasing the permeability

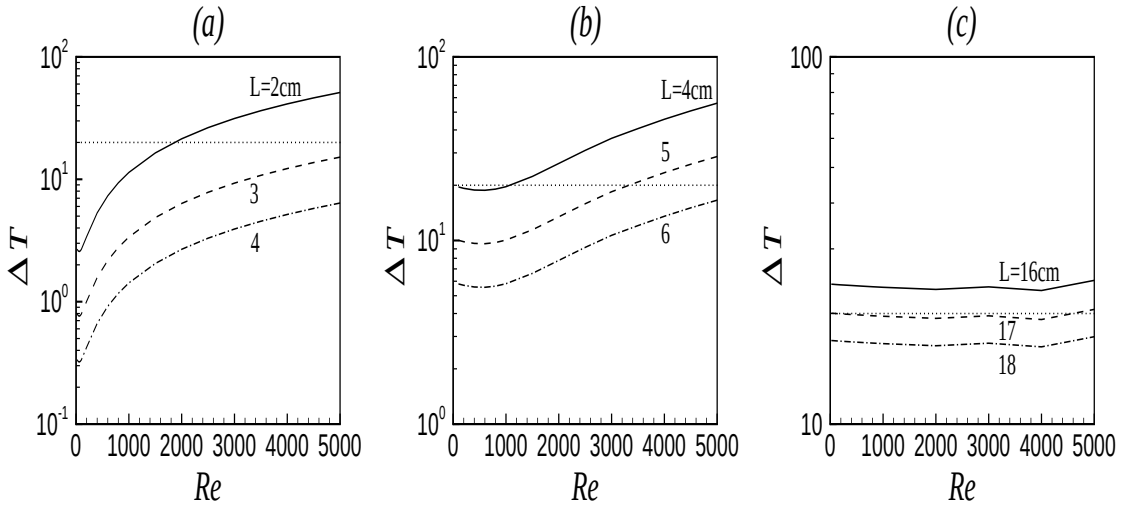

Figure 2.16: Variation of $\Delta T(^oC)$ w.r.t. Re for various values of half width of the channel: (a) $Da = 10^{-2}$, (b) $Da = 10^{-3}$ and (c) $Da = 10^{-4}$ for $Pr = 7$.

of the porous medium. Although the contribution of E_d in balancing the kinetic energy production decreases but its contribution even for Da equal to 10^{-3} is not negligible. E_b is completely balanced by E_D for Da equal to 10^{-4}. Quantitatively, when $Re = 100$, the percentages of contribution of E_d in balancing E_b for Da equal to 10^{-2}, 10^{-3} and 10^{-4} are 25.5, 11 and 4.8 respectively, whereas the same when $Re = 5000$ are 42.4, 28.8 and 4.4, respectively. The contribution of E_d and E_D in balancing the buoyant production depends on the values of Da as well as Re. Therefore we can conclude that for very low permeable medium E_b will be completely balanced by E_D.

As the density of fluid is approximated in the body force term by the Boussinesq approximation, so appropriate length scale and permeability of the porous medium is found out from dimensional analysis using the definition of Gr. Figure 2.16 shows what should be the appropriate half width of the channel in order to maintain temperature difference across the channel for laminar flow of water to take place under Boussinesq approximation [64]. For $Da = 10^{-2}$, corresponding to $L = 2$cm, the temperature difference across the channel is less than 20 ^{o}C upto $Re = 2000$. The corresponding permeability of the porous medium is 4×10^{-6}m^2. But, on increasing the Darcy number, channel with larger half width

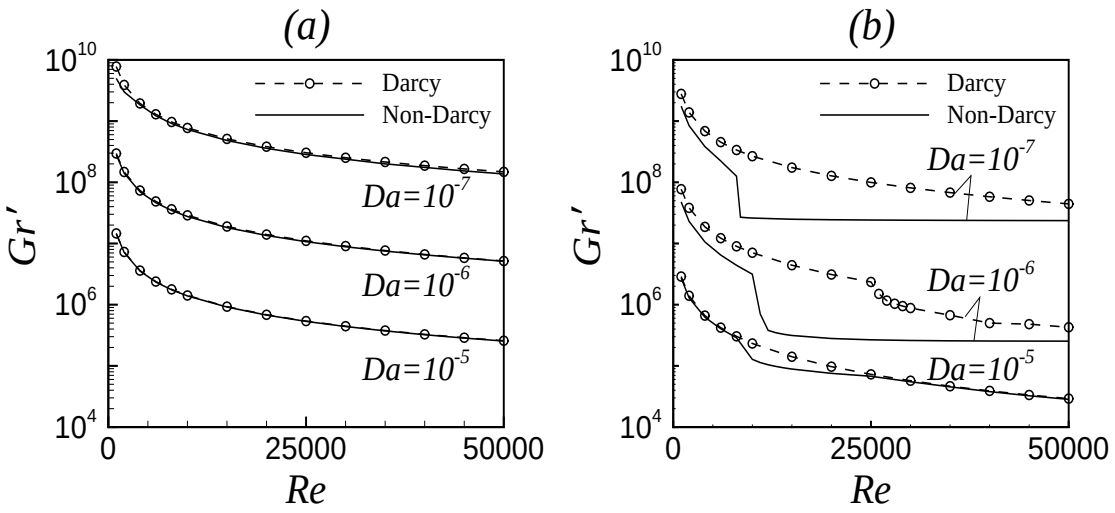

Figure 2.17: Variation of critical Gr' as a function of Re: *(a)* $Pr = 7$ and *(b)* $Pr = 70$ for $Da = 10^{-5}, 10^{-6}$ and 10^{-7}.

is required for Boussinesq approximation to hold. For example, when $Da = 10^{-3}$ and 10^{-4} the corresponding half widths of the channel should be at least 4cm and 16cm, respectively.

In order to understand the variation of instability boundaries for relatively low permeable media (i.e., LP) figure 2.17 is plotted using Darcy model as well as VANS without convective term. Qualitatively, here also the instability boundaries vary in a similar way as in the case of HP. However, following important observations can be pointed out. For $Pr = 7$, the instability curves under both models merge on each other for all the three considered values of Da. This result is also true for $Pr = 70$ except for $Da = 10^{-7}$ (see figure 2.17*b*). In general, the basic flow is more stable under Darcy model than under Darcy-Brinkmann model. For both models the instability curve possesses a jump for $Pr = 70$ when $Da = 10^{-6}$ and 10^{-7}.

So far we have discussed the role of Laplacian operator and instability mechanism for different porous media with varying permeability but fixed porosity. Now we are interested to analyze the instability mechanism and its dependence on porous media whose permeability is varied with porosity. The critical Gr' and critical α are calculated as a function of Da for two different cases: (i) constant porosity (CP) and (ii) variable porosity (VP).

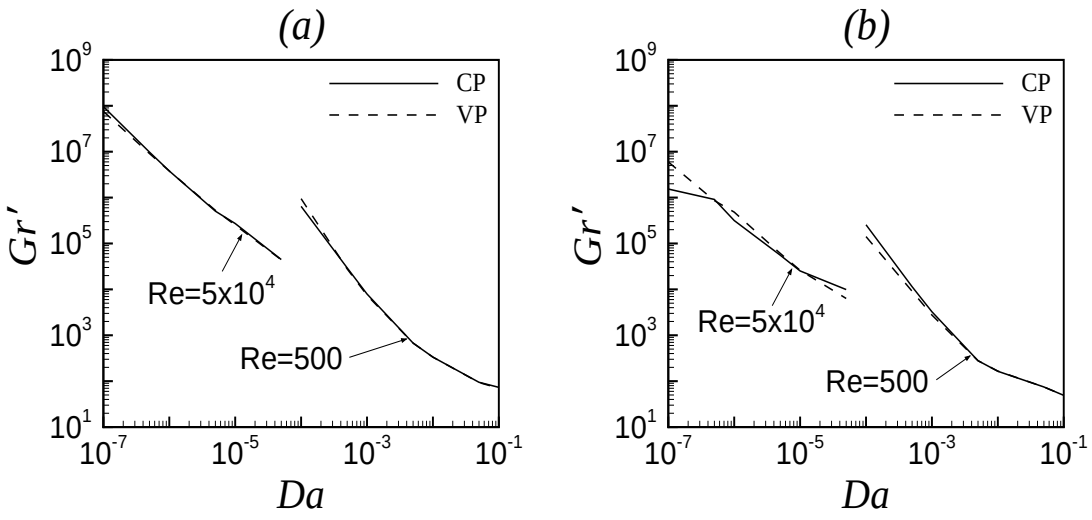

Figure 2.18: Variation of critical Gr' for constant porosity (CP) and variable poristy (VP) for (a) $Pr = 7$, and (b) $Pr = 70$ using Carman-Kozeny relation.

For case (ii), the well known expression relating the permeability of a porous medium with its porosity called as Carman-Kozeny relation, i.e., $K = D_\rho^2 \varepsilon^3 / 180(1-\varepsilon)^2$ has been used. Here, K is permeability of the medium, ε is porosity, and D_ρ depends on the integration of the density function for the distribution of particle diameters. The above relation is found to give satisfactory results when the porous medium is filled with particles of approximately spherical shape and whose diameters fall within a narrow range [76]. To analyse the effect of varying porosity figure 2.18 is plotted for a relatively high and a low permeable porous medium at *Re* equal to 500 and 50000, respectively. As can be seen from the above figure that the instability curves for VP and CP in (Da, Gr') plane almost merge on each other when $Pr = 7$. However the difference between both curves for $Pr = 70$ is more as compared to $Pr = 7$. It is also true for low permeable situation (LP) under Darcy model (figure not shown). As it has been observed in figure 2.16 that the critical values of ΔT across the channel width for relatively high permeable porous medium, i.e., when *Da* is equal to $10^{-2}, 10^{-3}$ and 10^{-4} are well within the Boussinesq limit. But the same for relatively low permeable porous medium, i.e., when *Da* is equal to $10^{-5}, 10^{-6}$ and 10^{-7} is not true. This shows that the basic flow is linearly stable as far as Boussinessq approximation holds. The

length of half width of the channel or permeabilty required for validity of the Boussinesq approximation is very high which is not feasible in realistic problems. Thus, the finite amplitude analysis by deriving a cubic Lanadu equation in the next section is carried out only for Da equal to $10^{-2}, 10^{-3}$ and 10^{-4}.

Some remarks:

Linear stability results for relatively high permeable porous medium show that the basic flow becomes unstable under mild heating conditions such that the Boussinesq approximation holds. The half width of the channel required for fully developed mixed convection flow to become unstable is 2cm, 4cm and 16cm when $Da = 10^{-2}, 10^{-3}$ and 10^{-4}, respectively. In the case of $Pr = 7$ the basic flow contains point of inflection when the flow is linearly unstable but in the case of $Pr = 70$ it is true only upto a certain value of Re. The above results are produced by keeping the porosity fixed. But, the variation of porosity and permeability by using the Carman-Kozeny relation showed negligible change in the linear instabilty boundaries. The byouant instabililty is the dominant mode of instability and the major part of dissipation in the whole domain of Re is due to surface drag.

Chapter 3

Linear stability of mixed convection flow in differentially heated vertical channel filled with porous-medium under LTNE state

The linear instability of parallel flow induced by external pressure gradient and buoyancy force in a differentially heated vertical channel filled with a fluid-saturated porous medium under local thermal non-equilibrium state is analyzed. This study is conducted to get a better perspective of how two different theories, namely local thermal equilibrium and local thermal non-equilibrium, of transfer of energy between solid and fluid phases inside the porous medium affect the instability of the considered flow. The interphase heat transfer coefficient (H) and porosity scaled thermal conductivity ratio of fluid and solid phases (γ) are new parameters in LTNE state whose effects are analyzed.

The objective of the present study is to analyze the stability characteristics of PMCF in a differentially heated channel filled with high permeable porous medium under LTNE state for fluids such as air and water. This analysis will be carried out in terms of interphase heat transfer coefficient (H) and porosity scaled thermal conductivity ratio (γ). Also,

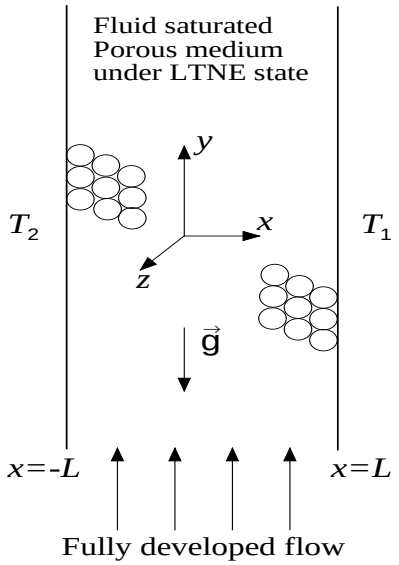

Figure 3.1: Schematic of the physical problem.

we want to find the appropriate non-isothermal parameter space as a function of Prandtl number, Reynolds number and Forchheimer number in which the parallel flow will remain stable, and identify the type of instability through energy analysis.

3.1 Mathematical model

3.1.1 Problem definition and governing equations

The flow investigated in this paper is mixed convection in a long vertical channel of width $2L$ and filled with fluid saturated porous medium. It is driven by an external pressure gradient and buoyancy force due to a constant temperature difference between the two channel walls. The right wall at $x = L$ and the left wall at $x = -L$ are maintained at constant temperatures T_1 and T_2 ($T_1 > T_2$) respectively, as shown in Figure 3.1. It is assumed that the fluid and porous medium are in local thermal non-equilibrium state, the porous medium

is homogeneous and hydro-dynamically as well as thermally isotropic, and the fluid is incompressible. The thermo-physical properties of the fluid are assumed to be constant except for the density dependence of the buoyancy term in the momentum equation which is satisfied by the Boussinesq approximation, i.e., density varies linearly with temperature as $\rho = \rho_f[1-\beta_T(T-T_0)]$, where $T_0 = (T_1+T_2)/2$. The gravitational force is aligned in the negative y-direction. Following Nield and Bejan [76] and our work in LTE case, the volume averaged Navier-Stokes (VANS) equation derived by Whitaker [123] is used as the momentum balance equation and the evolution of temperature fields of the fluid and solid phases of a rigid porous medium are given by two separate equations interconnected by interphase heat transfer coefficient.

The non-dimensional space coordinates (x^*, y^*, z^*), dependent variables $(\mathbf{v}^*, \theta, P^*)$ and time t^* are calculated after scaling the dimensional variables as follows:

$$\left.\begin{aligned} (x^*,y^*,z^*) = \frac{(x,y,z)}{L},\ \ \mathbf{v}^* = \frac{\mathbf{v}}{\overline{V}_0},\ \ \theta_f = (T_f - T_0)/(T_1 - T_2), \\ \theta_s = (T_s - T_0)/(T_1 - T_2),\ \ P^* = \frac{P}{\rho_f \overline{V}_0^2},\ \ t^* = \frac{t\overline{V}_0}{L} \end{aligned}\right\}, \tag{3.1}$$

where, $\mathbf{v}^* = (u^*, v^*, w^*)$, θ_f, θ_s, P^* and t^* are the dimensionless Darcy velocity vector, fluid temperature, solid porous matrix temperature, pressure and time, respectively. Furthermore, $\overline{V}_0$ and ρ_f are dimensional average basic velocity (bulk velocity) and fluid density, respectively.

After dropping asterisk, the non-dimensional governing equations can be written as

$$\nabla.\mathbf{v} = 0, \tag{3.2}$$

$$\frac{1}{\varepsilon}\frac{\partial \mathbf{v}}{\partial t} + \frac{1}{\varepsilon^2}(\mathbf{v}.\nabla)\mathbf{v} + F\mathbf{v}|\mathbf{v}| = -\nabla P + \frac{\lambda}{Re}(\nabla^2\mathbf{v}) - \frac{1}{DaRe}\mathbf{v} + \frac{Gr}{Re^2}\theta\hat{e}_y, \tag{3.3}$$

$$\frac{\partial \theta_f}{\partial t} + \frac{1}{\varepsilon}(\mathbf{v}.\nabla)\,\theta_f = \frac{1}{PrRe}(\nabla^2\theta_f) + \frac{H}{PrRe}(\theta_s - \theta_f), \tag{3.4}$$

$$\Gamma\frac{\partial \theta_s}{\partial t} = \frac{1}{PrRe}(\nabla^2\theta_s) + \frac{H\gamma}{PrRe}(\theta_f - \theta_s). \tag{3.5}$$

Here, subscripts f and s attached to variables refer to fluid and solid properties. In the above equations Gr, Pr, Da, Re, F, H, Γ and γ are Grashof number, Prandtl number, Darcy number, Reynolds number, Forchheimer number, interphase heat transfer coefficient, ratio of thermal diffusivities of fluid and solid phases, and porosity scaled thermal conductivity ratio of fluid and solid phases respectively. They are defined as

$$Gr = \frac{g\beta_T(T_1 - T_2)L^3}{\nu^2},\ Pr = \frac{\nu}{\alpha_f},\ Da = \frac{K}{L^2},\ Re = \frac{\overline{V}_0 L}{\nu},\ F = \frac{C_F L}{|K|^{1/2}},$$
$$H = \frac{hL^2}{\varepsilon k_f},\ \Gamma = \frac{\alpha_f}{\alpha_s},\ \text{and}\ \gamma = \frac{\varepsilon k_f}{(1-\varepsilon)k_s}. \tag{3.6}$$

Furthermore, g, $\hat{e}_y$, K, β_T, ν, ε, C_F, h, k_f, k_s, α_f, α_s denote the acceleration due to gravity, unit vector along y-direction, permeability of the porous medium, volumetric thermal expansion coefficient, kinematic viscosity, porosity, dimensionless form-drag constant, dimensional interphase heat transfer coefficient, thermal conductivity of the fluid, thermal conductivity of the solid, thermal diffusivity of the fluid, and thermal diffusivity of the solid phase, respectively. Also, λ is the ratio of effective viscosity to fluid viscosity $(\tilde{\mu}/\mu_f)$. Again, different values have been reported for $\tilde{\mu}$ in the literature [43, 55] leading to a λ other than unity. However, in the absence of any specific measured value, in this study $\lambda = 1$ has been taken.

3.1.2 Parallel mixed convective flow: Basic state

The basic flow whose stability analysis is going to be carried out is steady, fully developed, and one dimensional, i.e., PMCF. Under these conditions the governing equations (3.2)-(3.4) are simplified into following coupled ordinary differential equations.

$$\frac{d^2V_0}{dx^2} - \frac{1}{Da}V_0 + Gr'\Theta_f - F'|V_0|V_0 = Re\frac{dP_0}{dy}, \tag{3.7}$$

$$\frac{d^2\Theta_f}{dx^2} + H(\Theta_s - \Theta_f) = 0. \tag{3.8}$$

$$\frac{d^2\Theta_s}{dx^2} + H\gamma(\Theta_f - \Theta_s) = 0. \tag{3.9}$$

where, V_0, Θ_f, Θ_s, and P_0 are the basic velocity, basic fluid temperature, basic solid phase temperature and basic pressure, respectively. Here, $F' = FRe$ and $Gr' = Gr/Re$. The boundary conditions for the above basic state equations are given as:

$$V_0 = 0 \text{ at } x = \pm 1, \ \Theta_f = \Theta_s = \pm 1/2 \text{ at } x = \pm 1. \tag{3.10}$$

To solve the equations (3.7)-(3.10), the axial pressure gradient is determined using the global mass conservation,

$$\int_{-1}^{1} V_0 dx = 2. \tag{3.11}$$

Similar to the LTE case the above basic flow can be solved in three different cases: (i) for Darcy flow, i.e., dropping the second order derivative and quadratic terms in the momentum equation, (ii) for Darcy-Brinkman flow without form drag, i.e., $F = 0$, and, (iii) for Darcy-Brinkman flow with form drag. The basic temperature for all the three cases is given by

$$\Theta_f = \Theta_s = x/2. \tag{3.12}$$

Thus, the basic flow velocity functions for the first two cases are same as the LTE case as given below,

$$V_0 = \begin{cases} Gr'Da\left(\dfrac{x}{2}\right) + 1; & \text{(Darcy flow)} \\ s\left(1 - \dfrac{cosh(mx)}{cosh(m)}\right) + \dfrac{Gr'Da}{2}\left(x - \dfrac{sinh(mx)}{sinh(m)}\right); & \text{(when } F = 0\text{)} \end{cases} \tag{3.13}$$

where, $m = \dfrac{1}{\sqrt{Da}}$ and $s = m\left(\dfrac{sinh(2m)}{m(sinh(2m)) - cosh(2m) + 1}\right)$. However, in the third case, the basic flow velocity is obtained numerically using spectral method by solving equation (3.7) along with equations (3.10)-(3.12). The basic velocity and basic temperature functions in both LTE and LTNE cases are found to be equal. Similar to the LTE case, here also it is expected that the point of inflection in the velocity profile is a potential for instability of the basic flow. Hence, its linear stability analysis is carried out further through the use of normal modes.

3.2 Temporal linear stability

The linear stability of the above basic flow is investigated by imposing an infinitesimal disturbance on it. So, the field variables are split into the basic state and an infinitesimal disturbance, as

$$(\mathbf{v}, \theta_f, \theta_s, P) = (V_0(x)\hat{e}_y, \Theta_f(x), \Theta_s(x), P_0(y)) + (\mathbf{v}', \theta', p'). \tag{3.14}$$

These infinitesimal disturbances of corresponding field variables are separated into the normal mode form[32] as,

$$(\mathbf{v}', \theta_f', \theta_s', p') = (\hat{\mathbf{v}}(x), \hat{\theta}_f(x), \hat{\theta}_s(x), \hat{p}(x))e^{i(\alpha y+\beta z-\alpha ct)}, \tag{3.15}$$

where, α and β are the wavenumbers in streamwise and spanwise directions respectively, and $c = c_r + ic_i$ is a complex wave speed. The sign of c_i determines the growth or decay of the disturbances, i.e., the disturbances are classified as stable, neutrally stable, or unstable depending on whether $c_i < 0$, $c_i = 0$, or $c_i > 0$, respectively. On substituting the equations (3.14) and (3.15) into the governing equations (3.2)-(3.4), and subtracting the equations (3.7)-(3.9), the linear equations for the infinitesimal disturbances are obtained which are given as,

$$\frac{d\hat{u}}{dx} + i\alpha\hat{v} + i\beta\hat{w} = 0, \tag{3.16}$$

$$i\alpha Re\frac{1}{\varepsilon}\left(\frac{1}{\varepsilon}V_0 - c\right)\hat{u} + Re\frac{d\hat{p}}{dx} - \lambda\left(\frac{d^2\hat{u}}{dx^2} - (\alpha^2+\beta^2)\hat{u}\right) + \frac{1}{Da}\hat{u} + F'|V_0|\hat{u} = 0, \tag{3.17}$$

$$i\alpha Re\frac{1}{\varepsilon}\left(\frac{1}{\varepsilon}V_0 - c\right)\hat{v} + Re\frac{1}{\varepsilon^2}\frac{dV_0}{dx}\hat{u} + i\alpha Re\hat{p} - \lambda\left(\frac{d^2\hat{v}}{dx^2} - (\alpha^2+\beta^2)\hat{v}\right) + \frac{1}{Da}\hat{v} + 2F'|V_0|\hat{v} - Gr'\hat{\theta} = 0, \tag{3.18}$$

$$i\alpha Re\frac{1}{\varepsilon}\left(\frac{1}{\varepsilon}V_0 - c\right)\hat{w} + i\beta Re\hat{p} - \lambda\left(\frac{d^2\hat{w}}{dx^2} - (\alpha^2+\beta^2)\hat{w}\right) + \frac{1}{Da}\hat{w} + F'|V_0|\hat{w} = 0, \tag{3.19}$$

$$\frac{1}{\varepsilon}\frac{d\Theta_f}{dx}\hat{u}+i\alpha(\frac{V_0}{\varepsilon}-c)\hat{\theta}_f-\frac{1}{PrRe}\left(\frac{d^2\hat{\theta}_f}{dx^2}-(\alpha^2+\beta^2)\hat{\theta}_f\right)-\frac{H}{PrRe}(\theta_s-\theta_f)=0, \quad (3.20)$$

$$-\Gamma ic\alpha\hat{\theta}_s-\frac{1}{PrRe}\left(\frac{d^2\hat{\theta}_s}{dx^2}-(\alpha^2+\beta^2)\hat{\theta}_s\right)-\frac{H\gamma}{PrRe}(\theta_f-\theta_s)=0, \quad (3.21)$$

and, after eliminating the pressure we get,

$$\begin{aligned}\frac{d^4\hat{u}}{dx^4}-2(\alpha^2+\beta^2)\frac{d^2\hat{u}}{dx^2}+(\alpha^2+\beta^2)^2\hat{u}+i\alpha Re\frac{1}{\varepsilon^2}\frac{d^2V_0}{dx^2}\hat{u}+i\frac{\alpha\beta}{\alpha^2+\beta^2}F'\frac{d}{dx}(|V_0|\hat{\eta})\\+\left(i\alpha cRe\frac{1}{\varepsilon}-\frac{1}{Da}-i\alpha Re\frac{1}{\varepsilon^2}V_0\right)\left[\frac{d^2\hat{u}}{dx^2}-(\alpha^2+\beta^2)\hat{u}\right]+(\alpha^2+\beta^2)F'|V_0|\hat{u}\\-F'\left(\frac{\alpha^2}{\alpha^2+\beta^2}+1\right)\frac{d}{dx}\left(|V_0|\frac{d\hat{u}}{dx}\right)-i\alpha Gr'\frac{d\hat{\theta}}{dx}=0, \quad (3.22)\end{aligned}$$

$$\begin{aligned}\beta Re\frac{1}{\varepsilon^2}\frac{dV_0}{dx}\hat{u}+i\frac{\alpha\beta}{\alpha^2+\beta^2}F'|V_0|\frac{d\hat{u}}{dx}-\beta Gr'\hat{\theta}-\left(\frac{d^2\hat{\eta}}{dx^2}-(\alpha^2+\beta^2)\hat{\eta}\right)+\frac{1}{Da}\hat{\eta}\\+i\alpha Re\frac{1}{\varepsilon}\left(\frac{1}{\varepsilon}V_0-c\right)\hat{\eta}+\left(\frac{\beta^2}{\alpha^2+\beta^2}+1\right)F'|V_0|\hat{\eta}=0, \quad (3.23)\end{aligned}$$

$$\frac{1}{\varepsilon}\frac{d\Theta_f}{dx}\hat{u}+i\alpha(\frac{V_0}{\varepsilon}-c)\hat{\theta}_f-\frac{1}{PrRe}\left(\frac{d^2\hat{\theta}_f}{dx^2}-(\alpha^2+\beta^2)\hat{\theta}_f\right)-\frac{H}{PrRe}(\theta_s-\theta_f)=0, \quad (3.24)$$

$$-\Gamma ic\alpha\hat{\theta}_s-\frac{1}{PrRe}\left(\frac{d^2\hat{\theta}_s}{dx^2}-(\alpha^2+\beta^2)\hat{\theta}_s\right)-\frac{H\gamma}{PrRe}(\theta_f-\theta_s)=0, \quad (3.25)$$

where, $\hat{\eta}=\beta\hat{v}-\alpha\hat{w}$. Boundary conditions on the velocity as well as temperature perturbations are applied at both walls. The velocity perturbation satisfy the no-slip condition at the walls and the temperature perturbation satisfy the isothermal condition at the walls, i.e.,

$$\hat{u}=\frac{d\hat{u}}{dx}=\hat{\theta}_f=\hat{\theta}_s=\hat{\eta}=0 \text{ at } x=\pm 1. \quad (3.26)$$

These equations form a generalized eigenvalue problem with complex disturbance wavespeed as the eigenvalue.

3.2.1 Disturbance kinetic energy balance

As pointed out by Hart [46] the driving mechanisms of flow instability may be determined by the production and dissipation of disturbance kinetic energy (KE). Therefore, to ascertain the role played by heat transfer during the flow instability, it is necessary to keep track of KE. The balance of KE is given as,

$$\begin{aligned} Re\frac{1}{\varepsilon}\frac{\partial}{\partial t}\left\langle \frac{1}{2}(u'^2+v'^2+w'^2)\right\rangle &= -Re\frac{1}{\varepsilon^2}\left\langle u'v'\frac{dV_0}{dx}\right\rangle + Gr'\left\langle v'\theta'\right\rangle - F'\left\langle |V_0|(u'^2+2v'^2+w'^2)\right\rangle \\ &\quad -\frac{1}{Da}\left\langle (u'^2+v'^2+w'^2)\right\rangle - \left\langle (\nabla u')^2+(\nabla v')^2+(\nabla w')^2\right\rangle \\ &= E_s+E_b+E_F+E_D+E_d \end{aligned} \tag{3.27}$$

where, the symbol <> imply integration over the volume: $[-1,1]\times[0,2\pi/\alpha]\times[0,2\pi/\beta]$ of the disturbance cell. The integrals in above equation can be evaluated using the eigenvectors from the linear stability analysis. On the curve of neutral stability, the disturbances neither grow nor decay, and the left-hand side of (3.27) is zero. The first term on the right-hand side represents the gain (loss) of the KE from(to) the mean flow through Reynolds stress, referred to as shear production (destruction), represented as E_s. The second term represents the production of KE through work done by the fluctuating body force, and is the buoyant production term (E_b). The third term (E_F) represents the dissipation of KE due to form drag. The fourth term (E_D) represents the dissipation of KE energy due to work done by surface drag. The last term (E_d) represents the dissipation of energy due to viscous effects. Therefore, the equation (3.27) represents a balance of the production of KE by buoyant and shear mechanism with the dissipation of KE by surface drag, form drag, and viscous action. Since, at the critical level, the sum of all KE components must be equal to zero, therefore the relative error in kinetic energy balance is defined by $\delta_K = \dfrac{|E_s+E_b+E_D+E_F+E_d|}{|E_s+E_b|}$. For all the calculations presented in the following study δ_K is less than 3%.

3.3 Numerical method

The system of differential equations along with their boundary conditions in this paper are discretized in the interval $[-1,1]$ along x-direction at Gauss-Lobatto points by implementing the Chebyshev spectral collocation method [18] that uses Chebyshev polynomials as the basis functions. The collocation points are selected to be the extrema of the Nth-order Chebyshev polynomial so that the truncation error is minimized. The Gauss-Lobatto points of Nth-order Chebyshev polynomial are given as,

$$x_j = cos\left(\frac{\pi j}{N}\right), \tag{3.28}$$

where, $j = 0,1,2,\ldots N$ and N represents order of the base polynomial. The linear disturbance equations (3.22)-(3.25) along with homogeneous boundary conditions (3.26) are formulated as a generalized eigenvalue problem in the form

$$\mathbf{A}X = c\mathbf{B}X, \tag{3.29}$$

where, c is the complex eigenvalue, X is the representation of the eigenfunction, and $\mathbf{A}$ and $\mathbf{B}$ are the square complex matrices of order $3N+3$, where N represents order of the base polynomial in the collocation method. The eigenvalues of the above system are determined using the complex QZ algorithm [71] inbuilt in MATLAB.

The numerical code developed for the LTE condition is extended for the present problem by including the LTNE effects. Due to lack of numerical or experimental work in this direction it is difficult to match the present results with special case of any published work. However, the validation of our numerical code is carried out in two different ways. First, by performing a grid independence test of the least stable eigenvalue for the mixed convection flow in a porous medium. Second, by ensuring that the balance of disturbance kinetic energy at the critical level must be zero.

The convergence of the numerical scheme is checked by varying the number of terms in the Chebyshev collocation method. Table 3.1 shows that the least stable eigenvalue achieve 6-digit point accuracy with 51 terms at randomly selected values for various parameters. The results remain consistent with increase in number of terms. The same trend

N	Least stable eigenvalue
30	0.0000018550 - 0.0006378001i
40	0.0000018460 - 0.0006377899i
50	0.0000018163 - 0.0006385373i
51	0.0000018156 - 0.0006385384i
55	0.0000019819 - 0.0006383742i

Table 3.1: Convergence of the least stable eigenvalue by Chebyshev collocation method. Here, Pr=7, Re=1000, Gr'=5000, F'=1000, $Da = 10^{-3}$, ε=0.9, α=1, β=0, H=100, $\gamma =$ 0.01.

is observed with other values of parameters. It is observed that 51 terms of Chebyshev polynomials, i.e. $N = 51$, are usually sufficient to perform the numerical calculations with high accuracy. The final check is made by calculating energy growth rate around the critical point for a set of randomly chosen parameters, which is discussed in fig 3.2. It is clear from this figure that the growth rate of disturbance kinetic energy is negative when Gr' is less than its critical value (i.e., 6761) and equal to zero at the critical value. However, as the value of Gr' is increased further the growth rate becomes positive. This is true for other set of parameters also. The critical values of parameters thus obtained through linear stability analysis are used in the following section.

3.4 Results and discussion

It is to be noted that the basic flow (PMCF) under LTNE state is independent of the Prandtl number. The role played by Prandtl number in the stability of non-isothermal flow under LTE state has already been examined. As we have observed that the role of Pr in the stability of PMCF under LTE state is significant. So, the same is expected under LTNE state also. The present work intends to offer a comprehensive account of linear stability analysis of parallel mixed convective flow (PMCF) in a differentially heated vertical channel filled with fluid saturated high permeable porous medium under local thermal non-equilibrium state. Accordingly, the following analysis is made when the channel is filled with metallic

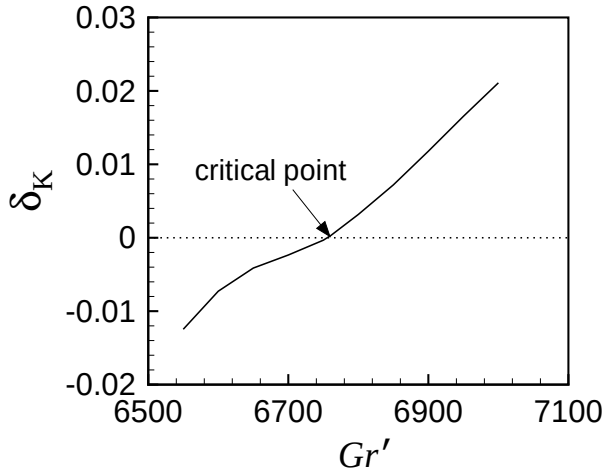

Figure 3.2: δ_K as a function of Gr' for $Pr = 7$ when Re = 1000, Da = 10^{-3}, F' = 1000, H=100 and $\gamma = 0.01$.

foam or any other porous medium having permeability in the range of 10^{-8}m^2 to 10^{-6}m^2 in SI unit with porosity of 0.9. Rigorous numerical computations reveal that the least stable mode is two-dimensional and spanwise independent. Thus, the linear stability boundaries are plotted for $\beta = 0$. This is in agreement with the results obtained while studying the linear stability of this mixed convection flow under LTE state as well as in the case of vertical channel with linearly varying wall temperature under LTNE state [9].

We have already studied this problem under LTE state where special attention was given on the influence of Prandtl number on instability mechanism of the flow. The results were presentd for a wide range of Pr to describe the effect of important parameters related to the porous medium such as Darcy number and modified Forchheimer number on the instability boundary. Now, we are interested to study the effect of LTNE state by considering the same range of parameters for Pr, Da, F' and Re. So, the range for parameters such as Pr,Re and F' considered in this study are [10^{-2}, 10^3], [100, 5000] and [0, 5×10^3], respectively. Three different values $(10^{-2}, 10^{-3}, 10^{-4})$ of Darcy number are chosen to depict high permeable porous medium. Due to the assumption of LTNE state

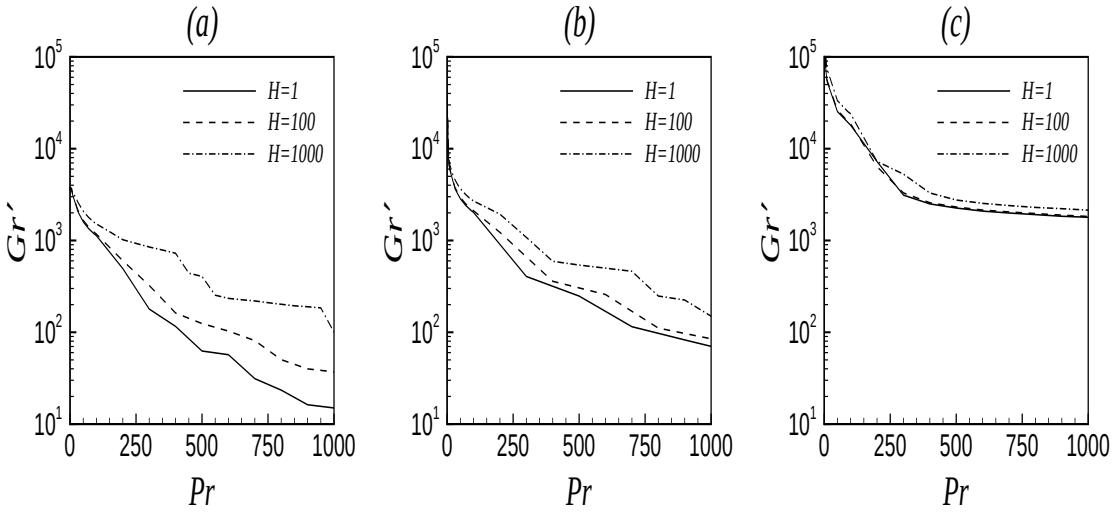

Figure 3.3: Variation of critical Gr' as function of Pr for (a) $Da = 10^{-2}$ and (b) $Da = 10^{-3}$ and (c) $Da = 10^{-4}$ when $\gamma = 0.01$, $Re = 1000$ and $F' = 1000$.

two new parameters are included namely H and γ. The practical values of these parameters for mixed convection and forced convection problems can vary in the range $[1, 10^3]$ for H and $[10^{-3}, 10^{-1}]$ for γ. The results are described using stability boundaries formed by critical modified Grashof number and wave numbers with respect to Prandtl number, Reynolds number, modified Forchheimer number, interphase heat transfer coefficient and porosity scaled thermal conductivity ratio of fluid and solid phases.

3.4.1 Influence of Prandtl number

To understand the relative influence of momentum diffusivity and thermal diffusivity on the instability boundary points, we have discussed about the instability boundary as a function of Pr. The instability boundary curves in (Pr, Gr') and (Pr, α) planes are shown in Figure 3.3. From our numerical experiments we have observed that γ has very little impact on the instability boundary with respect to Pr for a given value of other parameters. So, we have fixed the value of γ equal to 10^{-2} considering the other parameteric values. Several important observations can be made form the above figure. First, as in the case of LTE state, here also the instability boundary decreases monotonically with Pr and the rate of decrease

of critical Gr' decreases as the value of Pr is increased. This is true for all the considered values of H. Second, for a given value of Da, the interphase heat transfer coefficient has a stabilizing effect on the instability of the flow. As the value of H is changed from 1 to 100, the variation in instability boundary is negligible up to a certain value of Pr beyond which a significant variation can be seen. When H is increased further up to 1000 then the critical Gr' is much higher as compared to case $H = 1$ or 100. The relative change in critical Gr' as a function of H for $Da = 10^{-2}$ is higher than the same for $Da = 10^{-3}$ or 10^{-4} which shows that the impact of local thermal non-equilibrium state is relatively higher in high permeable porous medium.

The instability mechanism in the above figure can be best understood by recalling the definition of Prandtl number and interphase heat transfer coefficient. Also, from the governing equations, we see that the strength of momentum and thermal diffusions is measured by $(Re)^{-1}$ and $(RePr)^{-1}$, respectively. So, the Prandtl number signifies the relative strength of momentum and thermal diffusions. In general a low value of Pr causes an increase in the thermal diffusivity which itself suppresses the thermal fluctuations in the flow field. As a result, the flow remains stable even for larger values of Gr'. From the instability boundary curve we have observed that when the Prandtl number is of $O(1)$ then the thermal fluctuations quickly smooth out and all the least stable modes are induced by kinetic disturbances. This results in a rapid change in the critical value of Gr' up to a threshold value of Pr. But, with an increase in the value of Pr the corresponding relative momentum diffusivity increases and becomes a deciding factor in the instability characteristic of the flow. Also, an increase in the value of Pr increases the interaction between the porous substance and the fluid particles resulting in the reduced flow strength in the channel. So, beyond the above mentioned threshold value of Pr, a smooth and slow decreasing profile of instability boundary curve is expected. This explains the monotonic decrease in the critical Gr' as a function of Pr.

When other parameters along with Da are fixed, increasing the value of H increases

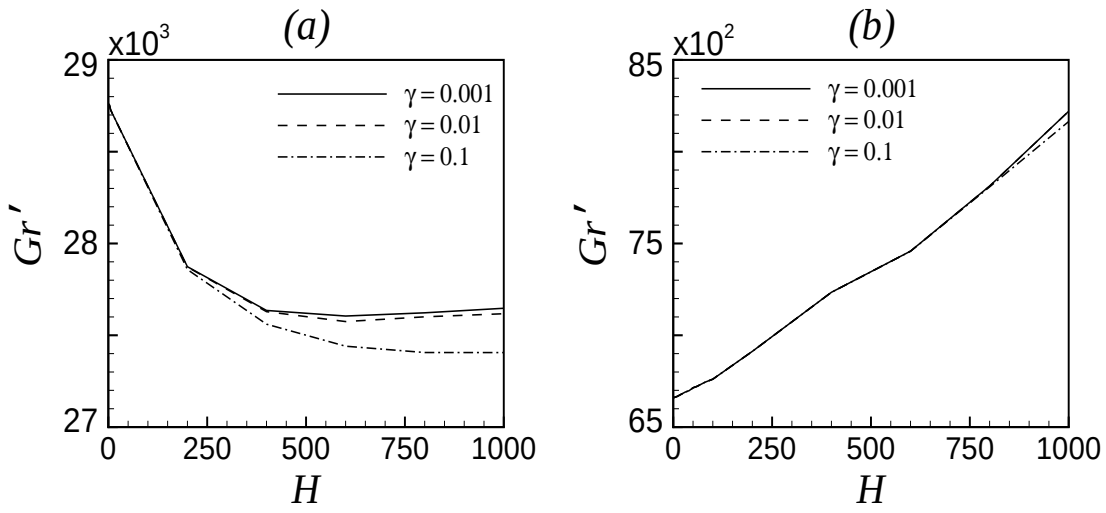

Figure 3.4: Variation of critical Gr' as function of H for (a) $Pr = 0.7$ and (b) $Pr = 7$ when $Da = 10^{-3}$, $Re = 1000$ and $F' = 1000$.

the interphase heat transfer coefficient. Due to this increase in the value of H the temperature distribution in the flow evens out and the flow tends toward local thermal equilibrium (LTE) state. Of course the rate at which this phenomenon takes place is a function of other paramters, especially, Darcy number. As the temperature distribution of solid and fluid phases gradually tends to local thermal equilibrium state on increasing the value of H, the thermal fluctuations due to infinitesimal disturbances decay which in turn makes the flow more stable. That is why the instability boundary curve for higher value of H is above the instability boundary curve for lower value of H for a given Da in the above figure. The above phenomena is also observed by Bera and Khandelwal [9] while studying the instability mechanism of non-isothermal Poiseuille flow in a vertical channel filled with porous-medium with linearly varying wall temperature.

To shed more light on the effect of H on the instability boundary figure 3.4 is plotted for two different types of fluid: air and water. It can be seen from the above figure that the instability boundary has a different trend for these fluids. For air, the instability boundary decreases monotonically with H, whereas for water the same increases monotonically with H. But the effect of γ is more significant for lower Prandtl number fluid such as air and

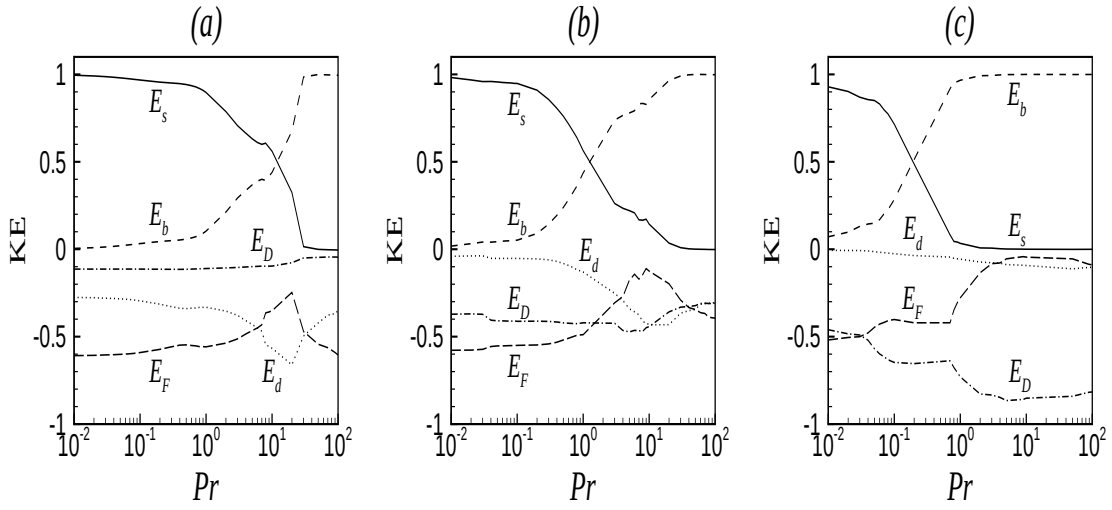

Figure 3.5: KE spectrum as a function of Pr under LTNE state for (a) $Da = 10^{-2}$ and (b) $Da = 10^{-3}$ and (c) $Da = 10^{-4}$ when $H = 1000$, $\gamma = 0.01$, $Re = 1000$ and $F' = 1000$.

the deviation in instability boundaries for different values of γ start to occur as early as $H = 200$. In the case of higher Pr such as water slight deviation can be observed at higher values of H. On increasing the value of γ for a fixed value of H there is a reduction in the conductivity of the solid porous material. This results in an increased fluid temeprature which in turn enhances the fluid velocity. Thus, the flow becomes more unstable.

To gain a further insight into the instability mechanism of the parallel mixed convective flow under LTNE state, the balance of disturbance kinetic energy as a function of Pr is shown in figure 3.5(a) to 3.5(c). The above figure is plotted at the critical level when $H = 1000$ and $\gamma = 10^{-2}$. Similar to the LTE state, here also we encounter three different types of instabilities namely shear, mixed and buoyant defined on the basis of contribution of energy production (or, destruction) by shear term (E_s) and buoyant term (E_b). If in the disturbance kinetic energy balance, contribution of E_s (E_b) is more than 70% then the type of instability is defined as thermal-shear (thermal-buoyant) else it is defined as interactive. Similar to the LTE state, here also, the type of instability for lower values of Pr is shear. At higher values of Pr the type of instability is buoyant. In between this two extremes there exists a mixed type of instability. But the range of Pr in which these three different types

of instabilities exist depends on the value of Da and other parameters. For $Da = 10^{-2}$ the shear instability is a dominant mode of instability in a larger range of Pr as compared to $Da = 10^{-3}$ and 10^{-4}, whereas for $Da = 10^{-4}$ the buoyant instability is dominant mode of instability in most of the domain of Pr. The range of Pr in which these types of instabilities occur for different values of Da is as follows. For $Da = 10^{-2}$, the different range for shear, mixed and buoyant instabilities are $0.01 \leq Pr < 3$, $3 \leq Pr < 20$ and $20 \leq Pr \leq 100$, respectively. For Da^{-3}, they are $0.01 \leq Pr < 0.6$, $0.6 \leq Pr < 3$ and $3 \leq Pr \leq 100$, respectively. Also, for Da^{-4}, they are $0.01 \leq Pr < 0.1$, $0.1 \leq Pr < 0.3$ and $0.3 \leq Pr \leq 100$, respectively. Thus, the range of Pr in which shear instability is dominant has increased for all considered values of Da due to local thermal non-equilibrium effect.

3.4.2 Influence of Reynolds number

We have observed from figure 3.4 that the higher values interphase heat transfer coefficient can have significant effect on the instability of the flow. But, it was seen only for $Re = 1000$. Figure 3.6 is plotted to show the effect of interphase heat transfer coefficient for the complete range of Re. In this section also we checked the instability boundary curves for all the three values $10^{-1}, 10^{-2}$ and 10^{-3} of γ. But the effect of γ on the istability curves, for different values of Pr, with respect to Re was found to be negligible. So, the value of γ is fixed at 10^{-2}. The values of F' and Da are also fixed at 10^3 and 10^{-3}, respectively. Figure 3.6 shows the variation of instability boundary in (Re, Gr')-plane when $\gamma = 0.01$, $Da = 10^{-3}$ and $F' = 1000$. Similar to the LTE state, here also the instability boundary curves for different values 1,100,1000 of H in (Re, Gr')-plane shows a rapid decrease in critical Gr' as Re is increased from very small value to a threshold value. However, as Re is increased beyond this threshold value the rate of decrease in Gr' is gradual and negligible. As we have already observed in the previous section that higher value of H renders the flow more stable. So, when the value of H increases from 1 to 100 the flow becomes more stable and a significant change can be observed in the instability boundary curve when H is changed to 1000. Moreover, the effect of H is significant in the case of $Pr = 7$ as compared

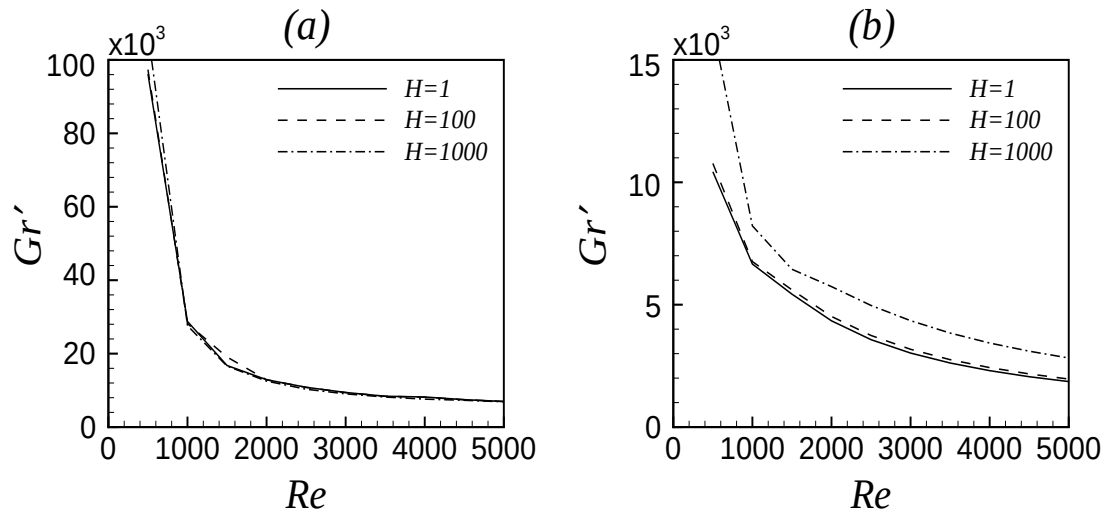

Figure 3.6: Variation of critical Gr' as function of Re for (a) $Pr = 0.7$ and (b) $Pr = 7$ when $Da = 10^{-3}$, $\gamma = 0.01$ and $F' = 1000$.

to $Pr = 0.7$. This can also be seen in the disturbance kinetic energy balance.

Figure 3.7 shows the disturbance KE balance w.r.t. Re for $Pr = 0.7$ and 7 when $H = 1000$ and $\gamma = 0.01$. Clearly, the balance of Re for $Pr = 0.7$ shows no change from the same under LTE state. But, when $Pr = 7$, it can be observed that the contribution of E_b has decreased whereas the contribution of E_s has increased by almost 10%. This may be the consequence of the fact that a fluid with higher value of Pr is more viscous in nature and hence it will generate higher internal shear stresses under mixed convection flow. These shear stresses will tend to destabilize the flow.

3.4.3 Influence of modified Forchheimer number

The results in previous two subsections were presented for a fixed value of F'. It is found that the point of inflection in the basic flow profile as well as back flow characteristic of the basic flow die out on incorporating the form drag in the momentum balance equation. So, it is important to study the role of inertia due to form drag which may play a significant role in the instability of the mixed convective flow under local thermal non-equilibriums state in porous medium [60]. We have already studied the influence of modified Forchheimer

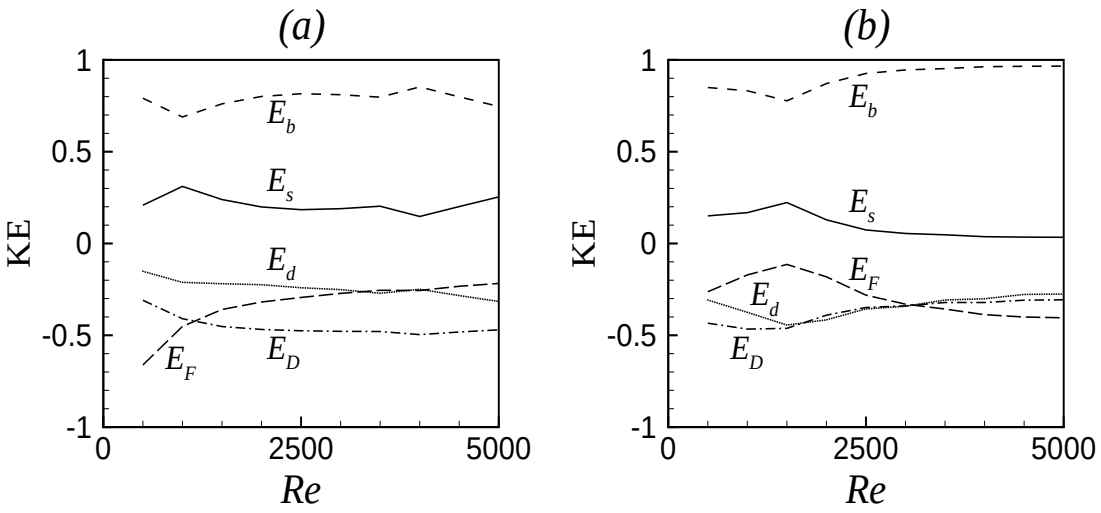

Figure 3.7: KE spectrum as a function of Re under LTNE state for (a) $Pr = 0.7$ and (b) $Pr = 7$ when $H = 1000$, $\gamma = 0.01$, $Da = 10^{-3}$ and $F' = 1000$.

number under LTE state. Although from the discussion in previous two subsections we know that H has a stabilizing effect on the considered flow. But, it may be interesting to see the effect of H when the form drag in the system is changed. So, we have plotted the variation of instability boundary w.r.t. F' in figure 3.8 for both fluids considered in this study when $\gamma = 0.01$, $Da = 10^{-3}$ and $Re = 1000$. For all the three values of H considered here, unlike the situtaion under LTE state, the effect of form drag for $Pr = 0.7$ is upto $F' = 10$ beyond which it is negligible. In the case of $Pr = 7$ the effect of form drag is similar to the LTE state. As expected, an increase in H increases the stability of the flow. This effect is more prominent for $Pr = 7$ and as the value of F' is increased the gap between the instability boundaries corresponding to different values of H tends to decrease. Since, the form drag itself has the tendency of stabilizing the flow. So, after a certain value of F', the effect of interphase heat transfer coefficient may not be significant.

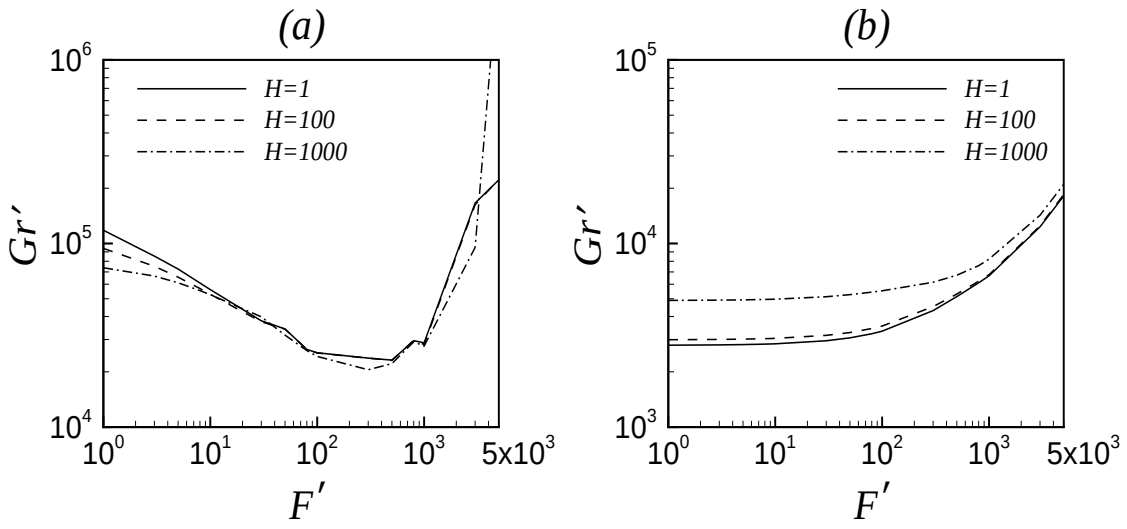

Figure 3.8: Instability boundaries in (F', Gr')-plane: *(a)* $Pr = 0.7$ and *(b)* $Pr = 7$ when $Da = 10^{-3}$, $\gamma = 0.01$ and $Re = 1000$.

3.5 Conclusion

We have analyzed the stability of parallel mixed convective flow (PMCF) under local thermal non-equilibrium state in a differentially heated vertical channel filled with incompressible fluid saturated porous medium. The entire study is made for a wide range of values of interphase heat transfer coefficient (H) and porosity scaled thermal conductivity ratio of fluid and solid phases (γ) to understand the effect of local thermal non-equilibrium state on the instability of flow.

The linear instability boundary shows that for a given value of Da, the interphase heat transfer coefficient has a stabilizing effect on the instability of the flow. The relative change in critical Gr' as a function of H for different values of Da shows that the impact of local thermal non-equilibrium state is relatively higher in the case of high permeable porous medium. The effect of γ on the istability of the flow was found to be negligible in almost all the cases. In comparison to local thermal equilibrium state, the disturbance kinetic energy balance at the critical level in local thermal non-equilibrium state showed that shear instability is dominant in larger range of Pr for all considered values of Da. For $Pr = 7$, the disturbance kinetic energy balance w.r.t. Re showed that the contribution

of E_b decreased whereas the contribution of E_s increased by almost 10% as compared to LTE state. The interphase heat transfer coefficient affects the instability of the flow when quadratic form drag is relatively low, i.e., up to $F' = 100$.

Chapter 4

Finite amplitude analysis of non-isothermal parallel flow in a vertical channel with linearly varying wall temperature and filled with porous medium

The finite amplitude analysis of stably stratified parallel mixed convection flow due to linearly varying wall temperature in vertical channel filled with porous medium has not been carried out yet. Thus, before studying the finite amplitude instability of the flow considered in Chapter 2, we consider the finite amplitude instability of stably stratified parallel mixed convection flow in a vertical channel filled with porous medium in this chapter. The objective of this study is to analyze the nature of bifurcation and the finite amplitude behavior of unstable disturbances that occur beyond the linear instability boundary, specially when the permeability of the medium and strength of the flow are reasonably high. This is accomplished by reviewing the linear stability results, and then a weakly nonlinear analysis is made to trace the evolution of finite amplitude perturbation. The linear stability analysis

is inadequate to describe the instabilities in the flow. It gives only the initial growth of the disturbance, but eventually it reaches such a size that Reynolds stresses (i.e., the mean force per unit area imposed on the mean flow by turbulent fluctuation) affect the mean flow and then it becomes difficult to explain the stability of the flow by linear theory. Nonlinear stability analysis gives some important information about size of disturbance and flow field that results from the linear instability. Here, we have developed a cubic Landau equation to analyze the nature of bifurcation and amplitude of most unstable wave beyond the critical value. Weakly nonlinear theories developed in [93, 100, 101, 127] have been shown to be very powerful tools for the analysis of stability of various flows. These nonlinear analyses are centered around the derivation of the Landau equation for the amplitude of disturbance wave. A cubic Landau equation is derived to study the limiting value of growth of instabilities under nonlinear effects. The nonlinear results are presented for air as well as water. The influence of nonlinear interaction of different superimposed waves on heat transfer rate, friction coefficient, nonlinear kinetic energy spectrum and disturbance flow is also studied in both supercritical as well as subcritical regimes. The effect of superimposed waves on the pattern of secondary flow, based on linear stability theory, is also studied.

4.1 Statement of the problem and governing equations

A pressure-driven non-isothermal flow in a vertical channel of width $2L$ filled with a porous medium is shown in figure 4.1. The wall temperature of the channel is assumed to vary linearly with y as $T_w = T_0 + Cy$, where C is a positive constant and T_0 is the upstream reference temperature. The gravitational force is aligned in the negative y-direction. The medium is assumed to be homogeneous and isotropic in permeability. The convective flow through the porous medium is governed by a non-Darcy model. The heat transfer equation is written under the assumption of local thermal equilibrium (LTE) state, i.e., the local temperatures of the fluid and solid phases are assumed to be identical. The thermophysical properties of the fluid are assumed to be constant except for density dependence

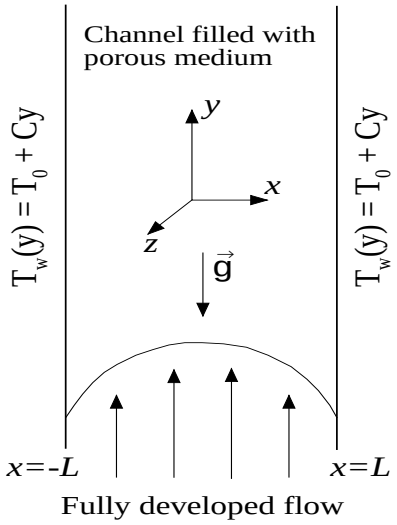

Figure 4.1: Schematic of the physical problem and coordinate system.

of the buoyancy term in the momentum equation, which is satisfied by the Boussinesq approximation. Since the flows through porous medium reveal inconsistencies in the usage of proper governing equations in the flow region, therefore a note on the considered model and consideration of different terms in the momentum equation for the present problem is made, which is given in Appendix A.

Following the discussion in above note, we consider non-Darcy volume averaged Navier-Stokes equations for the present theoretical investigation. The non-dimensionalized space coordinates (x^*, y^*, z^*), dependent variables $(\mathbf{v}^*, \theta, P^*)$ and time t^* are calculated after scaling the dimensional variables as follows:

$$\left.\begin{aligned}(x^*, y^*, z^*) = \frac{(x, y, z)}{L},\ \ \mathbf{v}^* = \frac{\mathbf{v}}{\overline{V}_0},\ \ \theta = \frac{(T - T_w)}{CLPrRe},\\ P^* = \frac{P}{\rho_f \overline{V}_0^2},\ \ t^* = \frac{t\overline{V}_0}{L}\end{aligned}\right\}, \tag{4.1}$$

where, $\mathbf{v}^* = (u^*, v^*, w^*)$, θ, P^* and t^* are the dimensionless Darcy velocity vector, temperature, pressure and time, respectively. Furthermore, $\overline{V}_0$ is dimensional average basic

velocity and ρ_f is fluid density. The dimensionless governing equations for continuity, momentum and energy, after dropping asterisks, can be written as

$$\nabla \cdot \mathbf{v} = 0, \tag{4.2}$$

$$\frac{1}{\varepsilon}\frac{\partial \mathbf{v}}{\partial t} + \frac{1}{\varepsilon^2}\mathbf{v}.\nabla\mathbf{v} + F\mathbf{v}|\mathbf{v}| = -\nabla P + \frac{Ra}{Re}\theta\mathbf{e_y} + \frac{\lambda}{Re}\nabla^2\mathbf{v} - \frac{1}{DaRe}\mathbf{v}, \tag{4.3}$$

$$\sigma\frac{\partial \theta}{\partial t} + \mathbf{v}.\nabla\theta = \frac{1}{RePr}(\nabla^2\theta - v). \tag{4.4}$$

The dimensionless parameters appearing in the problem are Rayleigh number (Ra), Reynolds number (Re), Prandtl number (Pr), Darcy number (Da), Forchheimer number (F) and viscosity ratio (λ). They are defined as

$$Ra = \frac{g\beta_T CL^4}{\nu k}, \quad Re = \frac{\overline{V}_0 L}{\nu}, \quad Pr = \frac{\nu}{k}, \quad Da = \frac{K}{L^2}, \quad F = \frac{C_F L}{K^{1/2}} \quad \text{and} \quad \lambda = \frac{\widetilde{\mu}}{\mu_f},$$

where, k is the thermal diffusivity, ν is the kinematic viscosity, β_T is the thermal expansion coefficient, ε is the porosity of the medium, C_F is the form drag coefficient, K is the permeability of the porous medium, g is gravitational acceleration, $\widetilde{\mu}$ is the effective viscosity, μ_f is the fluid viscosity and $\mathbf{e_y}$ is the unit vector in y-direction. In equation (4.4), σ denotes the ratio of the volumetric heat capacities of medium and fluid. It is important to mention here that although the problem in this paper is that of heated upward flow in a vertical channel, the results may also be used to the cooled downward flow in a vertical channel and vice versa. This is because the equations governing heated upward flow are identical to those of cooled downward flow, and the equations of cooled upward flow are identical to those of heated downward flow.

4.2 Linear stability analysis

4.2.1 Steady non-isothermal parallel flow: basic state

We assume that the flow is steady, unidirectional and fully developed which give rise to PMCF. Under these circumstances the above governing equations (4.2)-(4.4) are reduced

into a set of ordinary differential equations, which are defined in the operator form as:

$$L_y(V_0, \Theta_0, Ra, Da, F') = \frac{d^2V_0}{dx^2} - \frac{1}{Da}V_0 + Ra\Theta_0 - F'|V_0|V_0 = Re\frac{dP_0}{dy}, \tag{4.5}$$

$$L(V_0, \Theta_0) = \frac{d^2\Theta_0}{dx^2} - V_0 = 0, \tag{4.6}$$

with boundary conditions:

$$V_0 = \Theta_0 = 0 \quad \text{at} \quad x = \pm 1, \tag{4.7}$$

where V_0, Θ_0 and P_0 are the basic state velocity, basic state temperature and basic state pressure, respectively and $F' = FRe$. The quantity $Re\frac{dP_0}{dy}$ is determined by use of the global mass conservation:

$$\int_{-1}^{1} V_0 dx = 2. \tag{4.8}$$

The velocity profile contains points of inflection, which suggests a potential for the instability. But, these points of inflection in the velocity profile die out on decreasing the media permeability (see figure 4.18 in Appendix B).

4.2.2 Linear disturbance equations

To investigate the stability of above basic flow, the classical normal mode analysis [32] is used. The dependent variables are decomposed into basic state and infinitesimal disturbances. The velocity vector, temperature and pressure are written as:

$$\mathbf{v} = V_0(x)\mathbf{e_y} + \mathbf{v}', \quad \theta = \Theta_0(x) + \theta', \quad P = P_0(y) + p'. \tag{4.9}$$

These infinitesimal disturbances of corresponding field variables are separated into normal mode form as:

$$(\mathbf{v}', \theta', p')^T = e^{i(\alpha y + \beta z - \alpha ct)}(\hat{\mathbf{v}}, \hat{\theta}(x), \hat{p}(x))^T \tag{4.10}$$

where α and β are the wavenumbers in streamwise (y) and spanwise (z) directions, respectively, and $c = c_r + ic_i$ is a complex wave speed. The growth or decay of the disturbance

is determined from the sign of c_i. The flow is stable or neutrally stable or unstable accordingly as $c_i < 0$ or $c_i = 0$ or $c_i > 0$, respectively. On substituting equations (4.9) and (4.10) into the governing equations (4.2)-(4.4), the linearized disturbance equations are given in operator form as:

$$\mathscr{L}_o(\alpha,\beta,\hat{u},\hat{v},\hat{w}) = \frac{d\hat{u}}{dx} + i\alpha\hat{v} + i\beta\hat{w} = 0, \tag{4.11}$$

$$\begin{aligned}\mathscr{L}_x(\alpha,\beta,c,\hat{u},\hat{p},V_0,Da,F') &= i\alpha Re\frac{1}{\varepsilon}\left(\frac{1}{\varepsilon}V_0 - c\right)\hat{u} - \lambda\left(\frac{d^2\hat{u}}{dx^2} - (\alpha^2+\beta^2)\hat{u}\right) \\ &+ Re\frac{d\hat{p}}{dx} + \frac{1}{Da}\hat{u} + F'|V_0|\hat{u} = 0,\end{aligned} \tag{4.12}$$

$$\begin{aligned}\mathscr{L}_y(\alpha,\beta,c,\hat{u},\hat{v},\hat{p},\hat{\theta},V_0,Ra,Da,F') = i\alpha Re\frac{1}{\varepsilon}\left(\frac{1}{\varepsilon}V_0 - c\right)\hat{v} - \lambda\left(\frac{d^2\hat{v}}{dx^2} - (\alpha^2+\beta^2)\hat{v}\right) \\ +i\alpha Re\hat{p} + Re\frac{1}{\varepsilon^2}\frac{dV_0}{dx}\hat{u} + \frac{1}{Da}\hat{v} + 2F'|V_0|\hat{v} - Ra\hat{\theta} = 0,\end{aligned} \tag{4.13}$$

$$\begin{aligned}\mathscr{L}_z(\alpha,\beta,c,\hat{w},\hat{p},V_0,Da,F') &= i\alpha Re\frac{1}{\varepsilon}\left(\frac{1}{\varepsilon}V_0 - c\right)\hat{w} - \lambda\left(\frac{d^2\hat{w}}{dx^2} - (\alpha^2+\beta^2)\hat{w}\right) \\ &+ i\beta Re\hat{p} + \frac{1}{Da}\hat{w} + F'|V_0|\hat{w} = 0,\end{aligned} \tag{4.14}$$

$$\begin{aligned}\mathscr{L}(\alpha,\beta,c,\hat{u},\hat{v},\hat{\theta},V_0,\Theta_0) &= -i\alpha PrRe(V_0 - \sigma c)\hat{\theta} + \left(\frac{d^2\hat{\theta}}{dx^2} - (\alpha^2+\beta^2)\hat{\theta} - \hat{v}\right) \\ &- PrRe\frac{d\Theta_0}{dx}\hat{u} = 0.\end{aligned} \tag{4.15}$$

The corresponding boundary conditions for the perturbed field variables are:

$$\hat{u} = \hat{v} = \hat{w} = \hat{\theta} = 0 \ \text{ at } \ x = \pm 1. \tag{4.16}$$

The above equations are solved by eliminating the pressure terms along with no-slip and impermeability condition of velocity and zero temperature perturbation on the walls. These linear disturbance equations along with boundary conditions form a generalized eigenvalue problem for a complex disturbance wavespeed (c), which is given as

$$\mathbf{A}X = c\mathbf{B}X, \tag{4.17}$$

where X is the representation of the eigenfunction, and **A** and **B** are square complex matrices.

The linear stability theory is used to find the location of bifurcation point or critical point (α, Ra) and predict the form of developing disturbances. It does not provide any information about the actual size of the disturbances (amplitude) beyond the critical value. To analyze the amplitude of such disturbances, a weakly nonlinear stability analysis is required. The results of linear stability analysis are also required to carry out nonlinear analysis. Therefore, a brief review of linear stability results is presented below.

4.2.3 Review of linear stability results

The linear stability analysis of the present problem was studied by some authors [5, 19, 60] in the literature. In these studies, the rigorous numerical study of different controlling parameters as well as impact of drag forces and inertia on the stability of the PMCF were carried out. The problem contains eight important parameters such as Reynolds number (Re), Rayleigh number (Ra), Darcy number (Da), Prandtl number (Pr), modified Forchheimer number (F'), porosity (ε), viscosity ratio (λ) and heat capacity ratio (σ). The objective of the present study is to investigate the influence of nonlinear interaction of different harmonic modes on the instability of flow through high permeable porous medium. For this two fluids air ($Pr = 0.7$) and water ($Pr = 7$) are chosen. Apart from this, to avoid too many parametric studies, we have fixed some parameters for the present study. The porosity, viscosity ratio and heat capacity ratio are kept constant at 0.9, 1 and 1, respectively. Here, three different values $(10^{-2}, 10^{-3}$ and $10^{-4})$ of Darcy number along with three different values (1, $10^2, 10^3$) of F' are taken to examine the present problem. The chosen values of F' are based on the fact that the maximum value of C_F is around 0.1.

We revisit the linear stability results for air ($Pr = 0.7$) as well as water ($Pr = 7$) in (Re, Ra)-plane. The linear stability boundaries for three different values (1, 100, and 1000) of F', when fluid is air (solid line) and water (dashed line) are plotted in figures 4.2*(a)*, 4.2*(b)*, and 4.2*(c)*, respectively. For any of the considered values of Da, the critical value of

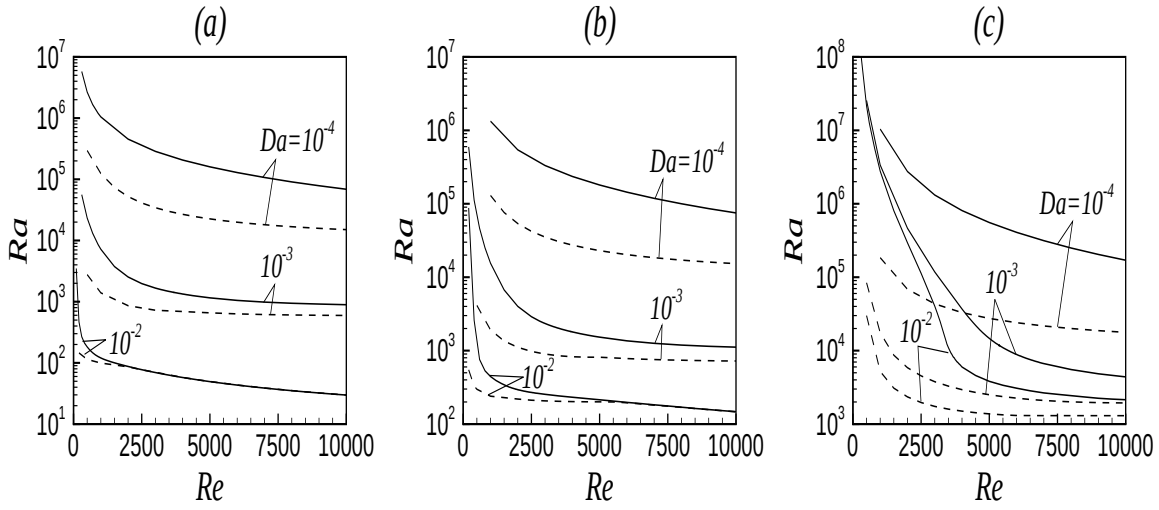

Figure 4.2: Linear stability boundaries in (Re, Ra)-plane: (a) $F' = 1$, (b) $F' = 100$ and (c) $F' = 1000$ where solid line is $Pr = 0.7$ and dashed line is $Pr = 7$.

Rayleigh number decreases with increasing Reynolds number and approaches a constant value beyond a threshold value of Re, which is true for air as well as water. As compared to the PMCF of air, the same of water is much more unstable. The instability boundaries show a more stable flow with decreasing media permeability. Apart from these, the induced form drag in the system delays the instability of the flow.

The disturbance kinetic energy (KE) balance corresponding to a neutral stability curve also provides some insight on the transport mechanisms during the flow instability. The mathematical details of the balance of KE can be seen in the paper by Bera and Khalili [6]. The different energy terms of the KE balance for air and water are plotted in figures 4.3*(a)* and 4.3*(b)*, respectively for different values of Darcy number. Because of similarity, the KE balance for $F' = 1$ and $F' = 1000$ are not shown here. As can be seen from the figure that based on the media permeability the type of instability may be buoyant, mixed, and shear. Here, the type of instability is defined on the basis of contribution of energy production (or, destruction) by shear term (E_s) and buoyant term (E_b). If, in the energy balance, the contribution of E_s (E_b) is more than or equal to 70% then the type of

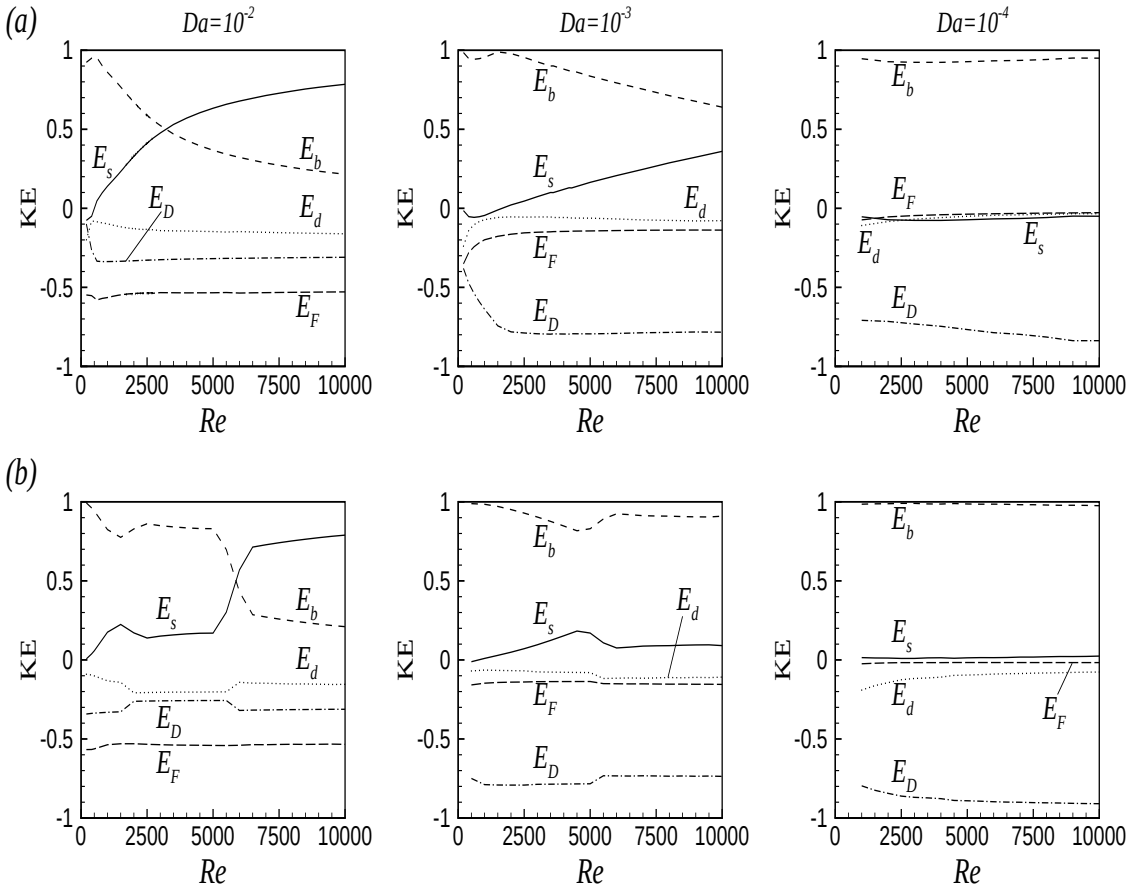

Figure 4.3: Linear disturbance kinetic energy (KE) balance at critical level: (a) $Pr = 0.7$ and (b) $Pr = 7$ when $F' = 100$.

instability is defined as shear (buoyant) else it is defined as mixed. The kinetic energy production for $Da = 10^{-2}$, when fluid is air (water), shows three different types of instability: buoyant for $Re \leq 1850$ ($Re \leq 5500$), mixed for $1850 < Re \leq 6500$ ($5500 < Re \leq 6500$) and shear instability for $Re > 6500$ ($Re > 6500$). Similarly for $Da = 10^{-3}$, it shows two types of instability: buoyant for $Re \leq 7000$ and mixed for $Re > 7000$ in case of air, whereas for water it is only buoyant type. For air as well as water, when $Da = 10^{-4}$, KE production due to buoyant term remains prominent in the entire range of Re considered in this study, consequently buoyant instability is the only type of instability. The type instability also depends on induced form drag in terms of F'. In general, induced form drag decelerates to attain mixed as well as shear instability of the flow (figure is not shown here). Note that for Da equal to 10^{-3} and 10^{-4} KE production or destruction is mainly balanced by dissipation of KE due to surface drag (E_D). However, for $Da = 10^{-2}$ it is different. Here, dissipation of KE is made through E_D as well as E_F. So it can be concluded that even though inertia due to convective term does not play any role in the basic flow but its impact on the instability boundary for relatively high permeable medium is not negligible.

The overview of linear stability results provides some suggestions regarding development of the disturbance. However, it can not provide any information about the amplitude of such disturbances and quantitative information about a disturbed flow. The occurrence of instability in a flow may lead to the replacement of the original laminar flow by a new laminar flow due to the superimposition of finite disturbances. This flow may be expected to persist for a certain range of Rayleigh number beyond the critical value and then become unstable at some new Rayleigh number against a new (second) type of disturbance. A new equilibrium flow, consisting of a mean flow with two superimposed modes of disturbance, is then conceivable for a range of Rayleigh number above the second critical value. In purely fluid domain, as the Rayleigh number is increased further, additional modes of disturbance may appear successively until the turbulence is achieved. In this way a sequence of instabilities may exist before it leads finally to turbulence [49]. Since turbulent flow in wall bounded porous media is possible [53], therefore, above similar phenomena may

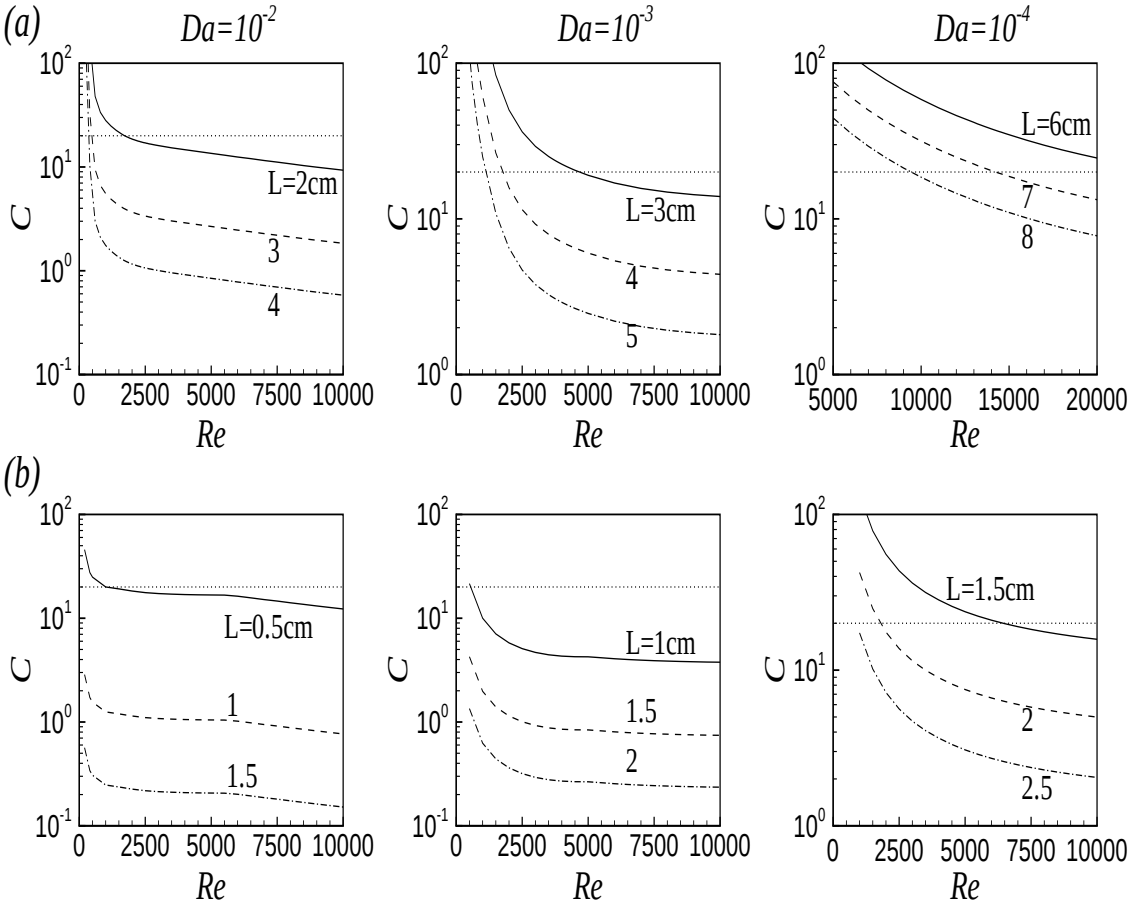

Figure 4.4: Variation of temperature gradient w.r.t. Re: (a) $Pr = 0.7$ and (b) $Pr = 7$ when $F' = 100$.

be expected in fluid flow through high permeable porous media. Therefore, a nonlinear stability is necessary to study the structure of the flow field that results from linear stability.

Before closing this subsection and moving to finite amplitude analysis of the above problem, we have calculated the minimum value of temperature gradient (C) for which the PMCF will be unstable and checked for what sort of values of permeability as well as Reynold's number the linear stability results under the Boussinesq approximation will remain valid. From the dimensional analysis we have $C = \dfrac{\nu k Ra}{g\beta_T L^4}$. Using our numerical data set of instability curve we have calculated the value of C at the critical points for air and water as a function of Re for $F' = 100$ and shown in figures 4.4*(a)* and 4.4*(b)*, respectively. To identify the minimum value of Re above which the value of C will be

less than or equal to 20^oC per unit length (i.e., the flow remains valid under Boussinesq approximation) a constant line $C = 20$ is also added in each sub-figure. Note that the value of C has been calculated from the definition of Ra which involves the characteristic length scale L. For a given value of Darcy number, the characteristic length is determined by the permeability (K) of the porous medium. So, the choice of permeability decides the temperature gradient which can be controlled by the experimentalist to obtain realistic and feasible results within the Boussinesq limit. Here, we have used the value of ν, β_T and k for air as 1.5×10^{-5}m^2/s, $3.4 \times 10^{-3}/^oC$ and 2.1×10^{-5}m^2/s, respectively, whereas for water as 8.7×10^{-7}m^2/s, $2.5 \times 10^{-4}/^oC$ and 1.5×10^{-7}m^2/s, respectively. In the following, the considered values of K are based on the fact that the metallic foam may have permeability as large as 8×10^{-6}m^2 [76].

Figure 4.4*(a)*, for $Da = 10^{-2}$, shows that when fluid is air the value of C is less than or equal to 20 for Re greater than or equal to 1720, 600 and 400 for K equal to 4×10^{-6}m^2, 9×10^{-6}m^2 and 1.6×10^{-5}m^2, respectively, or L equal to 2cm, 3cm and 4cm, respectively. In case of $Da = 10^{-3}$, C is less than or equal to 20 for Re greater than or equal to 4500, 2000 and 1500 for K equal to 9×10^{-7}m^2, 1.6×10^{-6}m^2 and 2.5×10^{-6}m^2, respectively. So, the minimum value of Re, beyond which the results from Boussinesq approximation will be appropriate, decreases on increasing the permeability of the medium. Similar observation can also be made for $Da = 10^{-4}$. However, when air is replaced by water then figure 4.4*(b)* for $Da = 10^{-2}$ shows that C is less than or equal to 20 for Re greater than or equal to 1000, 100 and 50 for K equal to 2.5×10^{-7}m^2, 10^{-6}m^2 and 2.25×10^{-6}m^2, respectively. For $Da = 10^{-3}$, C is less than or equal to 20 for Re greater than or equal to 500, 75 and 50 for K equal to 10^{-7}m^2, 2.25×10^{-7}m^2 and 4×10^{-7}m^2, respectively. This indicates that the domain of Re in which Boussinesq approximation remain valid for water even on reducing media permeability by one order is larger than the same for air. The above analysis also indicates the instability of PMCF in a high permeable porous medium under mild heating condition and a significant role of the buoyant term in the flow instability.

4.3 Formulation of finite amplitude equations

The nonlinear terms ignored in the linear stability analysis play a significant role when the amplitude of disturbance becomes finite. In this situation the exponential linear growth rate is modified by the nonlinearities in the governing equations. To study the nonlinear dynamic behavior we must take into account the nonlinear interactions between the various wave components. Therefore, a finite amplitude study using weakly nonlinear theory is made to capture the nonlinear effects in the problem. In this study, the field variables are separated into Fourier components of the most unstable linear wave, which is predicted from linear stability theory. Again, we decompose the functions for each harmonic component in terms of a suitable small parameter c_i (imaginary part of least linearly stable eigenvalue at critical point) and amplitude function. The amplitude expansion is given based on the analysis of various authors [95, 101]. The Fourier expansion of y-direction velocity component in separable form is:

$$\begin{aligned} v(x,y,z,t) &= V(x,\tau)E^0 + \hat{v}_1(x,\tau)E^1 + \hat{v}_2(x,\tau)E^2 + ... + c.c. \\ &= E^0\left[V_0(x) + c_i|B(\tau)|^2 V_1(x) + O((c_i)^2)\right] \\ &+ E^1[(c_i)^{\frac{1}{2}}Bv_{10} + (c_i)^{\frac{3}{2}}B|B|^2 v_{11} + O((c_i)^{\frac{5}{2}})] \\ &+ E^2[c_i B^2 v_{20} + O((c_i)^2)] + ... + c.c., \end{aligned} \tag{4.18}$$

where $E^j = e^{j[i\alpha(y-c_r t)+i\beta z]}$, j=0,1,2; α is the wavenumber corresponding to the critical Ra, and c_r is the real part of the wavespeed of most unstable disturbance wave. B denotes an amplitude function, which will be calculated from the Landau equation. c.c. stands for complex conjugate.

The method of multiple time scales is used to derive an evolution equation for slowly varying amplitude. Two types of timescales (fast timescale (t) & slow timescale (τ)) are used in the nonlinear stability analysis of the flow. The choice of the fast timescale is associated with the exponential development of the disturbance as in the linear stability analysis. The nonlinear terms become important when disturbance attains a finite amplitude. In this situation, the temporal behavior of the disturbances deviates from exponential

behavior. This is characterized by another timescale (slow timescale). The slow timescale leads to stages when the growth/decay of the disturbances is affected by nonlinearities of different order. The slow timescale $\tau = c_i t$ modifies the time derivative as:

$$\frac{\partial}{\partial t} \rightarrow \frac{\partial}{\partial t} + c_i \frac{\partial}{\partial \tau}. \tag{4.19}$$

The multiple timescale approach is valid when the amplitude dynamics change substantially as the disturbance develops. Similarly, we can write the expansions for the other dependent variables in terms of c_i and the amplitude function (B). The mathematical justification of perturbation expansion is as follows.

Stuart [99, 100] has shown that c_i is proportional to the difference between the actual and critical Rayleigh number (Δ). The author has also shown that the square of equilibrium amplitude (to be discussed later) is proportional to Δ. Consequently, the equilibrium amplitude is proportional to $(c_i)^{\frac{1}{2}}$. Hence, in α disturbance the amplitude of $\hat{v}_1$ is of order $(c_i)^{\frac{1}{2}}$. Field variables that are expanded in higher wave numbers are scaled according to the number of nonlinear interactions it takes to generate them. For example, 2α disturbances require the interaction of two α-perturbations, thus the amplitude of $\hat{v}_2$ is of order $(c_i)^1$. We also assume that $\frac{\partial}{\partial t}$ is never of greater magnitude than c_i, which is its order of magnitude according to the linear theory. The distortion of mean flow (V) is of order c_i, which arises from the part of the Reynolds stress [101].

4.3.1 Derivation of cubic Landau equation

On substituting equation (4.18) into the governing equations (4.2)-(4.4) and separating the harmonic components, the equations for the harmonic E^0 are

$$\begin{aligned} L_y(V_0, \Theta_0, Ra, Da, F') \quad &- \quad Re\frac{dP_0}{dy} + c_i|B|^2 \left\{ \lambda \frac{d^2V_1}{dx^2} - \frac{1}{Da}V_1 + Ra\Theta_1 - 2F'|V_0|V_1 \right. \\ &- \quad \left. Re\frac{dP_1}{dy} - \frac{Re}{\varepsilon^2}\left[\frac{d}{dx}(\tilde{v}_{10}u_{10} + v_{10}\tilde{u}_{10})\right]\right\} = O((c_i)^2), \end{aligned} \tag{4.20}$$

$$L(V_0, \Theta_0) + c_i|B|^2 \left\{ L(V_1, \Theta_1) - RePr\left[\frac{d}{dx}(\tilde{u}_{10}\theta_{10} + u_{10}\tilde{\theta}_{10})\right]\right\} = O((c_i)^2). \tag{4.21}$$

Similarly, the equation for the harmonic E^1 are:

$$(c_i)^{\frac{1}{2}} B\{\mathscr{L}_o(\alpha,\beta,u_{10},v_{10},w_{10})\} + (c_i)^{\frac{3}{2}} B|B|^2\{\mathscr{L}_o(\alpha,\beta,u_{11},v_{11},w_{11})\} = O(c_i^{\frac{5}{2}}), \quad (4.22)$$

$$(c_i)^{\frac{1}{2}} B\left\{\mathscr{L}_x(\alpha,\beta,c,u_{10},p_{10},V_0,Da,F')\right\} + (c_i)^{\frac{3}{2}}\left\{B|B|^2\mathscr{L}_x(\alpha,\beta,c,u_{11},p_{11},V_0,Da,F') - B|B|^2\mathscr{G}_x + \frac{Re}{\varepsilon}\frac{dB}{d\tau}u_{10} - \frac{\alpha BRe}{\varepsilon}u_{10}\right\} = O(c_i^{\frac{5}{2}}), \quad (4.23)$$

$$(c_i)^{\frac{1}{2}} B\left\{\mathscr{L}_y(\alpha,\beta,c,u_{10},v_{10},p_{10},\theta_{10},V_0,Ra,Da,F')\right\} + (c_i)^{\frac{3}{2}}\left\{B|B|^2\mathscr{L}_y(\alpha,\beta,c,u_{11},v_{11},p_{11},\theta_{11},V_0,Ra,Da,F') - B|B|^2\mathscr{G}_y + \frac{Re}{\varepsilon}\frac{dB}{d\tau}v_{10} - \frac{\alpha BRe}{\varepsilon}v_{10}\right\} = O((c_i)^{\frac{5}{2}}), \quad (4.24)$$

$$(c_i)^{\frac{1}{2}} B\left\{\mathscr{L}_z(\alpha,\beta,c,w_{10},p_{10},V_0,Da,F')\right\} + (c_i)^{\frac{3}{2}}\left\{B|B|^2\mathscr{L}_z(\alpha,\beta,c,w_{11},p_{11},V_0,Da,F') - B|B|^2\mathscr{G}_z + \frac{Re}{\varepsilon}\frac{dB}{d\tau}w_{10} - \frac{\alpha BRe}{\varepsilon}w_{10}\right\} = O((c_i)^{\frac{5}{2}}), \quad (4.25)$$

$$(c_i)^{\frac{1}{2}} B\{\mathscr{L}(\alpha,\beta,c,u_{10},v_{10},\theta_{10},V_0,\Theta_0)\} + (c_i)^{\frac{3}{2}}\left\{B|B|^2\mathscr{L}(\alpha,\beta,c,u_{11},v_{11},\theta_{11},V_0,\Theta_0) - B|B|^2\mathscr{G} - RePr\,\frac{dB}{d\tau}\theta_{10} + \alpha RePrB\theta_{10}\right\} = O((c_i)^{\frac{5}{2}}), \quad (4.26)$$

where $\mathscr{G}$'s are defined as:

$$\mathscr{G}_x = -\frac{Re}{\varepsilon^2}\left\{i\alpha V_1 u_{10} + 2i\alpha u_{20}\tilde{v}_{10} - i\alpha v_{20}\tilde{u}_{10} + \tilde{u}_{10}\frac{du_{20}}{dx} + u_{20}\frac{d\tilde{u}_{10}}{dx} - i\beta w_{20}\tilde{u}_{10} + 2i\beta\tilde{w}_{10}u_{20}\right\}, \quad (4.27)$$

$$\mathscr{G}_y = -\frac{Re}{\varepsilon^2}\left\{i\alpha V_1 v_{10} + u_{10}\frac{dV_1}{dx} + i\alpha v_{20}\tilde{v}_{10} + \tilde{u}_{10}\frac{dv_{20}}{dx} + u_{20}\frac{d\tilde{v}_{10}}{dx} - i\beta w_{20}\tilde{v}_{10} + 2i\beta\tilde{w}_{10}v_{20}\right\}, \quad (4.28)$$

$$\mathscr{G}_z = -\frac{Re}{\varepsilon^2}\left\{i\alpha V_1 w_{10} + 2i\alpha w_{20}\tilde{v}_{10} - i\alpha v_{20}\tilde{w}_{10} + \tilde{u}_{10}\frac{dw_{20}}{dx} + u_{20}\frac{d\tilde{w}_{10}}{dx} + i\beta w_{20}\tilde{w}_{10}\right\}, \quad (4.29)$$

$$\mathscr{G} = \quad RePr\Big\{ i\alpha V_1\theta_{10} + 2i\alpha\theta_{20}\tilde{v}_{10} - i\alpha v_{20}\tilde{\theta}_{10} + u_{10}\frac{d\Theta_1}{dx} + \tilde{u}_{10}\frac{d\theta_{20}}{dx} + u_{20}\frac{d\tilde{\theta}_{10}}{dx} - i\beta w_{20}\tilde{\theta}_{10} + 2i\beta\tilde{w}_{10}\theta_{20}\Big\}. \tag{4.30}$$

The equations for the harmonic E^2 are:

$$c_i B^2\{\mathscr{L}_o(2\alpha, 2\beta, u_{20}, v_{20}, w_{20})\} = O((c_i)^2), \tag{4.31}$$

$$c_i B^2\Big\{\mathscr{L}_x(2\alpha, 2\beta, c, u_{20}, p_{20}, V_0, Da, F') \quad + \quad \frac{Re}{\varepsilon^2}\Big(i\alpha u_{10}v_{10} + u_{10}\frac{du_{10}}{dx} + i\beta u_{10}w_{10}\Big)\Big\} = O((c_i)^2), \tag{4.32}$$

$$c_i B^2\Big\{\mathscr{L}_y(2\alpha, 2\beta, c, u_{20}, v_{20}, p_{20}, \theta_{20}, V_0, Ra, Da, F') \quad + \quad \frac{Re}{\varepsilon^2}\Big(i\alpha v_{10}^2 + u_{10}\frac{dv_{10}}{dx} + i\beta v_{10}w_{10}\Big)\Big\} = O((c_i)^2), \tag{4.33}$$

$$c_i B^2\Big\{\mathscr{L}_z(2\alpha, 2\beta, c, w_{20}, p_{20}, V_0, Da, F') \quad + \quad \frac{Re}{\varepsilon^2}\Big(i\alpha v_{10}w_{10} + u_{10}\frac{dw_{10}}{dx} + i\beta w_{10}^2\Big)\Big\} = O((c_i)^2), \tag{4.34}$$

$$c_i B^2\Big\{\mathscr{L}(2\alpha, 2\beta, c, u_{20}, v_{20}, \theta_{20}, V_0, \Theta_0) \quad - \quad RePr\Big(i\alpha v_{10}\theta_{10} + u_{10}\frac{d\theta_{10}}{dx} + i\beta w_{10}\theta_{10}\Big)\Big\} = O((c_i)^2). \tag{4.35}$$

Here $\sim$ denotes the complex conjugate. Consideration of higher order harmonics (E^3, E^4, etc.) in equation (4.18) is not necessary to obtain the first Landau coefficient. Therefore, these terms are not included in the series.

The systems of harmonic equations (4.20)-(4.35) can be solved sequentially in increasing power of c_i. At order $(c_i)^0$, the harmonic E^0 contains exactly the same basic state equations (4.5)-(4.6). The unknown functions V_0 and Θ_0 are obtained from equations (4.5)-(4.6). At order $(c_i)^{1/2}$, the harmonic E^1 contains linear stability equations and the contribution of other harmonics (E^0 and E^1) is zero. The functions u_{10}, v_{10}, w_{10} and θ_{10} are given by the eigenfunctions of linear stability equations at a particular wave number

as well as Ra. At order $(c_i)^1$, the harmonics E^0 and E^2 produce the non-homogeneous equations for the basic flow distortion functions V_1 and Θ_1 as well as for the functions u_{20}, v_{20}, w_{20} and θ_{20}, respectively. The non-homogeneous part of these equations contains the known variables u_{10}, v_{10}, w_{10}, θ_{10} and their derivatives, which are calculated from lower order analysis. At order $(c_i)^{3/2}$, the equations of harmonic E^1 become non-homogeneous. The left hand sides of these equations contain linear stability operators operating on u_{11}, v_{11}, w_{11}, θ_{11} and p_{11}, whereas, the right hand sides of these equations contain the terms proportional to $dB/d\tau$, B and $B|B|^2$. The coefficients of these terms on the right-hand sides are known from the lower-order analysis. The homogeneous form of the equations of E^1 is same as linear stability equations. For non-trivial solution of E^1 equations, the integrability condition can be used to determine the unknown amplitude function B. In order to formulate the integrability condition, the solution of homogeneous adjoint system corresponding to linear stability problem (see Appendix C) is required. Therefore, the right-hand sides of the non-homogeneous equations of E^1 at order $(c_i)^{3/2}$ must be orthogonal with the adjoint field variables. In this manner, multiplying the above right hand side terms by the adjoint field variables p^*, u^*, v^*, w^*, θ^*, and enforcing the condition (4.59), the following Landau equation results

$$\frac{dB}{d\tau} = \alpha B + a_1 B|B|^2, \tag{4.36}$$

where,

$$a_1 = \frac{1}{Re}\int_{-1}^{1} (\mathscr{G}_x u^* + \mathscr{G}_y v^* + \mathscr{G}_z w^* + \mathscr{G}\theta^*)\, dx, \tag{4.37}$$

and known as Landau constant, which is the first correction to linear growth rate. Landau equation (4.36) represents a modification to the exponential growth or decay of a disturbance predicted by linear theory.

In bifurcation theory, a field within mathematics, a pitchfork bifurcation is a particular type of local bifurcation where the system transitions from one fixed point to three fixed points. Based on the sign of real part of the Landau constant (a_1) pitchfork bifurcations may be supercritical or subcritical. If the real part of a_1 is positive then we predict a subcritical pitchfork bifurcation (or subcritical bifurcation), whereas, if it is negative then we predict

a supercritical Pitchfork bifurcation (or supercritical bifurcation). Note that a supercritical bifurcating solution is stable nonlinear states superimposed on the laminar flow to a small disturbance, whereas a subcritical bifurcating solution is unstable to a small disturbance. The supercritical bifurcating solution is a continuous process involving the smooth development of new modes of motion. However, the subcritical bifurcating solution is attracted to solution with larger amplitude. In short, we can say that a supercritical bifurcation makes it possible to achieve the controlled transition through stable nonlinear secondary motions, whereas a subcritical transition makes destabilizing influence of nonlinearities. The equilibrium amplitude of supercritical and threshold amplitude of subcritical bifurcations are given as [59]

$$A_e{}^2 = -\alpha c_i/(a_1)_r$$

and $A_t{}^2 = |\alpha c_i/(a_1)_r|$ respectively, where $(a_1)_r$ is the real part of a_1. The actual value of the Landau constant depends on the chosen normalization of eigenvectors obtained from linear stability.

4.3.2 Non-linear kinetic energy spectrum

To gain further insight on the mechanism of supercritical/subcritical bifurcation, an investigation of the energy transfer in the parallel mixed convective flow is made. The Reynolds stress has a significant impact on the basic flow in weakly nonlinear stability analysis. This distortion of the basic flow modifies the rate of the transfer of energy from the basic flow to the disturbance. The balance of kinetic energy for the fundamental disturbance is given

as [59, 88],

$$\begin{aligned}\frac{\partial}{\partial t}\left\langle \frac{1}{2}\frac{1}{\varepsilon}\left[\overline{u_1^2}+\overline{v_1^2}+\overline{w_1^2}\right]\right\rangle = & -\frac{1}{\varepsilon^2}\left\langle \overline{u_1 v_1}\frac{\partial V}{\partial x}\right\rangle + \frac{Ra}{Re}\left\langle \overline{v_1\theta_1}\right\rangle - \frac{1}{DaRe}\left\langle \overline{u_1^2}+\overline{v_1^2}+\overline{w_1^2}\right\rangle \\ & -\frac{1}{Re}\left\langle \overline{\left(\frac{\partial u_1}{\partial x}\right)^2}+\overline{\left(\frac{\partial u_1}{\partial y}\right)^2}+\overline{\left(\frac{\partial u_1}{\partial z}\right)^2}+\overline{\left(\frac{\partial v_1}{\partial x}\right)^2}\right. \\ & \left. +\overline{\left(\frac{\partial v_1}{\partial y}\right)^2}+\overline{\left(\frac{\partial v_1}{\partial z}\right)^2}+\overline{\left(\frac{\partial w_1}{\partial x}\right)^2}+\overline{\left(\frac{\partial w_1}{\partial y}\right)^2}+\overline{\left(\frac{\partial w_1}{\partial z}\right)^2}\right\rangle \\ & -\frac{1}{\varepsilon^2}\left\langle \overline{u_1^2\frac{\partial u_2}{\partial x}}+\overline{u_1 v_1\frac{\partial u_2}{\partial y}}+\overline{u_1 w_1\frac{\partial u_2}{\partial z}}+\overline{u_1 v_1\frac{\partial v_2}{\partial x}}+\overline{v_1^2\frac{\partial v_2}{\partial y}}\right. \\ & \left. +\overline{v_1 w_1\frac{\partial v_2}{\partial z}}+\overline{u_1 w_1\frac{\partial w_2}{\partial x}}+\overline{v_1 w_1\frac{\partial w_2}{\partial y}}+\overline{w_1^2\frac{\partial w_2}{\partial z}}\right\rangle \\ & -F\left\langle |V_0|(\overline{u_1^2}+2\overline{v_1^2}+\overline{w_1^2})\right\rangle . \end{aligned} \tag{4.38}$$

Here, bracket $\langle\rangle$ implies integration over the volume of disturbance wave and $\overline{GH}$ for some field variables G and H is defined as $G\tilde{H}+\tilde{G}H$. With the help of equation (4.36), the balance of kinetic energy leads to an amplitude equation [88]

$$\frac{d|B|^2}{d\tau} = 2\alpha|B|^2 + (P_{101}+E_{12}+P_{110}+T_{11}+D_{11}+K_{11}+F_{11})|B|^4. \tag{4.39}$$

The comparison of equations (4.36) and (4.39) shows that

$$2(a_1)_r = P_{101}+E_{12}+P_{110}+T_{11}+D_{11}+K_{11}+F_{11}, \tag{4.40}$$

where the right hand side quantities are defined as,

$$P_{101} = -\frac{1}{e_0\varepsilon^2}\left\langle \overline{u_{10}v_{10}}\frac{dV_1}{dx}\right\rangle, \tag{4.41}$$

$$\begin{aligned} E_{12} = -\frac{1}{e_0\varepsilon^2}\left\langle \overline{u_{10}^2\frac{\partial u_{20}}{\partial x}}+\overline{u_{10}v_{10}\frac{\partial u_{20}}{\partial y}}+\overline{u_{10}w_{10}\frac{\partial u_{20}}{\partial z}}\right. \\ +\overline{u_{10}v_{10}\frac{\partial v_{20}}{\partial x}}+\overline{v_{10}^2\frac{\partial v_{20}}{\partial y}}+\overline{v_{10}w_{10}\frac{\partial v_{20}}{\partial z}} \\ \left. +\overline{u_{10}w_{10}\frac{\partial w_{20}}{\partial x}}+\overline{v_{10}w_{10}\frac{\partial w_{20}}{\partial y}}+\overline{w_{10}^2\frac{\partial w_{20}}{\partial z}}\right\rangle, \end{aligned} \tag{4.42}$$

$$P_{110} = -\frac{1}{e_0 \varepsilon^2} \left\langle (\overline{u_{10} v_{11}} + \overline{v_{10} u_{11}}) \frac{dV_0}{dx} \right\rangle, \tag{4.43}$$

$$T_{11} = \frac{1}{e_0} \frac{Ra}{Re} \left\langle \overline{v_{10} \theta_{11}} + \overline{\theta_{10} v_{11}} \right\rangle, \tag{4.44}$$

$$\begin{aligned} D_{11} = \; & - \frac{1}{e_0} \frac{1}{Re} \left\langle \overline{\frac{\partial u_{10}}{\partial x} \frac{\partial u_{11}}{\partial x}} + \overline{\frac{\partial u_{10}}{\partial y} \frac{\partial u_{11}}{\partial y}} + \overline{\frac{\partial u_{10}}{\partial z} \frac{\partial u_{11}}{\partial z}} \right. \\ & + \overline{\frac{\partial v_{10}}{\partial x} \frac{\partial v_{11}}{\partial x}} + \overline{\frac{\partial v_{10}}{\partial y} \frac{\partial v_{11}}{\partial y}} + \overline{\frac{\partial v_{10}}{\partial z} \frac{\partial v_{11}}{\partial z}} \\ & + \left. \overline{\frac{\partial w_{10}}{\partial x} \frac{\partial w_{11}}{\partial x}} + \overline{\frac{\partial w_{10}}{\partial y} \frac{\partial w_{11}}{\partial y}} + \overline{\frac{\partial w_{10}}{\partial z} \frac{\partial w_{11}}{\partial z}} \right\rangle, \end{aligned} \tag{4.45}$$

$$K_{11} = -\frac{2}{e_0 Da Re} \left\langle \overline{u_{10} u_{11}} + \overline{v_{10} v_{11}} + \overline{w_{10} w_{11}} \right\rangle, \tag{4.46}$$

$$F_{11} = -\frac{2}{e_0} F \left\langle |V_0| (\overline{u_{10} u_{11}} + 2\overline{v_{10} v_{11}} + \overline{w_{10} w_{11}}) \right\rangle, \tag{4.47}$$

and

$$e_0 = \frac{1}{2\varepsilon} \left\langle \overline{u_{10}^2} + \overline{v_{10}^2} + \overline{w_{10}^2} \right\rangle. \tag{4.48}$$

The physical interpretation of different terms in the equation (4.40) is as follows. The term P_{101}, which is an integral of the product of Reynold's stress and the mean velocity gradient, denotes the gradient production of disturbance kinetic energy due to the interaction between the fundamental disturbance (quantities assigned with subscript 10) and the distorted mean flow strain rate. The energy needed for the distortion of the mean flow is obtained from the fundamental disturbance, consequently, the term will be negative. Hence, this term will reduce the growth rate of disturbance. The second term E_{12} represents the transfer of the disturbance energy from fundamental to the second harmonic wave (quantities assigned with subscript 20). The other five terms P_{110}, T_{11}, D_{11}, K_{11} and F_{11} account for the energy exchange due to modification of the shape of the fundamental disturbance wave. The term P_{110} arises because of modification in the gradient production of disturbance energy due

to change of the disturbance shape. This term may have positive or negative sign. If the term P_{110} is positive, the change in the shape of the disturbance will be more favorable for shear production of the disturbance energy. The term T_{11} leads to the modification in the buoyant production of disturbance kinetic energy due to change in the shape of the fundamental wave. The term D_{11} represents a modification in the rate of viscous dissipation of disturbance kinetic energy due to change in the disturbance shape. The term K_{11} denotes a modification in the surface drag dissipation of disturbance kinetic energy due to change in the disturbance shape. The last term F_{11} represents a modification in the dissipation of disturbance kinetic energy due to form drag through change in the shape of the fundamental wave. If T_{11} is positive, the modified disturbance shape will be more favorable for buoyant production of the disturbance energy, whereas a positive value of D_{11}, K_{11} and F_{11} will imply a decrease in the viscous dissipation rate, surface drag and form drag dissipation of the disturbance kinetic energy, respectively.

4.4 Numerical procedure

In the present work a spectral Chebyshev collocation method is employed to find the solution of the basic state, linear stability and nonlinear stability equations. The equations are discretized along x-direction by implementing the spectral collocation method that uses Chebyshev polynomials as the basis functions. The governing equations are collocated at Gauss-Lobatto points. The Gauss-Lobatto points of Nth-order Chebyshev polynomial are given as

$$x_j = cos\left(\frac{\pi j}{N}\right), \tag{4.49}$$

where $j = 0,1,2,.....N$ and N represents order of the base polynomial. The details of the spectral collocation technique can be seen in the book by Canuto *et. al.* [18]. The discretized linear disturbance equations (4.11)- (4.15) along with the homogeneous boundary conditions (4.16) are formulated as a generalized eigenvalue problem given by equation

	Published [59]			Present		
Re	Ra_c	α_c	(a_1)	Ra_c	α_c	(a_1)
100	41.65	0.875	-2.895 + 4.006i	41.647	0.875	-2.874 + 4.006i
500	32.65	1.22	-17.017+ 10.741i	32.65	1.22	-16.85+ 10.75i
1000	30.26	1.355	-29.188+ 7.55	30.26	1.34	-29.181+ 7.554i

Table 4.1: Comparison between published and present results.

(4.17). The square complex matrices **A** and **B** are of order $3N+3$ (after elimination of pressure term). The eigenvalues of the generalized eigenvalue problem (4.17) are calculated by the QZ-algorithm of **MATLAB** software using **eig** command. The adjoint eigenfunctions are used in the integrability condition to determine the first Landau coefficient. The set of adjoint equations of the linear stability problem are also solved by the same spectral method. For nonlinear stability analysis, we need to solve the related non-homogeneous differential equations in $\mathscr{A}X = b$ form, where $\mathscr{A} = \mathbf{A} - c\mathbf{B}$. In the case of E^2 harmonic component, the system $\mathscr{A} = \mathbf{A} - c\mathbf{B}$ is nonsingular as α and β in equations (4.31)-(4.35) are replaced by 2α and 2β respectively, and complex wavespeed (c) of the fundamental wave (E^1) is not an eigenvalue of this system. So, the eigenvalues are not identical and there is no theoretical difficulty in solving the equations of E^2 harmonic component. For the calculation of $u_{11}, v_{11}, w_{11}, p_{11}$ and θ_{11}, we encounter a singular system of equations $\mathscr{A}x = b$ which are solved by singular value decomposition (SVD) method which is in-built in the **MATLAB** software. These set of equations are also discretized by the same spectral collocation method and the integrals occurring everywhere are calculated by Gauss-Chebyshev quadrature integration formula.

The numerical code developed in the earlier work [59] for the stability of the non-isothermal Poiseuille flow in a vertical channel is extended for the present problem. The accuracy and validity of the numerical scheme are checked by comparing our general results with published results [20, 59], by taking $Da = 10^{12}$, $F' = 0$ and $\varepsilon = 1$ (see table 4.1).

The solution generated by the code is in excellent agreement with the published results. Apart from this, the results remain consistent when the order of polynomial (N) is 50 or more (table not shown), which is determined after many preliminary tests. Therefore, all the computations are reported by taking the order of polynomial as 50.

4.5 Results and discussion

To give an illustration, we carry out a finite amplitude instability analysis of stably stratified PMCF in a vertical channel filled with a fluid saturated porous medium. The linear stability results show that the two dimensional disturbance with $\beta = 0$ is the most unstable wave for stably stratified flow. As a consequence of it, the present nonlinear stability results are carried out for $\beta = 0$. The cubic Landau equation (4.36) derived in terms of the amplitude function is used to identify the supercritical/subcritical bifurcation.

4.5.1 Landau constant in the neighborhood of the bifurcation point

The Landau constant is calculated at $\delta_{Ra} = Ra/Ra_c - 1 = 0$ and at $\delta_{Ra} = 0.01$ (i.e., in the vicinity of the critical Rayleigh number) with respect to the most unstable linear wave (with critical wavenumber (α_c)) for both values 0.7 and 7 of Pr. The calculated values of $(a_1)_r$ for both values (0 and 0.01) of δ_{Ra} are almost identical for air, which is also true for water. Therefore, in the following, to identify the nature of bifurcation the real part of the Landau constant ($(a_1)_r$) as a function of Re is plotted at $\delta_{Ra} = 0.01$. The variation of $(a_1)_r$ when the porous medium is saturated by air is shown in figures 4.5*(a)*, 4.5*(b)*, and 4.5*(c)* for Da equal to 10^{-2}, 10^{-3} and 10^{-4}, respectively. The sign of $(a_1)_r$ is found to be negative for $Da = 10^{-2}$ with $F' = 1$, indicating the supercritical bifurcation (see figure 4.5*(a)*). The magnitude of $(a_1)_r$ increases on increasing the Reynolds number. The graph also shows supercritical bifurcation of PMCF when $F' = 100$ except in a small region $1900 \leq Re \leq 2100$ (positive value of $(a_1)_r$ with very small magnitude) where the bifurcation is subcritical. However, on replacing the value 100 of F' by 1000 the same figure shows supercritical

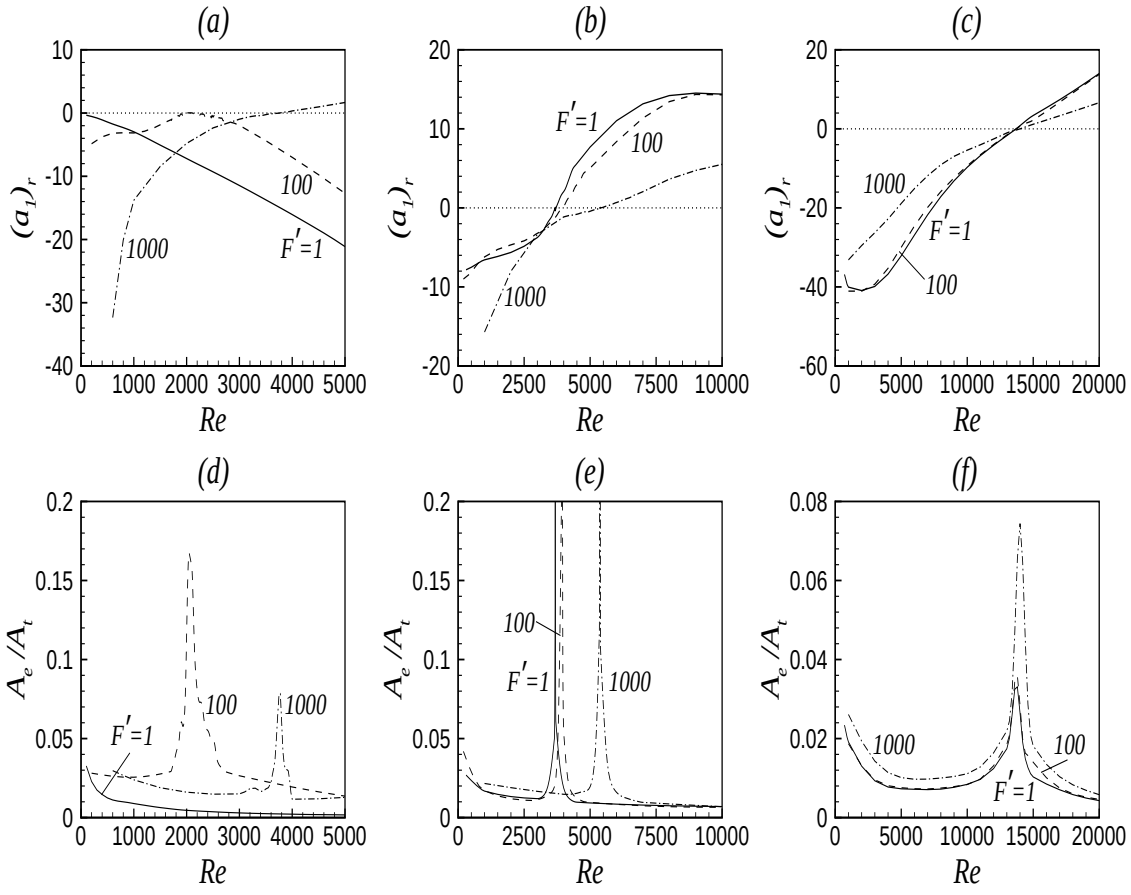

Figure 4.5: Variation of Landau constant ($(a_1)_r$) and equilibrium or threshold amplitude w.r.t. Re: (a,d) $Da = 10^{-2}$, (b,e) $Da = 10^{-3}$ and (c,f) $Da = 10^{-4}$ when $Pr = 0.7$.

bifurcation for $Re < 3800$ and subcritical bifurcation for $Re \geq 3800$. Furthermore, for each value of F', figure 4.5*(b)* shows the existence of a minimum value of Re below which the flow has supercritical bifurcation and above which it has subcritical bifurcation. Let Re_{sb} denote the value of Re at which the shifting of bifurcation takes place. The values of Re_{sb} for F' equal to 1, 100 and 1000 are 3678, 3952 and 5351, respectively. The shifting of bifurcation also takes place for $Da = 10^{-4}$ which can be seen from figure 4.5*(c)*. For F' equal to 1, 100 and 1000 the corresponding values of Re_{sb} are 13650, 13700 and 14100, respectively. Interestingly, Re_{sb} increases on increasing the value of F' as well as on decreasing the value of Da. It may be a consequence of the following fact. Since the decrease in media permeability or increase in form drag in general stabilizes the flow (see figure 4.3), therefore to achieve a change of bifurcation in PMCF in a porous medium in which permeability is relatively low or induced form drag is relatively high a relatively higher disturbance shear production is required.

The corresponding equilibrium amplitude (A_e) or threshold amplitude (A_t) for Da equal to 10^{-2}, 10^{-3} and 10^{-4}, are displayed in figures 4.5*(d)*, 4.5*(e)* and 4.5*(f)*, respectively. Each of the above figures manifests an important feature. The notable feature is an impulsive type of variation in the amplitude profile in the vicinity of Re_{sb}, where supercritical bifurcation changes to subcritical one or vice-versa. Partially, this may be the consequence of very small value of $(a_1)_r$ when the change of bifurcation takes place and A_e or A_t is inversely proportional to the square root of $(a_1)_r$. Note that the unpredictable jump in the amplitude profile shows a complex phenomena in the flow instability. More about the possible justification of this unpredictable jump will be discussed later in this section. From the above discussion and the discussion made in review of linear stability results, we can conclude that for the shear instability of PMCF the bifurcation is supercritical whereas for mixed or buoyant the same may be supercritical or subcritical.

To show the variation of $(a_1)_r$ as a function of Re, when the porous medium is saturated by water, figures 4.6*(a)*, 4.6*(b)* and 4.6*(c)* are drawn for Da equal to 10^{-2}, 10^{-3} and

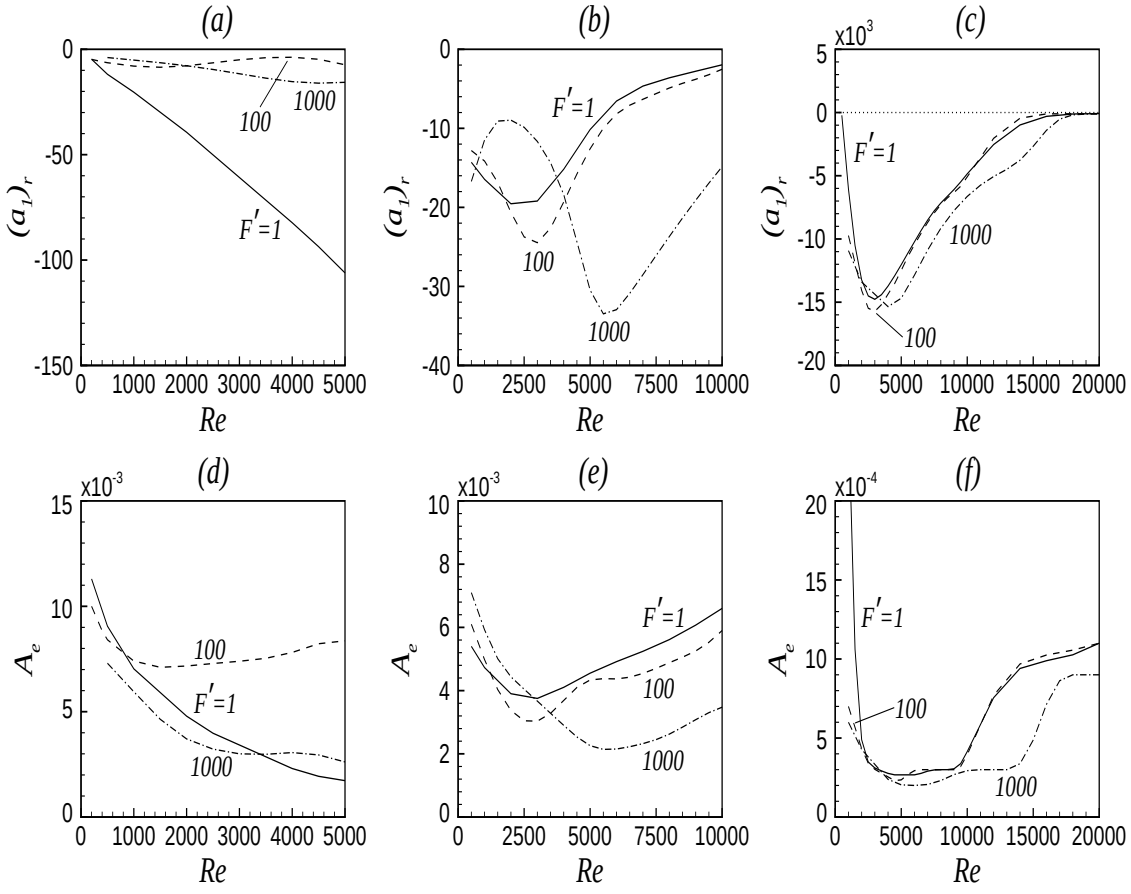

Figure 4.6: Variation of Landau constant ($(a_1)_r$) and equilibrium amplitude w.r.t. Re: (*a*,*d*) $Da = 10^{-2}$, (*b*,*e*) $Da = 10^{-3}$ and (*c*,*f*) $Da = 10^{-4}$ when $Pr = 7$.

10^{-4}, respectively. All these figures show only supercritical bifurcation. The corresponding amplitude profiles shown in figures 4.6*(d)*, 4.6*(e)* and 4.6*(f)* respectively vary smoothly for all Da as well as F'. Therefore, in the rest of this subsection we shall be restricted to only air saturated porous medium. Above observations make us curious to know about the variation of physical quantities like heat transfer rate in terms of Nusselt number and friction coefficient as a function of Re specially at the point where change of bifurcation takes place. As we have seen that in general F' delays the shifting whereas Da accelerates it. Therefore, in the rest of the analysis in this subsection, we have fixed the value of Da at 10^{-3}, F' at 100 and Pr at 0.7.

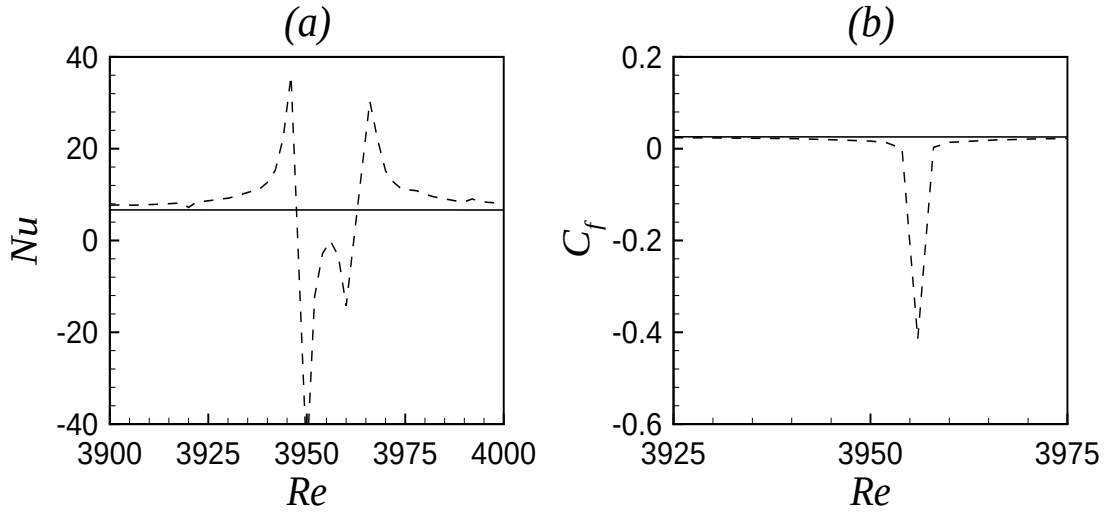

Figure 4.7: Variation of Nusselt number and friction coefficient w.r.t. Re when $Da = 10^{-3}$, $Pr = 0.7$ and $F' = 100$. Solid line and dashed line represents basic state and distorted state respectively.

4.5.1.1 Nusselt number and friction coefficient as a function of *Re*

The heat transfer rate in terms the Nusselt number is defined as

$$Nu = -2H_1/H_2,$$

where H_1 and H_2 are given by $\left.\frac{\partial \Theta}{\partial x}\right|_{x=1}$ and $\int_{-1}^{1} V\Theta dx / \int_{-1}^{1} V dx$, respectively. The functions V and Θ, calculated using the equilibrium amplitude, are given as $V_0 + {A_e}^2 V_1$ and $\Theta_0 + {A_e}^2 \Theta_1$, respectively. The functions V_1 and Θ_1 are the basic flow distortion functions. Similarly, the friction coefficient at the wall is given as [94]

$$C_f = -\frac{2}{Re} \left.\frac{\partial V}{\partial x}\right|_{x=1}.$$

The friction coefficient at the other wall of the channel ($x = -1$) is also same as the wall $x = 1$.

The impact of disturbance growth/decay on heat transfer rate is examined in figure 4.7*(a)*. Let, Nu_{bs} and Nu_{ds} be defined as Nusselt number predicted by the basic state (solid line) and distorted state (dashed line) respectively, in figure 4.7*(a)*. The results show that the Nusselt number estimated with the help of weakly nonlinear stability is more or less

same with the one calculated by the basic state except in the vicinity where the type of bifurcation gets changed. The impact of nonlinear interaction between different harmonic modes on the friction coefficient is displayed in figure 4.7*(b)*. The solid and dashed lines indicate the friction coefficient calculated by the basic state (C_{fbs}) and distorted state (C_{fds}), respectively. Similar to Nu_{ds}, the difference between C_{fds} and C_{fbs} is negligible, but the magnitude of C_{fds} increases drastically in the vicinity where change in bifurcation takes place.

In the context of complex behavior of flow mechanism, where a change from supercritical to subcritical (or reverse) bifurcation occurs, the basic flow $(V_0 \ \& \ \Theta_0)$ and basic flow correction distributions $(V \ \& \ \Theta)$ in the region of supercritical bifurcation as well as in the vicinity of Re_{sb} are examined. For this, we have chosen three different values 3000 (from supercritical zone), 3950(from supercritical zone), 3962(subcritical zone) of Re. Basic as well as distorted velocities and temperatures for above Re are shown in figures 4.8*(a)* and 4.8*(b)*, respectively. We note that the mean flow correction (lines other than solid), mainly in temperature (see figure 4.8*(b)*), loses the trend of the basic flow profile (solid line) in the vicinity of $Re_{sb} = 3952$, whereas it remains almost unchanged at $Re = 3000$. Furthermore, to understand the fluctuation of Nu_{ds} in the vicinity we have checked the variation of bulk temperature (given as $\int_{-1}^{1} V\Theta dy / \int_{-1}^{1} V dy$) and shown in figure 4.8*(c)*. As can be seen from this figure the bulk temperature goes on changing sign from negative to positive and again from positive to negative in the vicinity of $Re_{sb} = 3952$, resulting in the fluctuation of Nu_{ds} in the vicinity.

It should be noted that above phenomena (rapid change of Nu_{ds} as well as C_{fds} and negative Nu_{ds}) appearing in the vicinity of Re_{sb} was also reported for purely fluid medium [103] while studying nonlinear stability of mixed convection flow under non-Boussinesq condition in differentially heated channel. Thus we believe that the sudden appearance of subcritical bifurcation in the flow leads to a transverse mixing of the fluid layers in the transition mechanism. It is expected that the fluid motion near the bifurcation point will remain steady and parallel due to nearby stable branch of the supercritical bifurcation.

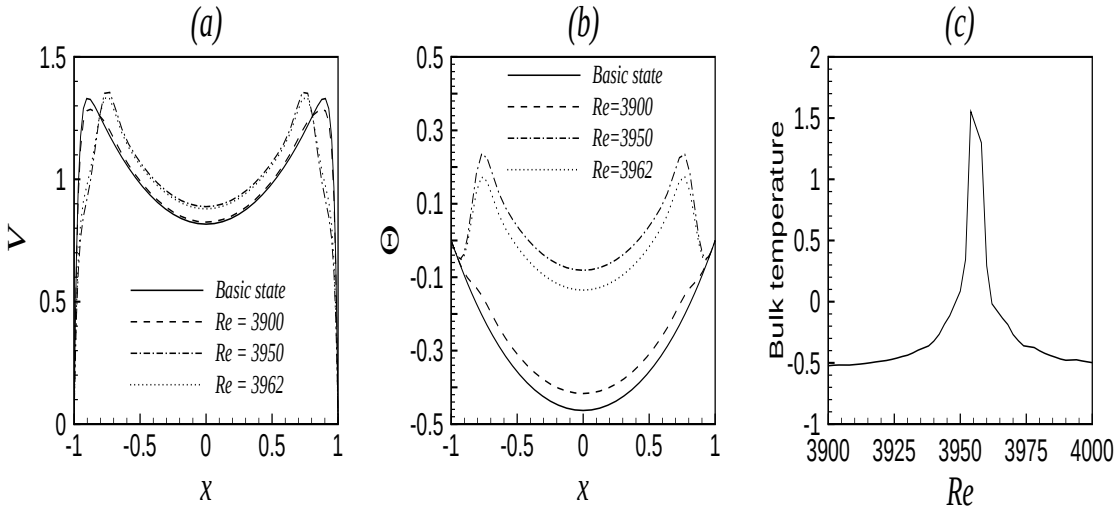

Figure 4.8: Variation of basic (solid line) and distorted (other lines) flow when $Da = 10^{-3}$, $Pr = 0.7$ and $F' = 100$: (a) velocity, (b) temperature and (c) bulk temperature.

4.5.1.2 Nonlinear energy spectrum as a function of *Re*

To understand the driving mechanisms of flow instability and change of bifurcation at a neighboring point ($\delta_{Ra} = 0.01$) of the least linearly stable point, the nonlinear KE spectrum in supercritical regime and subcritical regime is shown in figures 4.9*(a)* and 4.9*(b)*, respectively. From the figure 4.9*(a)* following points can be noted down. The term P_{101} is negative in this zone which implies that the gradient production of the KE for supercritical flow always tends to stabilize. It also remains almost constant. However, its contribution in the energy spectrum is negligible, i.e., gradient production through Reynolds stress is negligible. The magnitude of the term E_{12} is very small, i.e., the transfer of disturbance energy from fundamental to the harmonic wave is also negligible. The term T_{11} is positive through out the range of *Re*, i.e., the modified disturbance shape is favorable for buoyant production of the KE, whereas dissipation of KE through surface drag (K_{11}), which is the consequence of the change in the disturbance shape, is negative and increases as a function of *Re*. The term P_{110} is negative, i.e., the change in the shape of the disturbance is not favorable for shear production of the disturbance energy. As a result, it stabilizes the flow. In the subcritical zone, figure 4.9*(b)* shows that the terms P_{101}, E_{12} and F_{11} are negative with

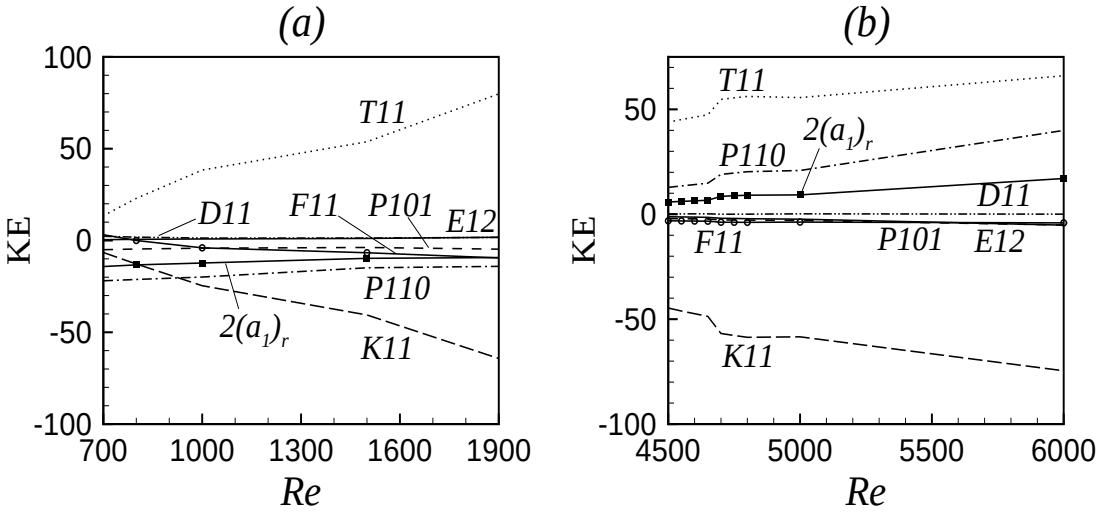

Figure 4.9: Variation of KE w.r.t. *Re* for $Da = 10^{-3}$, $Pr = 0.7$ and $F' = 100$: (*a*) Supercritical zone of *Re*, (*b*) Subcritical zone of *Re*.

very small magnitude, so their contribution in stabilizing the flow is almost negligible. In the KE spectrum, the term T_{11} and P_{110} are positive, i.e., the modified disturbance shape is favorable for buoyant production of the disturbance energy and the change in the shape of the disturbance is favorable for shear production of the disturbance energy. However, T_{11} plays the dominant role over P_{110} in the KE spectrum. The most dominant stabilizing term is K_{11}. So, we can conclude that the change of bifurcation from supercritical to subcritical is mainly due to the modification in the gradient production favorable for shear production of the KE.

Furthermore, the mathematical analysis of the nonlinear energy spectrum shows that the sum of different energy terms is twice the real part of Landau constant (see equation 4.40). Therefore, the type of bifurcation predicted by Landau constant can be reconfirmed through the sum of different energy terms. Consequently, the sum is shown in both figures 4.9*(a)* and 4.9*(b)*. As can be seen it supports the results obtained by Landau constant.

4.5.2 Bifurcation as a function of *Ra*

Weakly nonlinear analysis is only valid near the linear stability boundary point [32] and it addresses the question of what happens to an unstable flow. Rogers *et. al.* [88] have shown that the cubic Landau equation gives the correct results when the magnitude of c_i is small by comparison with the results from the direct numerical simulation as well as high-order weakly nonlinear results. They have also pointed out that the weakly nonlinear analysis is asymptotically correct for larger values of the Rayleigh number beyond the bifurcation point in the limit as c_i approaches zero. Based on this fact, for a given *Re*, we have studied the behavior of the Landau constant as well as equilibrium/threshold amplitude away from the critical *Ra*, as a function of δ_{Ra}. To check the transition mechanism at supercritical state as well as in the vicinity where the change of bifurcation as a function of *Re* takes place, two different values of *Re* one from supercritical zone and the other from subcritical zone are considered for a given *Da*. Accordingly, for three values 10^{-2}, 10^{-3} and 10^{-4} of *Da* three different respective values 1000, 1500 and 12000 of *Re* from the supercritical zone and three respective values 2030, 5000 and 15000 of *Re* from the subcritical zone are chosen. Here, F' is fixed at 100. From our numerical experiments we have checked that the magnitude of c_i for all the above values of *Re* is of the order of 10^{-2} in the considered range of δ_{Ra} (see figure 4.19 in Appendix B). Therefore, we also analyze the limiting value of growth of instabilities under nonlinear effects (i.e, nonlinear saturation) for larger values of the Rayleigh number beyond the bifurcation point (upto 3 times of critical *Ra*). However, a complete picture of nonlinear saturation can only be confirmed by use of direct numerical simulation, which is beyond the scope of the present work. Hence, a qualitative characteristic of the nonlinear interaction of different harmonic modes for larger values of *Ra* is also presented for the present problem. The variation of the Landau constant and amplitude as a function of δ_{Ra} for three values of *Re* chosen from super critical zone, are shown in figures 4.10*(a)* and 4.10*(b)*, respectively, whereas the same for *Re* chosen from the subcritical zone are shown in figures 4.10*(c)* and 4.10*(d)*, respectively. Figure 4.10*(a)* shows that the sign of $(a_1)_r$ is negative for all considered values of *Da* at and beyond

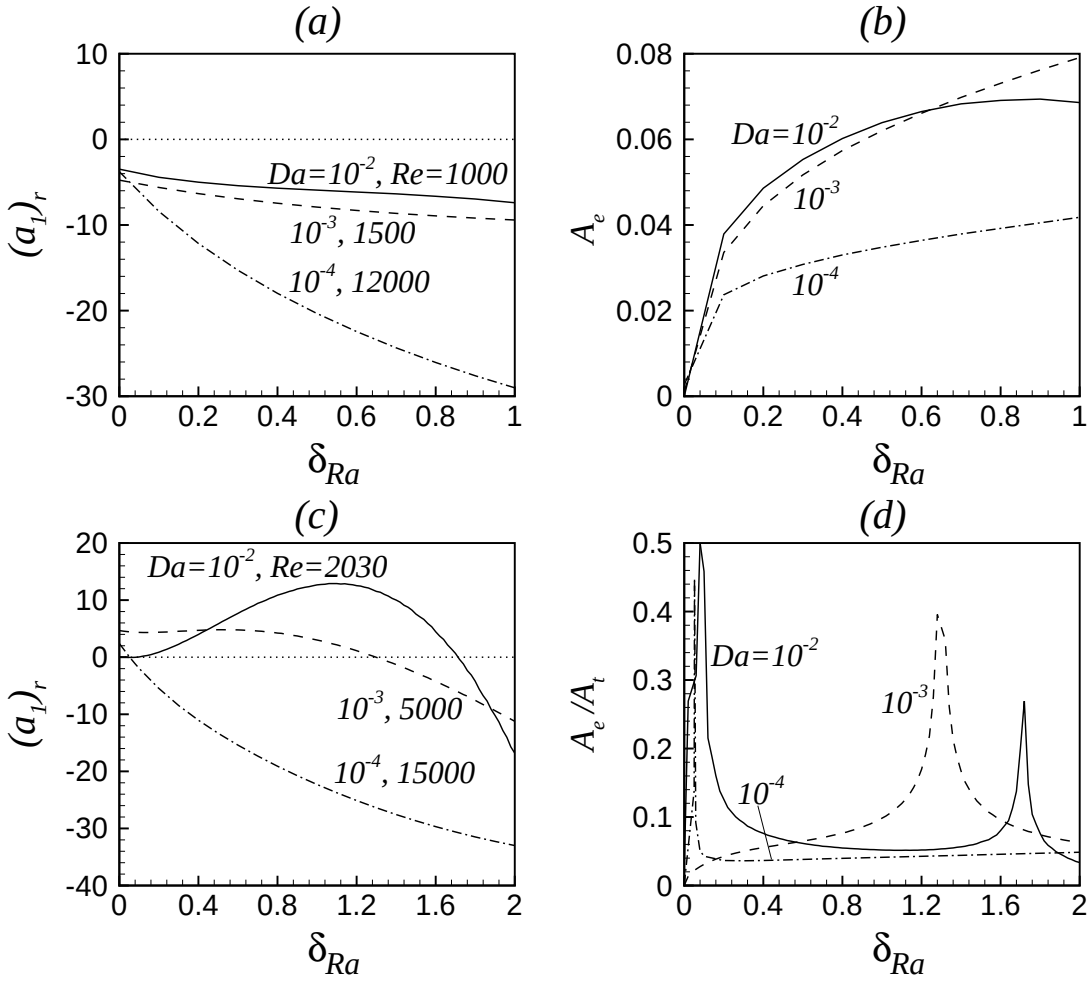

Figure 4.10: Variation of $(a_1)_r$ and amplitude w.r.t. δ_{Ra} when $Pr = 0.7$ and $F' = 100$:(a,b) Supercritical zone of Re, (c,d) Subcritical zone of Re.

the critical point which leads to supercritical bifurcation. The value of Landau constant decreases on increasing *Ra*. The corresponding equilibrium amplitude increases smoothly. This indicates that the supercritical bifurcation of the flow remains supercritical even when *Ra* is increased up to two times its critical value. Figure 4.10*(c)* shows that the sign of $(a_1)_r$ changes from positive to negative which leads to a change in bifurcation from subcritical to supercritical. Here also the equilibrium amplitude experiences a drastic change in the vicinity of point where change in bifurcation takes place (see figure 4.10*(d)*). Similar study is also made when the medium is saturated with water. However, the variation of Landau constant as a function of *Ra* predicts only supercritical bifurcation (see figure 4.20*(a)* in Appendix B) and the corresponding amplitude changes smoothly (see figure 4.20*(b)* in Appendix B). Therefore, in the rest of the section our analysis will be restricted to impact of non-linear interaction on PMCF of air only.

To understand the nonlinear impact on heat transfer rate away from the bifurcation point, figure 4.11*(a)* and 4.11*(b)* are drawn for *Re* equal to 1500 and 5000, respectively for $Da = 10^{-3}$. As can be seen from figure 4.11*(a)* that Nusselt number estimated with the help of weakly nonlinear stability is more than the one calculated by the basic state. The substantial increase in Nu_{ds} beyond the bifurcation point can be predicated due to instability of the flow. Quantitatively, we have observed that the increase in *Nu* due to nonlinear interaction is around 10% at $\delta_{Ra} = 0.5$. However, for *Re* in subcritical zone, Nu_{ds} increases steadily upto a threshold value of δ_{Ra} beyond which a fluctuation can be seen where it experiences positive and negative values. The friction coefficient, C_f, for above two values of *Re* is shown in figure 4.11*(c)* and 4.11*(d)*, respectively. The friction coefficient due to nonlinear interaction is less compared to the same calculated by basic state. It decreases as a function of *Ra*. Quantitatively speaking, the decrease in friction coefficient due to nonlinear interaction at $\delta_{Ra} = 0.5$ is 4.8%. Similar to Nusselt number, the profile of distorted state friction coefficient shows an abrupt change at larger values of the Rayleigh number due to shifting of the bifurcation.

The nonlinear spectrum of KE away from the critical point for $Da = 10^{-3}$ is shown

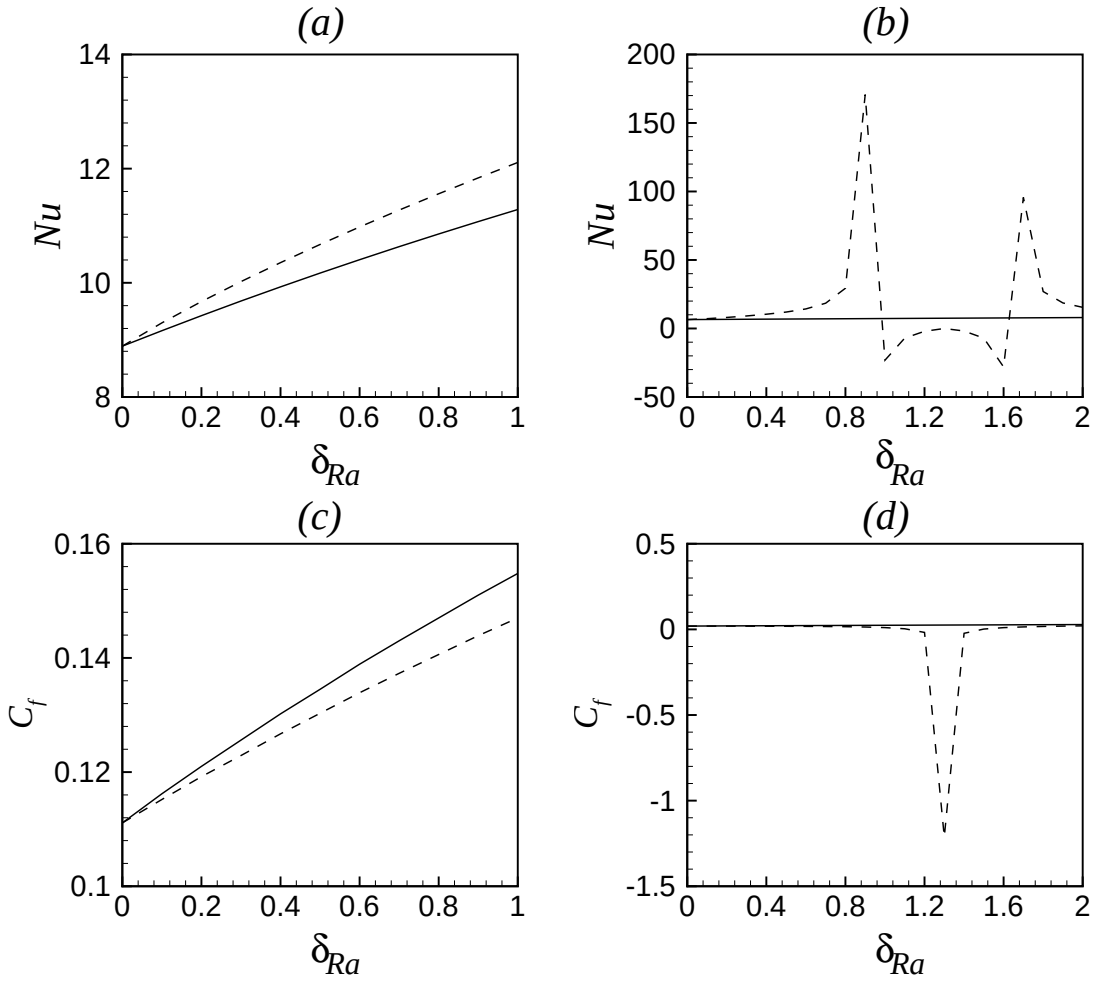

Figure 4.11: Variation of Nusselt number and friction coefficient w.r.t. δ_{Ra} for $Da = 10^{-3}$, $Pr = 0.7$ and $F' = 100$: (*a*,*c*) *Re*=1500 and (*b*,*d*) *Re*=5000. Solid line and dashed line represents basic state and distorted state respectively.

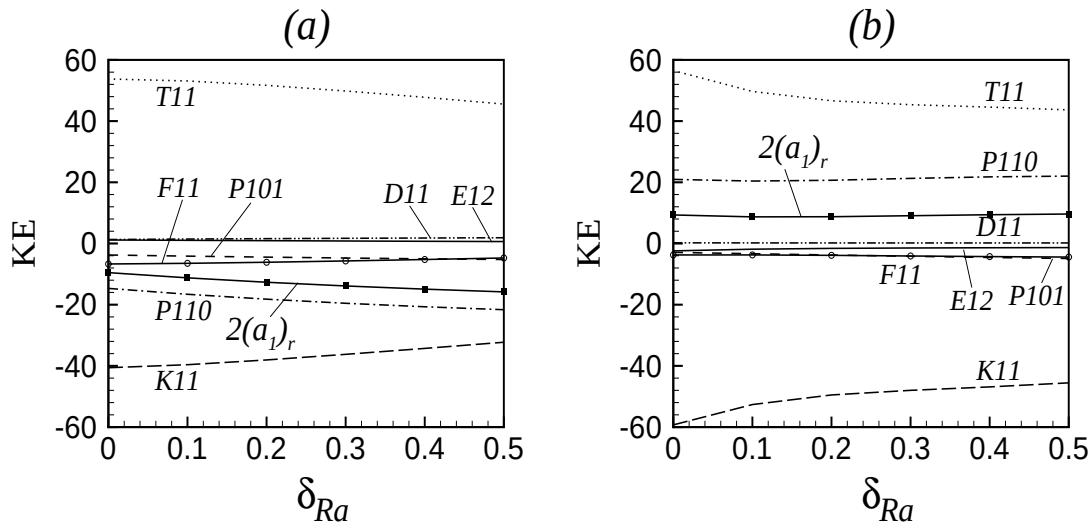

Figure 4.12: Variation of KE w.r.t. δ_{Ra} for $Da = 10^{-3}$, $Pr = 0.7$ and $F' = 100$: (*a*) *Re*=1500 and (*b*) *Re*=5000.

in figure 4.12*(a)* for supercritical zone and in figure 4.12*(b)* for subcritical zone of *Re*. The spectrum of KE in supercritical zone reveals that the term T_{11} is positive as a function of *Ra*, i.e., the modified disturbance shape is favorable for buoyant production of the KE and it is the main destabilizing factor. Although, the dissipation of KE through surface drag (D_{11}) is positive but it's impact is negligible as compared to T_{11}. The component K_{11}, which is the consequence of the change in disturbance shape, is negative and its magnitude decreases as a function of *Ra*. The term P_{110} is negative and its magnitude increases as a function of *Ra*. So it is not favorable for shear production of the disturbance energy. As a result, it is in favor of stabilizing the flow. It is to be noted that in the case of purely fluid domain [59] T_{11} was negative in supercritical zone and D_{11} was the main destabilizing factor. In the subcritical zone, similar to figure 4.9*(b)* here also P_{110} is positive and in favour of destabilizing the flow. The term K_{11} becomes the main stabilizing component (see figure 4.12*(b)*). So, we see that here also the change of bifurcation from supercritical to subcritical mainly occurs through the modification in the gradient production of disturbance energy due to the change of the disturbance shape. Also, the balance of KE supports the results obtained by Landau constant.

4.5.3 Bifurcation as a function of α

Since the lower-order weakly nonlinear analysis is asymptotically correct in the limit as c_i tends to zero, therefore the theory may be used to predict the behavior of the linear modes at the least-stable values of *Ra*. The variation of the neutral stability curve with wavenumber is also important because an instability that is supercritical for some wavenumber may be subcritical or supercritical at other nearby wavenumber [88]. In this situation, any of the potential unstable waves may grow and interact with other modes. Therefore, for the present problem we have chosen two different values of *Re*, one from supercritical zone and other from subcritical zone for a given *Da*. Accordingly, for three values 10^{-2}, 10^{-3}, and 10^{-4} of *Da* three different respective values 1000, 1500, and 12000 of *Re* from the supercritical zone and three respective values 2030, 5000 and 15000 of *Re* from the subcritical zone are chosen. Note that the corresponding critical points (α, Ra) for above chosen values of *Re* in supercritical zone are (1.76, 443.5), (1.42, 6701.3) and (1.4, 59067.2) and in subcritical zone are (2.04, 292), (1.58, 1525.4) and (1.32, 44423.4), respectively. For the above considered values of *Re* in supercritical as well as subcritical zone the type of instability is either buoyant or mixed (see figure 4.3*(a)*). The neutral stability curves $(c_i = 0)$ for different values of *Da* are plotted in figure 4.13. Here, solid and dashed line represents variation of *Ra* with α for a given *Re* from the supercritical and subcritical zone, respectively. It can be seen from the figure that, for $Da = 10^{-3}$, a large band of wavenumbers exists in which supercritical/subcritical bifurcation remains supercritical/subcritical. However, for $Da = 10^{-2}$ and $Re = 1000$, subcritical bifurcation can be seen for $\alpha < 0.9$ and supercritical for $\alpha \geq 0.9$. Similarly, for $Re = 2030$, supercritical bifurcation can be seen for $\alpha < 2.02$ and subcritical for $\alpha \geq 2.02$. In the case of $Da = 10^{-4}$, similar to $Da = 10^{-3}$, here also subcritical bifurcation for $Re = 15000$ remains subcritical for a large band of α, however, for $Re = 12000$ subcritical bifurcation can be seen for $\alpha < 1.3$ and supercritical for $\alpha \geq 1.3$. Note that for $Re = 12000$ the basic flow at the least linearly stable point (1.4, 59067.2) is supercritically stable whereas the same at nearby neutral point (1.3, 59530) is subcritically unstable. Similarly, for $Da = 10^{-2}$ the basic flow which is subcritically unstable at the

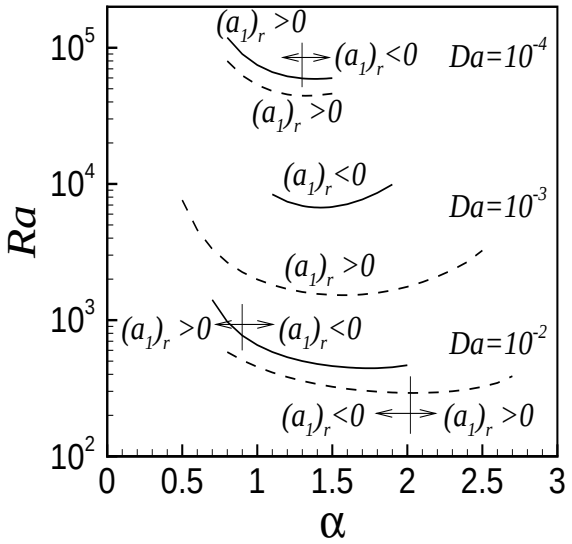

Figure 4.13: Neutral stability curve ($c_i = 0$) in (Ra,α)-plane for $Da = 10^{-2}$, $Da = 10^{-3}$ and $Da = 10^{-4}$ when $Pr = 0.7$ and $F' = 100$.

least linearly stable point (2.04, 291.9) is supercritically stable at the nearby neutral point (2.02, 292). From the above analysis we can point out that with the buoyant and mixed instabilities both subcritical and supercritical branches appear on the neutral curves.

4.5.4 Pattern of secondary flow

The overview of the above discussion suggests the existence of secondary flow with finite amplitude beyond the bifurcation point. We have seen that depending on the value of input parameter the bifurcation may be supercritical or subcritical. Apart from this, balance of kinetic energy depicts a different result relative to purely fluid domain, in supercritical zone. Therefore, nonlinear impact on secondary flow from linearly least stable wave is analyzed in supercritical as well as subcritical zone. The secondary flow under linear stability analysis is obtained from eigen function associated to linearly least stable eigen value and the same from weakly nonlinear analysis is calculated as a superposition of different harmonics (here, E^1 and E^2 in equation (4.18)). Following Khandelwal and Bera [59], the functions $\hat{u}_1$, $\hat{u}_2$, etc., for the secondary flow are calculated. The eigen function includes $\hat{u}$,

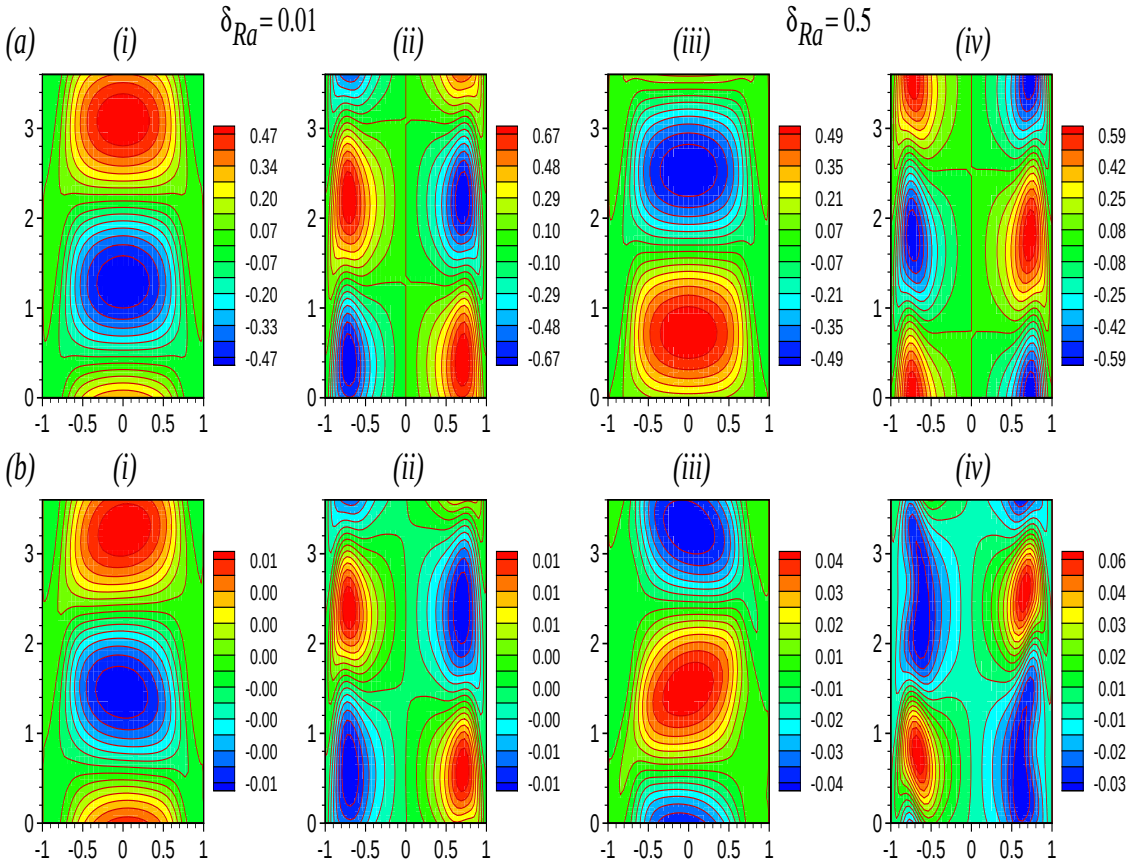

Figure 4.14: Pattern of secondary flow by (a) linear stability (b) non-linear stability when $Da = 10^{-2}$, Pr = 0.7, Re = 1000 and $\delta_{Ra} = 0.01$ as well as $\delta_{Ra} = 0.5$: (i) and (iii) disturbance u-velocity; (ii) and (iv) disturbance temperature.

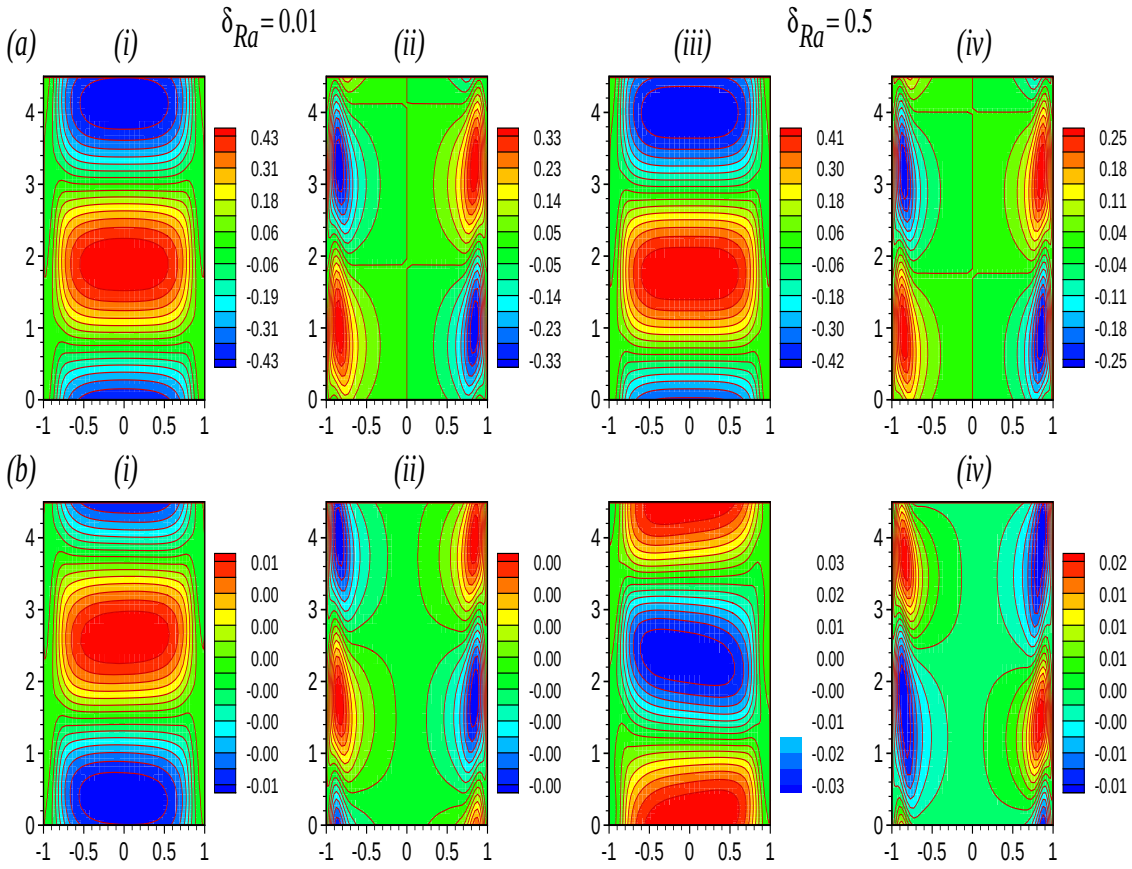

Figure 4.15: Pattern of secondary flow by (a) linear stability (b) non-linear stability when $Da = 10^{-3}$, Pr = 0.7, Re = 1500 and $\delta_{Ra} = 0.01$ as well as $\delta_{Ra} = 0.5$: (i) and (iii) disturbance u-velocity; (ii) and (iv) disturbance temperature.

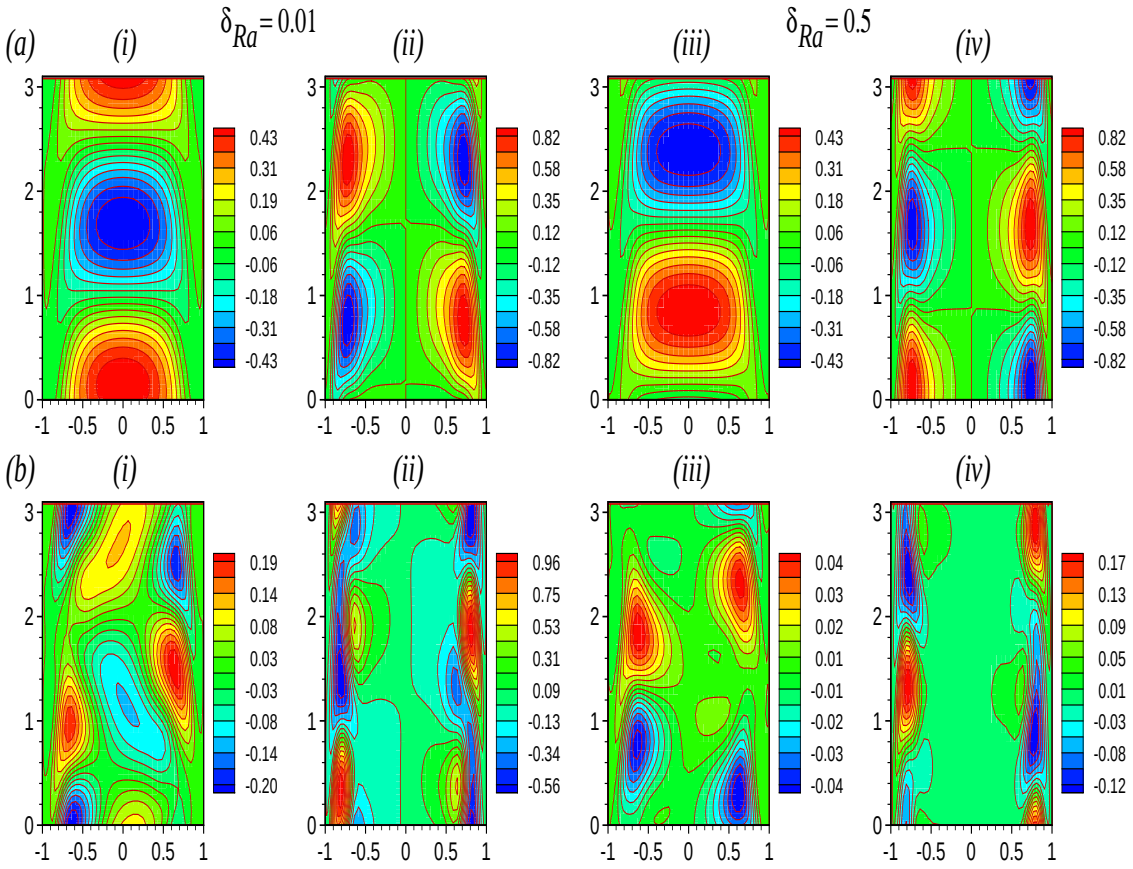

Figure 4.16: Pattern of secondary flow by (a) linear stability (b) non-linear stability when $Da = 10^{-2}$, Pr = 0.7, Re = 2030 and $\delta_{Ra} = 0.01$ as well as $\delta_{Ra} = 0.5$: (i) and (iii) disturbance u-velocity; (ii) and (iv) disturbance temperature.

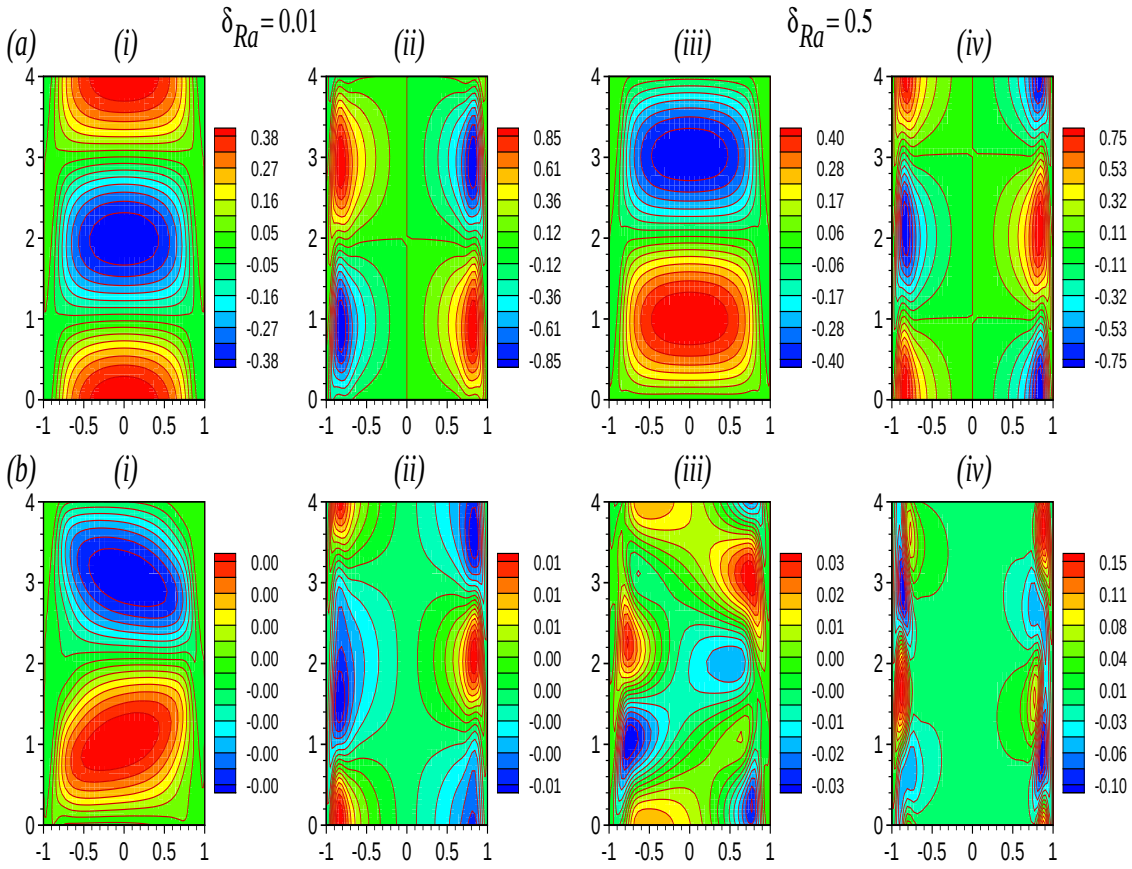

Figure 4.17: Pattern of secondary flow by (a) linear stability (b) non-linear stability when $Da = 10^{-3}$, Pr = 0.7, Re = 5000 and $\delta_{Ra} = 0.01$ as well as $\delta_{Ra} = 0.5$: (i) and (iii) disturbance u-velocity; (ii) and (iv) disturbance temperature.

$\hat{v}$, and $\hat{\theta}$. However, to avoid numerous figures the pattern of $\hat{v}$ is not shown in the following. We are interested to study the pattern of secondary flow very close to the bifurcation point ($\delta_{Ra} = 0.01$) as well as far away from the bifurcation point ($\delta_{Ra} = 0.5$) under linear as well as weakly nonlinear analysis. The patterns of secondary flow in supercritical regime, when $Re = 1000$ and $Da = 10^{-2}$, from linear stability theory and weakly non-linear stability theory are shown in figures 4.14*(a)* and 4.14*(b)*, respectively. As can be seen from the above figures that the difference between patterns of secondary flow using linear and weakly nonlinear theories at $\delta_{Ra} = 0.01$ is negligible as compared to the same at $\delta_{Ra} = 0.5$. However, magnitude wise it differs significantly at both values of δ_{Ra}. To check the above result for other value of Da we have plotted the same for $Da = 10^{-3}$ when $Re = 1500$ in figures 4.15*(a)* and 4.15*(b)*, respectively. It also gives similar impression. In subcritical zone for $Da = 10^{-2}$, figures 4.16*(a)* and 4.16*(b)* show that the uni-cellular structure of $\hat{u}$ from linear stability theory shift to deformed multicellular structure. Deformation of the secondary cells under subcritical bifurcation accelerates as one moves away from the bifurcation point. In order to cross check the same when Da is changed to $Da = 10^{-3}$, figure 4.17 is drawn for subcritical zone of $Re = 5000$. The remarks made for pattern deformation of the the secondary flow under linear stability theory due to non-linear interaction of different harmonics at $Da = 10^{-2}$ remains valid for this Darcy number too.

From the above analysis, we would like to mention that a jump in the amplitude profile of a physical problem leads to an abrupt transition from supercritical to subcritical flow and deformed the pattern of secondary flow under linear stability analysis drastically (see figures 4.16 and 4.17). Of course this kind of abrupt change does not occur in the laminar-transition. A higher order weakly nonlinear analysis may help to examine the clear interpretation towards the repeated bifurcation in the flow, which is also beyond the scope of present work. But in this situation we probably anticipate that similar to the pipe flow [44, 49], here also the transition to disorder flow may occur suddenly. In other situation, the deformation of pattern of secondary flow far away from the vicinity of Re_{sb} (see figures 4.14 and 4.15) shows a slow and smooth change as a function Ra. Therefore,

we can anticipate that, as in the case of pipe flow [77], here also the transition from smooth laminar to disorder turbulent flow may involve a sequence of instabilities.

4.6 Summary and Conclusions

This study considers the weakly non-linear stability analysis of stably stratified PMCF of air as well as water in a vertical channel filled with porous medium. The flow in the channel is governed by the volume-averaged forms of the Naiver-Stokes and continuity equations derived by Whitaker [123]. The purpose of this study is to analyze the nature of bifurcation and the finite amplitude behavior of unstable disturbances that occur beyond the linear instability boundary, especially when the permeability of the medium and strength of the flow are reasonably high. This is accomplished by reviewing the linear stability results, and then a weakly nonlinear analysis is made to trace the evolution of finite amplitude perturbation. From the review it has been checked through dimensional analysis that the non-isothermal PMCF becomes unstable under mild heating condition. For example, when the channel is filled with water saturated porous medium with permeability equal to $10^{-7}\mathrm{m}^2$, PMCF becomes unstable even when the temperature gradient $C = 3.7$. In the case when channel is filled with air saturated porous medium with permeability equal to $9 \times 10^{-7}\mathrm{m}^2$, PMCF becomes unstable when $C = 13.9$. The results obtained using Boussinesq approximation remains valid for wide range of input parameters.

To study the evolution of finite amplitude perturbation, first we have analyzed the variation of real part of Landau constant ($(a_1)_r$) and amplitude in the vicinity of the least linearly stable point as a function of Re for air as well as water. Depending on the flow strength as well as media permeability, the weakly nonlinear analysis predicts both supercritical and subcritical bifurcations for air and only supercritical bifurcation for water. In the case of air, an increase in Forchheimer number or decrease in media permeability delays the shift of bifurcation from supercritical to subcritical or vice versa in Reynolds number space. In general, compared to subcritical bifurcation, the supercritical bifurcation

occurs at relatively lower values of *Re*. The amplitude profile shows a peak, due to change in sign of $(a_1)_r$, at the Reynolds number where the shift in bifurcation from supercritical to subcritical takes place. The similar characteristic is also observed in physical quantities such as Nusselt number and friction coefficient, which is a consequence of the distortion in basic flow velocity and temperature.

For air, when $Da = 10^{-3}$, the nonlinear spectrum of kinetic energy in supercritical regime of *Re* shows that due to change in the shape of fundamental wave, modification in the buoyant production of KE (T_{11}) becomes main destabilizing factor, however modification in the gradient production (P_{110}) as well as modification in the surface drag dissipation (K_{11}) become major stabilizing factors. On the other hand in the subcritical regime of *Re*, P_{110} is a destabilizing factor along with T_{11}. Furthermore, based on very small value of c_i, we have analyzed the bifurcation away from the critical point for particular choice of *Re* in super as well as subcritical regimes. It has been found that for all considered values of *Da* the supercritical bifurcation as a function of *Ra* remains supercritical whereas in subcritical regime it may change to supercritical one. Also, the heat transfer rate (skin friction) increases (decreases) significantly and experiences jump in the neighbourhood of *Ra* where the change of bifurcation takes place. Furthermore, the analysis of nonlinear balance of kinetic energy for the disturbance also supports the results obtained through Landau constant, i.e., if the bifurcation of PMCF is found to be supercritical/subcritical from the Landau constant, then it also remains supercritical/subcritical under energy analysis. It is important to mention here that while studying mixed convection flow in vertical annulus Rogers *et. al.* [88] have found that the buoyant instability is supercritical at all wavenumbers whereas with the shear and interactive (or mixed) instabilities, both subcritical and supercritical branches appear on the neutral curves. In contrast to the above results it has been observed in the present study that with the buoyant and mixed instabilities both subcritical and supercritical branches appear on the neutral curves. Finally, for values of *Re* in supercritical regime, the disturbance temperature contours maintain the same shape but due to nonlinear interaction of waves they move towards the center of the channel and the

maximum magnitude of all the disturbance field variables reduce significantly. In the case of *Re* in subcritical regime, the shape of disturbance velocity as well as temperature contours gets changed drastically which in turn enhances the destabilizing characteristic of T_{11} and changes the stabilizing nature of P_{110} in supercritical bifurcation into a destabilizing nature in subcritical bifurcation.

The details of finite amplitude stability analysis for PMCF in a vertical porous-medium channel are of much interest. Although we have explored some important features including type of bifurcations, energy transfer and secondary flow. But the findings can also be viewed in a broader context of the stability behavior of the present flow with the help of higher order weakly nonlinear stability analysis and full numerical simulation. These analyses are left for our future study.

Appendix A: A note about model equations

Due to lack of unified theory for transport in porous media, different models have emerged based on empirical results (i.e., experimental data) as well as different theoretical approaches (i.e., volume-averaged analysis, matched asymptotic expansion, *etc.*). The volume-averaged Navier-Stokes (VANS) equation derived by Whitaker [123] for an incompressible viscous fluid flowing through a rigid, homogeneous, isotropic, porous medium is of the form

$$\rho_f \left[\frac{1}{\varepsilon} \frac{\partial \mathbf{v}}{\partial t} + \frac{1}{\varepsilon^2} \mathbf{v}.\nabla \mathbf{v} + C_F K^{-1/2} |\mathbf{v}| \mathbf{v} \right] = -\nabla P + \rho g \mathbf{e_y} + \widetilde{\mu} \nabla^2 \mathbf{v} - \mu_f \frac{\mathbf{v}}{K}, \tag{4.50}$$

where $\mathbf{v}$ is the Darcy velocity, P is the pressure, ε is the porosity of the medium, C_F is the form drag coefficient, K is the permeability of the porous medium, g is gravitational acceleration, $\widetilde{\mu}$ is the effective viscosity, μ_f is the fluid viscosity, ρ_f is fluid density, ρ is fluid density given by equation of state, and $\mathbf{e_y}$ is unit vector in the y-direction. In this equation, the Darcy term ($\mu_f \mathbf{v}/K$) represents a volume-averaged viscous drag, the Brinkman term ($\widetilde{\mu}\nabla^2\mathbf{v}$) represents a volume-averaged viscous diffusion, the Forchheimer term ($C_F K^{-1/2}|\mathbf{v}|\mathbf{v}$) represents form-drag due to inertial effects, and the convective term ($\rho_f \mathbf{v}.\nabla\mathbf{v}/\varepsilon^2$) represents another drag which arises from inertial effects. It is important to mention that volume averaging the convective term in the Navier-Stokes equation generates

the terms $\rho_f \mathbf{v}.\nabla\mathbf{v}/\varepsilon^2$ and $C_F K^{-1/2}|\mathbf{v}|\mathbf{v}$ when the difference between velocity of fluid and volume average velocity of fluid is negligible. Whitaker [123] found that the contribution of convective term $\rho_f \mathbf{v}.\nabla\mathbf{v}/\varepsilon^2$ is negligible in comparison with the dominant Forchheimer term, $C_F K^{-1/2}|\mathbf{v}|\mathbf{v}$. However, without a convective term, there is no mechanism for development of the flow field which leads to a physically flawed and unrealistic situation [119]. The literature review reveals some inconsistencies in the proper form of equations governing flow through porous media [42, 65, 123] but the form of equation by the volume-averaged method is particularly useful in channel flow [117, 131]. Note that Vafai *et. al.* [120] as well as Hsu *et. al.* [51] have also used volume averaging concept to derive porous flow equations similar to the above equation. Without diminishing the importance of their work, we also prefer the derivation of Whitaker [123] because it is, to the best of our knowledge, the most complete and formal.

The contribution of different terms in the above equation depends mainly on (i) the type of porous medium in which fluid flow is considered and (ii) the nature and strength of the flow. Darcy model is limited to describe the fluid flow in a porous medium when the Darcy velocity is small. It does not satisfy no-slip condition. To investigate the dynamics of pressure driven flow in a channel, Brinkman term is required to satisfy the no-slip condition [117]. Furthermore, if the porous medium is made of metallic foam then the Forchheimer-extended Darcy law is valid for most of the metal foams [131]. If the permeability of the medium is high and strength of the forced flow is also reasonably high then the contribution of $\rho_f \mathbf{v}.\nabla\mathbf{v}/\varepsilon^2$ is expected in evaluating the instability boundary point or critical point of a basic flow.

In this context a rigorous study is already reported by Kumar *et. al.* [60]. The authors have shown that if the permeability of the medium is not high then the results (i.e., instability boundary curve) from model containing Darcy and Brinkman terms and model containing Darcy, Brinkman and Forchheimer terms are same. Also, in this situation, results from model containing Darcy, Brinkman, and convective terms and model containing Darcy, Brinkman, convective and Forchheimer terms are same. They have also shown that

all the four models give almost same result when the fluid is water. Apart from these, while studying the effect of particle size of porous medium on forced convection from a circular cylinder without assuming local thermal equilibrium between phases, Al-Sumaily *et. al.* [1] have shown that the model containing all the four terms mentioned above gives a very good approximation to the experimental result. The appropriateness of inclusion of different terms in the momentum equation is still a matter of vital discussion in the literature.

Appendix B

B.1: Basic flow profiles

The basic velocity profile for different Da at $F' = 1$ and 100 are shown in figures 4.18*(a)* and 4.18*(b)*, respectively. As can be seen from the above figure that for each considered value of Da as well as F' the velocity profile contains point of inflection for $Ra = 500$, which is consequence of (i) no slip condition on the wall, (ii) acceleration of fluid near the wall due to buoyant term, and (iii) deceleration of the colder fluid near center due to mass conservation. The point of inflection dies out on decreasing the value of Da as well as F'. Appearance of inflection point indicates a potential of instability.

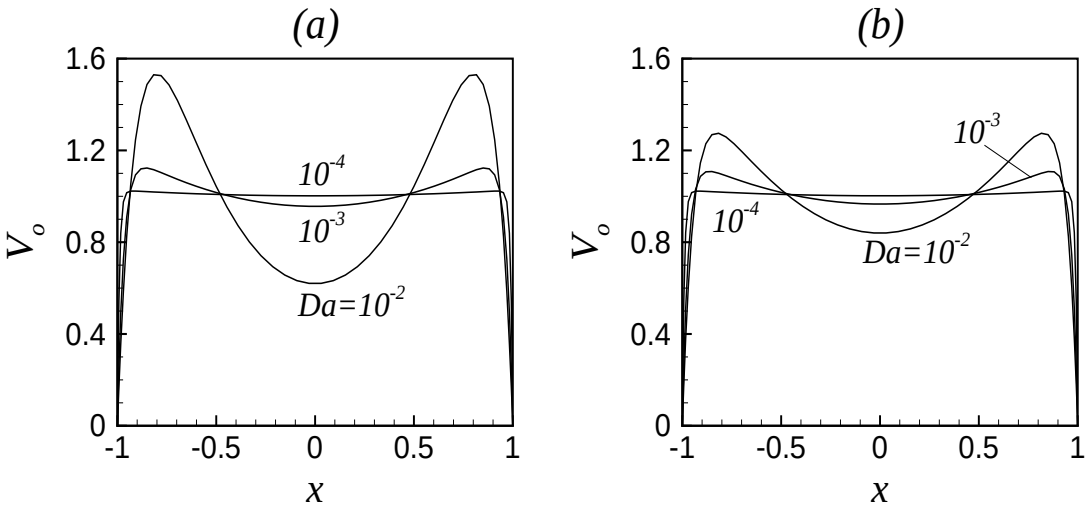

Figure 4.18: Basic velocity profile for different Da: (a) $F' = 1$ and (b) $F' = 100$ when $Ra = 500$.

B.2: Growth rate of disturbance

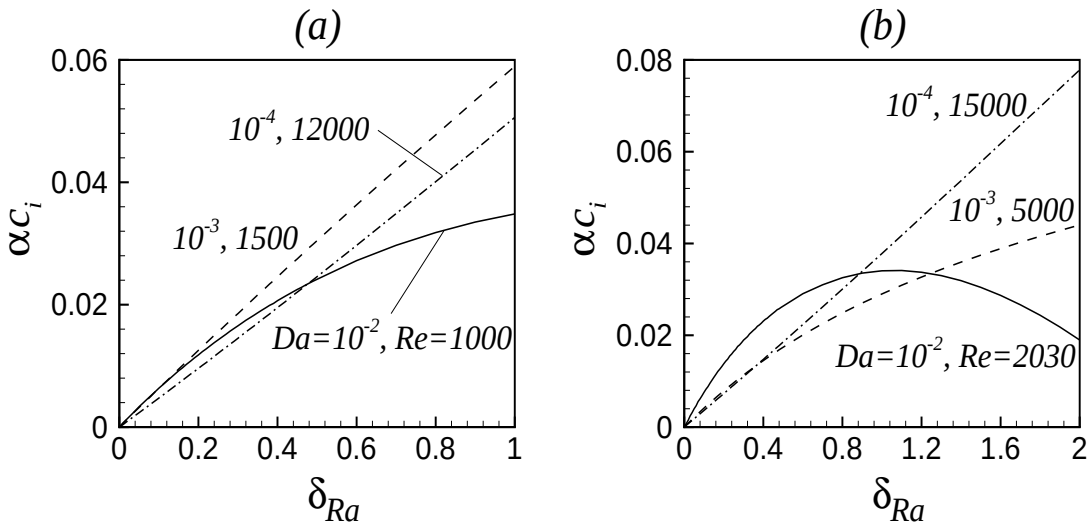

Figure 4.19: Variation of growth rate(αc_i) as a function of δ_{Ra}.

The growth rate as a function of *Ra* in supercritical and subcritical regimes of *Re* is shown in figures 4.19*(a)* and 4.19*(b)*, respectively. Both figures show the validity of linear variation of growth rate far away from the critical point for $Da = 10^{-3}$ and 10^{-4}. However, in case of $Da = 10^{-2}$ it is true for $\delta_{Ra} \leq 0.2$ and $\delta_{Ra} \leq 0.08$ for supercritical and subcritical cases, respectively.

B.3: Variation of Landau constant and amplitude for water

The variation of real part of Landau constant and the corresponding ampltitude are plotted in figures 4.20*(a)* and 4.20*(b)*, respectively when the porous medium is saturated by water. For all the three considered values of *Da* figure 4.20*(a)* shows that $(a_1)_r$ is negative, i.e., bifurcation at and beyond the critical point is supercritical. The corresponding equilibrium amplitude profile for two values 10^{-3} and 10^{-4} of *Da* indicates a smooth increase in magnitude, however the same for $Da = 10^{-2}$ increases upto $\delta_{Ra} = 1.1$ and beyond it the same decreases.

Appendix C: Linear adjoint equations

The solution of adjoint system of linear instability equations (4.11)-(4.15) is needed to obtain the Landau constant. The definition of adjoint operator is given as [59]

$$\langle LX, X^* \rangle = \langle X, L^* X^* \rangle, \tag{4.51}$$

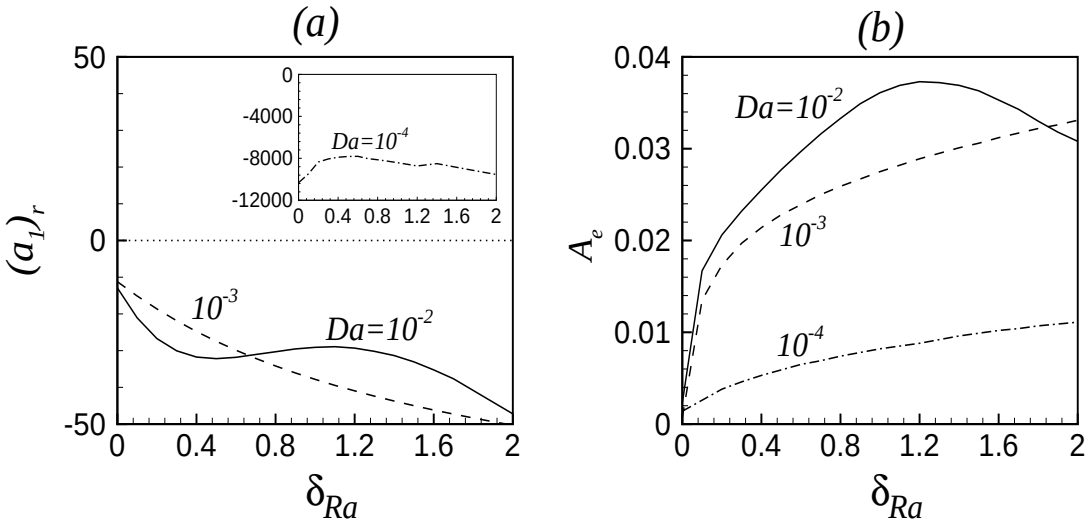

Figure 4.20: Variation of (a) $(a_1)_r$ and (b) amplitude w.r.t. δ_{Ra} when $Pr = 7$, $Re = 1000$ and $F' = 100$.

where $X^* = [u^*, v^*, w^*, \theta^*, p^*]$ is adjoint eigenfunction, $L = [\mathscr{L}_o, \mathscr{L}_x, \mathscr{L}_y, \mathscr{L}_z, \mathscr{L}]$ is the linear stability operator and $L^* = [\mathscr{L}_o^*, \mathscr{L}_x^*, \mathscr{L}_y^*, \mathscr{L}_z^*, \mathscr{L}^*]$ is corresponding adjoint operator. The inner product in this definition is the standard inner product given as

$$\langle Y(x), Z(x) \rangle = \int_{-1}^{1} Y^*(x) Z(x) dx = \int_{-1}^{1} \sum_{i=1}^{5} (y_i^*(x) z_i(x) dx, \tag{4.52}$$

where the superscript $*$ denotes the adjoint eigenfunction. The corresponding adjoint equations of linear stability equations (4.11)-(4.15) are given as:

$$\mathscr{L}_o^*(\alpha, \beta, u^*, v^*, w^*) = \frac{du^*}{dx} - i\alpha v^* - i\beta w^* = 0, \tag{4.53}$$

$$\begin{aligned}\mathscr{L}_x^*(\alpha, \beta, c, u^*, v^*, p^*, \theta^*, V_0, \Theta_0, Da, F') = i\alpha Re \frac{1}{\varepsilon}\left(\frac{1}{\varepsilon}V_0 - c\right)u^* + \frac{Re}{\varepsilon^2}\frac{dV_0}{dx}v^* \\ - \lambda\left(\frac{d^2u^*}{dx^2} - (\alpha^2+\beta^2)u^*\right) - \frac{dp^*}{dx} + \frac{1}{Da}u^* + F'|V_0|u^* - PrRe\frac{d\Theta_0}{dx}\theta^* = 0.\end{aligned} \tag{4.54}$$

$$\begin{aligned}\mathscr{L}_y^*(\alpha, \beta, c, v^*, p^*, \theta^*, V_0, Da, F') = & i\alpha Re \frac{1}{\varepsilon}\left(\frac{1}{\varepsilon}V_0 - c\right)v^* - \lambda\left(\frac{d^2v^*}{dx^2} - (\alpha^2+\beta^2)v^*\right) \\ & + i\alpha p^* + \frac{1}{Da}v^* + 2F'|V_0|v^* - \theta^* = 0,\end{aligned} \tag{4.55}$$

$$\mathscr{L}_z^*(\alpha,\beta,c,w^*,p^*,V_0,Da,F') = i\alpha Re\frac{1}{\varepsilon}\left(\frac{1}{\varepsilon}V_0 - c\right)w^* - \lambda\left(\frac{d^2w^*}{dx^2} - (\alpha^2+\beta^2)w^*\right) + i\beta p^* + \frac{1}{Da}w^* + F'|V_0|w^* = 0, \tag{4.56}$$

$$\mathscr{L}^*(\alpha,\beta,c,v^*,\theta^*,V_0,Ra) = -i\alpha PrRe(V_0-\sigma c)\theta^* + \left(\frac{d^2\theta^*}{dx^2} - (\alpha^2+\beta^2)\theta^*\right) - Ra\, v^* = 0. \tag{4.57}$$

The above equations are solved by eliminating the pressure terms along with no-slip and impermeability condition of velocity and zero temperature perturbation on the walls. The corresponding boundary conditions for adjoint system are:

$$u^* = v^* = w^* = \theta^* = 0 \quad \text{at} \quad x = \pm 1. \tag{4.58}$$

These adjoint eigenfunctions are also normalized to satisfy the equation

$$\int_{-1}^{1}\left[\frac{1}{\varepsilon}(\hat{u}u^* + \hat{v}v^* + \hat{w}w^*) - Pr\hat{\theta}\theta^*\right]dx = 1. \tag{4.59}$$

Chapter 5

Finite amplitude analysis of non-isothermal parallel flow in a differentially heated vertical channel filled with porous medium

As it was observed in chapter 4 that based on the values of different controlling parameters, both supercritical and subcritical bifurcations of non-isothermal parallel flow of air in vertical channel are possible. So, here also we are interested to see whether that type of change of bifurcation can take place or not when linearly heated vertical channel is replaced by differentially heated vertical channel. Therefore, in this chapter, we have investigated the finite amplitude stability of mixed convection flow in a differentially heated vertical channel filled with porous medium whose linear stability results are already discussed in Chapter 2. The results are presented with respect to two different fluids with Prandtl number equal to 0.7 and 7.

5.1 Finite amplitude analysis

The basic flow equations in operator form are given as:

$$L_y(V_0,\Theta_0,Gr',Da,F') = \lambda\frac{d^2V_0}{dx^2} - \frac{1}{Da}V_0 + Gr'\Theta_0 - F'|V_0|V_0 = Re\frac{dP_0}{dy}, \tag{5.1}$$

$$L(\Theta_0) = \frac{d^2\Theta_0}{dx^2} = 0, \tag{5.2}$$

with boundary conditions:

$$V_0 = \Theta_0 = 0 \quad \text{at} \quad x = \pm 1, \tag{5.3}$$

The linearized disturbance equations in operator form are given as:

$$\mathscr{L}_o(\alpha,\beta,\hat{u},\hat{v},\hat{w}) = \frac{d\hat{u}}{dx} + i\alpha\hat{v} + i\beta\hat{w} = 0, \tag{5.4}$$

$$\begin{aligned}\mathscr{L}_x(\alpha,\beta,c,\hat{u},\hat{p},V_0,Da,F') &= i\alpha Re\frac{1}{\varepsilon}\left(\frac{1}{\varepsilon}V_0 - c\right)\hat{u} - \lambda\left(\frac{d^2\hat{u}}{dx^2} - (\alpha^2+\beta^2)\hat{u}\right)\\ &+ Re\frac{d\hat{p}}{dx} + \frac{1}{Da}\hat{u} + F'|V_0|\hat{u} = 0,\end{aligned} \tag{5.5}$$

$$\begin{aligned}\mathscr{L}_y(\alpha,\beta,c,\hat{u},\hat{v},\hat{p},\hat{\theta},V_0,Gr',Da,F') &= i\alpha Re\frac{1}{\varepsilon}\left(\frac{1}{\varepsilon}V_0 - c\right)\hat{v} - \lambda\left(\frac{d^2\hat{v}}{dx^2} - (\alpha^2+\beta^2)\hat{v}\right)\\ &+ i\alpha Re\hat{p} + Re\frac{1}{\varepsilon^2}\frac{dV_0}{dx}\hat{u} + \frac{1}{Da}\hat{v} + 2F'|V_0|\hat{v} - Gr'\hat{\theta} = 0,\end{aligned} \tag{5.6}$$

$$\begin{aligned}\mathscr{L}_z(\alpha,\beta,c,\hat{w},\hat{p},V_0,Da,F') &= i\alpha Re\frac{1}{\varepsilon}\left(\frac{1}{\varepsilon}V_0 - c\right)\hat{w} - \lambda\left(\frac{d^2\hat{w}}{dx^2} - (\alpha^2+\beta^2)\hat{w}\right)\\ &+ i\beta Re\hat{p} + \frac{1}{Da}\hat{w} + F'|V_0|\hat{w} = 0,\end{aligned} \tag{5.7}$$

$$\begin{aligned}\mathscr{L}(\alpha,\beta,c,\hat{u},\hat{\theta},V_0,\Theta_0) &= -i\alpha PrRe(V_0 - \sigma c)\hat{\theta} + \left(\frac{d^2\hat{\theta}}{dx^2} - (\alpha^2+\beta^2)\hat{\theta}\right)\\ &- PrRe\frac{d\Theta_0}{dx}\hat{u} = 0.\end{aligned} \tag{5.8}$$

The corresponding boundary conditions for the perturbed field variables are:

$$\hat{u} = \hat{v} = \hat{w} = \hat{\theta} = 0 \ \text{ at } \ x = \pm 1. \tag{5.9}$$

As in the previous chapter, the Fourier expansion of the x-direction velocity in separable form in terms of c_i is given as [101]:

$$\begin{aligned} v(x,y,z,t) =& V(x,\tau)E^0 + \hat{v}_1(x,\tau)E^1 + \hat{v}_2(x,\tau)E^2 + \cdots + c.c. \\ =& E^0[V_0(x) + c_i|B(\tau)|^2 V_1(x) + O((c_i)^2)] + E^1[(c_i)^{1/2}Bv_{10} + (c_i)^{3/2}B|B|^2 v_{11} \\ &+ O((c_i)^{5/2})] + E^2[c_i B^2 v_{20} + O((c_i)^2)] + \cdots + c.c. \end{aligned} \tag{5.10}$$

where, $E = e^{[i\alpha(y-c_r t)+i\beta z]}$. The expansions for the other dependent variables can be written in similar way. Substituting (5.10) into the governing equations (2.2)-(2.4) and separating the harmonic components, the equations for the harmonic E^0 (mean flow) are given as

$$\begin{aligned} L_y(V_0,\Theta_0,Gr',Da,F') - Re\frac{dP_0}{dy} + c_i|B|^2\left\{\frac{d^2V_1}{dx^2} - \frac{1}{Da}V_1 + Gr'\Theta_1 - 2F'|V_0|V_1 - Re\frac{dP_1}{dy}\right\} \\ = O((c_i)^2), \end{aligned} \tag{5.11}$$

$$L(\Theta_0) + c_i|B|^2\left\{L(\Theta_1) - PrRe\left[\frac{\partial}{\partial x}(u_{10}\tilde{\theta}_{10} + \tilde{u}_{10}\theta_{10})\right]\right\} = O((c_i)^2). \tag{5.12}$$

The equations for harmonic E^1 can be written as

$$(c_i)^{1/2}B\{\mathscr{L}_o(\alpha,\beta,u_{10},v_{10},w_{10})\} + (c_i)^{3/2}B|B|^2\{\mathscr{L}_o(\alpha,\beta,u_{11},v_{11},w_{11})\} = O((c_i)^{5/2}), \tag{5.13}$$

$$\begin{aligned} (c_i)^{1/2}B\left\{\mathscr{L}_x(\alpha,\beta,c,u_{10},p_{10},V_0,Da,F')\right\} + (c_i)^{3/2}\left\{B|B|^2\mathscr{L}_x(\alpha,\beta,c,u_{11},p_{11},V_0,Da,F')\right. \\ \left. -\frac{\alpha}{\varepsilon}ReBu_{10} + \frac{Re}{\varepsilon}\frac{dB}{d\tau}u_{10} - B|B|^2\mathscr{G}_x\right\} = O((c_i)^{5/2}), \end{aligned} \tag{5.14}$$

$$\begin{aligned} (c_i)^{\frac{1}{2}}B\left\{\mathscr{L}_y(\alpha,\beta,c,u_{10},v_{10},p_{10},\theta_{10},V_0,Gr',Da,F')\right\} \\ + (c_i)^{\frac{3}{2}}\left\{B|B|^2\mathscr{L}_y(\alpha,\beta,c,u_{11},v_{11},p_{11},\theta_{11},V_0,Gr',Da,F')\right. \\ \left. - B|B|^2\mathscr{G}_y + \frac{Re}{\varepsilon}\frac{dB}{d\tau}v_{10} - \frac{\alpha BRe}{\varepsilon}v_{10}\right\} = O((c_i)^{\frac{5}{2}}), \end{aligned} \tag{5.15}$$

$$\begin{aligned} (c_i)^{1/2}B\left\{\mathscr{L}_z(\alpha,\beta,c,w_{10},p_{10},V_0,Da,F')\right\} + (c_i)^{3/2}\left\{B|B|^2\mathscr{L}_z(\alpha,\beta,c,w_{11},p_{11},V_0,Da,F')\right. \\ \left. -\frac{\alpha}{\varepsilon}ReBw_{10} + \frac{Re}{\varepsilon}\frac{dB}{d\tau}w_{10} - B|B|^2\mathscr{G}_z\right\} = O((c_i)^{5/2}), \end{aligned} \tag{5.16}$$

$$(c_i)^{1/2}B\{\mathscr{L}(\alpha,\beta,c,u_{10},\theta_{10},V_0,\Theta_0)\}+(c_i)^{3/2}\left\{B|B|^2\mathscr{L}(\alpha,\beta,c,u_{11},\theta_{11},V_0,\Theta_0)+\alpha RePrB\theta_{10}\right.$$
$$\left.-RePr\frac{dB}{d\tau}\theta_{10}-B|B|^2\mathscr{G}\right\}=O((c_i)^{5/2}), \tag{5.17}$$

where,

$$\mathscr{G}_x = -\frac{Re}{\varepsilon^2}\left\{i\alpha V_1u_{10}+2i\alpha u_{20}\tilde{v}_{10}-i\alpha v_{20}\tilde{u}_{10}+\tilde{u}_{10}\frac{du_{20}}{dx}\right.$$
$$\left.+u_{20}\frac{d\tilde{u}_{10}}{dx}-i\beta w_{20}\tilde{u}_{10}+2i\beta\tilde{w}_{10}u_{20}\right\}, \tag{5.18}$$

$$\mathscr{G}_y = -\frac{Re}{\varepsilon^2}\left\{i\alpha V_1v_{10}+u_{10}\frac{dV_1}{dx}+i\alpha v_{20}\tilde{v}_{10}+\tilde{u}_{10}\frac{dv_{20}}{dx}\right.$$
$$\left.+u_{20}\frac{d\tilde{v}_{10}}{dx}-i\beta w_{20}\tilde{v}_{10}+2i\beta\tilde{w}_{10}v_{20}\right\}, \tag{5.19}$$

$$\mathscr{G}_z = -\frac{Re}{\varepsilon^2}\left\{i\alpha V_1w_{10}+2i\alpha w_{20}\tilde{v}_{10}-i\alpha v_{20}\tilde{w}_{10}+\tilde{u}_{10}\frac{dw_{20}}{dx}+u_{20}\frac{d\tilde{w}_{10}}{dx}\right.$$
$$\left.+i\beta w_{20}\tilde{w}_{10}\right\}, \tag{5.20}$$

$$\mathscr{G} = RePr\left\{i\alpha V_1\theta_{10}+2i\alpha\theta_{20}\tilde{v}_{10}-i\alpha v_{20}\tilde{\theta}_{10}+u_{10}\frac{d\Theta_1}{dx}+\tilde{u}_{10}\frac{d\theta_{20}}{dx}\right.$$
$$\left.+u_{20}\frac{d\tilde{\theta}_{10}}{dx}-i\beta w_{20}\tilde{\theta}_{10}+2i\beta\tilde{w}_{10}\theta_{20}\right\}. \tag{5.21}$$

The equations for the harmonic E^2 are:

$$c_iB^2\{\mathscr{L}_o(2\alpha,2\beta,u_{20},v_{20},w_{20})\}=O((c_i)^2), \tag{5.22}$$

$$c_iB^2\left\{\mathscr{L}_x(2\alpha,2\beta,c,u_{20},p_{20},V_0,Da,F')+\frac{Re}{\varepsilon^2}\left(i\alpha u_{10}v_{10}+u_{10}\frac{du_{10}}{dx}+i\beta u_{10}w_{10}\right)\right\}$$
$$=O((c_i)^2), \tag{5.23}$$

$$c_iB^2\left\{\mathscr{L}_y(2\alpha,2\beta,c,u_{20},v_{20},p_{20},\theta_{20},V_0,Gr',Da,F')+\frac{Re}{\varepsilon^2}\left(i\alpha v_{10}^2+u_{10}\frac{dv_{10}}{dx}+i\beta v_{10}w_{10}\right)\right\}$$
$$=O((c_i)^2), \tag{5.24}$$

$$c_iB^2\left\{\mathscr{L}_z(2\alpha,2\beta,c,w_{20},p_{20},V_0,Da,F')+\frac{Re}{\varepsilon^2}\left(i\alpha v_{10}w_{10}+u_{10}\frac{dw_{10}}{dx}+i\beta w_{10}^2\right)\right\}$$
$$=O((c_i)^2), \tag{5.25}$$

$$c_i B^2 \left\{ \mathscr{L}(2\alpha, 2\beta, c, u_{20}, v_{20}, \theta_{20}, V_0, \Theta_0) \quad - \quad RePr\left(i\alpha v_{10}\theta_{10} + u_{10}\frac{d\theta_{10}}{dx} + i\beta w_{10}\theta_{10} \right) \right\} = O((c_i)^2). \tag{5.26}$$

Here, tilde denotes the complex conjugate. Higher order harmonics (E^3, E^4, etc.) are not considered in (5.10) as they are not necessary to obtain the first Landau coefficient. The system of equations through (5.11)-(5.26) can be solved sequentially in increasing powers of c_i. At order $(c_i)^0$, the harmonic E^0 contains the basic state equations (5.1)-(5.2) at the particular values of Gr' and Da. At order $(c_i)^{1/2}$, the E^1 equations are those of linear-instability where the functions u_{10}, v_{10},w_{10} and θ_{10} are given by the eigenvectors of the linear theory at the particular values of α and Ra. At order (c_i), the harmonics E^0 and E^2 produce the non-homogeneous equations for the distorted basic flow functions V_1 and Θ_1 as well as for the functions u_{20}, v_{20}, w_{20} and θ_{20}, respectively. The non-homogeneous part of these equations contains the known variables u_{10}, v_{10}, w_{10} and θ_{10}, and their derivatives, which are obtained from the lower order analysis. At order $(c_i)^{3/2}$, the equations of harmonic E^1 become non-homogeneous such that the linear-instability operators operate on u_{11}, v_{11}, w_{11} and θ_{11} on the left-hand sides while the right-hand sides are functions of B, $\frac{dB}{d\tau}$ and $B|B|^2$. As the homogeneous form of these equations admit non-trivial solutions (linear theory), therefore, for non-trivial solution of non-homogeneous E^1 equations the right hand-sides of these equations must be orthogonal to the solution of the corresponding homogeneous adjoint system of equations mentioned below.

The solution of adjoint system of linear instability equations is needed to obtain the Landau constant. The definition of adjoint operator is given as [59]

$$\langle LX, X^* \rangle = \langle X, L^* X^* \rangle, \tag{5.27}$$

where $X^* = [u^*, v^*, w^*, \theta^*, p^*]$ is adjoint eigenfunction, $L = [\mathscr{L}_o, \mathscr{L}_x, \mathscr{L}_y, \mathscr{L}_z, \mathscr{L}]$ is the linear stability operator and $L^* = [\mathscr{L}_0^*, \mathscr{L}_x^*, \mathscr{L}_y^*, \mathscr{L}_z^*, \mathscr{L}^*]$ is corresponding adjoint operator. The inner product in this definition is the standard inner product given as

$$\langle Y(x), Z(x) \rangle = \int_{-1}^{1} Y^*(x) Z(x) dx = \int_{-1}^{1} \sum_{i=1}^{5} (y_i^*(x) z_i(x) dx, \tag{5.28}$$

where the superscript $*$ denotes the adjoint eigenfunction. The corresponding adjoint equations of linear stability equations (5.4)-(5.8) are given as:

$$\mathscr{L}_0^*(\alpha,\beta,u^*,v^*,w^*) = \frac{du^*}{dx} - i\alpha v^* - i\beta w^* = 0, \tag{5.29}$$

$$\begin{aligned}\mathscr{L}_x^*(\alpha,\beta,c,u^*,p^*,\theta^*,V_0,\Theta_0,Da,F') &= -i\alpha cRe\frac{1}{\varepsilon}u^* - \lambda\left(\frac{d^2u^*}{dx^2} - (\alpha^2+\beta^2)u^*\right) - \frac{dp^*}{dx} \\ &+ \frac{1}{Da}u^* + F'|V_0|u^* - PrRe\frac{d\Theta_0}{dx}\theta^* = 0,\end{aligned} \tag{5.30}$$

$$\begin{aligned}\mathscr{L}_y^*(\alpha,\beta,c,v^*,p^*,V_0,Da,F') = -i\alpha cRe\frac{1}{\varepsilon}v^* - \lambda\left(\frac{d^2v^*}{dx^2} - (\alpha^2+\beta^2)v^*\right) + i\alpha p^* \\ + \frac{1}{Da}v^* + 2F'|V_0|v^* = 0,\end{aligned} \tag{5.31}$$

$$\begin{aligned}\mathscr{L}_z^*(\alpha,\beta,c,w^*,p^*,V_0,Da,F') = -i\alpha cRe\frac{1}{\varepsilon}w^* - \lambda\left(\frac{d^2w^*}{dx^2} - (\alpha^2+\beta^2)w^*\right) + i\beta p^* \\ + \frac{1}{Da}w^* + F'|V_0|w^* = 0,\end{aligned} \tag{5.32}$$

$$\begin{aligned}\mathscr{L}^*(\alpha,\beta,c,v^*,\theta^*,V_0,Gr') = -i\alpha PrRe(V_0-\sigma c)\theta^* + \left(\frac{d^2\theta^*}{dx^2} - (\alpha^2+\beta^2)\theta^*\right) \\ - Gr'v^* = 0.\end{aligned} \tag{5.33}$$

The above equations are solved by eliminating the pressure terms along with no-slip and impermeability condition of velocity and zero temperature perturbation on the walls. The corresponding boundary conditions for adjoint system are:

$$u^* = v^* = w^* = \theta^* = 0 \quad \text{at} \quad x = \pm 1. \tag{5.34}$$

Now, if these adjoint eigenfunctions are normailized so as to satisfy the equation

$$\int_{-1}^{1}\left[\frac{1}{\varepsilon}(\hat{u}u^* + \hat{v}v^* + \hat{w}w^*) - Pr\hat{\theta}\theta^*\right]dx = 1. \tag{5.35}$$

then the orthogonal product of right-hand sides of non-homogeneous E^1 equations and the adjoint eigenfunctions results in the following Landau equation:

$$\frac{\partial B}{\partial \tau} = \alpha B + a_1 B|B|^2, \tag{5.36}$$

where,

$$a_1 = \frac{1}{Re}\int_{-1}^{1} (\mathscr{G}_x u^* + \mathscr{G}_y v^* + \mathscr{G}_z w^* + \mathscr{G}\theta^*)\, dx, \tag{5.37}$$

If the real part of a_1, i.e. $(a_1)_r$, is positive then we predict a subcritical bifurcation, whereas, if it is negative then we predict a supercritical type of bifurcation. The equilibrium amplitude of supercritical and threshold amplitude of subcritical bifurcations are $|A_e|^2 = c_i|B|^2 = -\alpha c_i/(a_1)_r$ and $|A_t|^2 = |\alpha c_i/(a_1)_r|$, respectively.

The effect of the disturbance on the heat transfer rate may also be determined. An average Nusselt number at the right wall is defined as

$$Nu = 2\frac{\partial \Theta}{\partial x}|_{x=1} \tag{5.38}$$

The friction coefficient on the left and right channel walls is defined as

$$C_{fl} = \frac{2}{Re}\frac{\partial V}{\partial x}|_{x=-1} \text{ and } C_{fr} = -\frac{2}{Re}\frac{\partial V}{\partial x}|_{x=1}. \tag{5.39}$$

The functions V and Θ in above equations are calculated using equilibrium amplitude as $V = V_0 + |A_e|^2 V_1$ and $\Theta = \Theta_0 + |A_e|^2\Theta_1$. The numerical method is similar to the one used in previous chapter.

5.2 Results

The present problem contains six important parameters: namely *Gr*, *Pr*, *Da*, *Re*, *F* and ε which are Grashof number, Prandtl number, Darcy number, Reynolds number, Forchheimer number and porosity, respectively. Since, we are interested to study the finite amplitude stability of fully developed flow in a vertical channel filled with highly permeable porous medium, therefore three different values $10^{-2}, 10^{-3}$ and 10^{-4} of Darcy number are chosen

for a wide range (0, 5000) of Reynolds number. Although, we have mainly focused on finite amplitude stability of a fully developed flow in porous medium saturated with air or water, but other type of fluid has also been considered. To avoid numerous parametric study, we have fixed porosity at 0.9. Furthermore, the range of F' considered in this study is $[0, 5\times10^3]$.

Accordingly, the following analysis is made when the channel is filled with metallic foam or any other porous medium having permeability in the range of 10^{-5}m^2 to 10^{-7}m^2 in SI unit with porosity of 0.9. The linear stability theory predicts the transition point depicted as a stability diagram in the (Re, Gr') plane, as shown in Chapter 2. In the unstable region of the diagram (above the neutral stability curve), the ignored nonlinear terms in the linear stability analysis play significant role when the amplitude of disturbance becomes large enough. In this situation, the exponential linear growth rate is modified by the nonlinearities in the governing equations. To give an illustration, we carry out a finite amplitude analysis of the present problem. The linear stability results show that the two dimensional disturbance with $\beta = 0$ is the most unstable wave for this mixed convective flow. As a consequence, the present nonlinear stability results are carried out for $\beta = 0$. A cubic Landau equation (5.36) is derived in terms of the amplitude function to identify the type of bifurcation.

5.2.1 Landau constant at and beyond the critical point

In order to understand the nature of bifurcation, the variation of Landau constant as a function of Prandtl number is shown in figure 5.1(a), (b) and (c) for $Da = 10^{-2}$, 10^{-3} and 10^{-4}, respectively, where Re and F' are fixed at 1000. The above profile of $(a_1)_r$ is plotted at $\delta_{Gr'} = Gr'/Gr'_c - 1 = 0.01$. As can be seen from figure 5.1(a), (b) and (c), the real part of the Landau constant is negative for all Da as well as Pr. This shows that the type of bifurcation is supercritical at the critical point. Interestingly, for all three values of Da, it shows that magnitude of $(a_1)_r$ first increases rapidly up to a minimum value of Pr and beyond that its magnitude decreases drastically and finally asymptotically converge to

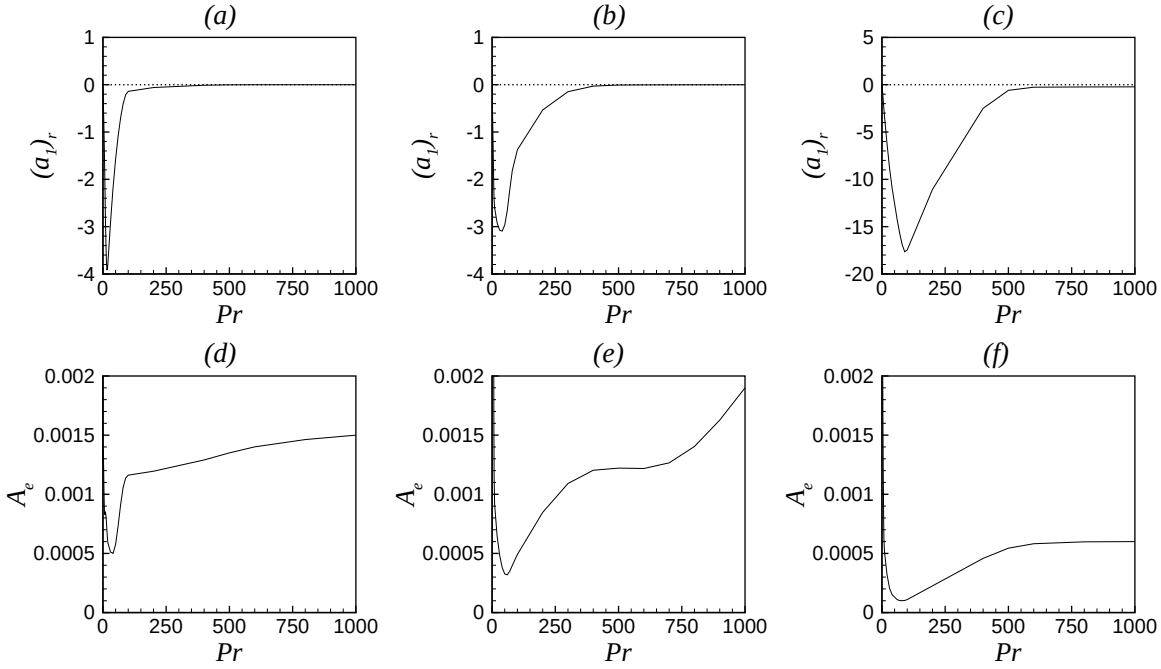

Figure 5.1: Variation of real part of Landau constant as a function of Pr for (a) $Da = 10^{-2}$, (b) $Da = 10^{-3}$ and (c) $Da = 10^{-4}$ when $Re = 1000$ and $F' = 1000$.

zero. as the value of Da decreases, the asymptotic convergence of the profile of $(a_1)_r$ gets delayed. The corresponding equilibrium amplitudes are shown in figure 5.1 (d), (e) and (f), respectively. The equilibrium amplitude for all three above values of Da initially decreases and then starts to increase as the value of Pr is increased.

In order to understand the nature of bifurcation, the variation of Landau constant as a function of modified Forchheimer number for two values: 0.7 and 7 of Pr are plotted in figure 5.2 (a) and (b), respectively when $Da = 10^{-3}$ and $Re = 1000$. For both values of Pr, the value of Landau constant is negative through out the range of F' predicting supercritical bifurcation of the flow. Interestingly, the real part of a_1 decreases drastically on increasing F' up to a threshold value around 100 when the channel is filled with air saturated porous medium. On further increase in F', the magnitude of $(a_1)_r$ increases. Similar trend can be seen for $Pr = 7$ when F' is around 5000.

The real part of the Landau constant $(a_1)_r$ as a function of Re is plotted in figure 5.3 for a wide range of Reynolds numbers and both the fluids. The Landau constant is

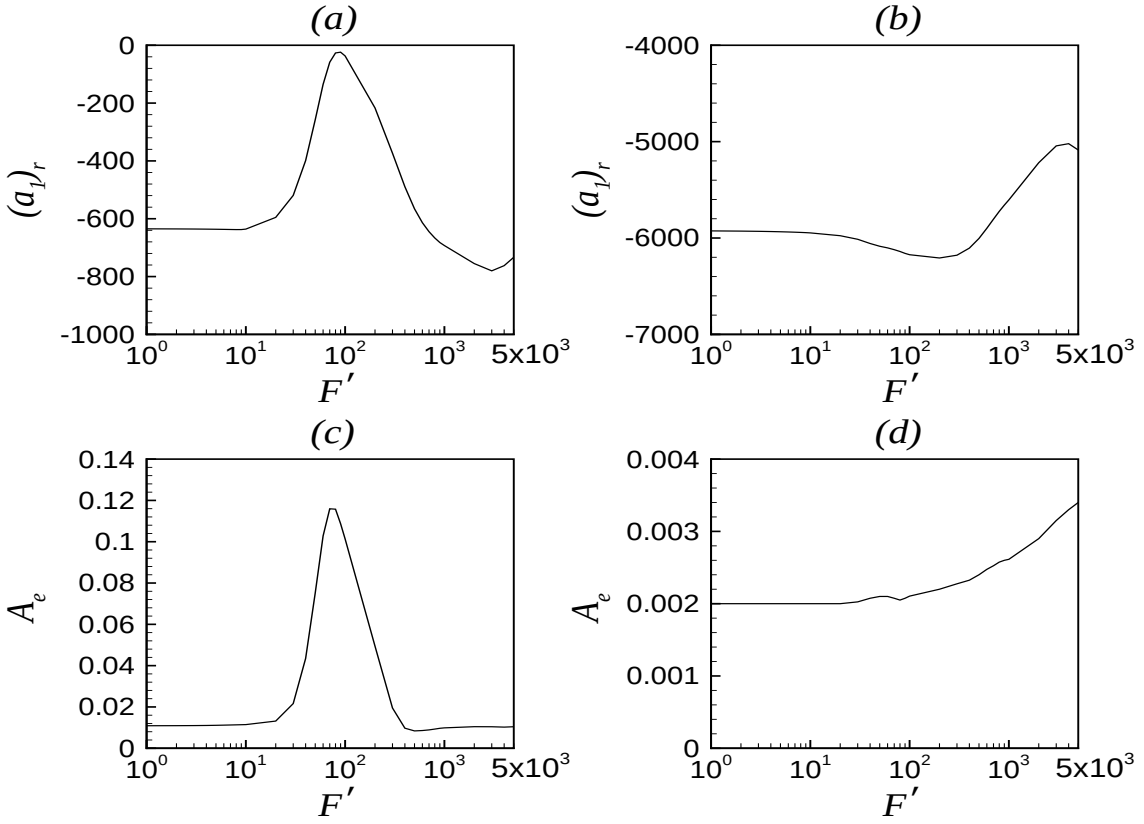

Figure 5.2: Variation of real part of Landau constant and equilibrium amplitude as a function of F' for (a,c) $Pr = 0.7$ and (b,d) $Pr = 7$ when $Da = 10^{-3}$ and $Re = 1000$.

calculated at $\delta_{Gr'} = Gr'/Gr'_c - 1 = 0$ and in the vicinity of the critical Gr' (i.e., $\delta_{Gr'} = 0.01$) with respect to the most unstable linear wave. The calculated values of $(a_1)_r$ for both values 0 and 0.01 of $\delta_{Gr'}$ are almost identical. As a result, the profile of $(a_1)_r$ is shown only at $\delta_{Gr'} = 0.01$ in the above figure. For both fluids, the sign of $(a_1)_r$ is found to be negative for all Da, indicating the supercritical bifurcation of the flow (see figures 5.3(a) and 5.3(b). The corresponding profiles of equilibrium amplitude (A_e) are shown in figure 5.3(c) and 5.3(d). The equilibrium amplitude decreases sharply up to a threshold value of Re and then converges asymptotically. Irrespective of the media permeability, the equilibrium amplitude at very low Reynold's number is very high due to very small magnitude of $(a_1)_r$ and it decreases on increasing the value of Re. The result is true for both fluids.

To identify the nature of bifurcation as well as variation of equilibrium amplitude far

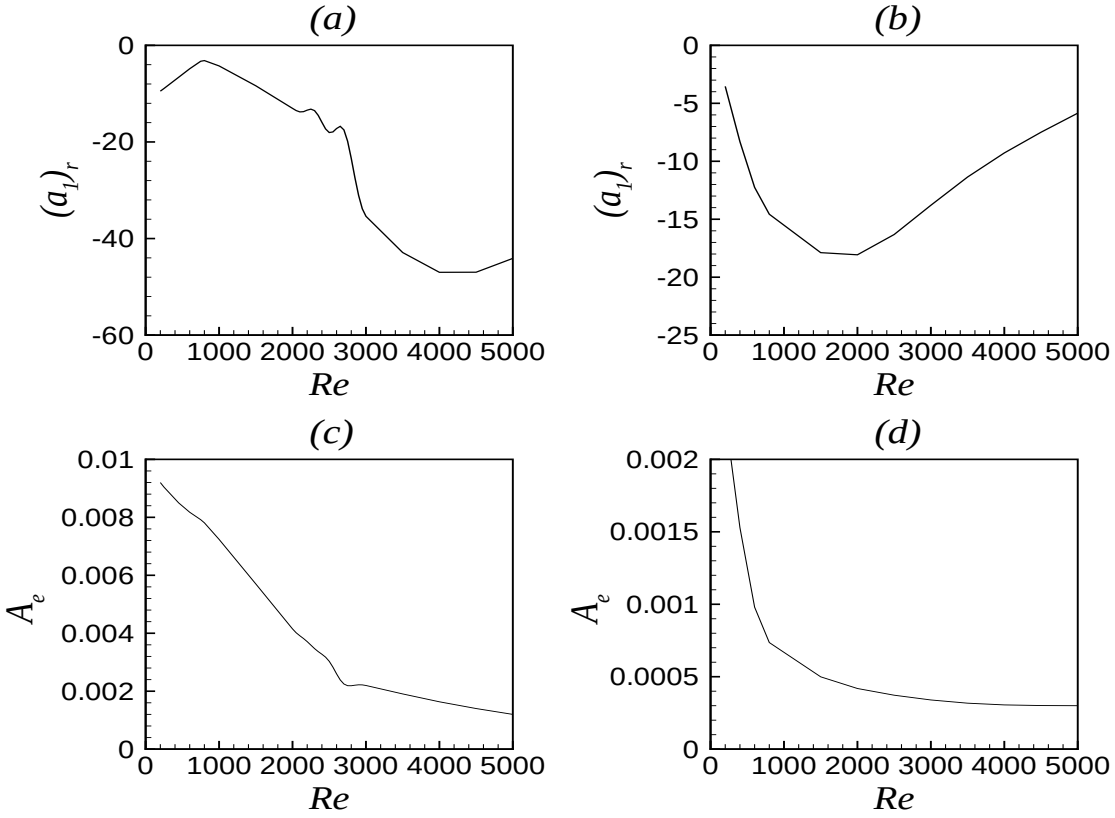

Figure 5.3: Variation of real part of Landau constant and equilibrium amplitude as a function of Re for (a,c) $Pr = 0.7$ and (b,d) $Pr = 7$.

away from the critical point, we have plotted the profiles of $(a_1)_r$ and A_e as a function of $\delta_{Gr'} = Gr'/Gr'_c - 1$ at $Re = 1000$, $F' = 1000$ and $Da = 10^{-3}$ in figures 5.4(a) and 5.4(b), respectively. The origin of the graphs shows the bifurcation point or critical point. The range of $\delta_{Gr'}$ is based on the magnitude of c_i. Rogers *et al.* [88] have shown that the cubic Landau equation gives correct result when the magnitude of c_i is small by comparison with direct numerical simulation as well as high-order weakly nonlinear results. They have also pointed out that the weakly nonlinear analysis is asymptotically correct for large values of Gr' beyond the bifurcation point in the limit as c_i approaches zero. In the present analysis the magnitude of c_i is less than or equal to 10^{-3} in the range [0, 1] of $\delta_{Gr'}$. Although we analyze the nonlinear saturation (i.e., the limiting value of growth of instabilities under nonlinear effects) for larger values of Gr' beyond the bifurcation point (upto 2 times of

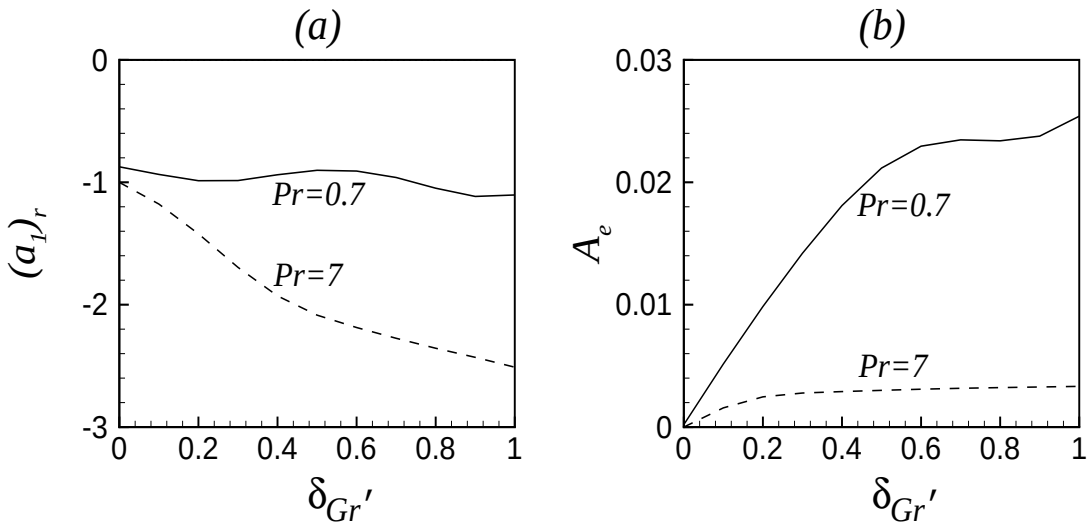

Figure 5.4: Variation of (a) real part of Landau constant, and (b) equilibrium amplitude as a function of Gr' for $Pr = 0.7$ and $Pr = 7$ at $Re = 1000$, $F' = 1000$ and $Da = 10^{-3}$.

critical Gr'), but a complete picture of nonlinear saturation can only be confirmed by use of direct numerical simulation, which is beyond the scope of the present work. Therefore, this analysis will present only a qualitative characteristic of the nonlinear interaction of different harmonic modes for larger values of Gr' beyond the bifurcation point. The bifurcation diagram presented in figure 5.4(a) shows only supercritical bifurcation. The amplitude profile increases smoothly with Gr' (see figure 5.4(b)).

To understand the finite amplitude analysis of the above problem under the non-Darcy model (VANS) without convective term an attempt is also taken and presented in Appendix A.

5.3 Summary and Conclusion

We have analyzed the finite amplitude stability of fully developed mixed convection flow in differentialy heated vertical channel filled with porous medium. The flow is governed by four parameters: Prandtl number (Pr), Grashof number (Gr), Reynolds number (Re) and Darcy number (Da). To illustrate the results, $Pr = 0.7$(air) and $Pr = 7$(water) are used

along with a wide range of Da, F' and Re. It should be noted that Re and $Gr' = Gr/Re$ based on half width of the channel are equivalent to $Re\sqrt{Da}$ and $Gr'Da$, respectively. A cubic Landau equation has been derived in terms of amplitude function to identify the type of bifurcation. We have mainly analyzed (i) the variation of real part of Landau constant as a function of Re, Gr' and α to determine the type of bifurcation, (ii) the variation of equilibrium amplitude.

The finite amplitude analysis predicts supercritical bifurcation of the flow at the critical point for both fluids as the sign of real part of Landau constant $(a_1)_r$ is found to be negative for all Da. Also, the magnitude of equilibrium amplitude decreases for higher values of Re. Also, only supercritical bifurcation is predicted in the neighborhood wavenumbers of the critical wavenumber.

Appendix A

To understand the finite amplitude analysis of the above problem under the non-Darcy model (VANS) without convective term, an attempt is made in this section. The procedure to derive the cubic Landau equation is same as explained in the previous chapter.

A.1: Landau constant at and beyond the critical point

In order to understand the nature of bifurcation, the variation of Landau constant as a function of modified Forchheimer number is analysed in figure 5.5. For all the considered values of Da and Pr, the value of Landau constant is positive throughout the range of F' predicting supercritical bifurcation of the flow. It should be noted that this range of F' covers a wide range of values of form drag coefficient (C_F) for high permeable porous medium [11]. Since, the variation of F' predicts only supercritical bifurcation, so its value is fixed as 1 in rest of the section. The real part of the Landau constant $(a_1)_r$ as a function of Re is plotted in figure 5.6 for a wide range of Reynolds numbers along with different media permeability. The Landau constant is calculated at $\delta_{Gr'} = Gr'/Gr'_c - 1 = 0$ and in the vicinity of the critical Gr' (i.e., $\delta_{Gr'} = 0.01$) with respect to the most unstable linear wave. The calculated values of $(a_1)_r$ for both values 0 and 0.01 of $\delta_{Gr'}$ are almost identical. As a result, the profile of $(a_1)_r$ is shown only at $\delta_{Gr'} = 0.01$ in the above figure. For both

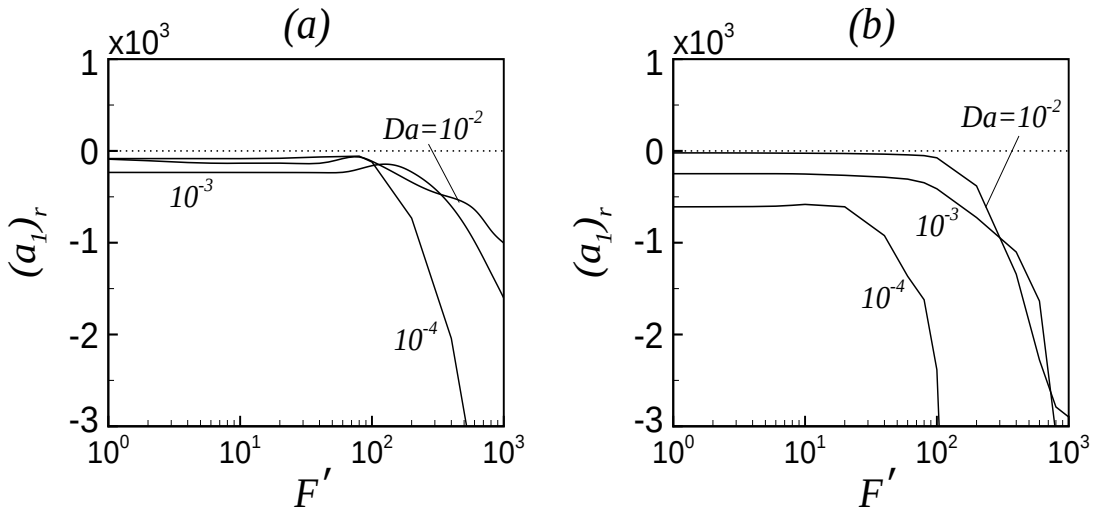

Figure 5.5: Variation of real part of Landau constant as a function of F' for *(a)* $Pr = 7$ and *(b)* $Pr = 70$ when $Re = 1000$.

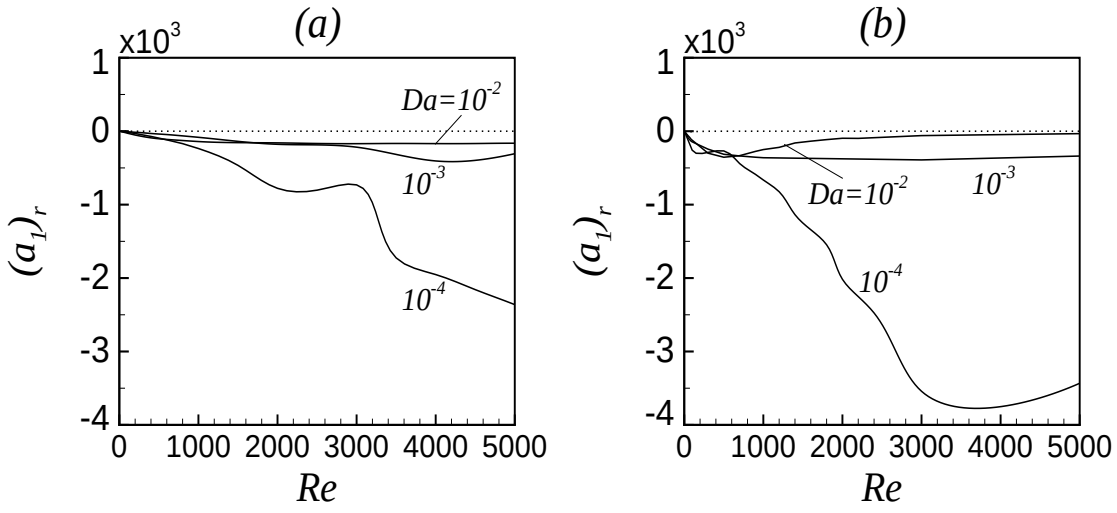

Figure 5.6: Variation of real part of Landau constant as a function of Re for *(a)* $Pr = 7$ and *(b)* $Pr = 70$.

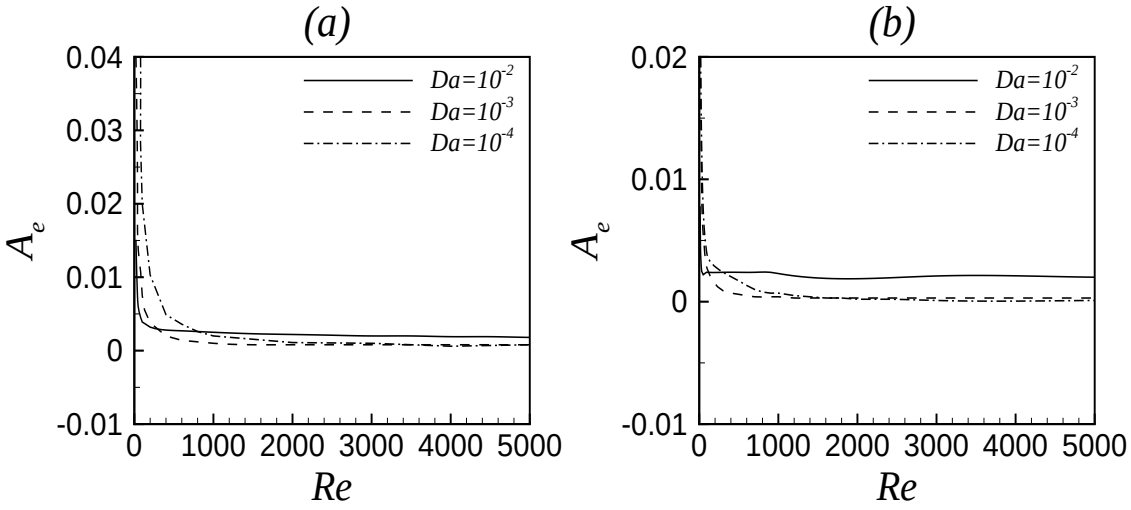

Figure 5.7: Variation of equilibrium amplitude as a function of *Re* for *(a)* $Pr = 7$ and *(b)* $Pr = 70$.

fluids, the sign of $(a_1)_r$ is found to be negative for all Da, indicating the supercritical bifurcation of the flow (see figures 5.6*a* and 5.6*b*). The corresponding profiles of equilibrium amplitude (A_e) are shown in figure 5.7. Irrespective of the media permeability the equilibrium amplitude at very low Reynold's number is very high due to very small magnitude of $(a_1)_r$ and it decreases on increasing the value of *Re*. The result is true for both fluids. Consequently, the value of *Pr* is fixed at 7 in the rest of the analysis.

To identify the nature of bifurcation as well as variation of equilibrium amplitude far away from the critical point, we have plotted the profiles of $(a_1)_r$ and A_e as a function of $\delta_{Gr'} = Gr'/Gr'_c - 1$ at $Re = 1000$ in figures 5.8*a* and 5.8*b*, respectively. The origin of the graphs shows the bifurcation point or critical point. The range of $\delta_{Gr'}$ is based on the magnitude of c_i. Rogers *et al.* [88] have shown that the cubic Landau equation gives correct result when the magnitude of c_i is small by comparison with direct numerical simulation as well as high-order weakly nonlinear results. They have also pointed out that the weakly nonlinear analysis is asymptotically correct for large values of Gr' beyond the bifurcation point in the limit as c_i approaches zero. In the present analysis the magnitude of c_i is less than or equal to 10^{-2} (for *Da* equal to 10^{-2}) or 10^{-3} (for *Da* equal to 10^{-3} and 10^{-4}) in the

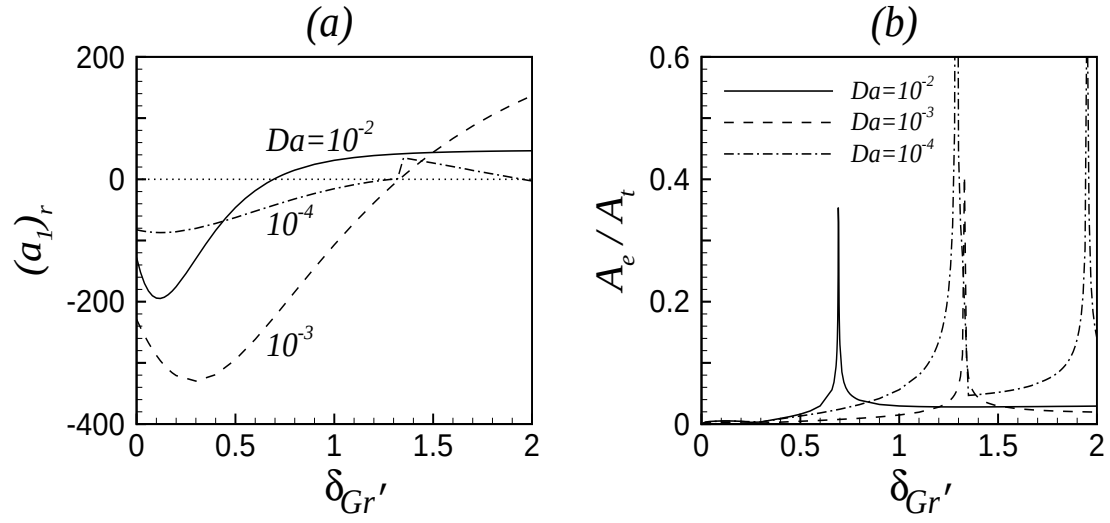

Figure 5.8: Variation of (a) real part of Landau constant, and (b) equilibrium amplitude as a function of Gr' for $Pr = 7$ at $Re = 1000$.

range [0, 2] of $\delta_{Gr'}$. Although we analyze the nonlinear saturation (i.e., the limiting value of growth of instabilities under nonlinear effects) for larger values of Gr' beyond the bifurcation point (upto 3 times of critical Gr'), but a complete picture of nonlinear saturation can only be confirmed by use of direct numerical simulation, which is beyond the scope of the present work. Therefore, this analysis will present only a qualitative characteristic of the nonlinear interaction of different harmonic modes for larger values of Gr' beyond the bifurcation point. The bifurcation diagram presented in figure 5.8*a* shows both types (subcritical and supercritical) of bifurcation for larger values of Gr'. The linearly unstable flow possesses a subcritical bifurcation for $\delta_{Gr'} \geq 0.7$, $\delta_{Gr'} \geq 1.4$ and $\delta_{Gr'} \geq 1.3$, for Da equal to 10^{-2}, 10^{-3} and 10^{-4}, respectively. Furthermore, for $Da = 10^{-4}$ the subcritical bifurcation again becomes supercritical at $\delta_{Gr'} = 2$. The amplitude profile shows an abrupt jump at the point where a change from supercritical to subcritical bifurcation occurs due to the change in sign of $(a_1)_r$ (see figure 5.8*b*).

The variation of the neutral stability curve with wavenumber is also important because an instability that is supercritical for some wavenumber may be subcritical or supercritical at other nearby wavenumber [88]. In this situation, any of the potential unstable

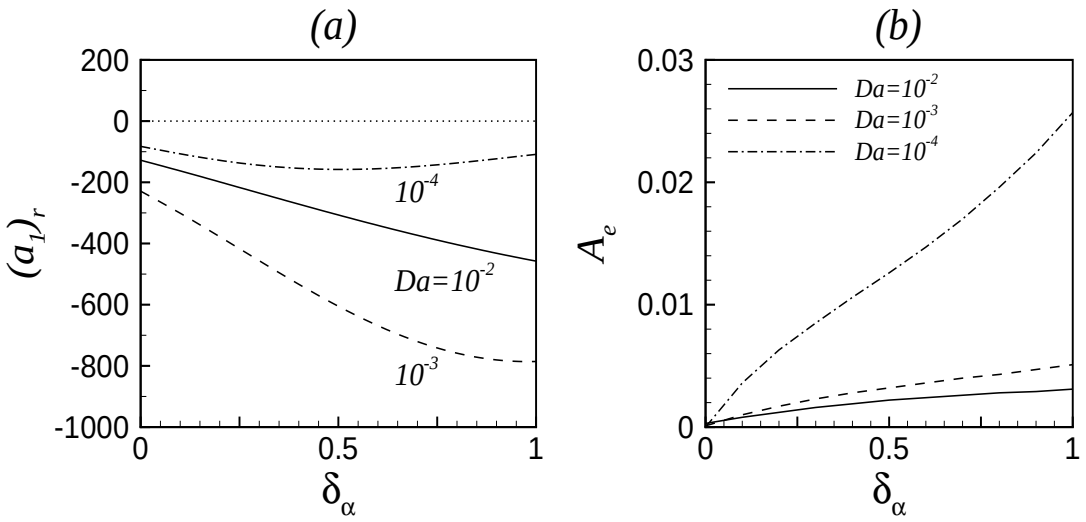

Figure 5.9: Variation of (a) real part of Landau constant, and (b) equilibrium amplitude as a function of α for $Pr = 7$ at $Re = 1000$.

waves may grow and interact with other modes. Thus, the profiles of $(a_1)_r$ and A_e as a function of $\delta_\alpha = \alpha/\alpha_c - 1$ for different values of Da are plotted in figure 5.9. The origin of the graphs shows the bifurcation point. From the numerical experiments we have found that for $\delta_\alpha < 1$ the value of c_i is less than 10^{-2} for all three values (10^{-2}, 10^{-3}, 10^{-4}) of Da. Consequently, the range of δ_α is [0, 1]. Figure 5.9 shows a large band of wavenumbers for all the above values of Da in which the type of bifurcation is supercritical.

As the weakly non-linear analysis is asymptotically correct in the limit as c_i approaches zero, so the behaviour of linear modes can be accurately predicted at the least stable values of Gr' and Re. Figure 5.6 shows supercritical instability at the least stable wavenumbers for the linear instability in the entire range of Re. This is true for all the considered values of Darcy and Prandtl numbers. We have seen from kinetic energy balance that the buoyant production of disturbance kinetic energy is dominant in the entire range of Re for all the considered values of Da and Pr. This buoyant instability is supercritical at all the nearby wavenumbers. This is illustrated in figure 5.10 for $Re = 10^3$. As can be seen from this figure that for the above buoyant instability there exist a large group of wavenumbers which are supercritically unstable for both considered fluids. This is true for

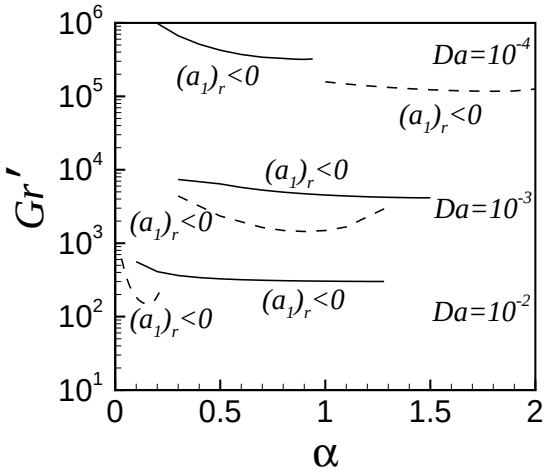

Figure 5.10: Neutral stability curve (c_i = 0) in (α, Gr') plane for at $Re = 10^3$. Solid line represents $Pr = 7$ and dotted line represents $Pr = 70$.

all the Darcy numbers considered here. The observations made above must be considered when one does complete simulation of this mixed convection flow.

A.2: Heat transfer rate and Friction coefficient

Since this is a non-isothermal flow, therefore the effect of interaction of different harmonics on some physical characteristics of the disturbed flow like heat transfer rate and friction coefficient on the hot wall of the channel for the region of supercritical bifurcation must be understood. Consequently, the basic as well as distorted heat transfer rate as a function of Re as well as Gr' are plotted in figures 5.11a and 5.11b, respectively. In figure 5.11, Nu_{bs} and Nu_{ds} are defined as Nusselt numbers predicted by the basic state and distorted state flow, respectively. Figure 5.11a is plotted at $\delta_{Ra} = 0.01$ in the region of supercritical bifurcation, and figures 5.11b and 5.11c are plotted at $Re = 1000$ in the region of supercritical as well as subcritical bifurcation. The results show that the Nusselt number for distorted flow is more than the same for basic flow. Whenever there is a shifting from supercritical to subcritical bifurcation, Nu_{ds} profile also experiences a jump (see figure 5.11b) similar to the amplitude profile. This indicates that the nonlinear interaction of different modes causes a substantial increase in Nusselt number. Figure 5.11c shows that the coefficient of

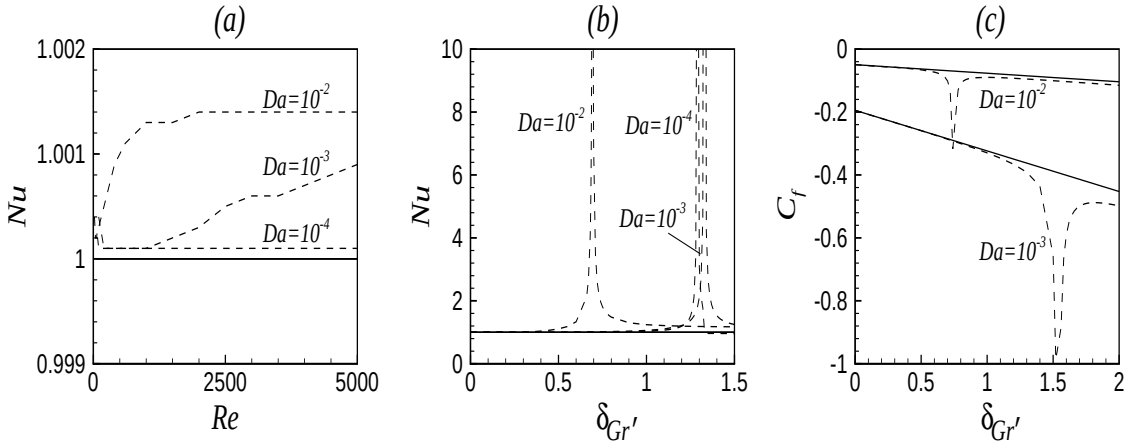

Figure 5.11: Variation of (a) Nu as a function of Re (b) Nu as function of Gr' and (c) Coefficient of friction as a function of Gr'. Solid and dotted lines represent physical quantities at basic and distorted state respectively.

friction at the hot wall for distorted flow (Cf_{ds}) as well as basic state (Cf_{bs}) are equal upto a threshold value of Gr' depending on the media permeability and beyond which (Cf_{ds}) becomes more than (Cf_{bs}).

A.3: Some important remarks

The finite amplitude analysis predicts supercritical bifurcation of the flow at the critical point for both fluids as the sign of real part of Landau constant $(a_1)_r$ is found to be negative for all Da. Also, the magnitude of equilibrium amplitude decreases for higher values of Re. For a fixed value of Re, subcritical bifurcation is also observed as the value of Gr' is increased beyond the critical value. The corresponding amplitude profile as function of Gr' experiences sudden peaks when the supercritical bifurcation becomes subcritical. Also, only supercritical bifurcation is predicted in the neighborhood wavenumbers of the critical wavenumber. Due to interaction of different harmonics, increased heat transfer rate and friction coefficient is obtained for distorted flow as compared to the same for basic flow.

Chapter 6

Conclusions and Future Scope

6.1 Conclusions

We have analyzed the stability of parallel mixed convection flow (PMCF) in a vertical channel filled with incompressible fluid saturated porous medium under Boussinesq approximation. Two different boundary conditions, walls are linearly heated and walls are differetially heated, are considered. The heat transfer and fluid flow mechanism of PMCF in a differentially heated channel filled with porous medium and its linear stability under local thermal equilibrium (LTE) state and under local thermal non-equilibrium (LTNE) state are studied in Chapter 2 and Chapter 3, respectively. A finite amplitude analysis is also carried out when the temperature of the walls of the channel vary linearly with the vertical co-ordinate. This is given in Chapter 4. The extension of this analysis to the non-isothermal parallel flow in differentially heated channel, whose linear stability is made in Chapter 2, is presented in Chapter 5. The non-Darcy volume averaged Navier-Stokes equation (VANS) is used as the momentum equation except in some special cases where VANS without convective term (see Appendix D of Chapter 2 and Appendix A of Chapter 5) as well as Darcy model are also used. Two different numerical methods: spectral Chebyshev collocation and spectral Galerkin method have been used for the solution of basic flow, linear disturbance equations and equations pertaining to non-linear analysis. A cubic

Landau equation is derived to identify regions of subcritical and supercritical bifurcations with the help of theories given by Stuart [100], Stewartson and Stuart [101] and Yao and Rogers [130]. The different governing parameters invloved in the study are Rayleigh number (Ra), Grashof number (Gr), Darcy number (Da), Prandtl number (Pr), Forchheimer number (F), Reynolds number (Re), porosity (ε), inter-phase heat transfer coefficient (H), and porosity scaled thermal conductivity ratio (γ). The following conclusions have been made in the end.

- The non-isothermal PMCF in a differetially heated channel possesses three different types of instability, namely thermal-shear, interactive, and thermal-buoyant, which depends on controlling parameters, mainly Pr. When Re is fixed at 1000, the appearance of point of inflection in the basic velocity for fluid with Pr less than 30 acts as a necessary condition for instability for all considered values of Darcy number.

- The linear instability boundary shows that for a given value of Da, the interphase heat transfer coefficient has a stabilizing effect on the instability of the flow. The effect of γ on the instability of the flow was found to be negligible.

- In contrast to the differentially heated channel filled with air saturated porous medium where supercritical bifurcation is the only type of bifurcation, in linearly heated channel filled with air saturated porous medium the type of bifurcation may be supercritical or subcritical depending on the value of Darcy number as well as Forchheimer number. However, in both the cases the type of bifurcation is always supercritical for water.

- In both the cases (when walls are heated differentially as well as when walls are heated linearly) heat transfer rate under distorted state as a function of Gr' or Ra increases and it is higher than the same under basic state, unless there is a change in the type of bifurcation.

- The physical quantities like heat transfer rate as well as skin friction coefficient also

experience a jump at the point wherever the type of bifurcation is changes from supercritical to subcritical.

- In general non-linear interaction of different harmonics on the pattern of secondary flow under supercritical bifurcation is negligible, whereas the same for subcritical bifurcation is significant, whic in turn enhances the destabilizing characteristic of the modification in the buoyant production of kinetic energy due to change in the shape of fundamental wave.

- The PMCF of air in differentially heated channel is found to have super as well as subcritical bifurcation far away from the critical point when VANS without convective term is used (see Appendix A in Chapter 5).

6.2 Scope for Further Research

The field of stability of the non-isothermal parallel mixed convective flow is a vast area. This thesis has addressed only a few aspects of it. Some more potential extension of the present work is also possible.

- The non-linear stability analysis could be further carried out for local thermal non-equilibrium situation to get a complete picture of stability under both LTE and LTNE theories.

- We have focused on the non-linear stability of stably stratified non-isothermal parallel flow in a vertical channel with linearly varying wall temperature, but the present analysis can be extended for unstably stratified flow too using higher order weakly nonlinear analysis.

- The solution of complete governing equations by Direct Numerical Simulation is also essential to get a clear picture of transition state.

These problems are left for a future study.

Bibliography

[1] Al-Sumaily, G. F., Nakayama, A., Sheridan, J. and Thompson, M. C., 2012, The effect of porous media particle size on forced convection from a circular cylinder without assuming local thermal equilibrium between phases, *Intl J. Heat Mass Transfer*, **55**, 3366–3378.

[2] Barletta, A., 2013, Instability of mixed convection in a vertical porous channel with uniform wall heat flux, *Phys. Fluids*, **25**, 084108–1–14.

[3] Barletta, A., 2015, A proof that convection in a porous vertical slab may be unstable, *J. Fluid Mech.*, **770**, 273–288.

[4] Barletta, A., 2016, Instability of stationary two-dimensional mixed convection across a vertical porous layer, *Phys. Fluids*, **28**, 014101–1–14.

[5] Bera, P. and Khalili, A., 2002, Stability of mixed convection in an anisotropic porous channel, *Phys. Fluids*, **14**, 1617–1630.

[6] Bera, P. and Khalili, A., 2006, Influence of Prandtl number on stability of mixed convective flow in a vertical channel filled with a porous medium, *Phys. Fluids*, **18**, 124103–1–10.

[7] Bera, P. and Khalili, A., 2007, Stability of buoyancy opposed mixed convection in a vertical channel and its dependency on permeability, *Adv. Water Res.*, **30**, 2296–2308.

[8] Bera, P., Kumar, J. and Khalili, A., 2011, Hot springs mediate spatial exchange of heat and mass in the enclosed sediment domain: A stability perspective, *Adv. Water Res.*, **34**, 817–828.

[9] Bera, P. and Khandelwal, M. K., 2016, A thermal non-equilibrium perspective on instability mechanism of non-isothermal Poiseuille flow in a vertical porous-medium channel, *Int. J. Thermal Sciences*, **105**, 159–173.

[10] Bhattacharya, A. and Mahajan, R.L., 2002, Finned metal foam heat sinks for electronics cooling in forced convection, *ASME J. Elect. Packag.*, **124**, 155–163.

[11] Bhattacharya, A., Calmidi, V. V. and Mahajan, R. L., 2002, Thermophysical properties of high porosity metal foams, *Int. J. Heat and Mass Trans.*, **45**, 1017–1031.

[12] Busse, F. H., 2003, The sequence-of-bifurcations approach towards understanding turbulent fluid flow, *Surveys in Geophysics*, **24**, 269–288.

[13] Borujerdi, A. N., Noghrehabadi, A. R. and Rees D. A. S., 2007, Onset of convection in a horizontal porous channel with uniform heat generation using a thermal nonequilibrium model, *Trans. in Porous Media*, **69**, 343–357.

[14] Brandt, L., 2014, The lift-up effect: The linear mechanism behind transition and turbulence in shear flows, *European J. Mechanics B/Fluids.*, **47**, 80–96.

[15] Bera, P., Eswaran, V. and Singh, P., 1998, Numerical study of heat and mass transfer in an anisotropic porous enclosure due to constant heating and cooling, *Numerical Heat Transfer, Part A: Applications*, **34**, 887–905.

[16] Bhargavi, D., Satyamurty, V.V. and Raja Sekhar, G.P., 2009, Effect of porous fraction and interfacial stress jump on skin friction and heat transfer in flow through a channel partially filled with porous material, *J. of Porous Media*, **12**, 1065–1082.

[17] Calmidi, V. V. and Mahajan, R. L., 2000, Forced convection in high porosity foams, *Trans. ASME J. Heat Transfer*, **122**, 557–565.

[18] Canuto, C., Hussaini, M. Y., Quarteroni, A. and Zang, T. A., 1988, *Spectral Method in Fluid Dynamics*, (Springer, New York Berlin Heidelberg).

[19] Chen, Y. C., 2004, Non-Darcy flow stability of mixed convection in a vertical channel filled with a porous medium, *Intl J. Heat Mass Transfer*, **47**, 1257–1266.

[20] Chen, Y. C. and Chung, J. N., 1996, The linear stability of mixed convection in a vertical channel, *J. Fluid Mech.*, **325**, 29–51.

[21] Chen, Y. C., Chung, J. N., Wu, C. S. and Lue, Y. F., 2000, Non-Darcy mixed convection in a vertical channel filled with a porous medium, *Intl J. Heat and Mass Transfer*, **43**, 2421–2429.

[22] Chen, Y. C. and Chung, J. N., 1998, Stability of shear flow in a vertical heated channel filled with a porous medium, *Proc. of Int. Heat Trans. conference 11*, 435–440.

[23] Chen, Y. C. and Chung, J. N., 1998, Stability of mixed convection in a differentially heated vertical channel, *ASME J. of Heat Transfer*, **120**, 127–132.

[24] Carbonell, R. G. and Whitaker, S., 1984, *Heat and Mass Transfer in Porous Media. In: Bear J., Corapcioglu M.Y. (eds) Fundamentals of Transport Phenomena in Porous Media*, (NATO ASI Series (Series E: Applied Sciences), **82**, Springer, Dordrecht).

[25] Criminale, W. O., Jackson, T. L., and Joslin, R. D., 2003, Theory and computation of hydrodynamic stability, *Cambridge University Press*.

[26] Chen, Y. C. and Chung, J. N., 2003, A direct numerical simulation of transition phenomenon in a mixed convection channel flow, *Computer and Fluids*, **32**, 795-822.

[27] Chen, Y. C. and Chung, J. N., 2008, A direct numerical simulation of early transition phenomenon in a buoyancy opposed vertical channel, *Numerical Heat Trans. Part A*, **53**, 787-806.

[28] Chanpreet, S., Tathgir, R.G. and Muralidhar, K., 2006, Experimental validation of heat transfer models for flow through a porous medium, *Heat Mass Transfer*, **43**, 55–72.

[29] Davey, A. and Drazin, P. G., 1969, The stability of Poiseuille flow in a pipe, *J. Fluid Mech.*, **36**, 209–218.

[30] Delache, A. and Ouarzazi, M. N., 2008, Weakly nonlinear interaction of mixed convection patterns in porous media heated from below, *Intl J. Thermal Sciences*, **47**, 709–722.

[31] Desaive, T., Lebon, G., and Hennenberg, M., 2001, Coupled capillary and gravity-driven instability in a liquid film overlying a porous layer, *Phys. Rev. E*, **64**, 066304-1-8.

[32] Drazin, P. G. and Reid, W. H., 2004, *Hydrodynamic Stability*, (Cambridge University Press).

[33] Dukhan, N., 2013, *Metals Foams: Fundamentals and Applications*, (DEStech publications).

[34] Dincov, D. D., Parrott, K. A. and Pericleous, K. A., 2004, Heat and mass transfer in two-phase porous materials under intensive microwave heating, *Journal of Food Engineering*, **65**, 403–412.

[35] Damm, D. L. and Fedorov, A. G., 2006, Local thermal non-equilibrium effects in porous electrodes of the hydrogen-fueled SOFC, *J. Power Sources*, **159**, 1153–1157.

[36] Duval, F., Fichot. F. and Quintard, M., 2004, A local thermal non-equilibrium model for two phase flow with phase change in porous media, *Int. J. Heat Mass Trans.*, **47**, 613–639.

[37] Dhiman, A. K., Anjaiah, N., Chhabra, R. P. and Eswaran, V., 2007, Mixed convection from a heated square cylinder to Newtonian and power-law fluids, *Journal of Fluids Engineering (Trans ASME)*, **129**, 506–513.

[38] Dhiman, A. K., Chhabra, R. P. and Eswaran, V., 2008, Steady mixed convection across a confined square cylinder, *Int. Comm. in Heat and Mass Trans.*, **35**, 47–55.

[39] Dey, B. and Raja Sekhar, G.P., 2016, An analytical study on hydrodynamics of an unsteady flow and mass transfer through a channel asymmetrically lined with deformable porous layer, *European J. of Mechanics B/Fluids*, **55**, 71–87.

[40] Divya, Sharma, R. C. and Sunil, 2005, Thermosolutal convection in a ferromagnetic fluid saturating a porous medium, *Journal Porous Media*, **8**, 393–408.

[41] Gill, A. E., 1969, A proof that convection in a porous vertical slab is stable, *J. Fluid Mech.*, **35**, 545–547.

[42] Giorgi, T., 1997, Derivation of the Forchheimer law via matched asymptotic expansions, *Transp. Porous Media*, **29**, 191–206.

[43] Givler, R. C. and Altobelli, S. A., 1994, A determination of the effective viscosity for the Brinkman-Forchheimer flow model, *J. Fluid Mech.*, **258**, 355–370.

[44] Grossmann, S., 2000, The onset of sheer flow turbulence, *Rev. Mod. Phys.*, **72**, 603–618.

[45] Gajjar, J.S.B. and Sibanda, P., 1996, The hydrodynamic stability of channel flow with compliant boundaries, *Theoretical and Computational Fluid Dynamics*, **8**, 105–129.

[46] Hart, J. E., 1971, Stability of the flow in a differentially heated inclined box, *J. Fluid Mech.*, **47**, 547–576.

[47] Hadim, H. A. and Chen, G., 1994, Non-Darcy mixed convection in a vertical porous channel with asymmetric wall heating, *J. Thermophysics*, **8**, No.4, 805–808.

[48] Hadim, A. and Govindarajan, S., 1988, Development of laminar mixed convection in a vertical porous channel, *ASME HTD*, **105**, 145–153.

[49] Hof, B. et. al., 2004, Experimental observation of nonlinear travelling waves in turbulent pipe flow, *Science*, **305**, 1594–1598.

[50] Hof, B. et. al., 2006, Finite lifetime of turbulence in shear flows, *Nature*, **443**, 59–62.

[51] Hsu, C. T. and Cheng, P., 1990, Thermal dispersion in a porous medium, *Intl J. Heat Mass Transfer*, **33**, 1587–1597.

[52] Hayes, A. M., Khan, J. A., Shaaban, A. H. and Spearing, I. G., 2008, The thermal modelling of a matrix heat exchanger using a porous medium and the thermal nonequilibrium model, *Int. J. Therm. Sci.*, **47**, 1306–1315.

[53] Jin, Y. and Kuznetsov, A. V., 2017, Turbulence modeling for flows in wall bounded porous media: An analysis based on direct numerical simulations, *Phys. Fluids*, **29**, 045102-1–18.

[54] Joseph, D. D., Nield, D. A. and Papanicolaou, G., 1982, Nonlinear equation governing flow in a saturated porous medium, *Water Res. Research*, **18**, 1049–1052.

[55] Kaviany, M., 1991, *Principles of Heat Transfer in Porous Media*, (Springer, New York).

[56] Khalili, A., Basu, A. J., Pietrzyk, U. and Raffel, M., 1999, An experimental study of recirculating flow through fluid-sediment interfaces, *J. Fluid Mech.*, **383**, 229–247.

[57] Kamath, P. M., Balaji, C., and Venkateshan, S. P., 2011, Experimental investigation of flow assisted mixed convection in high porosity foams in vertical channels, *Int. J. Heat Mass Transfer*, **54**, 5231–5241.

[58] Khandelwal, M. K. and Bera, P., 2012, A thermal non-equilibrium perspective on mixed convection in a vertical channel, *Int. J. of Thermal Sciences*, **56**, 23–34.

[59] Khandelwal, M. K. and Bera, P., 2015, Weakly nonlinear stability analysis of non-isothermal Poiseuille flow in a vertical channel, *Phys. Fluids*, **27**, 064103-1-24.

[60] Kumar, J., Bera, P. and Khalili, A., 2010, Influence of inertia and drag terms on the stability of mixed convection in a vertical porous-medium channel, *Intl J. Heat Mass Transfer*, **53**, 5261–5273.

[61] Kurtbas, I. and Celik, N., 2009, Experimental investigation of forced and mixed convection heat transfer in a foam-filled horizontal rectangular channel, *Int. J. Heat Mass Transfer*, **52**, 1313–1325.

[62] Kwok, L. P. and Chen, C. F., 1987, Stability of thermal convection in a vertical porous layer, *Trans. ASME J. Heat Transfer*, **109**, 889–893.

[63] Kou, H. S. and Lu, K. T., 1993, Combined boundary and inertia effects for fully developed mixed convection in a vertical channel embedded in porous media, *Int. Comm. Heat Mass Transfer*, **20**, 333–345.

[64] Kizildag. D., Rodriguez. I., Oliva, A. and Lehmkuhl, O., 2014, Limits of the Oberbeck-Boussinesq approximation in a tall differentially heated cavity filled with water, *Int. J. of Heat and Mass Trans.*, **68**, 489-499.

[65] Lage, J. L., 1998, The fundamental theory of flow through permeable media from Darcy to turbulence, Transport Phenomena in Porous Media (ed. D. B. Ingham & I. Pop), *Pergamon*, , 1-30.

[66] Lefebvre, L. P., Banhart, J., and Dunand, D. C., 2008, Porous Metals and Metallic Foams: Current Status and Recent Developments, *Advanced Engineering Materials*, **10**, 775–787.

[67] Lewis, S., Bassom, A. P. and Rees, D. A. S., 1995, The stability of vertical thermal boundary-layer flow in a porous medium, *Eur. J. Mech. B/Fluids*, **14**, 395–407.

[68] Lee, Y. and Korpela, S. A., 1983, Multicellular natural convection in a vertical slot, *J. Fluid Mech.*, **126**, 91–121.

[69] Landahl, M. T., 1975, Wave breakdown and turbulence, *SIAM J. Appl. Math.*, **28**, 735–756.

[70] Lundgren, T. S., 1972, Slow flow through stationary random beds and suspensions of spheres, *J. Fluid Mech.*, **51**, 273–299.

[71] Moler, C. B. and Stewart, G. W., 1973, An algorithm for generalized matrix eigenvalue problems, *SIAM J. Numer. Anal.*, **10**, 241–256.

[72] Motsa, S. S. and Sibanda, P., 2003, On the stability analysis of thermally stratified channel flow with a compliant boundary, *International Journal of Heat and Mass Transfer*, **46**, 939–948.

[73] Muralidhar, K., 1987, Stability of mixed convection flow, *International Journal of Heat and Mass Transfer*, **8**, 228–234.

[74] Muralidhar, K., 1989, Mixed convection flow in a saturated porous annulus, *International Journal of Heat and Mass Transfer*, **32**, 881–888.

[75] Muralidhar, K., 1990, A review of free, forced and mixed convection flow in a saturated porous annulus, *Sadhana*, **15**, 1–41.

[76] Nield, D. A. and Bejan, A., 2013, *Convection in Porous Media*, (Springer, New York).

[77] Niemela, J. J., Skrbek, L., Sreenivasan, K. R. and Donnelly, R., 2005, Turbulent convection at very high Rayleigh numbers, *Nature*, **404**, 837–840.

[78] Nield, D. A., Kuznetsov, A. V. and Xiong, M., 2002, Effect of local thermal non-equilibrium on thermally developing forced convection in a porous medium, *Int. J. Heat and Mass Transfer*, **45**, 4949–4955.

[79] Orszag, S. A., 1971, Accurate solution of the Orr-Sommerfeld stability equation, *J. Fluid Mech.*, **50**, 689–703.

[80] Prasad, V., Kulacki, F. A. and Keyhani, M., 1985, Natural convection in porous media, *J. Fluid Mech.*, **150**, 89–119.

[81] Pu, W. L., Cheng, P., and Zhao, T. S., 1999, Mixed-convection heat transfer in vertical packed channels, *J. Thermophysics and Heat Transfer*, **13**, No.4, 127–132.

[82] Phanikumar, M. S. and Mahajan, R. L., 2002, Non-Darcy natural convection in high porosity metal foams, *Int. J. Heat Mass Trans.*, **45**, 3781–3793.

[83] Partha, M.K., and Raja Sekhar, G.P., 2005, Mixed convection heat and mass transfer with thermal radiation in a non-Darcy porous medium, *J. of Porous Media*, **8**, 541–549.

[83a] Payne, L. E. and Straughan, B., 1998, Structural stability for the Darcy equations of flow in porous media, *Proceedings of the Royal Society A: Mathematical, Physical and Engineering Sciences*, **454**, 1691–1698.

[84] Qin, Y., and Kaloni, P. N., 1993, A nonlinear stability problem of convection in a porous vertical slab, *Phys. Fluids A*, **5**, 2067–2069.

[85] Ramachandran, A., Saikia, B., Sinha, K., and Govindarajan, R., 2016, Effect of Prandtl number on the linear stability of compressible Couette flow, *Int. J. Heat Fluid Flow*, **61**, 553–561.

[86] Rachedi, R., and Chikh, S., 2001, Enhancement of electronic cooling by insertion of foam materials, *Heat Mass Transf.*, **37**, 371–378.

[87] Riahi, N., 1983, Nonlinear convection in a porous layer with finite conducting boundaries, *J. Fluid Mech.*, **129**, 153–171.

[88] Rogers, B. B., Moulic, S. G., and Yao, L. S., 1993, Finite-amplitude instability of mixed convection, *J. Fluid Mech.*, **254**, 229–250.

[89] Rees, D. A. S., 1988, The stability of Prandtl-Darcy convection in a vertical porous layer, *Int. J. Heat Mass Transfer*, **31**, 1529–1534.

[90] Rees, D. A. S., 2011, The effect of local thermal nonequilibrium on the stability of convection in a vertical porous channel, *Transp. Porous Media*, **87**, 459–464.

[91] Rubinstein, J., 1986, Effective equations for flow in random porous media with a large number of scales, *J. Fluid Mech.*, **170**, 379–383.

[92] Rees, D. A. S., Bassom, A. P. and Siddheshwar, P. G., 2008, Local thermal non-equilibrium effects arising from the injection of a hot fluid into a porous medium, *J. Fluid Mech.*, **594**, 379–398.

[93] Reynolds, W. C., Potter, M. C., 1967, Finite-amplitude instability of parallel shear flows, *J. Fluid Mech.*, **27**, 465–492.

[94] Schlichting, H. and Gersten, K., 2004, Boundary layer theory, *Springer 8th edition*.

[95] Schmid, P. J. and Henningson, D. S., 2001, Stability and Transition in Shear Flows, *Springer*.

[96] Slattery, J. C., 1969, Single-phase flow through porous media, *AIChE J.*, **15**, 866–872.

[97] Shukla, P. and Alam, M., 2011, Weakly nonlinear theory of shear-banding instability in a granular plane Couette flow: analytical solution, comparison with numerics and bifurcation, *J. Fluid Mech.*, **666**, 204–253.

[98] Straus, J. M., 1974, Large amplitude convection in porous media, *J. Fluid Mech.*, **64**, 51–63.

[99] Stuart, J. T., 1958, On the non-linear mechanics of hydrodynamic stability, *J. Fluid Mech.*, **4**, 1–21.

[100] Stuart, J. T., 1960, On the non-linear mechanics of wave disturbances in stable and unstable parallel flows. Part 1. The basic behavior in plane-Poiseuille flow, *J. Fluid Mech.*, **9**, 353–370.

[101] Stewartson, K. and Stuart, J. T., 1971, A non-linear instability theory for a wave system in plane Poiseuille flow, *J. Fluid Mech.*, **48**, 529–545.

[102] Su, Y. C. and Chung, J. N., 2000, Linear stability analysis of mixed-convection flow in a vertical pipe, *J. Fluid Mech.*, **422**, 141–166.

[103] Suslov, S. A. and Paolucci, S., 1999b, Nonlinear stability of mixed convection flow under non-Boussinesq condition: Part 2. Mean flow characteristics, *J. Fluid Mech.*, **398**, 87–108.

[104] Scott, N. L. and Straughan, B., 2013, A nonlinear stability analysis of convection in a porous vertical channel including local thermal nonequilibrium, *J. Math Fluid Mech.*, **15**, 171–178.

[105] Scheele G.F. and Hanratty T.J., 1962, Effect of natural convection on stability of flow in a vertical pipe, *J. Fluid Mech.*, **14**, 244–256.

[106] Straughan, B., 1988, A nonlinear analysis of convection in a porous vertical slab, *Geophys. Astrophys. Fluid Dyn.*, **42**, 269–275.

[107] Samanta, A., Vinuesa, R., Lashgari, I., Schlatter, P. and Brandt, L., 2015, Enhanced secondary motion of the turbulent flow through a porous square duct, *J. Fluid Mech.*, **784**, 681–693.

[108] Saeid, N. H., 2004, Analysis of mixed convection in a porous layer using non-equilibrium model, *Int. J. Heat Mass Transfer*, **47**, 5619–5627.

[109] Singh, C., Tathgir, R. G. and Muralidhar, K., 2009, Energy storage in fluid saturated porous media subjected to oscillatory flow, *Heat Mass Transfer*, **45**, 427–441.

[110] Schmid, P. J. and Brandt, L., 2014, Analysis of fluid systems: stability, receptivity, sensitivity, *Applied Mechanics Reviews*, **66**, 024803.

[111] Sibanda, P., Motsa, S.S. and Shateyi, S., 2004, Linear stability of two-dimensional flow to three-dimensional perturbations in a channel with a flexible wall, *Archives of Mechanics*, **56**, 293–311.

[112] Shankar, V. and Kumaran, V., 1999, Stability of non-parabolic flow in a flexible tube, *Journal of Fluid Mechanics*, **395**, 211–236.

[113] Shankar, V. and Kumaran, V., 2000, Stability of fluid flow in a flexible tube to non-axisymmetric disturbance, *Journal of Fluid Mechanics*, **407**, 291–314.

[113a] Kumaran, V., 1995, Stability of the viscous flow of a fluid through a flexible tube, *Journal of Fluid Mechanics*, **294**, 259–281.

[114] Sunil, Divya and Sharma, R. C., 2005, The effect of magnetic field dependent viscosity on thermosolutal convection in a ferromagnetic fluid saturating a porous medium, *Transport in Porous Media*, **60**, 251–274.

[115] Sunil, Sharma, P. and Mahajan, A., 2011, Onset of Darcy-Brinkman ferroconvection in a rotating porous layer using a thermal non-equilibrium model: A nonlinear stability analysis, *Transport in Porous Media*, **88**, 421–439.

[116] Tang, W. H., Wu, Q. H. and Richardson, Z. J., 2002, Equivalent heat circuit based power transformer thermal model, *IEE Pros. Electr. Power Appl.*, **149**, 87–92.

[117] Tilton, N. and Cortelezzi, L., 2008, Linear stability analysis of pressure-driven flows in channels with porous walls, *J. Fluid Mech.*, **604**, 411–445.

[118] Umavathi, J. C., Kumar, J. P., Chamkha, A. J. and Pop, I., 2005, Mixed convection in a vertical porous channel, *Transp. Porous Media*, **61**, 315–335.

[119] Vafai, K. and Kim, S. J., 1995, On the limitations of the Brinkman-Forchheimer-extended Darcy equation, *Intl J. Heat and Fluid Flow*, **16**, 11–15.

[120] Vafai, K. and Tien, C. L., 1981, Boundary and inertia effects on flow and heat transfer in porous media, *Intl J. Heat Mass Transfer*, **24**, 195–203.

[121] Vafai, K. and SÃűzen, M., 1990, Analysis of energy and momentum transport for fluid flow through a porous bed, *ASME J. Heat Transfer*, **112**, 390âĂŞ399.

[122] Vafai, K., 2000, *Handbook of Porous Media*, (Marcel Dekker, New York).

[123] Whitaker, S., 1996, The Forchheimer equation: A theoretical development, *Transp. Porous Media*, **25**, 27–61.

[124] Wooding, R. A., 1957, Steady state free thermal convection of liquid in a saturated permeable medium, *J. Fluid Mech.*, **2** 273–285.

[125] Wolanski, E. J., 1973, Convection in a vertical porous slab, *Phys. Fluids*, **16**, 2014–2016.

[126] Wong, K. C. and Saeid, N. H., 2009, Numerical study of mixed convection on jet impingement cooling in a horizontal porous layer under local thermal non-equilibrium conditions, *Int. J. of Thermal Sciences*, **48**, 860–870.

[127] Watson, J., 1960, On the non-linear mechanics of wave disturbances in stable and unstable parallel flows. Part 2. The development of a solution plane-Poiseuille flow and for plane-Couette flow, *J. Fluid Mech.*, **9**, 371–389.

[128] Yang, J., Wang, J., Bu, S., Zeng, M., Wang, Q., and Nakayama, A., 2012, Experimental analysis of forced convective heat transfer in novel structured packed beds of particles, *Chem. Eng. Sci.*, **71**, 126–137.

[129] Yao, L. S. and Rogers, B. B., 1989, The linear stability of mixed convection in a vertical annulus, *J. Fluid Mech.*, **201**, 279–298.

[130] Yao, L. S. and Rogers, B. B., 1992, Finite-amplitude instability of non-isothermal flow in a vertical annulus, *Proc. R. Soc London, Ser.*, **437**, 267–290.

[131] Zhang, W., Li, W. and Nakayama, A., 2015, An analytical consideration of steady-state forced convection within a nanofluid-saturated metal foam, *J. Fluid Mech.*, **769**, 590–620.

[132] Zorrilla, S.E. and Rubiolo, A.C., 2005, Mathematical modeling for immersion chilling and freezing of foods. Part I. Model development, *Journal of Food Engineering*, **66**, 329–338.